TOOLS FOR THE PROFESSIONAL DEVELOPMENT OF HORN LOUDSPEAKERS

Von der Fakulät für Elektrotechnik und Informationstechnik der
Rheinisch-Westfälischen Technischen Hochschule Aachen
zur Erlangung des akademischen Grades eines
DOKTORS DER INGENIEURWISSENSCHAFTEN
genehmigte Dissertation

vorgelegt von

Diplom-Ingenieur
Michael Makarski
aus Mainz

Berichter: Universitätsprofessor Dr. rer. nat. Michael Vorländer
Universitätsprofessor Dr.-Ing. Bernhard Rembold

Tag der mündlichen Prüfung: 20. April 2006

Bibliografische Information Der Deutschen Bibliothek

Die Deutsche Bibliothek verzeichnet diese Publikation in der Deutschen Nationalbibliografie; detaillierte bibliografische Daten sind im Internet über http://dnb.ddb.de abrufbar.

ISBN 3-8325-1280-2

Logos Verlag Berlin
Comeniushof, Gubener Str. 47,
10243 Berlin
Tel.: +49 030 42 85 10 90
Fax: +49 030 42 85 10 92
INTERNET: http://www.logos-verlag.de

Contents

Abstract - Zusammenfassung **vii**

1 Introduction **1**

2 Basic Principles of a Horn Driver - Horn Combination **7**
2.1 Horn Driver 8
2.2 Horn 14
2.3 Discussion on Driver Modelling and Horn Calculations 16

3 Investigation of the Interface between Horn Driver and Horn **19**
3.1 Scanning of Pressure and Velocity Profile at the Driver's Mouth 20
3.1.1 Measurement Technique 20
3.1.2 Velocity Measurement 23
3.1.3 Mesh Requirements 24
3.2 Modal Decomposition 27
3.3 Analysis 30
3.3.1 Theoretical Considerations 30
3.3.2 Decomposition Results 33
3.4 Discussion of the Results 35

4 Separation of Horn Driver and Horn **41**
4.1 Full Cross Modal Description 42
4.2 Simplified Descriptions 47
4.3 How many Modes should be considered? 51

5 Determination of the Horn Parameters **53**
5.1 BEM 53
5.2 Calculation of the Modal Data Set for the Horn 56
5.2.1 Simulation of the Modal Surface Pressure Distribution 56
5.2.2 Calculation of the Modal Throat Impedance Matrix from the Modal Surface Pressure 58
5.2.3 Calculation of Modal Transfer Impedance Vectors 66

6 Determination of the Driver Parameters **71**
6.1 Fundamental Mode Model 72
6.1.1 Definitions and Reciprocity 72
6.1.2 Basic Considerations for the Measurement of the Fundamental Mode Model's Parameters 73

6.1.3 Method I - Using Two Different Drivers . . . 76
6.1.4 Method II - Using Two Identical Drivers . . . 80
6.1.5 Some Application Examples for the Fundamental Mode Model . . . 83
6.1.6 Discussion . . . 87

7 Simulation of Nonlinear Properties 89
7.1 Nonlinear Wave Equation . . . 91
7.2 Calculation of Harmonic Distortion in Horns . . . 92
7.3 Calculation of the Maximum Sound Pressure Level . . . 94
7.3.1 Horn Related Distortion . . . 95
7.3.2 Driver Related Distortion . . . 96
7.4 Measurements and Simulations . . . 100
7.5 Discussion . . . 103

8 Professional Development of Loudspeakers 105
8.1 Horn Optimization . . . 106
8.1.1 Development of the Geometry . . . 106
8.1.2 Nonlinear Simulations . . . 115
8.2 Investigation of Horn Drivers and Properties of the Coupled System Driver/Horn . . . 116
8.2.1 Linear Properties Based on Fundamental Mode Two-port Measurements and Simulations . . . 117
8.2.2 Investigation of the Higher Order Mode Influence . . . 118
8.2.3 Simulation of the Max-SPL . . . 122
8.3 Final Conclusions and Measurements . . . 123
8.3.1 Measurements of the Combination Driver B/Horn 10hr . . . 124

9 Summary 127

10 Kurzfassung 133
10.1 Einleitung . . . 133
10.2 Funktionsweise einer Horntreiber/Horn-Kombination . . . 134
10.3 Experimentelle Untersuchung der Schnittstelle von Horntreiber und Horn . 134
10.4 Beschreibung der Schnittstelle von Horntreiber und Horn . . . 135
10.5 Bestimmung der Parameter für das Horn . . . 136
10.6 Bestimmung der Parameter für den Treiber . . . 137
10.7 Simulation von nichtlinearen Eigenschaften . . . 137
10.8 Professionelle Entwicklung von Hornlautsprechern . . . 138
10.9 Zusammenfassung und Ausblick . . . 139

A Glossary 141

B Discretised Decomposition 144

C Solution of the System of Equations using Method I, page 76 146

D Solution of the System of Equations using Method II, page 80 148

E Nonlinear wave equation **149**
E.1 Second order equation 150

Danksagung **153**

Lebenslauf **154**

Bibliography **155**

Abstract – Zusammenfassung

Abstract

This thesis deals with methods for the professional development of horn loudspeakers. The basic idea is to separately describe the acoustic source (horn driver) and the device to guide the wave (horn or wave guide). The separate description of both systems allows one to freely combine the data of any driver and horn which yields an enormous flexibility when developing new driver/horn combinations.

At first, it is investigated by measurements which properties of the sound wave can be found at the common interface between driver and horn. Different driver/horn combinations are analysed by decomposing the pressure and velocity profiles into orthogonal eigenfunctions.

Based on the practical measurement results, several modal models for the interface are derived. On the one hand, the models must be capable to describe the three-dimensional properties of the sound wave at the interface. On the other hand, it must be possible to measure or calculate the model's parameters in practice.

Then, it is described how the modal horn parameters are calculated using numerical methods (Boundary Element Method) combined with modal excitation and decomposition. The driver's parameters are acquired using a particular measurement technique.

Additionally to the linear modal modelling, a method to calculate harmonic distortion in horn loudspeaker is developed and verified.

Finally, it is demonstrated how to use the methods in practice. A complete development process of a horn loudspeaker is described and the results are verified by measurements. The practical relevance of the methods results not only from the high accuracy, but also from the effective application when developing horn loudspeakers.

Zusammenfassung

Im Rahmen dieser Arbeit werden Methoden zur professionellen Entwicklung von Hornlautsprechern hergeleitet, verifiziert und in zahlreichen praktischen Messungen und Anwendungsbeispielen erprobt. Grundidee der beschriebenen Methoden ist eine konsequente Trennung zwischen Schallquelle (Horntreiber) und Schallführung (Horn). Die Auftrennung an einer gemeinsamen Schnittstelle erlaubt es, Datensätze verschiedener Treiber und Hörner frei zu kombinieren, wodurch ein Höchstmaß an Effektivität und Flexibilität bei der Entwicklung neuer Lautsprechersysteme erreicht wird.

Es wird zunächst mit Hilfe von Messungen an verschiedenen Horntreiber/Hornkombinationen untersucht, welche Eigenschaften die sich in der gemeinsamen Schnittstelle ausbreitende Schallwelle besitzt und wie die Rückwirkung der Schallführung auf die eingeprägte Wellenform zu bewerten ist. Die Analyse der gemessenen Schallfelder erfolgt durch eine modale Zerlegung in orthogonale Eigenfunktionen.

Basierend auf diesen Ergebnissen werden modale Modelle mit unterschiedlicher Anzahl von Freiheitsgraden hergeleitet. Ziel ist es, an dieser Stelle den bestmöglichen Kompromiss zwischen Genauigkeit und Komplexität der Modelle zu finden. Die dreidimensionalen Eigenschaften des Schallfeldes im Übergang Treiber/Horn müssen erfasst werden und es muss natürlich möglich sein, die Modelle praktisch zu realisieren.

Es wird dann ausführlich beschrieben, wie die modalen Daten für das Horn durch die Anwendung von numerischen Verfahren (Boundary Elemente Methode kombiniert mit modaler Anregung/Dekomposition) bestimmt werden können. Die Parameter für das Treibermodell werden durch ein spezielles Messverfahren bestimmt.

Zusätzlich zu den linearen, modalen Modellen wird ein erweitertes Berechnungsverfahren für die Bestimmung der harmonischen Verzerrungen eines Hornlautsprechers entwickelt und verifiziert.

Abschließend wird die Anwendung aller beschriebenen Verfahren anhand eines kompletten Entwicklungszyklus einer professionellen Horntreiber/Hornkombination demonstriert. Die praktische Relevanz der entwickelten Verfahren ergibt sich hier nicht nur durch die hohe Modellierungsgenauigkeit, sondern gerade auch durch die effektive Umsetzbarkeit in die Praxis.

Chapter 1

Introduction

Horns used as sound reinforcement devices have been known for several centuries. They were used not only for speech reinforcement and as musical instruments but also as ear-trumpet and loudspeaker. Hence, the mathematical treatment also goes back to this time. Famous scientists like Euler, Lagrange, Webster, and others are associated with the theory of horn physics. The theoretical approaches of this time mainly concentrated on methods to calculate properties of the horn using a plane wave at the horn throat[1] as "input signal". Furthermore, the models used in the early time of horn theory are simplified to a one-dimensional treatment of the wave propagation. These two ideas lead to the famous "Webster's equation" which appears in a huge number of articles. Eisner's paper "Complete Solution of the "Webster" horn equation" [Eis66] includes more than 200 references to this topic.

An important property of a horn is the horn throat impedance: the ratio of pressure and volume velocity in the cut plane of the horn throat. When connecting an acoustic source, like an electro-mechanical transducer, a "human voice", an embouchure of a musical instrument, or any device which can generate sound volume velocity, an acoustic interaction takes place: the horn acts like a load on the source, and, thus, influences the sound power emitted by the source. In a one-dimensional acoustic model, this can directly be translated into electric circuits. Hence, the throat impedance corresponds to a terminating impedance and accordingly influences the efficiency of the whole apparatus. As the horn enables to increase the acoustic load for the source (most mechanical sources are mismatched to the sound field), it enables to increase the emitted sound power.

The potential increase of efficiency, actually, was the reason to use a horn to amplify the mechanical oscillation of a pin running in a groove of a disc: the gramophone (Figure 1.1(a)). With the invention (G.R. Carey, 1875) and mass production of electron tubes (RCA,

[1] The horn throat is the geometrical beginning of the horn.

1920), it also became popular to use electro-acoustic transducers to generate sound from electric signals. As the transducers of this era featured a low efficiency, it was necessary to combine them with acoustic horns. The better efficiency of a *horn driver/horn combination* and the increased acoustic gain enabled the sound reinforcement for large audience areas (Figure 1.1(b)).[2]

(a) Gramophone (b) Movie talker

Figure 1.1: Historical horn applications

The invention of the transistor (Walter Brattain, 1947) later offered the possibility to build amplifiers of significant larger capability. With increasing power and decreasing costs of the amplifiers, the optimisation of the electro-acoustic efficiency was not the primary goal of horn development anymore. But also the electro-acoustic transducers became more efficient, as better materials for the permanent magnet were used. Hence, modern horn and transducer design concentrates on the radiation pattern of the horn and optimization of nonlinear properties of horn and transducer. Today, the horn is seen as *directivity controlling device*. This paradigm shift took place in the 90s of the 20th century. As a result, new models were needed to predict the three dimensional radiation patterns and nonlinear properties of horn loudspeakers. The “simple” one-dimensional models of a horn based on the Webster’s horn equation were replaced (or modified) by more sophisticated analytical or combined analytical/numerical models and methods (see for example [MR93], [Ged89],

[2]The horn concentrates the sound power on a smaller volume, compared to a conventional loudspeaker. The ratio of sound intensity of the omni-directionally radiated sound power and maximum sound intensity of the directed sound is called gain.

[Ged93], [NKP96], [AKP97], [BJ74a], [BJ74b], [Pis03] [Put93] [Put96]) or pure numerical methods based on the linear sound field equation ([MKS79], [Hen93], [GH96], [Bri03], [Joh94], [Mak03] [Kel02]).

The treatment of electro-acoustic transducers is even more complex. As the transducer is the source of volume velocity for the acoustic sound field, a lot of research is done on it. The methods used to model the transducer range from applying lumped elements [CG87] [Kee77] [WML78] in one-dimensional models to nonlinear models [Kli96] [SBSH95] [SBB97] [SB95] [Voi02] [SMPX99] and very complex numerical methods [Dod03] [Bel98] [RLK+97]. Beside the modelling of the transformation of electrical power into radiated sound power, thermal models of voice coil, magnetic circuit and mechanical components are used to predict their temperature over the input power. Furthermore, the adhesives, membrane materials and voice coil materials are of great importance for the power handling capabilities of the transducer. Hence, properties of such materials are normally confidential (in the case such properties are known) and not open to the public to use as input data in numerical simulations.

As there exist a lot of modelling methods for both, the horn and the transducer, the question comes up what is left to be further investigated? Comparing the methods described in literature and the methods often used in practice to develop horn driver/horn combinations one finds a large discrepancy: although the state of the art methods exist (see literature) they are usually not applied in “everyday development processes”. In fact, the development of a commercial driver/horn system is usually a combination of trial and error, experience of the engineer (the knowledge which driver may be suitable) and rules of thumb for the development of the horn geometry. Accordingly, it is necessary to build a number of horn prototypes and combine them with a number of drivers. Then, the acoustic properties of these combinations are measured to find the most suitable one. This procedure is expensive (building the horn prototypes) and time consuming (making the measurements) and, thus, it does not seem to be the optimum.

But why are the methods described in literature, normally, not applied in practice? This may have several reasons which can be discussed using a typical loudspeaker development process: a public address[3] system has to be developed. The transducer of type “XY” with a circular 1.4” outlet has to be used for the high frequency unit in this project. The coverage angle[4] should be, for instance, 60° in the horizontal plane and 40° in the vertical plane. The

[3] A public address system is a loudspeaker designed to cover large audience areas

[4] The coverage angle is the angle where the sound pressure level is -6 dB referred to the main axis of the horn.

lower cut-off should be at 2 kHz and the sound-pressure level at 10% harmonic distortion must be at a minimum of 120 dB SPL[5] for the complete high frequency band and at about 130 dB SPL at the lower cut-off. Furthermore the shape of the horn mouth[6] is defined to be rectangular with the dimension a x b and the maximum length of the horn is l. The on-axis frequency response of the driver "XY" combined with the horn to be developed should, additionally, be as smooth as possible. Of course, the project has to be finished within two weeks.

The engineer who has to develop the horn geometry is obviously confronted with a lot of practical constraints. Before starting the development he, furthermore, has to decide if it is generally possible to fulfil all constraints or not[7]. At first, he has to get some information about the transducer. Since such transducers, especially the so-called horn drivers[8], are rather complex electromechanical systems, a simple lumped element model might not be accurate enough. A numerical model of the transducer is also not feasible, as the development of such a model is a task of several weeks or even months. Concerning the driver, the developer will finally try to characterise the transducer by electric and acoustic measurements. After that, the horn geometry can be developed. Looking at the numerous analytical or combined analytical/numerical methods to calculate horns, one finds that it is extremely complex to calculate a geometry varying from a circular one at the beginning to a rectangular one at the end and to additionally include diffraction at the cabinet of the whole loudspeaker. From this, one can conclude that pure numerical methods are probably the most direct way to solve the linear sound field equation and to use the results to calculate the radiation pattern, throat impedance and other properties of the horn. Besides these considerations, there are some other points to be discussed. As the source and the horn are treated separately, one has to decide how to couple (numerically) the measured data of the transducer to the simulated or calculated data of the horn and how to calculate common properties of the acoustically coupled systems. Another question is how accurate the driver description has to be and how to treat other sources than horn drivers.

Using this actually rather simple example one could discuss a lot of other ideas and methods to solve the problems found in practical development processes. This is exactly the content of this thesis. The basic idea of this work is to treat the acoustic source (a

[5] dB SPL: Sound Pressure Level $L(\tilde{p}) = 20\log_{10}(\tilde{p}/20\,\mu\text{Pa})$

[6] The horn mouth is the output of the horn

[7] The author knows from his own practical experience that such projects sometimes are like a mission impossible.

[8] A horn driver is a transducer designed for high performance applications in combination with a horn as loading and directivity controlling device.

horn driver, dome tweeter, midrange cone speaker, ribbon tweeter, ...) and the horn or waveguide[9] separately. Provided that suitable descriptions are used for both systems and that the measurement or simulation technique is capable to derive the needed parameters, this technique allows to greatly reduce time and effort to simulate the complete system of acoustic source and horn.

The thesis begins with some basic considerations and discussions on conventional driver and horn modelling. Chapter 3 contains a practical investigation of the most common source, the typical horn driver. The properties of real sources are the basis for discussing the separation of the two coupled systems and which method can be used to describe the two separated systems (Chapter 4). Chapters 5 and 6 describe methods to determine the parameters for the driver and the horn description. The calculation of some nonlinear properties of wave propagation in horns is treated in Chapter 7. The thesis concludes with the description of a typical application example one can find in practice and demonstrates how to use the described techniques (Chapter8).

[9]The expression waveguide is often used for horn geometries designed to create particular wave fronts, like plane coherent waves for line array applications. Other authors use this expressions also for conventional horns in order to emphasize that the horn is used as directivity controlling device.

Chapter 2

Basic Principles of a Horn Driver - Horn Combination

Today, the variety of audio transducers is immense. They differ in the mechanism of transforming electrical into mechanical energy, in the materials used for membrane and other components, and in shape and mode of membrane movement. Despite this diversity, there exist typical configurations in professional loudspeaker applications. The low and mid-frequency range is, normally, covered using cone speakers with or without horn whereas the high-frequency range, usually, is realized using a horn driver combined with a horn. These frequency ranges are not clearly defined, but it is possible to classify the typical horn drivers found on the market by their driver outlet. The outlet is normally circular, but some types exist featuring rectangular outlets for particular applications. For the types with circular outlet, some standard sizes exist on the market and one can approximately assign the following frequency ranges to these sizes:

- 2”-diameter covers 500 Hz to 13 kHz, in some rare cases even up to 20 kHz
- 1.4” and 1.5” cover 800 Hz to 15 kHz, most popular size
- 1” covers 1.3 kHz to 20 kHz
- 0.75” covers 2 kHz to 20 kHz, but this size is not very popular

The widespread use of the horn driver/horn combination is in fact a consequence of physical constraints and the practical requirements of a public address system. The acoustic properties needed for loudspeaker applications can be summarized in a few points. The sound pressure level should not vary in the audience area. Additionally, it is not desired to radiate sound into unwanted directions like the ceiling or backwards to the stage. Furthermore, it must be possible to cluster several loudspeakers in order to cover larger audience

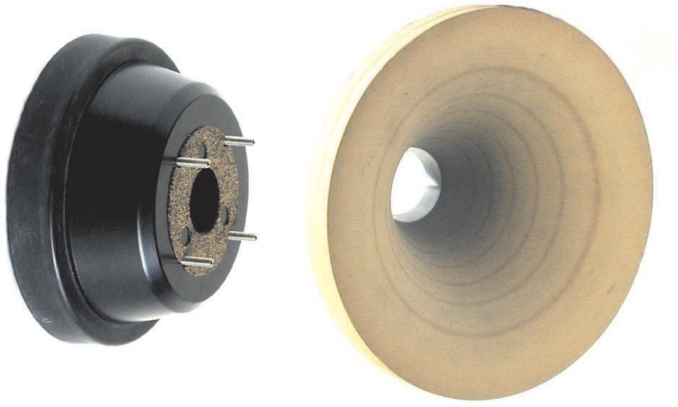

Figure 2.1: Typical horn driver and horn combination. The driver outlet diameter is 2”. The horn shown here is a so-called tractrix horn.

areas as would be possible using a single system. In this case too, the pressure distribution has to be almost constant, which in practice is not fulfilled due to more or less strong interferences between neighboured systems. Hence, a PA-system should radiate sound with a well-defined spatial distribution to fulfil the needs in practice. The sound pressure signal measured at any position in the audience area should match the electrical signal which is fed into the amplifiers as closely as possible. This, of course, must be ensured even at high sound pressure levels.

The functionality of such a typical horn driver/horn combination is explained in the following, starting with the horn driver. Although the functional principle of the driver is of no importance for the separation of horn driver and horn at their common interface, which will be described in the following Chapters, the basic idea of this combination is discussed briefly.

2.1 Horn Driver

A horn driver usable for professional sound reinforcement has to fulfil two basic requirements: firstly, the electrical power is to be transformed as efficiently as possible into acoustical power. Secondly, the shape of the wave front leaving the driver should be suitable for coupling the driver to a horn. The wave front is influenced by the mode of excitation and the wave guiding components. Hence, the mechanical construction of the driver allows, at least to a certain degree, to influence the velocity profile at the driver’s mouth.

Figure 2.2 shows a sectional view of a typical horn driver. A common method to describe such systems is to use lumped elements to model the electro-acoustic transducer. The following electro-mechanical analogies are used [ZZ93]: the mechanical force F corresponds to a voltage, the mechanical velocity V is the current. Accordingly, the ratio of force and velocity is a mechanical impedance Z_m and can be used in the same way as

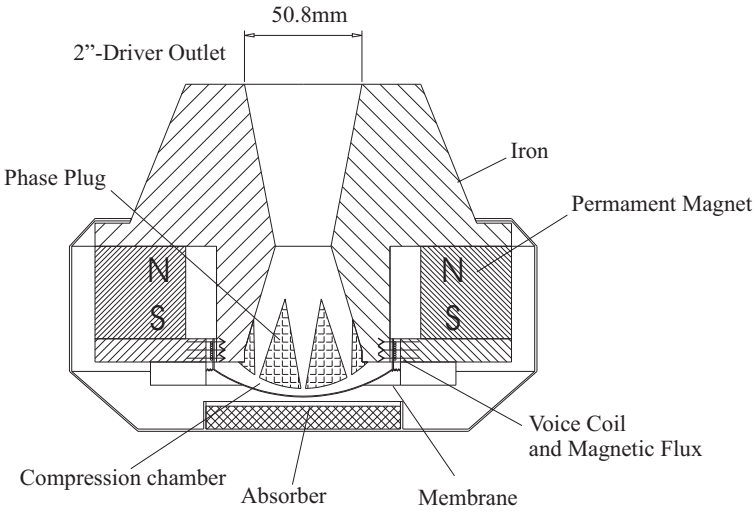

Figure 2.2: Sectional view of a typical (old-fashioned) horn driver.

electric impedances in an electric network.

The transformation from electric signals to the force driving the membrane can be basically described by a network, as shown in Figure 2.3(a). The electric current, fed into

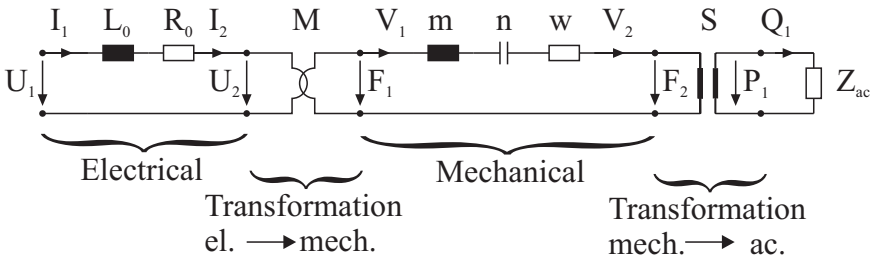

(a)

M	Force factor Bl	N/A
Z_e	Electric impedance	Ω
S	Membrane area	m^2
m	Mechanical mass	kg
n	Mechanical compliance	m/N
w	Mechanical losses	N s/m
R_0	DC-resistance of the voice coil	Ω
L_0	Voice coil inductance	H
Z_m	Mechanical impedance	N s/m

(b)

Figure 2.3: Standard lumped element network and of an electro dynamic transducer (a) and physical quantities (b)

the voice coil of the transducer, is transformed into a force perpendicular to the cut-plane of the voice-coil. For an ideal electro-dynamic transducer, the magnetic field crosses the wire perpendicularly at any point. Hence, the force can be expressed omitting the vector

product:

$$F = BlI, \tag{2.1}$$

where B is the flux density, l is the length of the wire (within the magnetic field) and I is the current. If the coil is moved by an external force, there will also be a back EMF. The open circuit voltage is then

$$U = BlV. \tag{2.2}$$

These two equations can be combined in a T-matrix

$$\begin{pmatrix} F_1 \\ V_1 \end{pmatrix} = \begin{pmatrix} 0 & M \\ \frac{1}{M} & 0 \end{pmatrix} \begin{pmatrix} U_2 \\ I_2 \end{pmatrix} \tag{2.3}$$

where $M = Bl$. This matrix describes the transformation of electrical into mechanical energy under ideal circumstances. Additionally, a T-matrix for the losses and the inductance of the coil (eq. (2.4)) and a matrix describing the mechanical oscillator (eq. (2.5)), consisting of dynamical mass, suspension, and mechanical losses of the membrane has to be used:

$$\begin{pmatrix} U_2 \\ I_2 \end{pmatrix} = \begin{pmatrix} 1 & -Z_e \\ 0 & 1 \end{pmatrix} \begin{pmatrix} U_1 \\ I_1 \end{pmatrix} \tag{2.4}$$

$$\begin{pmatrix} F_2 \\ V_2 \end{pmatrix} = \begin{pmatrix} 1 & -Z_m \\ 0 & 1 \end{pmatrix} \begin{pmatrix} F_1 \\ V_1 \end{pmatrix} \tag{2.5}$$

$$Z_e = R_0 + j\omega L_0 \tag{2.6}$$

$$Z_m = w + j\omega m + \frac{1}{j\omega n} \tag{2.7}$$

The membrane is driven by a certain force, depending on the properties of this matrices, and transforms this force into a motion. Accordingly, the moving membrane accelerates a volume of the surrounding fluid. The volume velocity Q_1 of the accelerated fluid is proportional to the effective membrane area S. The transducer is now described up to the membrane by the most simple model possible.

To study the properties of a real transducer the parameters were measured[1] at a dismounted driver (RCF 980, phase-plug removed):

$S = 2.12 \cdot 10^{-3}\ \mathrm{m}^2$ $\quad m = 1.3\ \mathrm{g}$ $\quad n = 3.8\ \mu\mathrm{m/N}$ $\quad w = 4\ \mathrm{Ns/m}$

$R_0 = 4\ \Omega$ $\quad L_0 = 55\ \mu\mathrm{H}$ $\quad M = 8\ \mathrm{Vs/m}$

If such a transducer - without phase-plug - is used for the radiation of sound, the sound field will provide a mechanical reaction on the membrane as the acceleration of a portion of fluid

[1] The measurement of transducer parameters is described in [Goe99]

needs a certain pressure. This interaction of fluid and driving membrane is called radiation impedance. It is dependent on size and shape of the membrane and can be calculated analytically for some geometries like circular or rectangular pistons and pulsating or oscillating spheres (see [MI68]). A common property of all simple, piston-like geometries is that the radiation impedance converges to the specific impedance $\rho_0 cS$ of the fluid[2] when the wavelength is small compared to the membrane dimensions. Hence, the membrane is *loaded* by this ratio of force and velocity. In order to effectively excite sound waves, the source, consisting of driving membrane and the electro-mechanical transformer, should be matched to this impedance. A perfectly matched sound source would have an inner impedance which is conjugate complex to the *acoustic load* Z_{ac}, which is in this consideration simply the radiation impedance of the membrane.

The inner mechanical impedance of the transducer, connected to an ideal voltage source, seen from the membrane down into the network can be calculated by

$$Z_{m,i} = \left(\frac{j\omega L_0}{M^2} + \frac{R_0}{M^2}\right)^{-1} + j\omega m + \frac{1}{j\omega n} + w. \tag{2.8}$$

Figure 2.4 shows the calculated inner mechanical impedance (equation (2.8)), based on the measured parameters. At the resonance frequency of the transducer the impedance

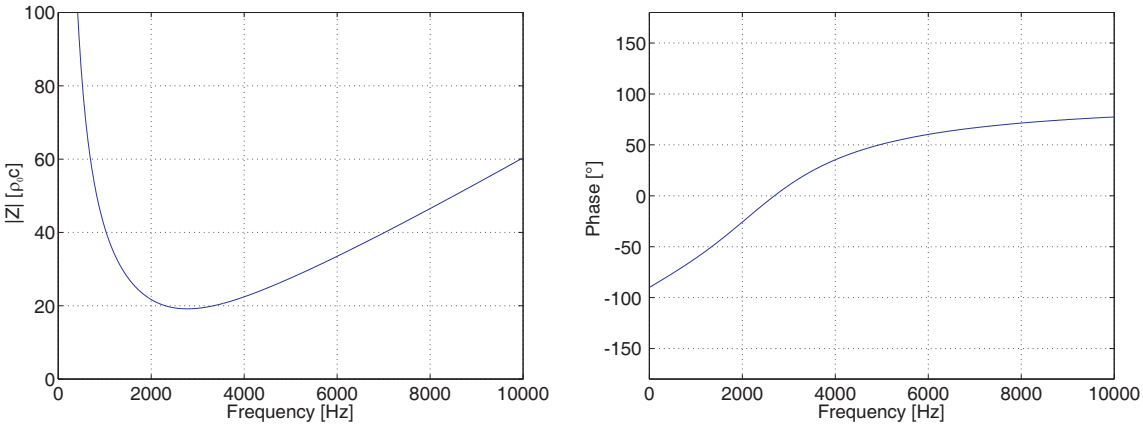

(a) Magnitude (b) Phase

Figure 2.4: Inner mechanical impedance normalized to $\rho_0 cS$

reaches the absolute minimum at a value of about 20 times $\rho_0 c$. For higher frequencies it is dominated by the dynamic mass. Below the compliance is dominant. It is obvious that a source with such a characteristic is mismatched to the sound field and, therefore, cannot effectively radiate sound waves in a medium like air. To transform the source impedance to

[2] ρ_0 is the density and c is the phase velocity of the unperturbed fluid

a lower value, the large area of the membrane has to be coupled to a compression chamber (Figure 2.5).

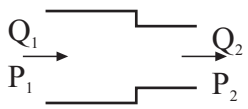

Figure 2.5: Compression chamber

In a first order approximation, this configuration works like an acoustic transformer. At the cross-sectional jump, volume flow and pressure have to be constant, thus, increasing the particle velocity by the ratio of the cross-sectional cut-planes. Additionally, the distance from different parts of the membrane to the driver outlet have to be balanced to avoid interference effects within the horn driver which is realized by a phase-plug. Again, making a first order approximation for the phase plug as conical bore (see Figure 2.2) the T-matrix for the compression chamber and phase-plug is

$$\begin{pmatrix} P_3 \\ Q_3 \end{pmatrix} = \frac{a}{R} \begin{pmatrix} -\cos(kl) & -jZ(\eta(0))\sin(kl) \\ j\frac{1}{Z(\eta(l))}\sin(kl) & \frac{Z(\eta(0))}{Z(\eta(l))}\cos(kl) \end{pmatrix} \begin{pmatrix} P_2 \\ Q_2 \end{pmatrix}, \tag{2.9}$$

where

$$Z(\eta(0)) = \frac{\rho_0 c}{S_2} \frac{jk\eta(0)}{1 + jk\eta(0)} \qquad \eta(0) = \frac{al}{R-a} \tag{2.10}$$

$$Z(\eta(l)) = \frac{\rho_0 c}{S_3} \frac{jk\eta(l)}{1 + jk\eta(l)} \qquad \eta(l) = l + \frac{al}{R-a} \tag{2.11}$$

and l is the length, d the radius at the beginning, R the radius at the end of the conical tube.

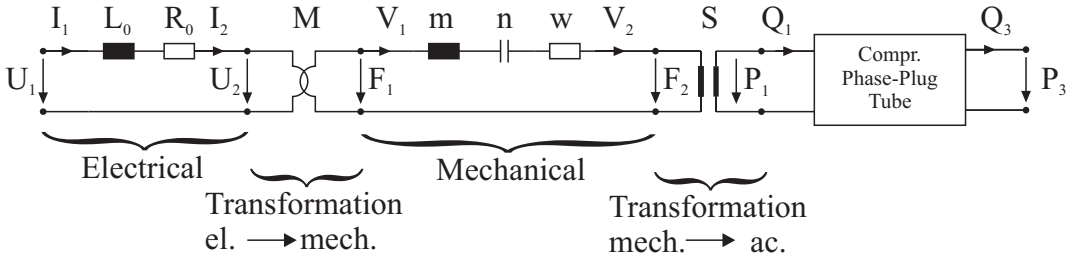

Figure 2.6: Network for a horn driver including phase-plug

The source impedance of this configuration calculated at the plane of the driver outlet is

$$Z_{ac,i} = Z(\eta(l)) \frac{\frac{1}{S_1^2}\frac{Z_{m,i}}{Z(\eta(0))} + j\tan(kl)}{j\frac{1}{S_1^2}\frac{Z_{m,i}}{Z(\eta(0))}\tan(kl) + 1}, \tag{2.12}$$

where $S_1 \approx S_3$ and $S_2/S_1 \approx 1/20$ were measured at the dismounted driver. Figure 2.7(a) shows a comparison of measured and computed source impedance [Mak01]. There is a

good accuracy for high frequencies (4 kHz to 10 kHz). At frequencies below 4 kHz the simple model cannot predict the measured curve, as the resonance is split up into some more resonances. The behaviour is typical (comparable to a ported enclosure) for this kind of compression chamber and can be modelled more accurately by adding an additional resonator to the network [CG87]. The absolute value of the source impedance of the complete

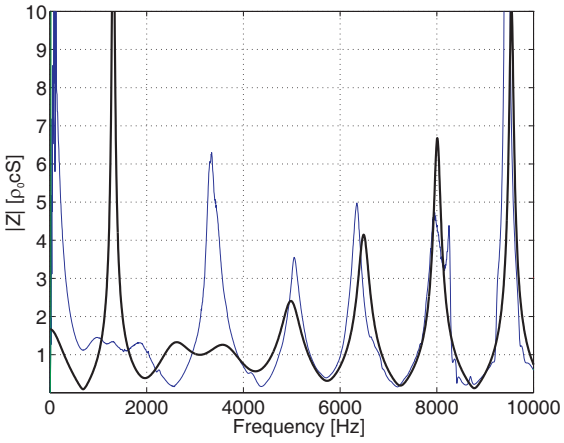

(a) Magnitude of computed/measured source impedance

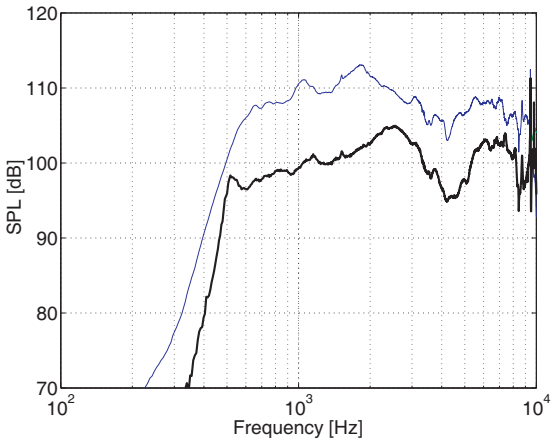

(b) Frequency response with/without phase plug

Figure 2.7: Comparison of measured (thin line) and computed (bold line) source impedance normalized to $\rho_0 cS$ and measured frequency response curves with (thin curve) and without phase plug (bold curve)

driver is now toddling around the specific impedance of the fluid as it was the initial goal for a matched acoustic source. This can be underlined by comparing the measured frequency response of the driver with and without phase plug. The mismatch of the directly radiating system results in a loss of about 10 dB SPL, which corresponds to a 10 times smaller radiated sound power. A more detailed description and some extra measurement results are presented in [Mak01]. A more precise model of a conical tube is described in [Mec02].

Although a horn driver is a rather effective sound source, it is in its basic form not usable as loudspeaker for professional applications. The sound wave leaving the driver outlet will create an undirected radiation at low frequencies and is highly directive at high frequencies. Furthermore, the radiation impedance of the driver outlet is rather small at low frequencies. To improve the system performance a device is needed that increases the load at low frequencies and at the same time can control the directivity. This, exactly, is the functionality of a horn.

2.2 Horn

The “recipe” to calculate wave propagation in a horn of arbitrary geometry and termination at the throat and mouth can be summarized up in one sentence: “simply” solve the Helmholtz equation for the given boundary conditions. In examples of practical importance this leads to severe mathematical difficulties and can be realized just for some separable coordinate systems and particular boundary conditions. For more advanced analytical calculations the reader is referred to [Ged02] and [MI68]. The techniques needed to do this are beyond the scope of this section. The intention is to discuss some basic properties common to all horns using an example of reasonable complexity.

A very basic horn geometry is the conical, axisymmetric horn (Figure 2.8)[3]. For this

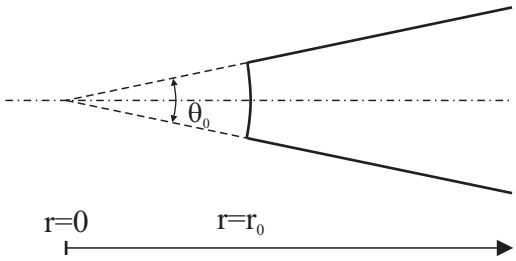

Figure 2.8: Conical, axisymmetric horn

particular boundary value problem, spherical coordinates are useful. The Helmholtz equation in spherical coordinates is (omitting φ-dependency in the axisymmetric case)

$$\frac{1}{r^2}\frac{\partial}{\partial r}\left(r^2\frac{\partial \Psi}{\partial r}\right) + \frac{1}{r^2 sin(\theta)}\frac{\partial}{\partial \theta}\left(\sin(\theta)\frac{\partial \Psi}{\partial \theta}\right) - k^2\Psi = 0, \tag{2.13}$$

where the complex exponential $\Psi(r,\theta,t) = \Psi(r,\theta)e^{j\omega t}$ is used for the time dependency of the velocity potential. It can be solved by a standard separation leading to the following solution:

$$\Psi(r,\theta,t) = \sum_n A_n P_n(\cos(\theta))h_n(kr)e^{j\omega t} \tag{2.14}$$

where P_n are the normal Legendre polynomials of order n and h_n is the spherical Hankel function of the second kind of order n (n is an integer).

Let’s consider a *pulsating* spherical cap of radius r_0 as source of volume velocity. If only outgoing waves are regarded, thus, implying that the wave is not reflected at the end of the horn , the velocity potential is

$$\Psi = A_0\frac{e^{j(\omega t - kr)}}{r} \tag{2.15}$$

[3]This geometry is rarely found in practical examples as the directivity is not very useful.

with $n = 0$, in order to fulfil the boundary condition at r_0: the pulsating cap generates a velocity profile at $r = r_0$ which is not dependent on the angle θ. At the same time, the velocity in θ-direction has to be zero for $\theta = \theta_0$ (rigid wall assumed):

$$grad_\theta(\Psi(r, \theta = \theta_0, t)) = \frac{1}{r}\frac{\partial \Psi}{\partial \theta}\bigg|_{\theta=\theta_0} = 0 \tag{2.16}$$

The solution for this particular boundary value problem is simply the fundamental mode ($n = 0$) propagating down the horn. To calculate the interaction of horn and driving cap, the acoustic impedance[4] on the cap has to be determined. The velocity in radial direction is calculated by

$$v_r = -grad_r(\Psi) = A_0 \frac{e^{j(\omega t - kr)}}{r}\frac{1 + jkr}{r} \tag{2.17}$$

and the pressure on the cap is

$$p = \rho_0 \frac{\partial \Psi}{\partial t} = \rho_0 j\omega A_0 \frac{e^{j(\omega t - kr)}}{r} \tag{2.18}$$

Hence the *fundamental mode impedance* is given by

$$Z_0 = \rho_0 c \frac{1}{1 + (jkr)^{-1}} \tag{2.19}$$

One could even go one step ahead and calculate the radiation from the horn mouth. To do this, a termination at the mouth has to be used that can be analytically described. A common geometry is to surround the horn by a sphere with rigid walls where the horn mouth cuts out a spherical cap of the sphere's surface. This "mounting" also fits into the spherical coordinates and is not so far away from realistic mountings. At the mouth, the velocity profile has to be determined and with this profile the radiation into the far-field of the horn can be calculated.

A more realistic example is the *piston-like* vibrating sphere, which corresponds to a dome-tweeter found in real applications. The velocity distribution generated by such a source does not fit exactly into one of the possible solutions of the wave equation. To calculate the wave-propagation for this particular source, the velocity profile has to be expanded into a series using Legendre polynomials *and* at the same time it has to be assured that the boundary conditions at the walls are fulfilled. Using normal Legendre polynomials this is only given for $n = 0$ but not for higher order modes of wave propagation. To calculate this example, the Legendre polynomials have to be modified using the boundary conditions defined for the rigid wall in eq. (2.16) and after expanding the velocity profile into this new series one could calculate the *modal impedances* for this particular source. Even this

[4]The acoustic impedance is the ratio of pressure and velocity.

small variation of the problem will lead into complicated calculations and therefore is not considered at this point.

Now, consider a horn driver as described in the previous section. Without further analysis one can predict that in most cases the wave front leaving the driver's mouth will not exactly fit, for instance, into a spherical cap, but may be of arbitrary shape. Furthermore one can assume that a certain feedback concerning the shape of the wave front will exist. The two spherical caps considered in the previous examples were assumed as *ideal* sources, which means that the velocity distribution on their surfaces is not influenced by the geometry of the horn. A horn driver, even in its most idealized description, will not behave like this when connected to different horns. The velocity profile found at the driver's outlet will show a certain dependency on the shape of the horn. This reaction on the wave front is accordingly a consequence of the system of modes that can propagate down the horn. This feedback is expressed by the modal impedances, the reaction of the particular horn geometry on the driving source.

2.3 Discussion on Driver Modelling and Horn Calculations

Two conventional methods of horn driver and horn modelling were introduced in the previous sections. These examples give a basis to discuss briefly the problems found. The driver model, though capable to describe the transformation of electric signals into mechanical force and velocity, cannot deal with the 3-dimensional properties describing the reaction of the horn on the driving source. To combine these two separate descriptions the driver model has to include all these effects. An analytical description for the wave propagation from membrane to driver outlet seems impossible for the geometries are two complex. Furthermore, the membrane might not behave like an ideal membrane (vibrating axially), but is also a complex system vibrating with its eigenmodes. As we have seen studying the simple conical horn, this membrane vibration is one of the boundary conditions to calculate wave propagation analytically and, thus, it has of course to be known.

Concerning the horn, it can be said that for an appropriate description of the connection of driver and horn, the velocity profile should be expanded into the system of eigenfunctions of the boundary value problem. Then, the feedback can be described by the modal horn throat impedances. As the eigenfunctions are different for each coordinate system, this cannot be used in a generalized approach and needs some further considerations.

The main aspect of this thesis is to find descriptions for horn driver and horn that are

effectively usable in professional development of horn loudspeakers. Calculating the directivity, the most important property in modern horn development, is possible (analytically or numerically) if the wave propagation within the horn *and* the velocity profile at the horn throat is known. To fulfil this it is not necessary to know every detail of the driver's mechanical construction, but it is sufficient to know the relation of electric input and acoustic output and how the modal throat impedances influence the velocity profile at the driver's outlet. A suitable description is, for example, the two-port or multi-port description as used later in this thesis, which enables to exactly fulfil these requirements.

Before diving into discussions which modal basis is best and how to calculate horns, properties of commercial horn drivers are studied more intensively in the next Chapter. The analysis of the results and the practical constraints of the measurement technique will finally dictate the way of modeling the system of driver and horn.

Chapter 3

Investigation of the Interface between Horn Driver and Horn

In this Chapter, the interaction of horn driver and horn is investigated by measurements of real driver/horn combinations. The intention is to prepare the separation of both coupled systems at their common interface (Chapter 4).

Basically, there exist several possibilities to define an interface of a driving acoustic source and a device to guide the wave. If sources with a "visible" membrane are considered, like cone drivers, dome tweeters, and ribbon tweeters[1], it is possible to directly measure the properties of the driving membrane. Hence, it is for this particular class of drivers a convenient approach to separate the waveguide and the driver exactly at the face of the membrane.

Unfortunately, the horn drivers used in professional applications do not belong to the directly radiating sources. Accordingly, it is not possible to use approaches based on direct measurements of the membrane. The "interface" which is necessary to model these drivers has to be based on acoustic properties of the sound wave travelling through both systems. Consider a sound wave travelling through a face of arbitrary shape: to completely characterise the wave, the pressure and normal velocity profile on this face has to be known.

Beside the description of the (theoretical) case where any pressure/velocity profile is possible, it is of great practical importance to know which simplifications in the description of driver and horn are allowed for practical development processes. This, actually, corresponds to find common properties for all horn drivers. To be more precise, there exist some basic questions which can be answered by analysing the pressure/velocity profiles at the interface of driver and horn:

- Which are the common properties at the interface of different drivers?

[1] Chapters 1 to 4 in [Vor05] give an introduction to different transducer principles

- Is there a significant feedback from the horn to the driver's pressure/velocity profile?
- Are the profiles measured at the interface unique for each type of driver?

The investigation of these questions is done in two steps: measuring the profile of different driver/horn combinations and applying a modal decomposition to separate the profile into orthogonal eigenfunctions.

3.1 Scanning of Pressure and Velocity Profile at the Driver's Mouth

To perform the scanning of pressure and/or velocity there exist in general some standard measurement techniques. The most popular device for velocity scanning might be the *scanning laser vibrometer* which allows to directly measure the point velocity of vibrating surfaces via the optical doppler effect [Pol] without physical contact. Though this is a state of the art method, it is not useful for horn drivers with their "hidden" membranes. Some experiments to adapt this technique by using an auxiliary "cling film membrane" at the driver's mouth just showed that another method has to be used for scanning horn drivers.

A part of the technique described in the following was developed, tested and used in the context of a diploma thesis by [Joe04]. The thesis also includes a comprehensive overview of the investigated drivers and horns, so that a description is skipped here. First results were presented in [BM04] and [Mak04b].

3.1.1 Measurement Technique

The equipment and the software for the analysis used here was developed during the last years and adapted several times to new requirements. Basically, the machine used for the measurements allows to move the device under test (DUT) in two axes (x and y-axis). Figure 3.1 shows a photography of the machine during a measurement. The positioning of the DUT is computer controlled. The probe can be moved by hand in the z-axis and be adjusted with a fine thread and precisely measured by a nonius. The data for the automatic positioning can be generated by CAD-software and is fully compatible with the meshes (Figure 3.3) used for numerical simulations. Thus it is possible to use the same data for the scanning process and for the simulation. Figure 3.2 shows the data-flow for the scanning measurement.

The positions where the sound pressure is acquired are defined by the nodes of the mesh. For drivers with a driver outlet of 2" or less, the probe must not be too large. Anyhow, if

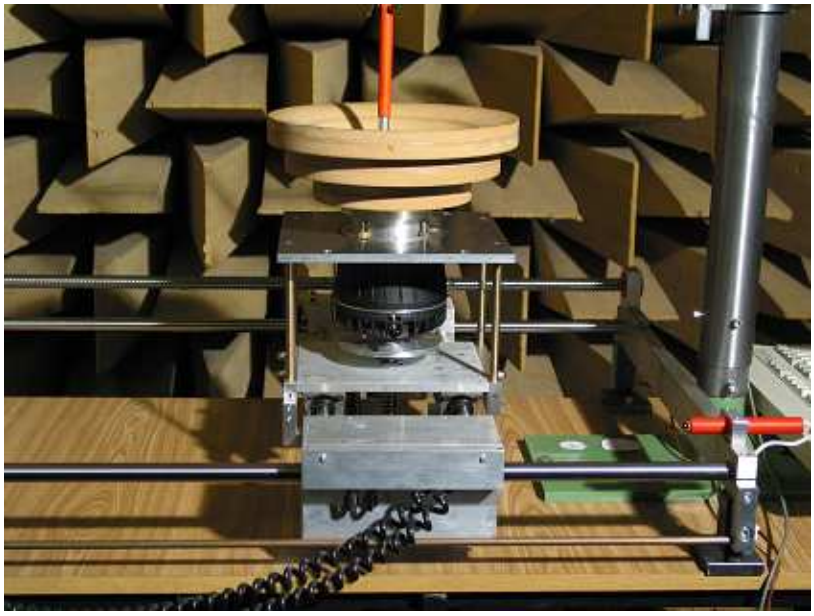

Figure 3.1: Scanning table with a 2"driver mounted to a tractrix horn. The probe is inside the horn.

the sound field is to be investigated up to 20 kHz, the probe should be significantly smaller than a half wavelength to minimize the influence on the result.

The probes used here are a combination of a standard 1/2"-condenser microphone and a very thin probe tube (see for example [BK]). Unfortunately, this kind of probe suffers from a non-flat frequency response. The deviations from an ideal response increase with frequency and probe length, while a smaller probe diameter decreases the sensitivity. But to scan long, narrow horns it is absolutely necessary to use a long probe with a small diameter. Accordingly, we find here some contradictory boundary conditions: while a small and long probe is desired to reach the driver outlet if connected to a narrow horn, the sensitivity and frequency response get worse.

Figure 3.4 shows some frequency responses of a loudspeaker measured with a standard 1/2" condenser microphone and two different microphone probes. One can clearly see the lower sensitivity at high frequencies. Furthermore, the tube causes resonances (depending on the tube length) which are visible as comb filter in the results. Though the magnitude and phase response can be corrected by inverse filtering, the loss in the dynamic range of about 40 dB is painful. Although it is not obvious at this point, it will be in fact the limiting factor for the measurements. Assuming a dynamic range for the complete measurement components (AD and DA converter, pre-amplifier, power amp, microphone) of 100 dB, which seems to be lot for this kind of measurements, only 60 dB are left for the high frequencies. Due to a non-optimal configuration of the measurement system, only 40 dB dynamic range are reached practically.

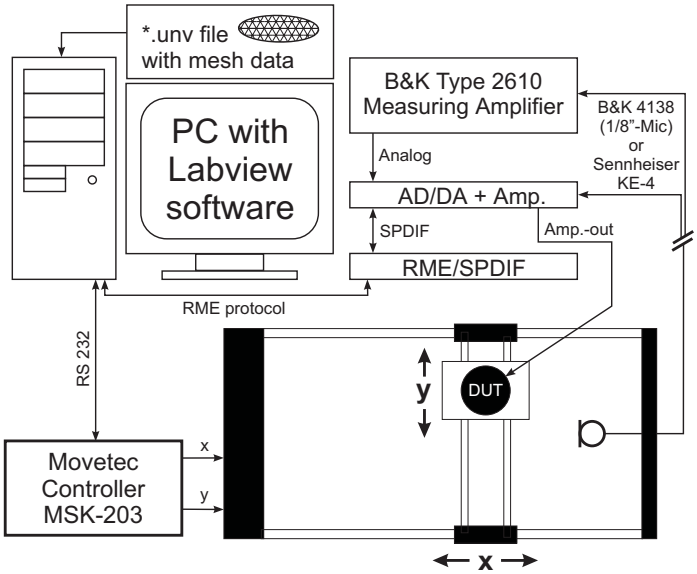

Figure 3.2: Measurement setup

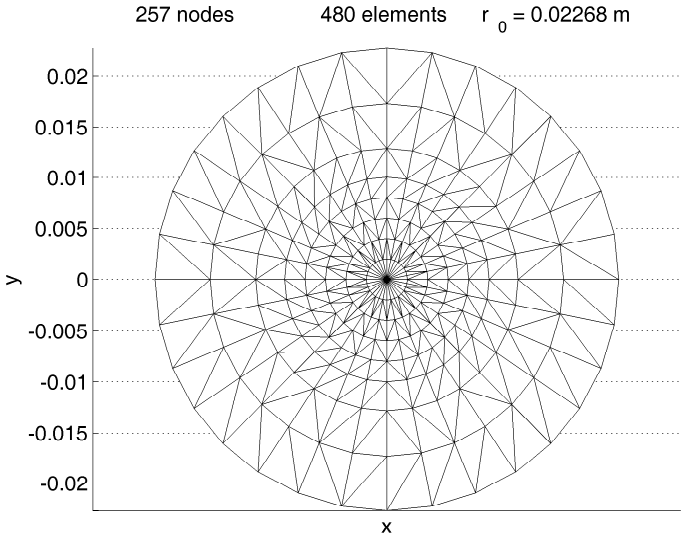

Figure 3.3: Triangular mesh describing the junction of driver and horn.

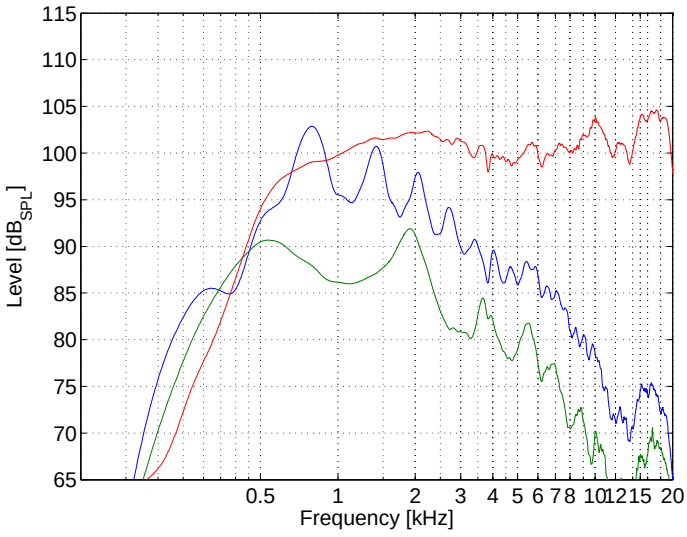

Figure 3.4: Frequency response of a loudspeaker measured with a 1/2" microphone (top), a 2 mm probe (middle) and a 1 mm probe (bottom).

3.1.2 Velocity Measurement

In the authors opinion, no accurate devices to directly measure particle velocity are existent. Hence, it was calculated from the gradient of the sound pressure. The pressure field at the driver outlet was scanned in planes with a distance Δz. The z-component of the particle velocity can be calculated with

$$v_z = -grad_z\left(\frac{p}{j\omega\rho_0}\right) \approx \frac{p(z) - p(z+\Delta z)}{j\omega\rho_0\Delta z} \tag{3.1}$$

A specific problem of this standard method is to find a suitable distance(s) for the measurement. At low frequencies, the distance must provide a significant phase difference which requires as much as possible large distances. At the same time, the distance must be shorter than half a wavelength to avoid spatial aliasing. This is mainly a problem at high frequencies. To cover the complete frequency range it is accordingly necessary to use several distances and to combine the frequency bands according to the different Δz. A convenient set of plane distances is for example 16 mm (up to 2.5 kHz), 8 mm (2.5 kHz - 5 kHz), 4 mm (5 kHz - 10 kHz) and 2 mm (10 kHz - 20 kHz)[2]. At first glance this seems to be a good solution, but in the particular situation of measuring the "cut plane" of driver and horn, one problems occurs: many drivers do not allow measurements at negative z-values, as it is not possible to measure inside the driver. Hence, it is in general necessary to measure only outside which moves the plane of reference also outside the driver. For example, a two-plane measurement with 0 mm (directly within the cut plane) and 2 mm above the cut plane would yield a reference plane for further calculations at a z-value of 1 mm. This can be accepted, as the error introduced may only occur at very high frequencies. But when considering a 0 mm and 16 mm plane measurement, the reference plane is at 8 mm. Besides this, an additional error is introduced due to the flaring of the horn: the measurement plane does not cover the complete cut plane. This also introduces an additional error for measurements with large distances. A practical measurement result can be studied to give an example what can happen qualitatively. Figure 3.5 shows an impedance measurement result for different pairs of measurement planes. The impedance is calculated with

$$Z(z, \Delta z) = \frac{p(z) + p(z+\Delta z)}{2v_z} \tag{3.2}$$

Hence, the plane of reference is at 1, 2 and 8 mm for the illustrated example. At high frequencies the aperture error introduced by the approximation of the gradient in eq. (3.1) yields a zero at 12 kHz for the 16 mm distance followed by a pole at the double frequency.

[2] A detailed textbook about sound intensity measurements is for example [Fah89].

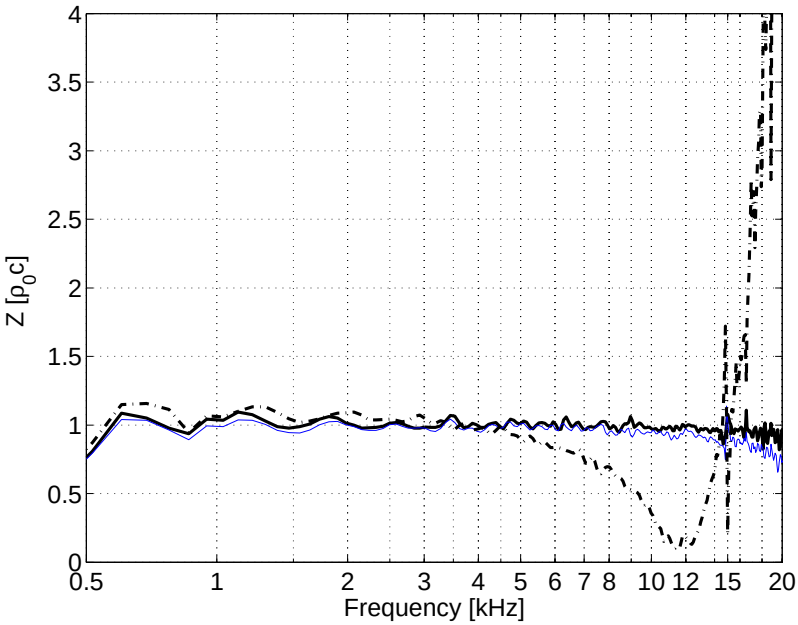

Figure 3.5: Comparison of impedance measurements at different distances in the cut plane of a 2" driver/horn combination: 0 and 2 mm (bold), 0 and 4 mm (thin), 0 and 16 mm (dotted bold)

The same behaviour is encountered at the 4 mm measurement, whereas the frequencies are now shifted by a factor of 4. More interesting is the low frequency error introduced by the incomplete scanning of the horn's cut plane: the measured impedance is too large. Consequently, the use of such large plane distances has to be avoided for further measurements. Fortunately, the probe frequency responses only decrease the high-frequency dynamic range. Hence, at low frequencies the full dynamic range can be used. As compromise a combination of a 4 mm measurement for the range up to 10 kHz and a 2 mm measurement for the rest can be used. Anyhow, velocity measurements with a *high precision and a high dynamic range and a high bandwidth* are an unsolved problem and should be avoided if possible.

3.1.3 Mesh Requirements

The last point of practical interest is how many measurement positions are needed and how these positions should be distributed in the measurement plane. Basically, a continuous physical property is to be characterized by some discrete measurement points. Hence, to correctly sample the quantity one has to fulfil the Shannon theorem [Lük95]. A unique result, without aliasing effects, is obtained if at least a minimum of 2 measurements per wavelength are used. Hence, to give a correct number and distribution of measurement positions one has to know which is the smallest spatial wavelength.

Figure 3.6 shows some pressure patterns at different frequencies as example for a typical driver horn combination. The measurement was made with about 1000 equidistantly

distributed measurement positions to avoid spatial aliasing. One can clearly see how the pattern changes with increasing frequency from a nearly constant distribution to more complex patterns at high frequencies. But, the use of 1000 or more positions is not a feasible approach for the later described decomposition technique. Simply consider the time needed for such a measurement: if a measurement signal of degree[3] 18 with 4 times averaging and an appropriate windowing of the impulse response is used to increase the signal to noise ratio, the measurements will need about 6 1/2 hours for one plane plus the time needed for the probe positioning. Thus, a 5-plane measurement takes about 3 days if the operator does not sleep aside the measuring machine. Anyhow, experiments with such an extremely high number of measurement points just showed that the result of a *single* measurement position can be improved, but the *decomposition* result is not greatly improved. There are several explanations for this. One might be that the system is a little bit time variant as humidity and temperature vary over such a long measuring time. Additionally, the voice coil and magnetic circuit may warm up and thus change the behaviour.

Accordingly, in practice one has to find a compromise between the number of points for the measurements and the signal quality of a single measurement. A good quality for each measuring position is, for instance, necessary if the result is used for a visualization of the particle velocity [Mak]. For the mathematical transformation used later to analyse the measured profiles it is, however, not necessary to improve the signal-to-noise ratio of a single measurement. A series of measurements using different meshes and excitation signals was made to find an optimum configuration. It turned out that 300 to 500 positions measured with a short excitation signal, for example a sweep of degree 14, is appropriate to acquire a 2" driver outlet. A feasible distribution of points is shown in Figure 3.3. The mesh was generated with respect to the system of eigenfunctions used later in this thesis (see also Figure 3.7).

Finally, it is pointed out to one property one can find at the measured pressure patterns shown in Figure 3.6. Although it is difficult to interpret such patterns without further mathematical analysis, one important thing should be noted here: the horn is completely axisymmetric, as well as the connecting cut plane and also the inner mechanical construction of the horn driver. Regardless of the axisymmetric boundary conditions, the patterns are definitively not axisymmetric. The measurements show a significant dependency of the angle (using cylindrical coordinates), starting at about 8 kHz. Accordingly, this particular behaviour *must* be a property of the internal membrane movement.

[3]Degree 18 means 2^{18} samples. For detailed information about measurement signals and processing of the results it is referred to [MM01].

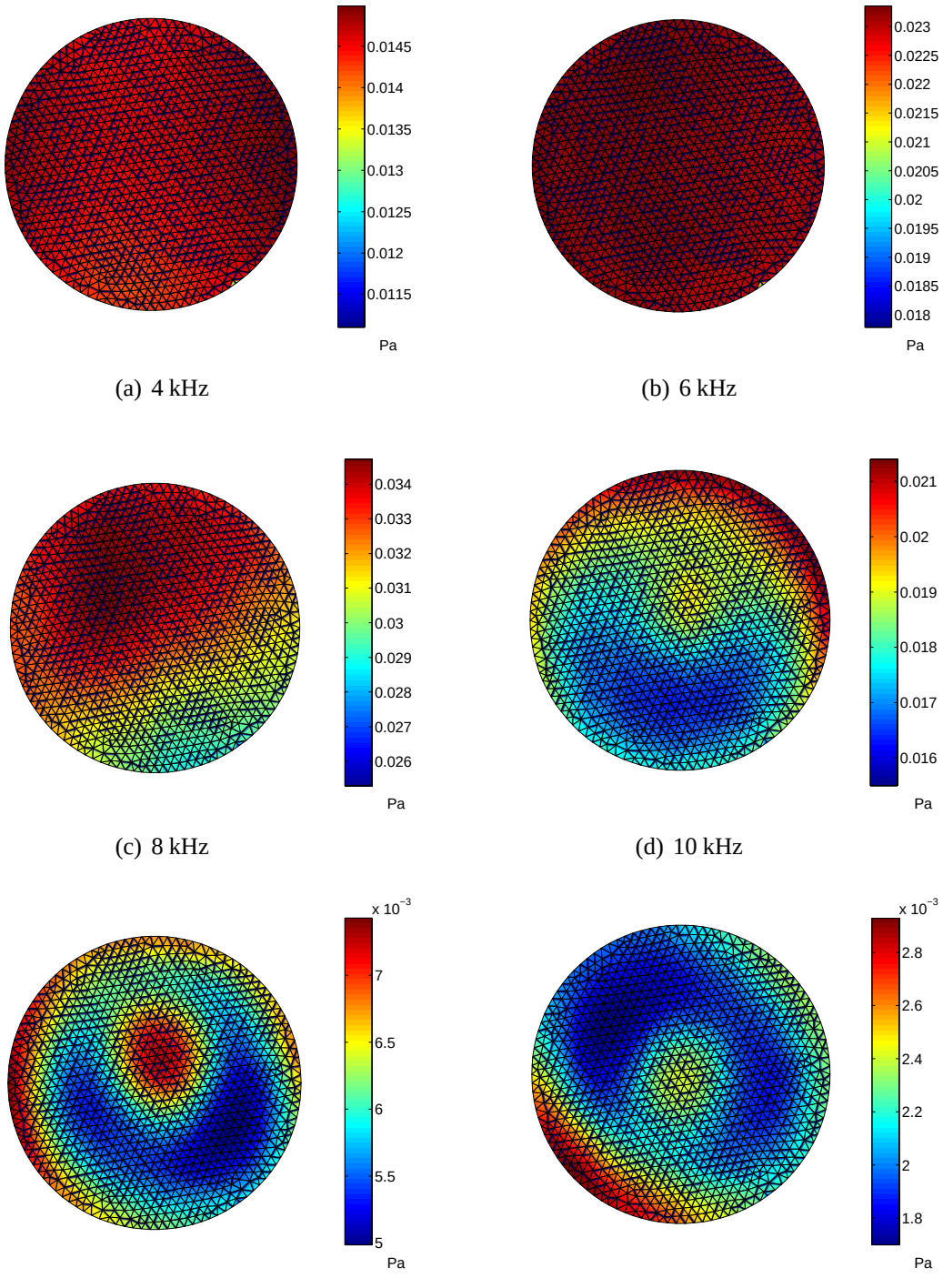

(a) 4 kHz (b) 6 kHz

(c) 8 kHz (d) 10 kHz

(e) 12 kHz (f) 14 kHz

Figure 3.6: Pressure patterns at different frequencies for a 2” driver connected to a (axisymmetric) tractrix horn.

3.2 Modal Decomposition

To further analyse the measured sound fields, a technique is needed to separate the complicated patterns into a set of orthogonal eigenfunctions. In principle, any set of eigenfunctions could be used. For example, the solutions for the spherical wave function provides an orthogonal set consisting of the Legendre polynomials for the θ-direction and sin/cos functions for the φ-direction. As the measurements were performed directly in the cut plane of the driver outlet, a more convenient set of eigenfunctions is provided by the solution of the Helmholtz equation in cylindrical coordinates for a cylindrical duct with rigid walls and a radius corresponding to the radius r_0 of the driver outlet[4]:

$$\frac{1}{r}\frac{\partial}{\partial r}\left(r\frac{\partial \Psi}{\partial r}\right)+\frac{1}{r^2}\frac{\partial^2 \Psi}{\partial \varphi^2}+\frac{\partial^2 \Psi}{\partial z^2}=\frac{1}{c^2}\frac{\partial^2 \Psi}{\partial t^2}. \tag{3.3}$$

The coordinates r and φ describe the cut plane of the scanning measurements, respectively, the cut plane of the duct for the boundary value problem. The solutions can be obtained by a standard separation yielding the velocity potential

$$\Psi(r,\varphi,z,t) = J_m(\kappa_{mn} r)\Phi(\varphi)e^{-jk_{z,mn}z}e^{j\omega t} \tag{3.4}$$

$$k_{z,mn} = \sqrt{k^2-{\kappa_{mn}}^2} \tag{3.5}$$

$$\Phi(\varphi) = \begin{matrix}\cos(m\varphi)\\ \sin(m\varphi)\end{matrix} \tag{3.6}$$

where J_m is the m-th Bessel-function. The constant κ_{mn} is determined by the boundary condition, which for the rigid wall is

$$v_r = -grad_r(\Psi) = \left.\frac{\partial}{\partial r}J_m(\kappa_{mn} r)\Phi(\varphi)e^{-jk_{z,mn}z}e^{j\omega t}\right|_{r=r_0} = 0 \tag{3.7}$$

Table 3.1 shows some values for $\kappa_{mn} r_0$ where the zeros of the first derivative of the m-th Bessel-function are found. Hence, the variable n counts the zeros of eq. (3.7). The transverse eigenfunctions

$$\Psi^{\sigma}_{mn} = \begin{matrix}\cos(m\varphi)\\ \sin(m\varphi)\end{matrix} J_m(\kappa_{mn} r) \tag{3.8}$$

are a complete set of orthogonal functions fulfilling the orthogonality relationship

$$\int_0^{2\pi}\int_0^{r_0}\Psi^{\sigma}_{mn}\Psi^{\sigma'}_{m'n'}\, r\, dr\, d\varphi = \begin{cases}0 & \sigma\neq\sigma' \text{ or } m\neq m' \text{ or } n\neq n'\\ \pi {r_0}^2\Lambda_{mn} & \sigma=\sigma \text{ and } m=m' \text{ and } n=n'\end{cases} \tag{3.9}$$

with

$$\Lambda_{mn} = \frac{1}{\epsilon_m}\left[1-\frac{m^2}{\kappa_{mn}^2 r_0^2}\right]J_m^2(\kappa_{mn} r_0). \tag{3.10}$$

[4]For a more detailed description it is referred to Chapter 9.2 “Higher Order Modes in Ducts” in [MI68]

Table 3.1: First three solutions of eq. (3.7) up to order $m = 8$ for the Bessel function. n counts the zeros of the first derivative of the Bessel-function.

$\kappa_{mn} r_0$			
m/n	0	1	2
0	0	3.832	7.016
1	1.841	5.331	8.536
2	3.054	6.706	9.969
3	4.201	8.015	11.346
4	5.318	9.282	12.682
5	6.416	10.520	13.987
6	7.501	11.735	15.268
7	8.578	12.932	16.529
8	9.647	14.116	17.774

and $\epsilon_m = 1$ when $m = 0$, $\epsilon_m = 2$ for $m > 0$. $\sigma = 1$ is used for the $\cos(m\varphi)$ factor and $\sigma = -1$ is used for the $\sin(m\varphi)$ factor in the eigenfunctions. Figure 3.7 shows the profile for some eigenfunctions up to order $n = 2$ and $m = 4$. Any pressure or velocity distribution can be expanded in terms of these eigenfunctions, as it can be expressed as weighted sum of eigenfunctions

$$p_0(r,\varphi) = \sum_{m=0}^{\infty} \sum_{n=0}^{\infty} \sum_{\sigma=-1}^{\sigma=+1} P_{mn}^{\sigma} \Psi_{mn}^{\sigma} \tag{3.11}$$

The task is to find the complex, frequency dependent coefficients P_{mn}^{σ} for a particular measured profile at the cut plane. To perform the decomposition of the measurements into the participation coefficients, the orthogonality is used:

$$\int_0^{2\pi} \int_0^{r_0} p_0(r,\varphi) \Psi_{mn}^{\sigma} \, r \, dr \, d\varphi =$$

$$\int_0^{2\pi} \int_0^{r_0} \sum_{m'=0}^{\infty} \sum_{n'=0}^{\infty} \sum_{\sigma'=-1}^{\sigma'=+1} \left(P_{m'n'}^{\sigma'} \Psi_{m'n'}^{\sigma'} \right) \Psi_{mn}^{\sigma} \, r \, dr \, d\varphi = P_{mn}^{\sigma} \pi \, {r_0}^2 \, \Lambda_{mn}$$

$$\Rightarrow P_{mn}^{\sigma} = \left(\pi \, {r_0}^2 \, \Lambda_{mn} \right)^{-1} \int_0^{2\pi} \int_0^{r_0} p_0(r,\varphi) \Psi_{mn}^{\sigma} \, r \, dr \, d\varphi \tag{3.12}$$

Eq. (3.12) cannot be applied directly, as at first the patterns have to be interpolated on the surface to enable the integration. Based on the measurement points a continuous interpolation of the profile has to be calculated and, additionally, eq. (3.12) has to be discretised (see Chapter B). The discretised decomposition formula applied on a linearly

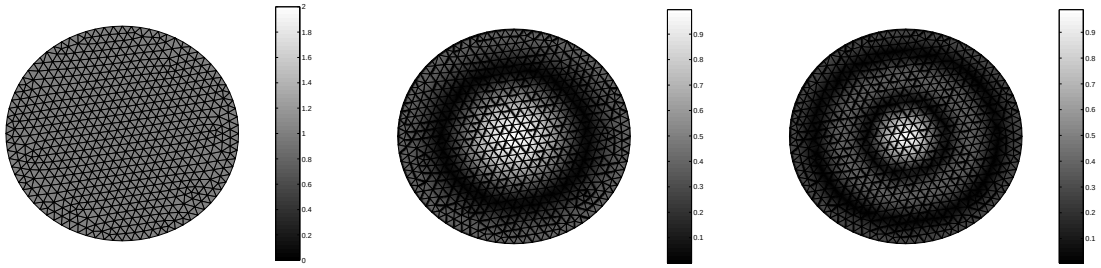

(a) Ψ_{00}

(b) Ψ_{01}

(c) Ψ_{02}

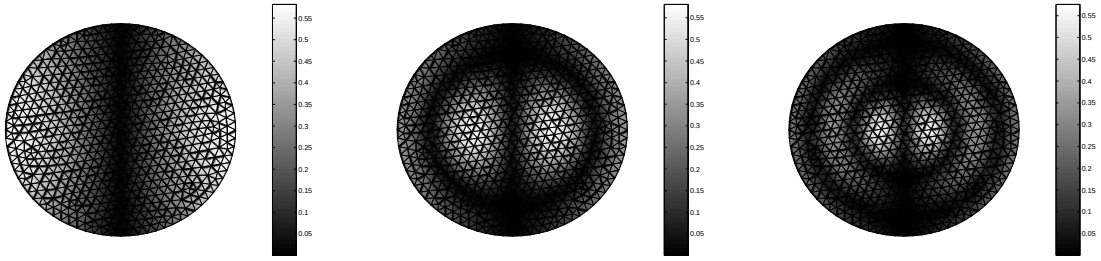

(d) $\Psi_{10\,\cos}$

(e) $\Psi_{11\,\cos}$

(f) $\Psi_{12\,\cos}$

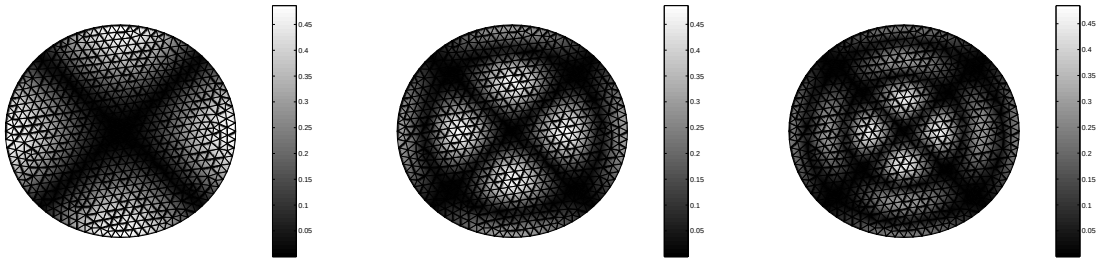

(g) $\Psi_{20\,\cos}$

(h) $\Psi_{21\,\cos}$

(i) $\Psi_{22\,\cos}$

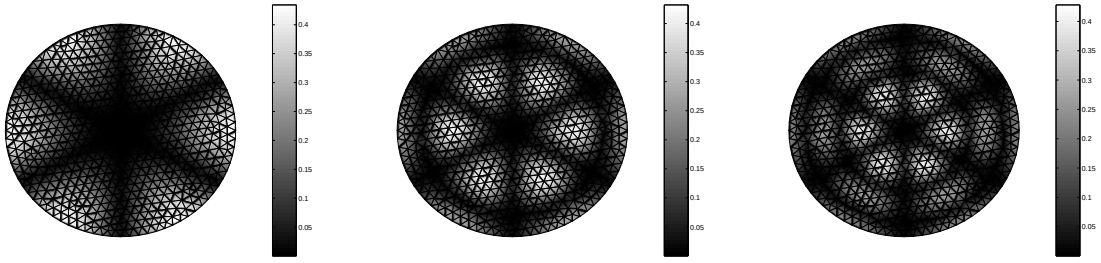

(j) $\Psi_{30\,\cos}$

(k) $\Psi_{31\,\cos}$

(l) $\Psi_{32\,\cos}$

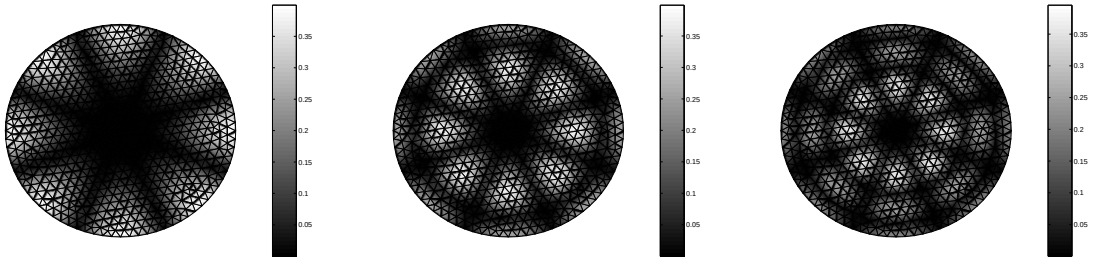

(m) $\Psi_{40\,\cos}$

(n) $\Psi_{41\,\cos}$

(o) $\Psi_{42\,\cos}$

Figure 3.7: Transverse eigenfunctions up to order $m = 4$ and $n = 2$. Figure (a) is the fundamental mode Ψ_{00}.

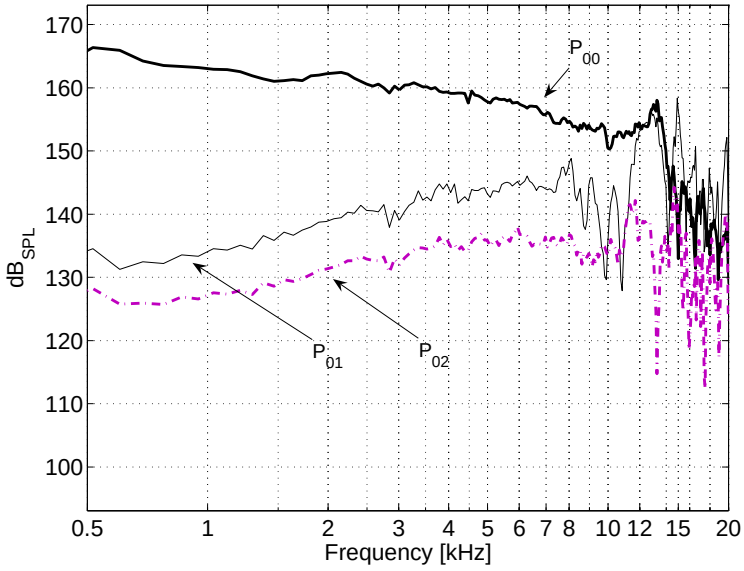

Figure 3.8: Decomposition of a measured pressure profile of a typical 2” driver connected to a tractrix horn. The curves belong to the fundamental mode and the first two pure radial modes

interpolated function over the cut plane is

$$P^{\sigma}_{mn} = \left(\pi {r_0}^2 \Lambda_{mn}\right)^{-1} \sum_{k=1}^{N} \frac{S_k}{3} \sum_{n=1}^{3} p_0(k,n) \Psi^{\sigma}_{mn}(r,\varphi) \tag{3.13}$$

$$r = \sqrt{x^2(k,n) + y^2(k,n)}$$

$$\varphi = \arctan\left(\frac{y(k,n)}{x(k,n)}\right)$$

$p(k,n)$ is the pressure measured at the n-th node of the k-th element, $\Psi^{\sigma}_{mn}(r,\varphi)$ is the value of the transverse eigenfunction at the coordinate of the node and S_k is the area of the k-th element.

Equation (3.13) has then to be applied on each measured frequency, resulting in a frequency response for each eigenfunction. Figure 3.8 shows a typical pressure decomposition result for the fundamental and the two radial modes.

3.3 Analysis

Before going into details of the decomposition results, some basic properties of mode propagation in cylindrical ducts are discussed. Although the cylindrical duct is of course not a horn, it also shows some characteristic properties of horns like mode cut-off.

3.3.1 Theoretical Considerations

The cut-off frequency of a mode is defined as the frequency where the mode starts to propagate without attenuation. Below the cut-off, the mode is called evanescent, as the wavenumber is imaginary. Table 3.2 shows some cut-off frequencies for a 2” duct, calculated

f_{mn} [kHz]			
m/n	0	1	2
0	0	8.26	15.12
1	3.97	11.49	18.39
2	6.58	14.45	21.49
3	9.06	17.28	24.46
4	11.46	20.00	27.34
5	13.83	22.68	30.15
6	16.17	25.29	32.91
7	18.49	27.87	35.63
8	20.79	30.43	38.31

Table 3.2: Cut-off frequencies f_{mn} for a 2-inch duct filled with air. m counts the nodal lines in the angular direction, respectively, the order of the Bessel function. n counts the nodal lines in the radial direction, respectively, the number of zeros of the first derivative of the Bessel-function

using eq. (3.4) and table 3.1. For smaller driver outlets, the corresponding cut-offs will be at higher frequencies.

It has to be awaited that for horns with a moderate flaring and no cross-sectional jumps at the beginning these cut-off frequencies are more or less also found. In section 3.1.3, it was mentioned that it is a priori not known how many measurement points are needed to avoid spatial aliasing. With the estimation of the duct cut-off frequencies it is possible to estimate the minimum requirements for the measurement. For instance: to cover all modes with cut-off frequencies below 20 kHz it is necessary to consider at least the first 54 eigenfunctions[5].

Although a large number of modes can propagate in the considered frequency range, the capability to transmit power may be rather different. The transmitted power for the duct can be calculated which yields a rough estimation for power transmitted by a horn. The transmitted sound power of an eigenfunction is evaluated by integrating the intensity $I_{z,mn}$ over the cut plane of the duct:

$$I_{z,mn} = \frac{1}{2}\Re\left\{p\, v^*_{z,mn}\right\} \tag{3.14}$$

$$v_{z,mn} = \frac{k_{z,mn}}{\omega\rho_0} p(r,\varphi,z,t) \tag{3.15}$$

$$\mathbf{P}_{mn} = \int_0^{2\pi}\int_0^{r_0} \frac{p_0^2 k_{z,mn}}{2\omega\rho_0} (\Psi^\sigma_{mn})^2\, r dr d\varphi \text{ if } k \geq \kappa_{mn}. \tag{3.16}$$

Relationship (3.16) can be evaluated by the orthogonality relationship (3.9) and (3.10).

$$\mathbf{P}_{mn} = \frac{p_0^2\sqrt{k^2-\kappa^2_{mn}}}{2\omega\rho_0}(\pi r_0^2 \Lambda_{mn}) \tag{3.17}$$

[5]This number is, actually, not exact and was chosen to be on the safe side. In fact, less than 54 (only 42) eigenfunctions have to be considered but the numerical implementation uses, for simplicity, all eigenfunctions. Hence, the number of measurement points should be compatible with the implementation

Λ_{mn}			
m/n	0	1	2
0	1	0.162	0.090
1	0.119	0.058	0.037
2	0.068	0.045	0.031
3	0.046	0.036	0.027
4	0.035	0.031	0.024
5	0.027	0.026	0.021
6	0.023	0.023	0.019
7	0.019	0.021	0.017
8	0.016	0.018	0.016

(a)

$P'_{mn}[\mathrm{dB}_{\mathrm{rel}P_{00}}]$			
m/n	0	1	2
0	0	−8.3	−12.3
1	−9.3	−13.3	−18.5
2	−11.9	−15.1	–
3	−13.9	−17.4	–
4	−15.5	–	–
5	−17.0	–	–
6	−18.9	–	–
7	−21.5	–	–
8	–	–	–

(b)

Figure 3.9: The constant Λ_{mn} up to order $m = 8$, $n = 2$ (a) and normalized power $\mathbf{P}'_{mn}$ at 20 kHz in dB for a 2” duct (b)

Thus, the equation for the transmitted sound power of a mode consists of a frequency dependent term and the constant Λ_{mn} multiplied by the area of the junction. The fundamental mode power is simply the plane wave power and, thus, the only mode capable to transmit power within the complete audio frequency range ($\kappa_{00} = 0$ and $\Lambda_{00} = 1$, see also table 3.1 and 3.9(a)). From this consideration one can clearly state that the most important eigenfunction excited at the driver’s outlet is the fundamental mode.

To compare the higher order mode power to the fundamental mode power, it is convenient to normalize the higher order modes to the fundamental mode. Accordingly, the normalized modal sound power is

$$P'_{mn} = \sqrt{1 - \frac{\kappa_{mn}^2}{k^2}}\Lambda_{mn} \tag{3.18}$$

This is a very interesting equation. It says that the maximum normalized sound power is Λ_{mn}. The result, of course, is only valid if the amplitude of the mode is equal to the amplitude of the fundamental. Table 3.9(a) shows the Λ_{mn} for the first modes. One can find, for example, that the ($m = 0$, $n = 1$)-mode transmits a maximum of -7.9 dB of the fundamental mode power[6]. Additionally, taking into consideration that the frequency range of interest is below 20 kHz, the maximum of the normalized power can be calculated (Table 3.9(b)).

Concerning this calculation, it has to be remarked that the results presented in Table 3.9(b) are, strictly speaking, only valid for a duct of infinite length. Thus, a more ore less

[6]This value is calculated from table 3.9(a): $-7.9\,\mathrm{dB} = 10\log_{10}(0.162)$

deviating influence of higher order modes has to be expected. This, of course, will depend on the geometry of the horn. A horn with a long horn throat will surely behave more as a long duct than as a short conical horn. Describing this more complicated geometries analytically, will lead too deep into mathematics at this point. A closer look at this field of investigation leads to systems of linear equations for each mode. Interesting work was done on this field, by, for example, [Pis03], [NKP96] and [AKP97].

3.3.2 Decomposition Results

This section contains a selection of decomposition results of measured driver/horn combinations. The intention is to present typical combinations one can find in practice, and, with the results found at these combinations to discuss the questions bought up at the beginning of this Chapter (see page 20)

General properties and pressure/velocity comparison Figure 3.10 shows a typical measurement result of a 2” compression driver connected to a horn. The curves show the pressure decomposition result for the first 54 eigenfunctions.

The fundamental mode dominates the low frequencies, as predicted by theory. For this particular driver/horn combination this is true up to approximate 12 kHz. Looking at this frequency range, one also finds that most of the modes are far below the fundamental[7]. This also corresponds to the estimation of the duct cut-off frequencies. Nevertheless, there are some modes with significant level. These are the first two radial modes and the first two angular modes for this example.

In the following, the decomposition results are normalized to the fundamental mode. As the fundamental mode dominates the profile and transmits most of the sound power this will be a convenient approach. Furthermore, a normalization is necessary to compare results of different driver/horn combinations. As abbreviation for the notation of the eigenfunction, for instance, 01 for the $m = 0$, $n = 1$ eigenfunction is used. Figure 3.11 shows the first normalized pressure/velocity modes for the EV-DH1A/Tractrix combination. The pressure and the velocity show, except for details, the same characteristic behaviour. Furthermore, it seems that the slope of the eigenfunctions increases with increasing mode order (see also Figure 3.11). While these observations are just of qualitative nature and maybe only valid for this particular combination, some further combinations are studied in the following.

[7] The dynamic range is at low frequencies about 60 to 80 dB and the results of most of the higher order modes is dominated here by noise at such low levels.

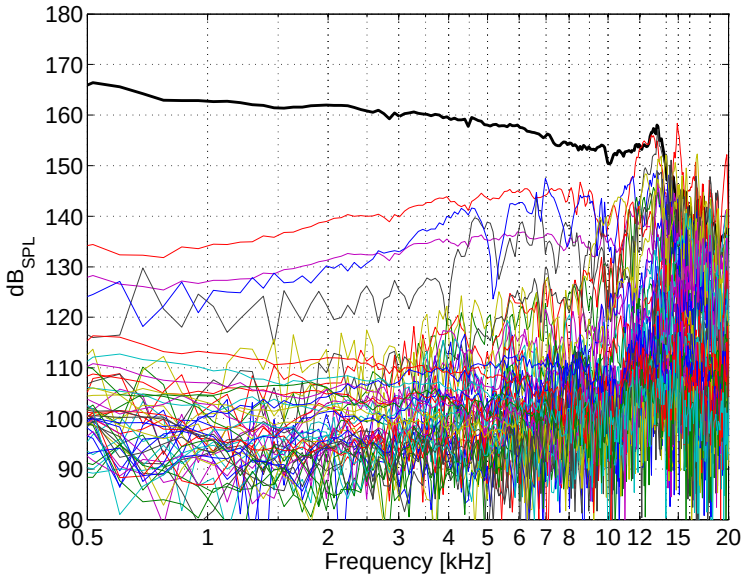

Figure 3.10: Pressure magnitude decomposition up to order $m = 8$ and $n = 2$ for a 2"-driver (EV-DH1A) connected to a tractrix horn. The bold curve is the fundamental mode.

One driver and different horns Figure 3.12 shows decomposition results of a JBL 2445 2”-driver connected to different horns. Besides the tractrix horn, a very long and narrow horn with square mouth and a short, about 10 cm long, cylindrical tube as acoustic load is used. While the two “real horns” are not expected to show significant differences, the short tube should force a different modal behaviour at the driver’s mouth: the abrupt cross sectional jump at the end of the tube will cause the propagating modes to be reflected.

Figure 3.12 shows the 01 and 02 coefficients for the normalized pressure/velocity. The differences between the two horns are, at least at high frequencies, very small. It is interesting to note that the velocity coefficients of the long, square horn do not show the same slope as the results of the tractrix horn. They are at a constant level of about -20 dB below 8 kHz. The results of the tube show some significant changes around 2 kHz and 8 kHz at the pressure coefficients as well as at the velocity coefficients. For higher frequencies the coefficients are, except for some details, not significantly different from the horn measurements.

To further analyse the differences between the modal feedback of the acoustic loads, the modal impedances were calculated. Figure 3.13 shows the modal impedances of the two horns and the short tube. The curves merely show the quotient of the pressure coefficient and the according velocity coefficient. For instance, Figure 3.13(a) shows the normalized fundamental mode impedance $Z_{00} = P_{00}/(\rho_0 c V_{00})$ and the first radial mode impedance $Z_{01} = P_{01}/(\rho_0 c V_{01})$.

It will be shown later in Chapter 5 that the modal impedances measured at the interface are even dependent on the particular combination of modes at the driver’s mouth. Thus,

the interpretation of the modal impedances is not straightforwardly possible, as the modal interaction has to be taken into account. Anyhow, the results are interesting, and, as far as the author knows, new in this field of investigation.

One horn and different drivers Figure 3.14 shows the normalized 01- and 02 pressure participation coefficients for different horn drivers, among them also one modified driver with phase plug removed (RCF 980-opp), measured all with the tractrix horn. At low frequencies they almost behave the same, the pressure increases with about 6 dB/octave. At a certain frequency the modes become dominant. For this frequency range the frequency responses are significant different of all drivers, although the acoustic load is the same.

3.4 Discussion of the Results

Although the results presented in this section can of course not cover all possible combinations of drivers and horns, it may be allowed to sum up the significant tendencies found at the measurements. The first important result was that most of the frequency range is dominated by the fundamental mode. As long as no “extreme” acoustic load is connected to the driver like a short, abrupt ending tube, the transition frequency where the modes become dominant seems to be more or less a property of the driver and is not influenced by the horn. However, it has to be remarked that the dominate behaviour of the fundamental is not only a consequence of the physical properties of waves propagating in ducts. It is also related to the exciting membrane and the construction of the phase plug. While some 2”-drivers have a transition frequency at 10 kHz, one can also find drivers with dominating fundamental mode up to 16 kHz (see Figure 3.14). Furthermore, it should be noted here that smaller drivers will of course have higher transition frequencies. To answer the question of common driver properties: the dominating fundamental mode for a large frequency range is common to most drivers found on the market. One can even go one step ahead and predict that the reason for a non-smooth frequency response at high frequencies is caused by dominating higher order modes. This seems obvious as the decomposition results show also non-smooth higher order mode responses for all investigated drivers at high frequencies. Thus, the measurement of the pressure/velocity profile may also serve as indicator for the quality (of the linear properties) of the driver.

The second point of interest was, if a feedback of the horn to the driver could be measured at the common interface. If one driver is connected to different acoustic loads the

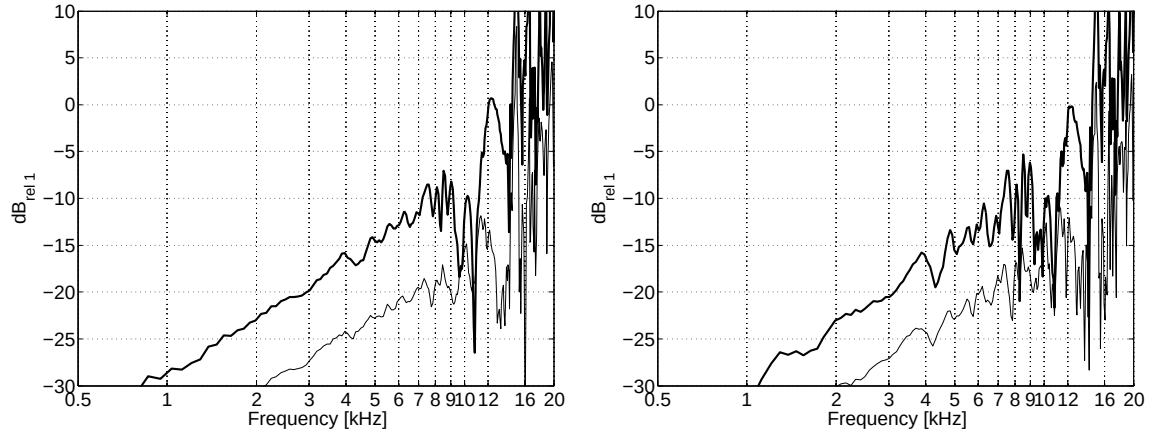

(a) Pressure 01 (bold) and 02

(b) Velocity 01 (bold) and 02

(c) Pressure 10cos (bold) and 10sin

(d) Velocity 10cos (bold) and 10sin

(e) Pressure 20cos (bold) and 20sin

(f) Velocity 20cos (bold) 20sin

Figure 3.11: Normalized pressure and velocity participation coefficients of the EV-DH1A/tractrix horn combination

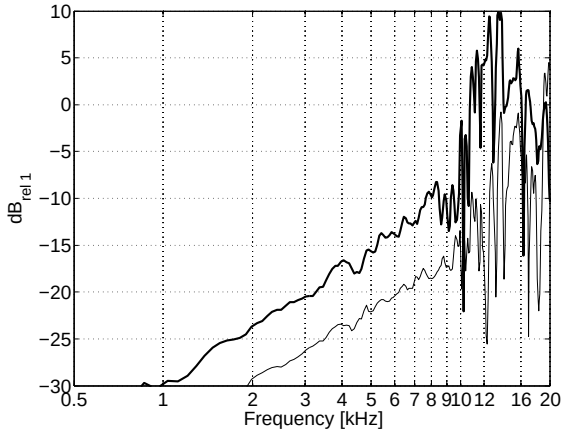

(a) Pressure 01 (bold) and 02 with tractrix horn

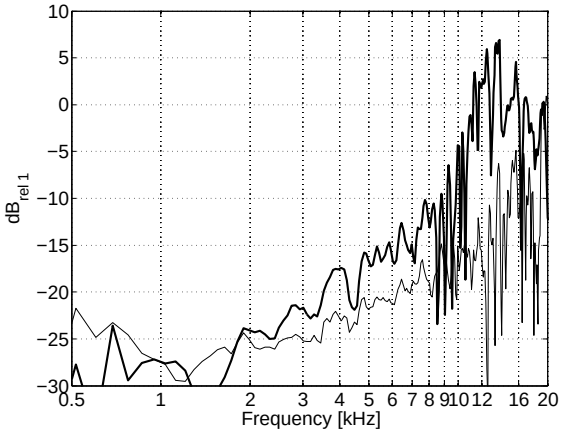

(b) Velocity 01 (bold) and 02 with tractrix horn

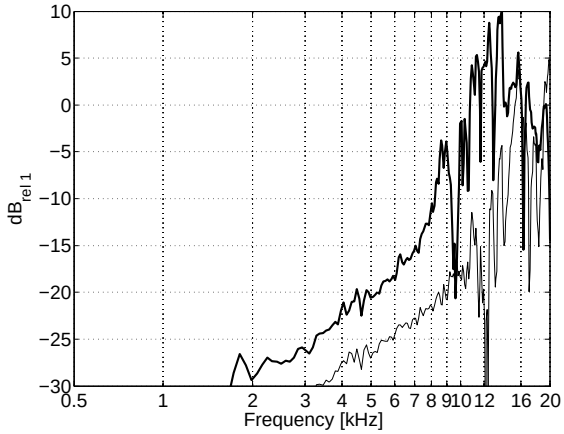

(c) Pressure 01 (bold) and 02 with square horn

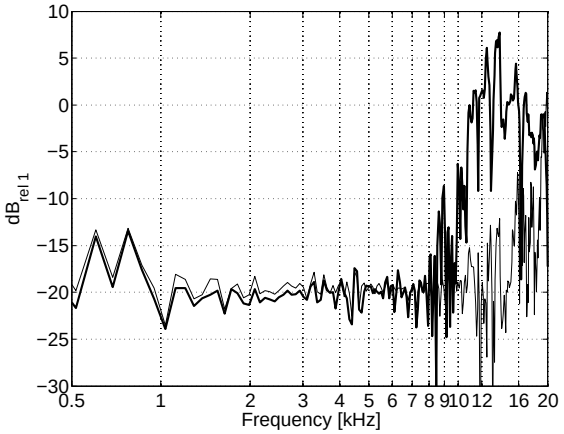

(d) Velocity 01 (bold) and 02 with square horn

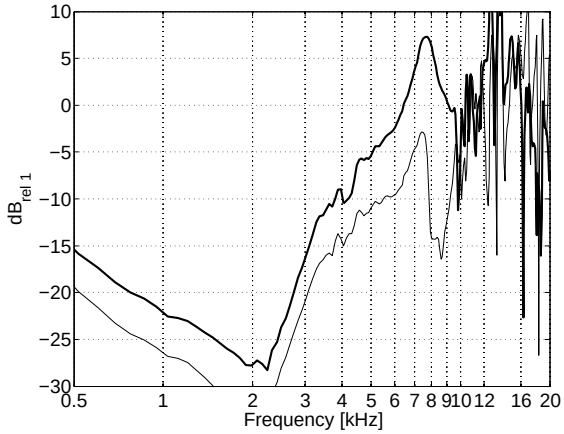

(e) Pressure 01 (bold) and 02 with short tube

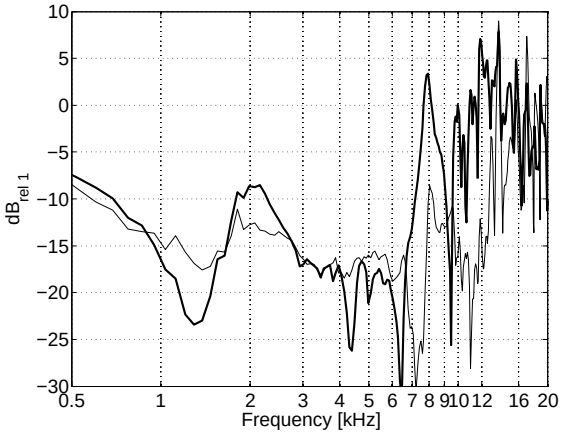

(f) Velocity 01 (bold) and 02 with short tube

Figure 3.12: Normalized magnitude of 01 and 02 pressure/velocity participation coefficients for the JBL2445 driver and different horns

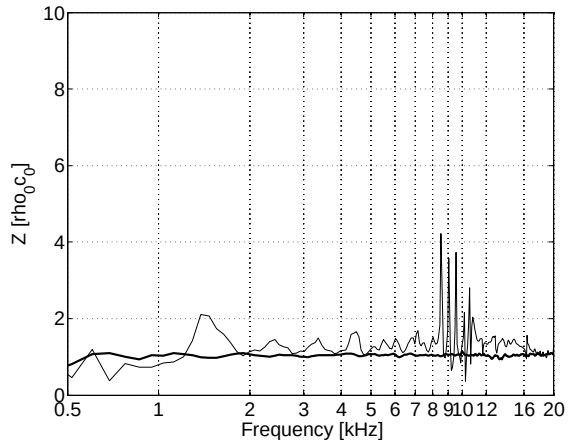

(a) Impedance 00 (bold) and 01 at the tractrix horn

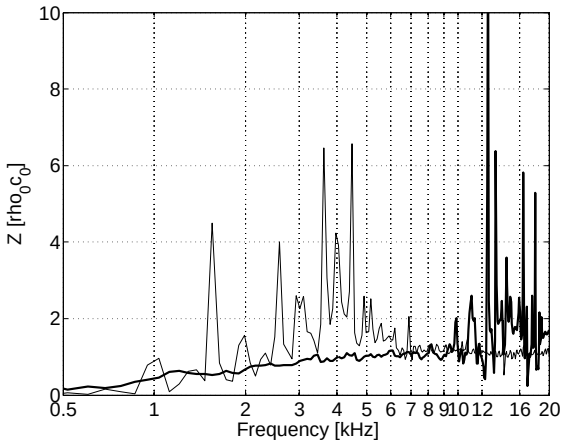

(b) Impedance 02 (bold) and 10 at the tractrix horn

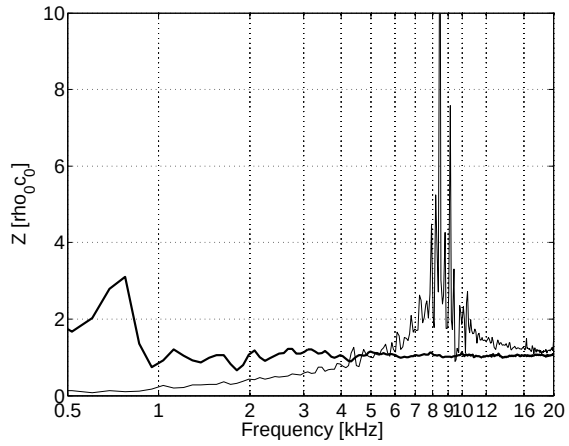

(c) Impedance 00 (bold) and 01 at the square horn

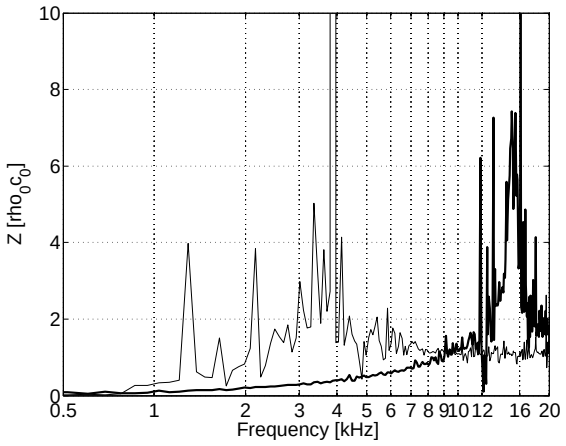

(d) Impedance 02 (bold) and 10 at the square horn

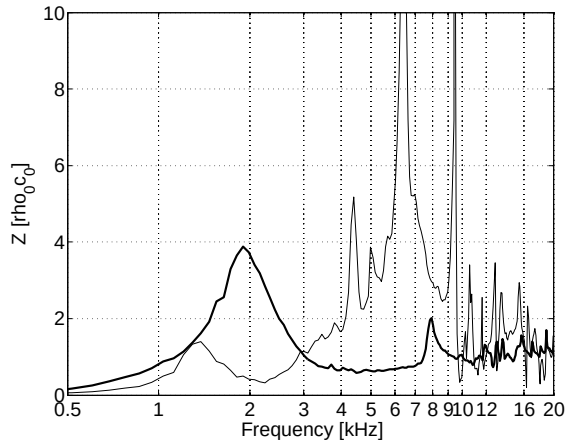

(e) Impedance 00 (bold) and 01 at the short tube

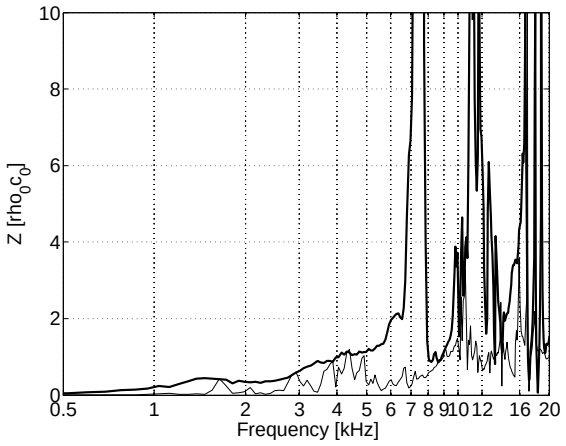

(f) Impedance 02 (bold) and 10 at the short tube

Figure 3.13: Normalized modal impedances of the 00, 01, 20 and 10 pressure/velocity participation coefficients for the JBL2445 driver at different horns

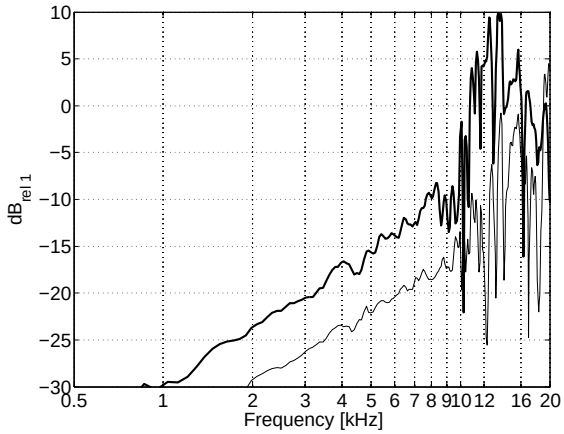

(a) Pressure 01 (bold) and 02 JBL2445/tractrix horn

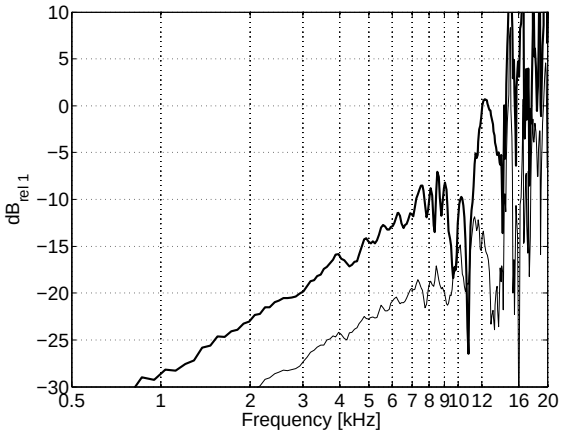

(b) Pressure 01 (bold) and 02 EV-DH1A/tractrix horn

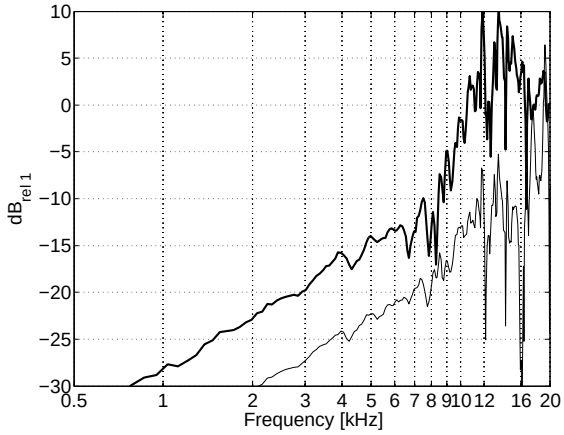

(c) Pressure 01 (bold) and 02 Radian 950 PB-16/tractrix horn

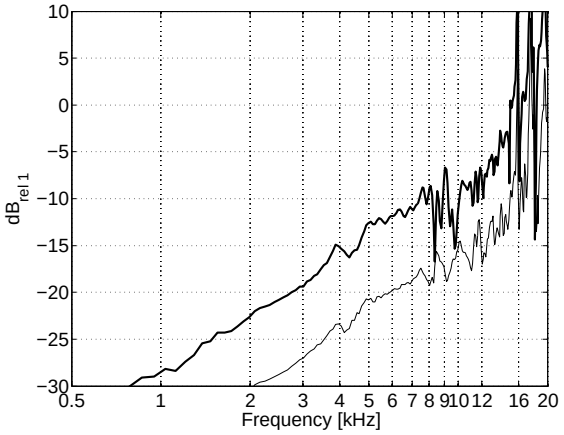

(d) Pressure 01 (bold) and 02 RCF 980/tractrix horn

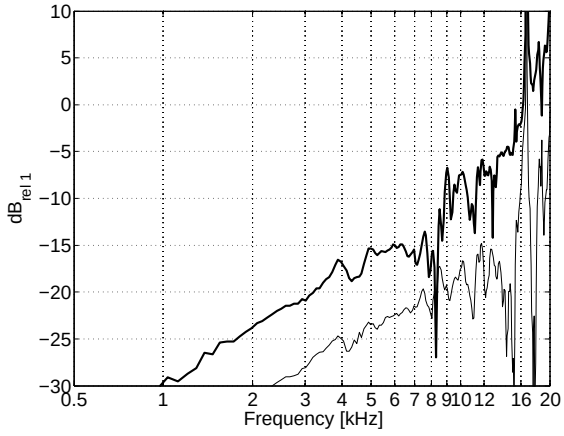

(e) Pressure 01 (bold) and 02 RCF 980-opp/tractrix horn

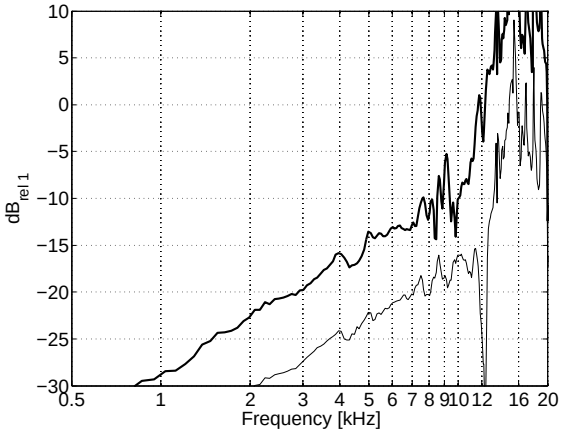

(f) Pressure 01 (bold) and 02 RCF ND2030-T3/tractrix horn

Figure 3.14: Normalized 01 and 02 pressure participation coefficients for different driver and the tractrix horn

pressure/velocity profile must also show significant changes, at least if the driver is not extremely mismatched to the sound field. In Figure 3.12 results for different load cases are presented and Figure 3.13 shows the measured modal impedances for the first 4 modes. From these results, one can say that the feedback is not only existent for the fundamental mode but also for higher order modes at the driver's mouth. It has to be remarked here, that the calculation of the modal impedances as ratio of decomposed pressure and velocity has to be reconsidered, as the propagating modes are not orthogonal any more when they leave the driver's mouth. They may convert to other modes while they travel through the horn and thus may also influence other modal impedances. In other words: different velocity profiles may cause different modal impedances! This will be treated later more comprehensively in Chapter 5.

The third question was: are the pressure and velocity profiles at the interface unique for each type of driver?

Besides the differences in the level of the participation coefficients, one can say that especially the composition of higher order modes is unique for each driver. By simply comparing the normalized 01 and 02 modes for different drivers measured at the same horn in Figure 3.14 one finds, for instance, that the transition frequencies vary from 10 kHz to 16 kHz. Furthermore, the relation of fundamental mode amplitude and higher order mode amplitude above this frequency also shows large differences between these drivers.

Chapter 4

Separation of Horn Driver and Horn

Based on the practical investigation of the acoustic field at the cut-plane between driver and horn (Chapter 3), a separate description for both systems is developed in this Chapter. In the most general case, the description has to consider any distribution of velocity and pressure and, furthermore, also has to describe any possible feedback from horn to horn driver. This, of course, also includes any feedback from the acoustic field to the electric properties. The only required assumption is linearity and time invariance of the system (LTI system). Without further proof, it is stated here that systems which are not at least dominant in their linear behaviour and stable enough concerning their time dependent properties are also not usable for professional sound reinforcement systems and, thus, are not of interest to be described within this context.

To manage this task, two methods are combined:

- The acoustic pressure and velocity profiles at the separating interface are expanded into orthogonal eigenfunctions. Hence, the systems are described by their "modal coordinates"
- The interaction between acoustic properties and electric properties is described by a modal multiport

Similar methods are, for instance, also used to simulate horn antennas of arbitrary shape by combined mode matching and numerical methods [BBA99] or to describe piezoelectric actuators by a multi-port [DHD91], [KSH91].

This Chapter starts with a complete description which includes all linear effects between the two systems. This description will be called *full cross modal description*. As this model has many degrees of freedom, it is more or less of theoretical nature. In fact, it serves in this thesis as basis to derive descriptions with fewer free parameters. The intention is, actually, to find models which can also be used in practical implementations.

All these descriptions will finally lead to mathematical representations using matrices for the systems and vectors for the input and output of the system. A complex frequency domain representation is used in the following. The entries of the vectors and matrices are themselves complex frequency vectors (see for instance [Küp84] and [Mak01]).

$$\begin{pmatrix} P(f) \\ Q(f) \end{pmatrix} = \begin{pmatrix} T_{11}(f) & T_{12}(f) \\ T_{21}(f) & T_{22}(f) \end{pmatrix} \begin{pmatrix} U(f) \\ I(f) \end{pmatrix} = \mathbf{T}(f) \begin{pmatrix} U(f) \\ I(f) \end{pmatrix} \tag{4.1}$$

The operation between vector entries and matrix entries is a complex, element by element multiplication.

The modal descriptions in this thesis are based on a modal basis, a system of eigenfunctions fulfilling the two-dimensional orthogonality relationship. The numbering of the eigenfunctions Ψ is realized by two indexes m and n.

$$\iint_A \Psi_{mn} \Psi_{m'n'} \, dA = \begin{cases} 0 & m \neq m' \text{ or } n \neq n' \\ A\Lambda_{mn} & m = m' \text{ and } n = n', \end{cases} \tag{4.2}$$

Λ_{mn} is a particular normalization constant for each mode and each modal basis. This set of functions can represent any two-dimensional profile in the separating interface area A between the two systems as superposition of weighted eigenfunctions. The weighting coefficients are called participation coefficients and can be complex valued. The modal basis used for the investigation of the horn drivers was derived by the solution of the cylindrical duct with hard walls of infinite length. Other useful basises are, for example, the set of eigenfunctions belonging to the rectangular duct (would be applied to all drivers with rectangular outlets, like many ribbon tweeters and planar magnetic drivers) or the circular membrane or rectangular membrane (comprehensive treatment in Morse's famous book [MI68]).

4.1 Full Cross Modal Description

In general, a multi-port can be used to describe any LTI-system with any number of inputs and outputs. In the context of this thesis, each acoustic port consists of a pair of pressure and velocity participation coefficients, describing the amplitudes of the particular eigenfunctions with the numbers m, n. Using this black box description, results in a matrix describing all possible couplings between all connections of the multi-port (eq. (4.6)). The size of the matrix varies with the number of eigenfunctions taken into consideration. For instance, if the first j eigenfunctions are considered, the size of the matrix is $j + 1$, as one terminal is required for the electric port.

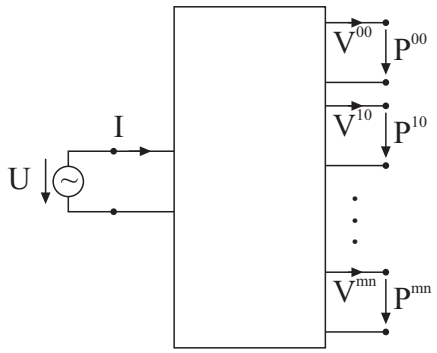

Figure 4.1: Modal multi-port of the horn driver connected to an ideal voltage source

Both sides of the system, the electric and the acoustic ports, are connected by the matrix $\mathbf{Z_d}$ as defined in (4.3)

$$\begin{pmatrix} U \\ \mathbf{P} \end{pmatrix} = \mathbf{Z_d} \begin{pmatrix} I \\ \mathbf{V} \end{pmatrix} \tag{4.3}$$

$$\mathbf{P} = (P_{00}\, P_{01} \ldots P_{mn})^t \tag{4.4}$$

$$\mathbf{V} = (V_{00}\, V_{01} \ldots V_{mn})^t \tag{4.5}$$

$\mathbf{P}$ and $\mathbf{V}$ are the vectors of pressure and velocity participation coefficients, U is the voltage and I is the current. As the decomposition projects the two-dimensional distribution at the interface onto one-dimensional coefficients, a mathematical unambiguous description is realized. The connection matrix $\mathbf{Z_d}$ contains electric, acoustic and mixed impedances:

$$\mathbf{Z_d} = \begin{pmatrix} Z_d^{U,I} & Z_d^{U,00} & \cdots & Z_d^{U,mn} \\ Z_d^{00,I} & Z_d^{00,00} & \cdots & Z_d^{00,mn} \\ \vdots & \vdots & \ddots & \vdots \\ Z_d^{mn,I} & Z_d^{mn,00} & \cdots & Z_d^{mn,mn} \end{pmatrix} \tag{4.6}$$

For example, $Z_d^{U,I} = U/I$, $Z_d^{U,00} = U/V_{00}$, $Z_d^{mn,mn} = P_{mn}/V_{mn}$, and so on. The four parameters in the upper left corner of the matrix are the coefficients related to the fundamental mode model. To get a more convenient representation for calculations, the variables within the matrix are combined in vectors containing the mixed electro-acoustic impedances and a sub-matrix including only acoustic variables.

$$\mathbf{Z_d^{U,V}} = \left(Z_d^{U,00}, \cdots, Z_d^{U,mn}\right) \tag{4.7}$$

$$\mathbf{Z_d^{P,I}} = \left(Z_d^{00,I}, \cdots, Z_d^{mn,I}\right)^t \tag{4.8}$$

$$\mathbf{Z_d^{P,V}} = \begin{pmatrix} Z_d^{00,00} & \cdots & Z_d^{00,mn} \\ \vdots & \ddots & \vdots \\ Z_d^{mn,00} & \cdots & Z_d^{mn,mn} \end{pmatrix} \tag{4.9}$$

Using this notation, $\mathbf{Z_d}$ can be written in a very compact form:

$$\mathbf{Z_d} = \begin{pmatrix} Z_d^{U,I} & \mathbf{Z_d^{U,V}} \\ \mathbf{Z_d^{P,I}} & \mathbf{Z_d^{P,V}} \end{pmatrix} \tag{4.10}$$

Coupling of driver and acoustic load If an acoustic load is connected to the driver, the ratio of velocity and pressure is determined by the loading impedance. The coupling of an acoustic load will accordingly be modelled by a modal horn throat impedance matrix. This

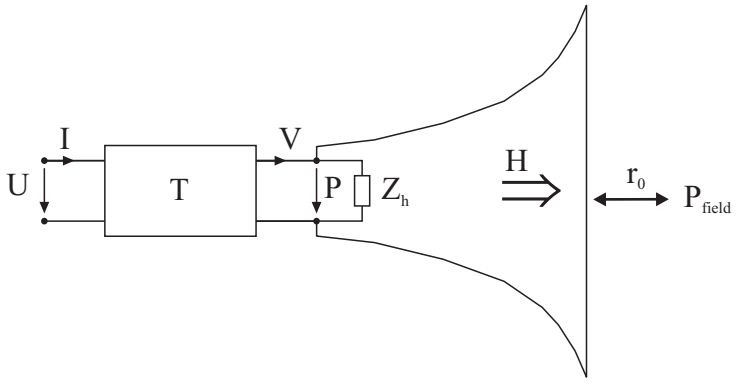

Figure 4.2: Coupling of horn driver and horn

impedance matrix includes all possible modal coupling enforced by the horn geometry:

$$\mathbf{Z_h} = \begin{pmatrix} Z_h^{00,00} & \cdots & Z_h^{00,mn} \\ \vdots & \ddots & \vdots \\ Z_h^{mn,00} & \cdots & Z_h^{mn,mn} \end{pmatrix} \tag{4.11}$$

The definition of the matrix components is according to the driver matrix. For instance, the entry $Z_h^{00,00}$ is the ratio of pressure coefficient P_{00} and velocity coefficient V_{00}. This particular entry exactly corresponds to the fundamental mode horn throat impedance. The entry $Z_h^{00,mn}$ is the ratio of P_{00} and V_{mn}, and so on. Hence, the diagonal elements of the impedance matrix contain the impedance coupling of the modes with the mode itself. All the other elements contain the modal cross coupling. Figure 4.2 shows the two coupled systems, whereas for simplicity the modal ports are combined in one port.

With the impedance matrix connected to the driver matrix, it is possible to calculate the *coupled system's* property. For instance, the vector of velocity within the connecting cut-plane for a particular driver/horn combination results in the solution of a system of equations. If the driver is connected to an ideal voltage source, the following system is to be solved for the velocity and current coefficients:

$$\begin{pmatrix} U \\ \mathbf{Z_h V} \end{pmatrix} = \mathbf{Z_d} \begin{pmatrix} I \\ \mathbf{V} \end{pmatrix} \tag{4.12}$$

The first line of this equation can be solved for the unknown current I:

$$U = Z_d^{U,I} I + \mathbf{Z_d^{U,V}} \mathbf{V} \qquad \Rightarrow \qquad I = \frac{U}{Z_d^{U,I}} - \frac{1}{Z_d^{U,I}} \mathbf{Z_d^{U,V}} \mathbf{V} \tag{4.13}$$

The second line of (4.12) together with (4.13) can be solved for the velocity vector

$$\mathbf{Z_h V} = \mathbf{Z_d^{P,I}} I + \mathbf{Z_d^{P,V}} \mathbf{V} \qquad \Rightarrow \qquad \mathbf{V} = \left(\mathbf{Z_h} + \frac{1}{Z_d^{U,I}} \mathbf{Z_d^{P,I}} \mathbf{Z_d^{U,V}} - \mathbf{Z_d^{P,V}} \right)^{-1} \mathbf{Z_d^{P,I}} \frac{U}{Z_d^{U,I}} \tag{4.14}$$

Please note that the multiplication of $\mathbf{Z_d^{P,I}}$ and $\mathbf{Z_d^{U,V}}$ again results in a matrix of correct size, as a row-vector is multiplied by a column-vector.

In the same way other properties of the coupled system driver/horn can be calculated. For instance, the electric input impedance can be expressed in terms of the driver and the horn matrix as

$$Z_e = \frac{Z_d^{U,I}}{1 - \mathbf{Z_d^{U,V}} \left(\mathbf{Z_h} + \left(Z_d^{U,I} \right)^{-1} \mathbf{Z_d^{P,I}} \mathbf{Z_d^{U,V}} - \mathbf{Z_d^{P,V}} \right)^{-1} \mathbf{Z_d^{P,I}} \left(Z_d^{U,I} \right)^{-1}} \tag{4.15}$$

Power flow and electro-acoustic efficiency If no energy is generated within the two systems, the total electric input power has to be identical to the total acoustic output power plus the sum of all thermal and other losses which do not contribute to the acoustic output of the coupled systems. With the flow definition of Figure 4.1 the following relationship has to be fulfilled:

$$\Re \{UI^*\} = \Re \left\{ \sum_{m=0}^{\infty} \sum_{n=0}^{\infty} \iint_A P_{mn} V_{mn}^* \Psi_{mn}^2 dA \right\} + P_{loss} \tag{4.16}$$

The right side represents the sum of the power transmitted by all acoustic modes plus the losses. Using the matrix for the acoustic load and the vector for the velocity participation coefficients together with the orthogonality defined in eq. (4.2) yields a more elegant representation,

$$\Re \{Z_e II^*\} = \Re \left\{ A \left(\mathbf{\Lambda Z_h V} \right)^t \mathbf{V}^* \right\} + P_{loss} \tag{4.17}$$

where $\mathbf{\Lambda}$ is a diagonal matrix of the normalization coefficients defined by the orthogonality relationship. The electric impedance can be determined with eq. (4.15) and the modal velocity vector is given by eq. (4.14). The electro-acoustic efficiency can, accordingly, be calculated as ratio of acoustic output to electric input power:

$$\eta = \frac{\Re \left\{ A \left(\mathbf{\Lambda Z_h V} \right)^t \mathbf{V}^* \right\}}{\Re \{Z_e II^*\}} \tag{4.18}$$

Calculation of radiation Up to this point, it is possible to calculate any linear property related to the driver and the velocity or pressure profile at the acoustic interface between the driver and the horn. In general, with the velocity profile at the horn throat (and of course the geometry of the horn and other boundary conditions) the calculation of the far field sound pressure, velocity and other properties of the loudspeaker is possible. It is a convenient approach to describe the relation of far field properties and velocity profile at the horn throat in terms of the same set of eigenfunctions, too. This methodology is, in general,

independent of the method used to calculate the radiation into the far field. Anyhow, the storage space needed for the simulation/calculation result is significantly smaller if the horn is described by modal coordinates.

Theoretically, there exist a large number of possibilities to describe the spatial sound field of a loudspeaker. To describe the idea of a *modal horn data set* it is sufficient to concentrate on the most common property, the so-called on-axis frequency response. Normally, the on-axis frequency response is referred to a distance of $r = 1$ m from the loudspeaker and also referred to a nominal input power of 1 W. The normalized on-axis frequency response is called *sensitivity* (see also Figure 4.2). The modal data set for this particular configuration consists of a modal transfer function, which simply is the ratio of the sound pressure at 1 m distance to the velocity participation coefficient. This can also be interpreted as modal transfer impedance:

$$H_{mn} = \frac{P|_{r=1\mathrm{m},V_{mn}}}{V_{mn}} \tag{4.19}$$

To avoid confusion with all the other impedances, the modal transfer impedance is denoted as H as shown in Figure 4.2. For the sake of a more compact reading, the transfer function is written as modal row vector:

$$\mathbf{H} = \left(\frac{P|_{r=1\mathrm{m},V_{00}}}{V_{00}}, \ldots, \frac{P|_{r=1\mathrm{m},V_{mn}}}{V_{mn}} \right) \tag{4.20}$$

Assuming that the nominal impedance of the driver under investigation is R_n[1], the sensitivity of the driver/horn combination is:

$$P|_{1\mathrm{m},\,1\mathrm{W}} = \mathbf{H} \left(\mathbf{Z_h} + \frac{1}{Z_d^{U,I}} \mathbf{Z_d^{P,I}} \mathbf{Z_d^{U,V}} - \mathbf{Z_d^{P,V}} \right)^{-1} \mathbf{Z_d^{P,I}} \frac{U_0}{Z_d^{U,I}} \tag{4.21}$$

where $U_0^2 R_n = 1$ W.

In the same way, sets of transfer functions can be defined for other field points located on circles around the horn in the horizontal plane, vertical plane or field points on a sphere.

Thus, a data set for the horn consists of the modal throat impedance matrix $\mathbf{Z_h}$ as defined in eq. (4.11) and a set of modal transfer functions for the field points of interest, like the on-axis field point at 1 m distance as defined in eq. (4.20). Although there exists an informal convention which sets of field points are used for the spatial characterization, it might be useful to calculate the sound field at other points, too. To manage this task, it is also possible to store the pressure distribution $\mathcal{P}_{mn}$ on the radiating surface S, related to the exciting eigenfunction V_{mn}. Using the Helmholtz-Kirchhoff integral equation of radiation,

[1] The nominal impedance is defined in [DIN03], section 16.1

it is, then, possible to calculate the sound pressure at any field point in dependency of the exciting eigenfunction:

$$\iint_S \left[\mathcal{P}_{mn} \frac{\partial g(r_0, y)}{\partial n(y)} + j\omega\rho_0 \Psi_{mn} V_{mn} g(r_0, y) \right] dS = P_{mn}(r_0), \tag{4.22}$$

where y is a spatial point on the surface, r_0 is the spatial point which the sound pressure is calculated for and $g(r_0, y)$ is the free space green's function. Thus, $P_{mn}(r_0)$ is the sound pressure at the field point with the coordinates r_0 when the horn is excited at the horn-throat by a velocity profile Ψ_{mn} with the amplitude V_{mn}. This idea is, actually, adopted from numerical methods of acoustics and will later be treated more comprehensively in Chapter 5 where it is described how to numerically calculate the horn data and the surface pressure distribution.

4.2 Simplified Descriptions

The vector matrix notation as presented before enables a very compact notation and effective calculation of the coupled system's properties. This might be misleading concerning the applicability of the full cross-modal driver description. Especially, it might be very difficult (or at last impossible) to *practically* measure the entries of the fully occupied driver matrix for a large number of eigenfunctions.

A simple example will reveal this: if the driver matrix should be measured for the first j eigenfunctions, it is necessary to measure the driver under $j+1$ *significantly* different acoustic conditions, which will result in system of $(j+1)^2$ equations for the $(j+1)^2$ unknown variables. Of course, a numerical model would enable to determine the complete matrix. But as pointed out in the introduction: the development of such models is a complicated task and it is definitively not a feasible approach in a normal loudspeaker development process.

Although a full modal description for the driver is nice to have, practical constraints dictate to apply simplified descriptions. Besides the problems of determining the driver's parameters, it is, maybe, not necessary to apply such a precise modal model. For now, some useful and reasonable simplifications are discussed at the end of this Chapter. How to determine the driver data will be described in detail (Chapter 6).

Modal description One step of complexity below the full cross modal description is to leave out the cross-interaction of the modes among each other. This *modal description* assumes that the loading impedances also show a weak modal cross coupling, which, as

will be shown later, is approximately true for most common horn geometries. The matrices $\mathbf{Z_d^{P,V}}$ and $\mathbf{Z_h}$ which describe the acoustic interaction of the eigenfunctions between each other can be greatly reduced by assuming that this cross-interaction of modes of different order can be neglected. In other words, the loading matrix and the acoustic impedance matrix just consist of their diagonal elements. At this point, it has to be noted that the cross interaction of modes occur only if the modal basis is not identical with the "natural" system of coordinates of the acoustic problem. For instance, if sound propagation in a conical tube is described in Cartesian coordinates, an infinite number of modes has to be taken into consideration. Unfortunately, for most interesting horn geometries and particularly for the phase plug/membrane interaction of the driver, normally, no separable coordinate system exists. Thus, the modal basis will be a more or less good compromise. The better the eigenfunctions fit into the problem, the weaker the cross interaction is and accordingly the more diagonalized the impedance matrices are. However, simulation results of different horn geometries presented later in this thesis show that the horn matrix is dominated by its diagonal elements, even if the basis of the cylindrical duct is used.

The most important consequence of this approach is the reduced number of unknown variables to determine. To be more precise, the modal description requires $3j+1$ equations as the vectors $\mathbf{Z_d^{P,I}}$, $\mathbf{Z_d^{U,V}}$ and the diagonal matrix $\mathbf{Z_d^{P,V}}$ each have j unknown variables. Accordingly, three significant different load cases are required, independent of the number of modes. This is a rather remarkable result and above all, it seems to be a realistic task to manage.

Modal source/impedance model An interesting alternative description is the modal source/impedance model. Instead of considering all possible couplings, the electric side is terminated by an ideal voltage source feeding the driver with the voltage U_0. This configuration is very close to many practical configurations as modern amplifiers feature a very low inner impedance compared to the electric impedance of the connected loudspeakers. For the representation there exist two common methods: a pressure source and an inner impedance in series, as shown in Figure 4.3, or a velocity source connected to an impedance in parallel to the source. Using the formalism developed in this Chapter, the parameters can be calculated. The second line of eq. (4.10) directly yields the relationship

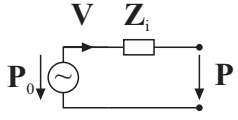

Figure 4.3: Pressure source

between voltage U_0 and pressure $\mathbf{P_0}$, if the driver is connected to an infinite impedance,

thus enforcing the velocity vector to be zero:

$$\mathbf{P_0} = \mathbf{Z_d^{P,I}} \frac{U_0}{Z_d^{U,I}} \tag{4.23}$$

The velocity source can be calculated with eq. (4.14) if the acoustic load $\mathbf{Z_h}$ is set to zero, which enforces the pressure vector to be zero:

$$\mathbf{V_0} = \underbrace{\left(\frac{1}{Z_d^{U,I}} \mathbf{Z_d^{P,I}} \mathbf{Z_d^{U,V}} - \mathbf{Z_d^{P,V}} \right)^{-1}}_{\mathbf{Z_i}^{-1}} \underbrace{\mathbf{Z_d^{P,I}} \frac{U_0}{Z_d^{U,I}}}_{\mathbf{P_0}} \tag{4.24}$$

To calculate the inner impedance, these two equations could also be used, but it is more illustrative to make a “virtual measurement” at the driver’s multi-port. Instead of connecting an acoustic load to the acoustic ports, a device is connected generating a defined velocity $\mathbf{V}$, while the source impedance of this device is infinite. Thus, this virtual measuring instrument could be called ideal modal velocity source. As the device is terminated by a

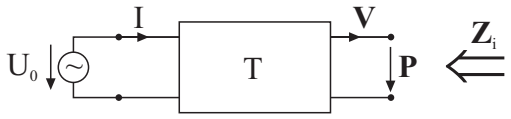

Figure 4.4: Determination of the source impedance

short-cut at the electric side, the following equations directly result from the driver matrix eq. (4.10):

$$0 = Z_d^{U,I} I - \mathbf{Z_d^{U,V}} \mathbf{V} \tag{4.25}$$

$$\mathbf{P} = \mathbf{Z_d^{P,I}} I - \mathbf{Z_d^{P,V}} \mathbf{V} \tag{4.26}$$

Please note the changed sign of the velocity due to the flow conventions. Eliminating the current I yields

$$\mathbf{P} = \underbrace{\left(\frac{1}{Z_d^{U,I}} \mathbf{Z_d^{P,I}} \mathbf{Z_d^{U,V}} - \mathbf{Z_d^{P,V}} \right)}_{\mathbf{Z_i}} \mathbf{V}. \tag{4.27}$$

Pressure and velocity are related to each other by the inner impedance matrix $\mathbf{Z_i}$. If, additionally, cross-coupling is neglected in order to decouple the modal sources and modal inner impedances, the number of unknown variables for this model is $2j$, j unknown variables for the source pressure or velocity and j variables for the diagonal elements of the source impedance $\mathbf{Z_i}$. This special model, accordingly, requires two different modal load cases with the dimension j to be completely characterized.

Fundamental mode description From the mathematical point of view this model does not attract much attention, but for practical purposes it will be, not at least due to the more or less simple practical determination of its parameters, the most attractive description. As mentioned on page 43 (see also eq. (4.6)), the upper left four entries of the driver matrix are related to fundamental mode model, which accordingly yields now a merely one-dimensional modal model. In other words, the fundamental mode model can be described as two-port. Since the formalism is exactly the same as for the modal multi-port, it is not necessary to repeat this here.

For practical purposes, it will, later, be convenient to use the two-port not as impedance matrix, but as transfer matrix. The velocity coefficient of the fundamental is replaced here by the volume velocity Q generated at the acoustic port:

$$\begin{pmatrix} P \\ Q \end{pmatrix} = \begin{pmatrix} T_{11} & T_{12} \\ T_{21} & T_{22} \end{pmatrix} \begin{pmatrix} U \\ I \end{pmatrix} = \mathbf{T} \begin{pmatrix} U \\ I \end{pmatrix}. \tag{4.28}$$

The flow direction of the physical properties is defined in Figure 4.5 according to the modal multi-port. The T-matrix parameters can be calculated from the driver matrix by the following relations:

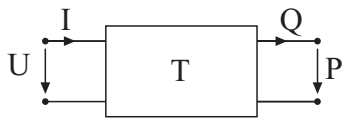

Figure 4.5: Electro-acoustic two-port

$$T_{11} = \left.\frac{P}{U}\right|_{I=0} = \frac{Z_d^{00,I}}{Z_d^{U,00}} \tag{4.29}$$

$$T_{12} = \left.\frac{P}{I}\right|_{U=0} = Z_d^{00,I} - Z_d^{00,00}\frac{Z_d^{U,I}}{Z_d^{U,00}} \tag{4.30}$$

$$T_{21} = \left.\frac{Q}{U}\right|_{I=0} = \frac{A\Lambda_{00}}{Z_d^{U,00}} \tag{4.31}$$

$$T_{22} = \left.\frac{Q}{I}\right|_{U=0} = -A\Lambda_{00}\frac{Z_d^{U,I}}{Z_d^{U,00}} \tag{4.32}$$

Reduced modal description The last model to discuss is in fact a combination of the fundamental mode model and the modal source/impedance model. For the fundamental mode the formalism described before is used, thus including any feedback to the electric side concerning the fundamental mode. Higher order modes are described by an ideal velocity source. The inner admittance is assumed to be zero here. Although this model does not even consider the acoustic feedback between horn and higher order modes, it should yield good results if the measurement of the velocity source coefficients is made together with a representative acoustic load.

4.3 How many Modes should be considered?

The previous sections of this Chapter describe modal models of driver and horn which enable a separate description of both systems. Several simplified driver models were discussed. This section discusses briefly if a further reduction in the modal models can be achieved by simply reducing the number of modes taken into consideration.

In section 3.3.1, the influence of higher order modes was estimated by calculating their power transmission and the related cut-off frequencies of the cylindrical duct. It turned out that a lot of cut-off frequencies are below 20 kHz (2” duct considered), but only some modes are capable to significantly transmit sound power (see table 3.9(b) on page 32): the most important mode was, of course, the fundamental mode. Beside this, there are (for the 2”-duct) only two modes which transmit more than -10 dB of the fundamental mode power: the first radial mode (01) transmits at 20 kHz about -8.3 dB and the first angular mode (10) transmits at 20 kHz -9.3 dB if excited by the same amplitude as the fundamental. Although these modes are excited at the driver’s mouth (see section 3.3.2), the influence on the far field response of the horn might be negligible. Exactly this question was investigated by simulations and theoretical considerations in [Mak04b]. It turned out that many modes are excited at the driver’s outlet but their influence vanishes at the far field. Furthermore, it is possible to exclude any mode with an asymmetrical eigenfunction when the focus is on the development of a horn geometry. For instance, the fundamental mode and the pure radial modes are the only modes of practical importance if circular outlets are considered. All other modes of this particular system of eigenfunctions yield an asymmetrical radiation pattern which is only useful in very rare case. It should also be noted that the patterns created by angular modes are, of course, dependent on the mounting position of the driver. Simulation and measurements presented later will show that these asymmetrical patterns do exist and can be simulated by the techniques described in this thesis.

Chapter 5

Determination of the Horn Parameters

For the determination of the modal horn parameters it has to be considered how to simulate or calculate sound radiation of a closed, finite surface. The surface is described by its geometry and boundary conditions: surface admittance, the ratio of pressure and normal velocity, and a distribution of vibration on the surface acting as excitation. The problem described here is known as one of the standard problems of numerical acoustics: the radiation problem ([Mec02]). Although it is always better to analytically derive solutions with general character, this is not possible for arbitrary geometries defining the radiation problem.

In Chapter 4, it was described which modal data is needed to couple the horn, the acoustic load, to the driver. It was also pointed out that in a more general way any linear property of the sound field created by the radiating surface is included in the modal surface pressure distribution $\mathcal{P}_{mn}$ of the solved radiation problem. The modal data, the modal throat impedance matrix as defined in eq. (4.11) and a set of modal transfer functions defined in eq. (4.20), can accordingly be derived for each eigenfunction if the surface pressure $\mathcal{P}_{mn}$ is known. For the determination of a horn data set, it is, however, irrelevant how to derive the solution. In this work, the boundary element method (BEM) is used and, therefore, it will be described shortly. After that, the modal data for some particular horn geometries of practical importance will be presented.

5.1 BEM

During the last decades, a couple of formulations to numerically solve exterior field problems have been developed. In the following, the most popular formulation based on the Helmholtz-integral equation is presented representatively for all similar formulations. This formulation, called direct form or sometimes basic form, is also used in this thesis. The

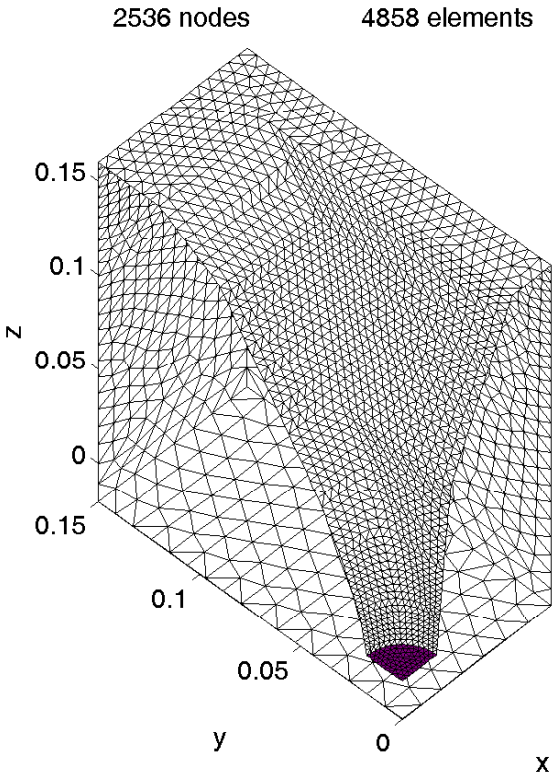

Figure 5.1: Discretised surface of a quarter sectional view of a horn mounted in a box. The boundary conditions belong to a standard simulation. The dark panels are defined as vibrating with normal velocity of $1\frac{\mathrm{m}}{\mathrm{s}}$, the white panels are non-vibrating with a surface admittance of zero (rigid wall)

Helmholtz-integral equation is

$$\iint_S \left[p(y)\frac{\partial g(x,y)}{\partial n(y)} - \frac{\partial p(y)}{\partial n(y)} g(x,y) \right] ds = \begin{cases} p(x) & , x \in B_e \\ C(x)p(x) & , x \in S \\ 0 & , x \in B_i \end{cases} \tag{5.1}$$

with

$$g(x,y) = \frac{1}{4\pi\tilde{r}} e^{-jk\tilde{r}} \tag{5.2}$$

$$\tilde{r} = \|x - y\| \tag{5.3}$$

$$C(x) = 1 + \frac{1}{4\pi} \iint_S \frac{\partial}{\partial n(y)} \left(\frac{1}{\tilde{r}(x,y)} \right) ds(y). \tag{5.4}$$

S describes a closed surface, B_e is the exterior field room, B_i is the interior field room, y is a spatial point on the surface, x is the location of a field point. C(x) is the solid angle seen from x. Eq. (5.1) simply says, that the pressure at any field point can be calculated by integrating all monopoles and dipoles located on the surface. Unfortunately, this distribution is not known a priori. A standard problem, like sound radiation from a horn loudspeaker, is defined by vibrating regions of the surface and a distribution of admittance over the surface, as shown in Figure 5.1. The pressure distribution on the left side of (5.1) has to be calculated from this boundary conditions. This is the task of the BEM. The second line of eq. (5.1) also gives the correct relation of surface pressure to monopole and dipole

distribution on the surface. As the pressure on the surface is on both sides of the equation, one has to solve this equation for the surface pressure.

To use this formula for computations, it has to be discretised and the integration has to be done numerically. This causes some problems since the numerical integration is not possible for singular integral kernels as it is the case here. Besides this, the equation suffers from the so-called non-uniqueness problem. Both problems are described and solved in literature and therefore not worth to be discussed in this context. A detailed description of the BEM and specific problems can be found, for instance, in [Mec02]. The non-uniqueness problem is discussed comprehensively in the famous Burton-Miller Paper [BM71]. Methods of discretisation and interpolation on surfaces are described in [Zie77].

The discretised form of the Helmholtz-integral equation for the surface pressure is

$$\sum_{k=1}^{N} \iint_{S_k} \left[p(y) \frac{\partial g(x_i, y)}{\partial n(y)} + j\omega\rho_0 v_n(y) g(x_i, y) \right] ds = C(x_i) p(x_i), \tag{5.5}$$

with the normal velocity

$$\frac{\partial p(y)}{\partial n(y)} = -j\omega\rho_0 v_n(y). \tag{5.6}$$

The integration is split into a sum of integrations over the N surface elements. In the example shown in Figure 5.1 the elements are planar-triangular. The variable i counts the points on the surface where the solutions are obtained. For instance, if a linear interpolation of the functions is used, three points per triangle are needed. Together with the used interpolation scheme (see section 3.2 and also [Mak04b]) the equation can be expressed as system of equations in terms of matrices and vectors:

$$\mathbf{D}\mathcal{P} + \mathbf{MV} = \mathbf{C}\mathcal{P} \tag{5.7}$$

The system can be solved for the unknown pressure distribution $\mathcal{P}$

$$\mathcal{P} = \mathbf{A}^{-1}(-\mathbf{MV}) \tag{5.8}$$

$$\mathbf{A} = \mathbf{D} - \mathbf{C}. \tag{5.9}$$

The system matrix **A** which contains the dipole terms and the diagonal matrix **C** of the solid angles is fully populated and complex and, thus, leads to non-optimum conditions for its inversion. The time needed depends on the algorithm. Standard methods show a time dependency of approximate $t_{solving} \propto I^{2.7}$ for the inversion of a matrix with I^2 entries. The vector **V** defines the excitation of the radiation problem. It is obvious that the system matrix has to be inverted once and can then be used to process a set of solutions for different

velocity excitation vectors. This configuration enables to effectively process the modal data by fast matrix-vector multiplications. It is, however, not possible in practice to store the inverted matrices and, then, to calculate the sound field resulting from arbitrary excitations as the following example will show: to get an accurate result a certain number of computation points on the surface are needed, for linear interpolations 6 points per wavelength are needed at least in the regions of high sound pressure. The examples shown later in this Chapter use about 7000 nodes for the simulation, thus leading to a matrix with $49 \cdot 10^6$ entries. Each entry is stored as complex double. This yields a size of 784 MB per frequency. A usual simulation contains 256 frequency lines to cover the complete audio band. In this case about 200 GB disk space would be needed for each simulation which is not practical at the moment of writing.

A better solution for this comes with the idea of a modal excitation which will be described in the following. This also allows to calculate the sound field for (nearly) arbitrary excitations. The storage space needed for the same problem size as discussed above is merely 1.0 GB if the complete surface potentials for the first 54 eigenfunctions are stored, 200 times less as the inverted matrices. If only the final modal data set is stored, the storage problem is not worth to be discussed.

5.2 Calculation of the Modal Data Set for the Horn

The modal horn data set as described in Chapter 4 consists of two parts: the modal horn throat impedance matrix defined in eq. (4.11), and a set of transfer impedance vectors (eq. (4.20)) describing the relation between exciting eigenfunction and far-field sound pressure. It was also pointed out that it is a good idea to store the surface pressure related to each eigenfunction to be able to process further sets of transfer impedance vectors without starting a new simulation.

5.2.1 Simulation of the Modal Surface Pressure Distribution

The first step of a BEM-simulation is to generate the geometry as a surface mesh. The interface where the driver normally is connected, is of course just a part of the surface here. To be exact, this separating face between the two systems serves as exciting part of the radiation problem, the rest of the surface is defined as non-vibrating. It is reasonable to use a geometry for this acoustic interface that fits into the system of coordinates used for the modal description. If, for instance, the eigenfunctions of the cylindrical duct are used, one should choose a planar, circular acoustic interface. If spherical coordinates are involved,

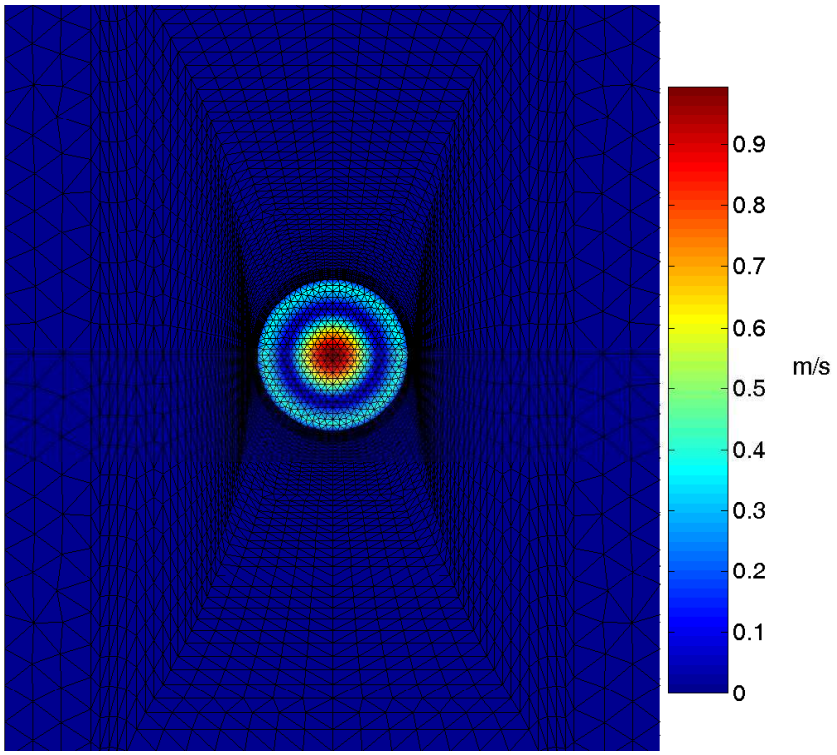

Figure 5.2: Excitation of a 60x40-horn with the first radial mode Ψ_{01} of a cylindrical duct as velocity distribution

the exciting area is a spherical cap and so on. In theory, it is not necessary, but not doing so requires an unnecessary large number of eigenfunctions and, thus, is not very useful. The acoustic interface shown in Figure 5.1 is a planar, circular disk that would be used with the cylindrical eigenfunctions.

It is assumed in the following that the geometry and the acoustic interface is described according to the chosen modal basis and that the inverted matrix is computed. The next step is to calculate the pressure distributions by multiplying $\mathbf{A}^{-1}$ with the velocity eigenfunction up to a certain order required to precisely describe all distributions possible at the interface. Figure 5.2 shows as an example the excitation of a horn with the first radial mode of the cylindrical duct. Some estimations concerning the highest order necessary for the eigenfunctions are described in section 3.3.1 based on the cut-off frequencies for the modes. As the additional computational time is negligible, one should use some more eigenfunctions if necessary. Accordingly, the modal pressure distribution is calculated by:

$$\mathcal{P}_{mn} = -\mathbf{A}^{-1}\mathbf{M}V_{mn}\Psi_{mn} \tag{5.10}$$

Actually, this equation is not exact, as the eigenfunction Ψ_{mn} with amplitude V_{mn} is only related to the separating surface between driver and horn. It has to be interpreted as the velocity vector describing the velocity distribution on the whole surface: it is zero for all

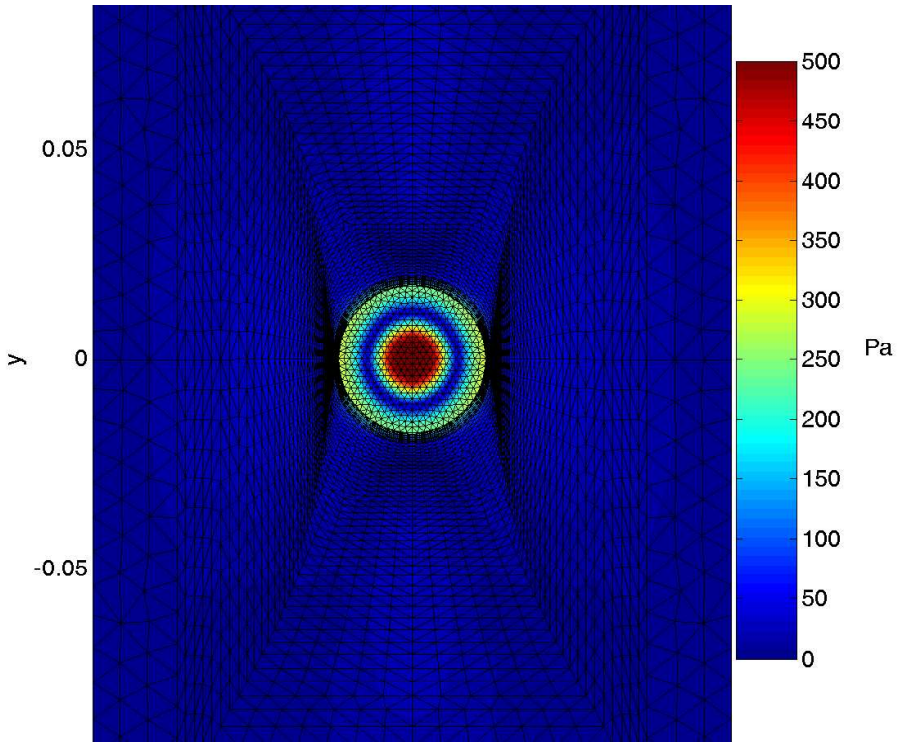

Figure 5.3: Surface pressure $\mathcal{P}_{01}$ at 10 kHz of a 60x40-horn as result of an excitation with the first radial mode velocity profile Ψ_{01} of a cylindrical duct

elements not belonging to the separating surface and Ψ_{mn} for the separating surface.

Using this idea of orthogonal eigenfunctions as excitation for the simulation, leads to a pressure distribution $\mathcal{P}_{mn}$ for the *mn*-th eigenfunction acting as exciting velocity distribution at the horn throat. Some examples for modal surface pressures of a horn are shown in Figures 5.3 to 5.5.

5.2.2 Calculation of the Modal Throat Impedance Matrix from the Modal Surface Pressure

This section describes how the modal throat impedance matrix defined in Chapter 4 is calculated from the surface pressure. First, two properties inherent each horn are discussed studying qualitatively an example of wave propagation in a typical horn geometry: mode conversion and reflection of modes at the end of the horn.

The excitation at the horn throat causes a propagating wave. While this wave travels along the horn, the initial shape of the wavefront changes due to the geometry of the horn. Figure 5.6 shows the phase distribution of a 60x40-horn at 10kHz, using the fundamental mode (plane wave) as velocity excitation. It can clearly be seen that the shape of the wave changes in order to fulfil the boundary conditions defined by the geometry and the

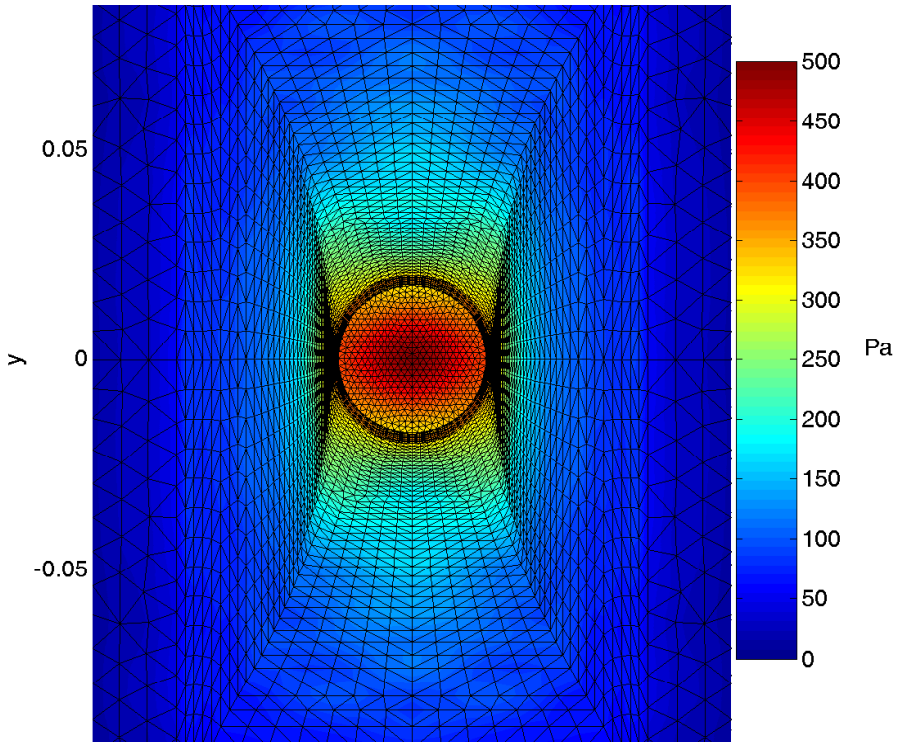

Figure 5.4: Surface pressure $\mathcal{P}_{00}$ at 10 kHz of a 60x40-horn as result of an excitation with a fundamental mode velocity profile Ψ_{00} of a cylindrical duct

surface admittance. Hence, the initial mode changes to a superposition of different modes. When the wave finally arrives at the horn mouth or other discontinuities, the modes are reflected and travel backwards to the horn throat. Figure 5.7 shows a pressure pattern at 10 kHz for plane wave excitation. It is obvious that the pattern does not belong to a pure plane wave, but to a plane wave and some superposed higher order modes. This is the reason for coupling of modes at the horn throat area. From this simple considerations it can be concluded, that axis-symmetric horns with low flare-rate have a weak modal coupling. Rectangular horns with high flare-rate, diffraction slot and other sharp bends will have a stronger modal coupling. A surface admittance unequal to zero would also cause modal coupling, even if the geometry fits into a separable system of coordinates. But as it is rather unusual to make horns with a significant different surface admittances from zero, this effect is not discussed here. Anyhow, by modifying the surface admittance it is possible to influence the directivity pattern (due to modal conversion) of the horn. This was investigated by Piscoya in [Pis03] with a rather complicated mathematical treatment. To calculate the horn throat impedance matrix from simulation results, the modal decomposition, as described in section 3.2, has to be applied to the simulated pressure distribution at the horn throat

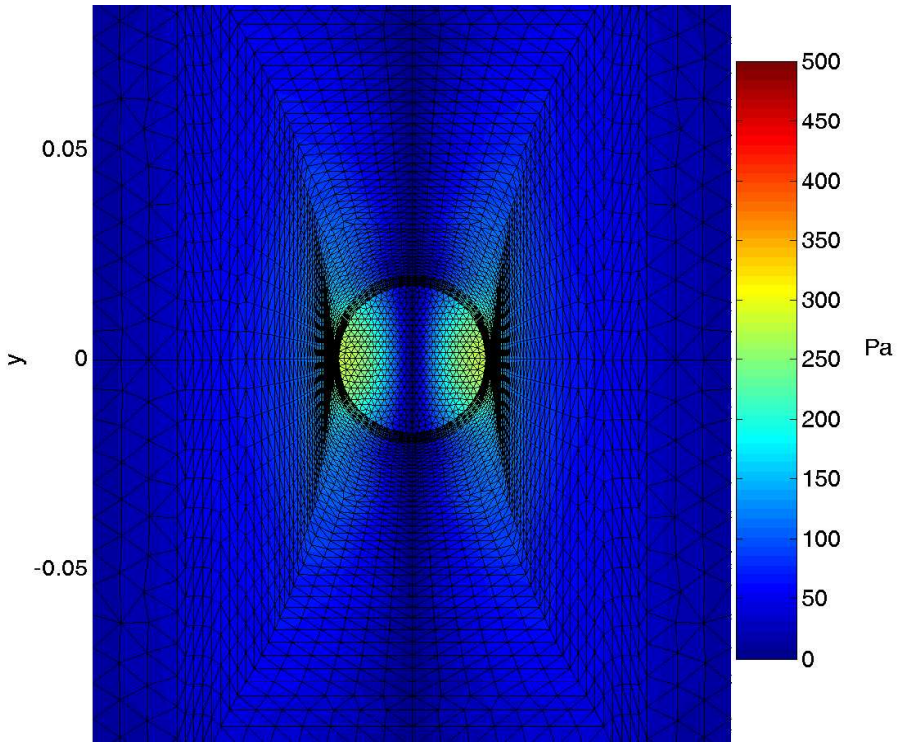

Figure 5.5: Surface pressure $\mathcal{P}_{10}$ at 10 kHz of a 60x40-horn as result of an excitation with the first angular mode velocity profile Ψ_{10} of a cylindrical duct

membrane area A (indicated by $\mathcal{P}^A_{mn}$)

$$P_{mn,m'n'} = (A\,\Lambda_{m'n'})^{-1} \iint_A \mathcal{P}^A_{mn}\,\Psi_{m'n'}\,dA. \tag{5.11}$$

The result is the pressure participation coefficient at the horn throat for the m'n'-th eigenfunction, when the horn is excited by the eigenfunction of amplitude V_{mn}. Thus, one entry of the modal throat impedance matrix is calculated by

$$Z_h^{mn,m'n'} = \frac{P_{mn,m'n'}}{V_{mn}}. \tag{5.12}$$

This equation has to be applied to all eigenfunctions of interest to fill the impedance matrix $\mathbf{Z_h}$ up to a certain order with its entries. If the maximum order of excitation is the same as the maximum decomposition order, the impedance matrix is square.

In the following a selection of modal impedance matrix entries is presented. The results belong to three different horns each of them representing a class of common horns. The eigenfunctions used for these simulations are derived by the rigid wall cylindrical duct and are described comprehensively in Chapter 3.2. Hence, the acoustic interface is a planar disk at the horn throat.

The first example is a 60x40 horn with a rectangular shaped mouth. It is straightforward constructed and does not feature sharp bends or a diffraction slot. The second example is

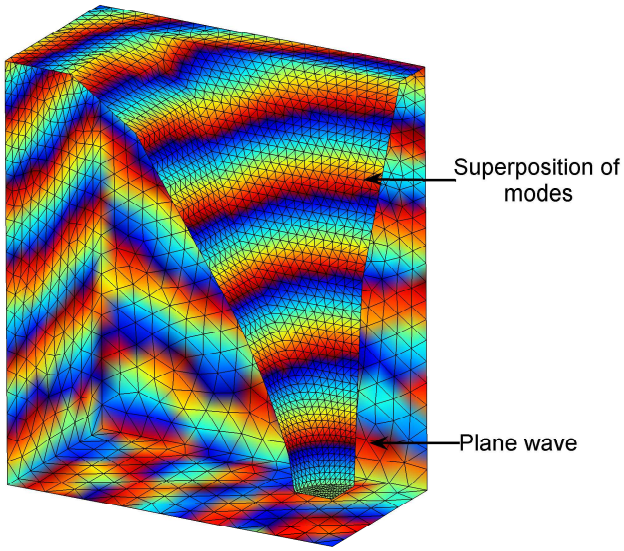

Figure 5.6: Phase distribution of the 60x40 at 10kHz excited by the fundamental mode velocity of a cylindrical duct (Ψ_{00}, plane wave)

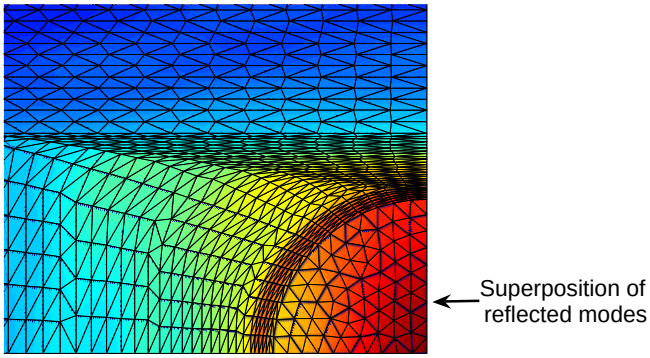

Figure 5.7: Horn throat pressure magnitude at 10kHz with fundamental mode excitation (V^{00}, plane wave)

a square mouth 90x40 horn with diffraction unit. As last example, a tractrix horn is shown here. It serves as a kind of “contrast” to the 90x40 horn.

60x40 horn with a 12x6 inch flange and 1.4 inch driver The mesh shown in Figure 5.8(a) consists of about 7000 nodes and 13000 elements. It has to be noted at this point that the simulation using eigenfunctions as excitation at the horn throat requires to simulate the complete model. It is not possible to use planes of symmetry within the mesh which normally helps to greatly reduce the calculation time. Figure 5.8(b) shows the modal throat impedances of the fundamental mode and the cross coupling with the other modes. The decomposition was calculated up to order $m = 8$ and $n = 2$. Hence, the plots corresponds to the first column of the modal impedance matrix of this horn. One can clearly see the different behaviour of the fundamental mode and coupled higher order modes. The plane wave throat impedance reaches values around $\rho_0 c$ even at low frequencies. The coupling of the fundamental mode with higher order modes is weak and only the 01-mode shows a

little coupling around 12 kHz. If the horn is excited using the 01-mode (Figure 5.8(c)), the result looks completely different. Below a cut-off frequency, the wave is evanescent and, hence, the corresponding throat impedance is small for low frequencies. Furthermore, the 01-mode does not show a coupling with other modes. Looking at Figure 5.8(d), one can notice that the 10cos-mode throat impedance has a lower cut-off than the other modes and that, especially, this mode converges to $\rho_0 c$ even within the audio frequency range. The modal coupling is very weak. Similar properties can be found for other modes, whereas the cut-off frequencies are shifted to higher frequencies.

90x40 horn with a 12x12 inch flange and 1.4 inch driver The geometry of this horn represents the typical square-mouth horn types with diffraction slot to get the desired horizontal radiation pattern. Figure 5.9(a) shows a phase-plot of this horn at 10 kHz. The velocity distribution used here was the fundamental mode. One can clearly see how the initial wave changes while it travels through the diffraction unit. The wave converts from a circular plane wave to a mixture of a cylindrical wave and an elliptical wave. As consequence of this conversion, it has to be expected that this type of horn enforces a stronger modal coupling, and, furthermore, that a difference in the horizontal and vertical direction of the modes with nodal lines on the angular axis can be found. Figure 5.9(b) shows the fundamental mode throat impedance. In contrast to the 60x40-horn, a stronger coupling of the 00-mode with some higher order modes can be found. Especially, the first two angular modes (10- and 20-mode) and the first radial mode (01-mode) are now involved. The 01-mode throat impedance shown in Figure 5.9(c) has a significant resonant behaviour and additionally a coupling with the 20cos-mode. Figure 5.9(d) and 5.9(e) show the 10sin-mode and 10cos mode. The impedances have the expected difference due to the geometry of the horn.

Tractrix horn with 20 cm mouth diameter and 1.4” throat diameter As last example, some results for a 1.4” tractrix horn with 20 cm mouth diameter are presented (Figure 5.10). The weak modal coupling that can be expected intuitively is now verified by simulation results. Furthermore, the plane wave throat impedance (Figure 5.10(b)) shows a perfect behaviour as it is known from theory. The higher order modes (Figure 5.10(c) - 5.10(d)) have a nearly non-existent coupling and, additionally, they are very smooth over the complete frequency range.

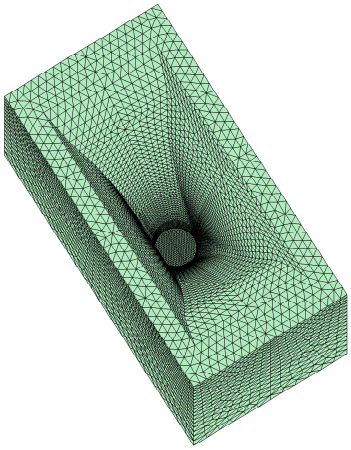

(a) Mesh of the 60x40-horn with 12x6 inch flange and 1.4 inch driver outlet

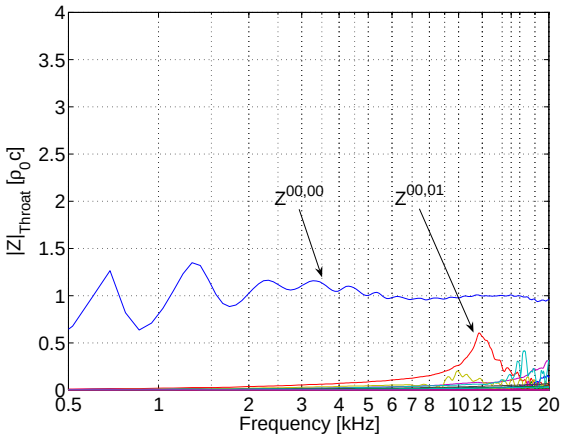

(b) $Z^{00,ii}$

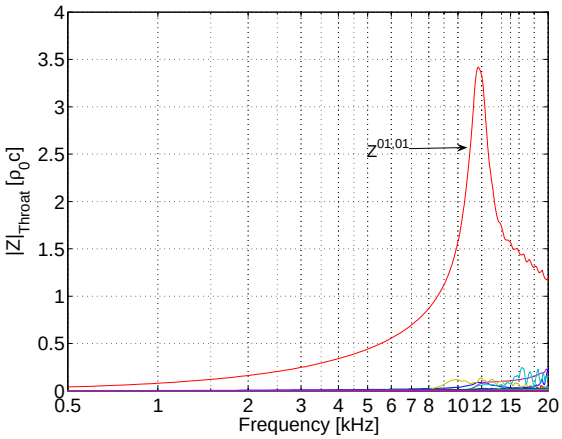

(c) $Z^{01,ii}$

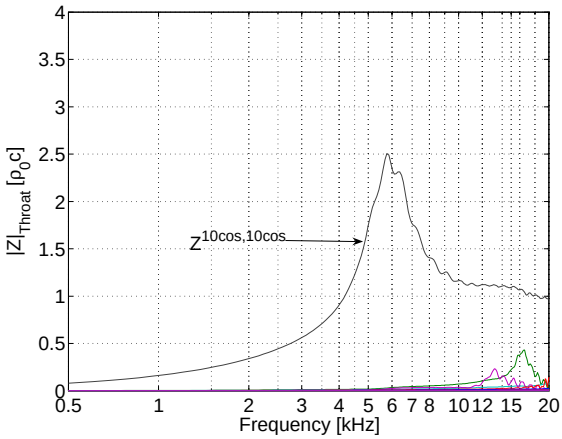

(d) $Z^{10cos,ii}$

Figure 5.8: Normalized modal throat impedance of the 60x40 horn

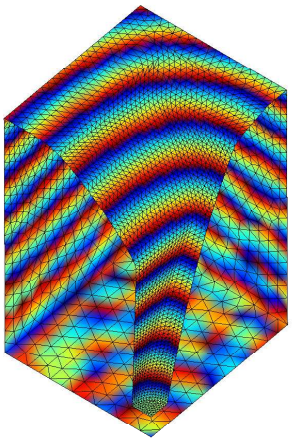

(a) Phase-plot of the 90x40 horn at 10kHz with fundamental mode velocity excitation

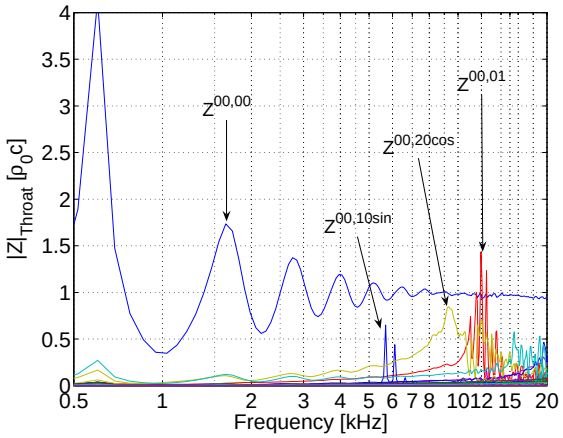

(b) $Z^{00,ii}$

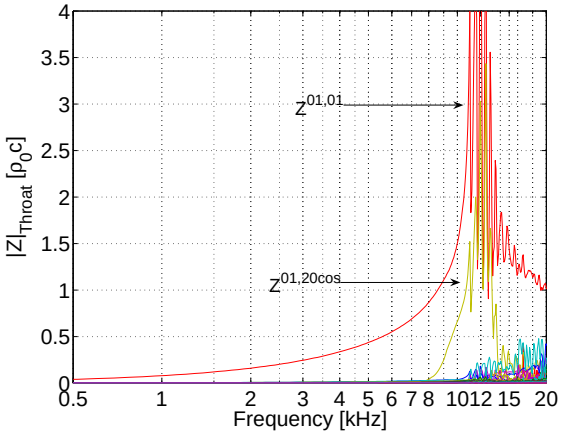

(c) $Z^{01,ii}$

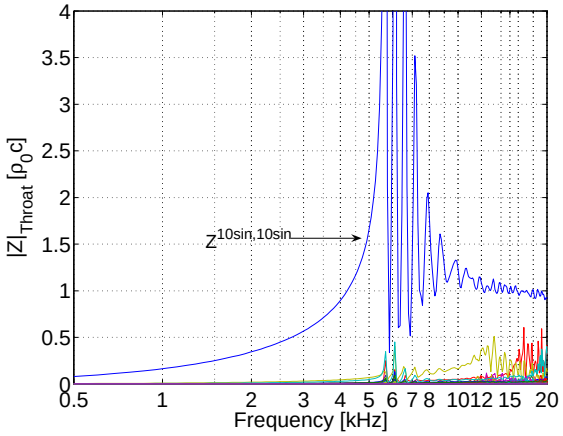

(d) $Z^{10sin,ii}$

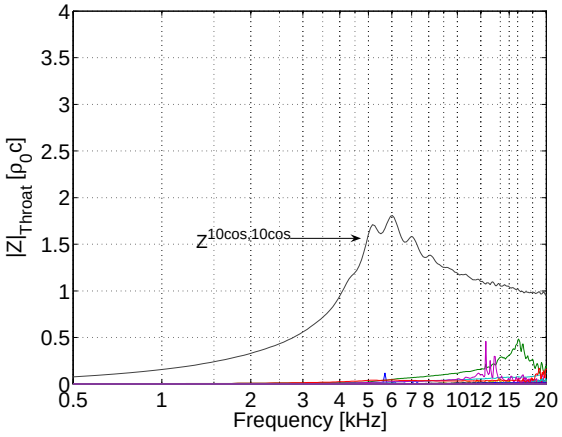

(e) $Z^{10cos,ii}$

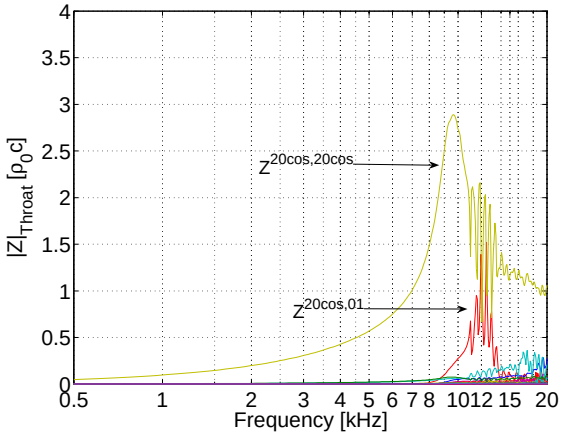

(f) $Z^{20cos,ii}$

Figure 5.9: Normalized modal throat impedance of the 90x40 horn

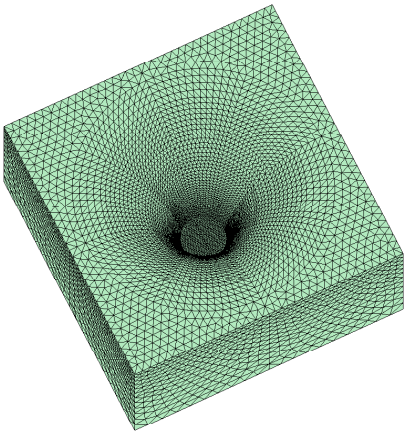

(a) Tractrix horn with 20 cm mouth diameter and 1.4” driver

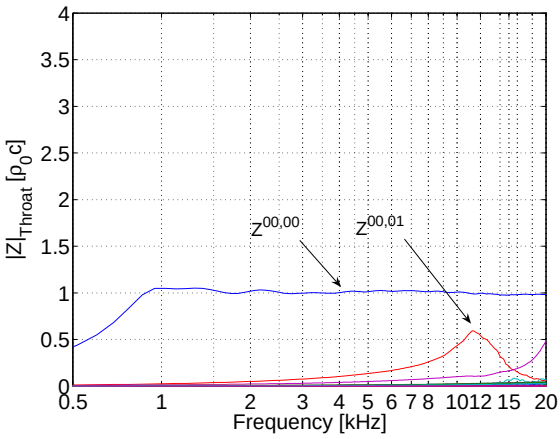

(b) $Z^{00,ii}$

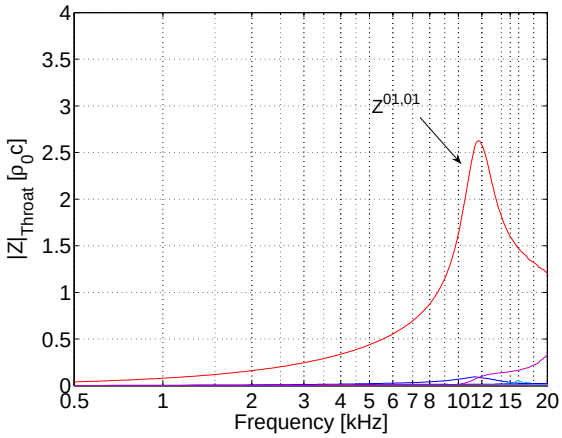

(c) $Z^{01,ii}$

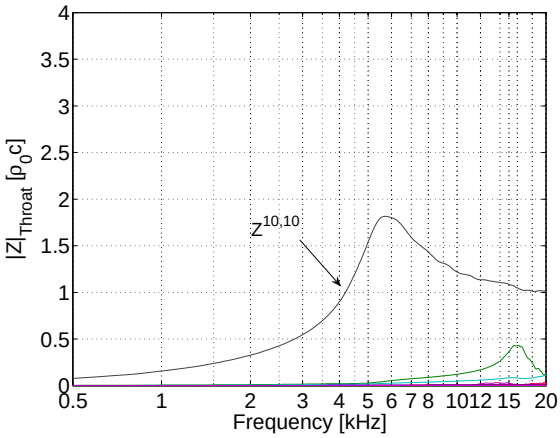

(d) $Z^{10sin,ii}$

Figure 5.10: Normalized modal throat impedance of the tractrix horn

5.2.3 Calculation of Modal Transfer Impedance Vectors

The second part of the modal horn data is a set of transfer impedance vectors defined in eq. (4.20). Each entry describes the relation of the sound pressure at a certain field point to the exciting velocity eigenfunction at the horn throat. While the impedance matrix is needed to calculate the modal velocity vector at the separating acoustic interface, the transfer functions are needed to relate the velocity vector to the far-field of the horn.

To calculate the transfer functions, the pressure frequency response has to be processed using eq. (5.5) together with the simulated surface pressure of the mn-th eigenfunction: [1]

$$\iint_S \left[\mathcal{P}_{mn} \frac{\partial g(r_0, y)}{\partial n(y)} + j\omega\rho_0 \Psi_{mn} V_{mn} g(r_0, y) \right] ds = P_{mn}(r_0). \tag{5.13}$$

With this result the entries of the modal transfer function vector from the horn throat to this far-field point can be calculated:

$$H_{mn} = \frac{P_{mn}(r_0)}{V_{mn}}. \tag{5.14}$$

To characterize the radiation pattern of the horn it is most usual to make measurements or simulations at the following field points:

- on the main axis of the horn at the distance $|r_0|$
- on a circle in the horizontal plane around the horn with radius $|r_0|$
- on a circle in the vertical plane around the horn with radius $|r_0|$

The on-axis point serves here to characterize the far-field frequency response of the loudspeaker. This frequency response is often normalized to a measurement distance of 1 m and an electrical nominal input power of 1 W if a real transducer is considered. The two circles are of course not sufficient to characterize the complete radiation pattern but they represent the most important informations. A typical spacing for the field points on the circles is 5°, thus leading to 72 points for each circle (Figure 5.11). Additionally, the pressure results on the circles are normalized to the 0° axis, which is for both circles identical to the on-axis direction. Figures 5.12(a) to 5.12(f) show some examples for the transfer function vectors simulated for the horizontal and vertical field point circles. The results belong to the 60x40 horn shown in Figure 5.8(a). All frequency responses are normalized to the 0°-response of the fundamental mode excitation. The normalization enables to compare different horns and, especially, in this context, to compare the influence of different modal excitations.

[1] Again, this equation is not exact as the eigenfunction is only related to the acoustic interface

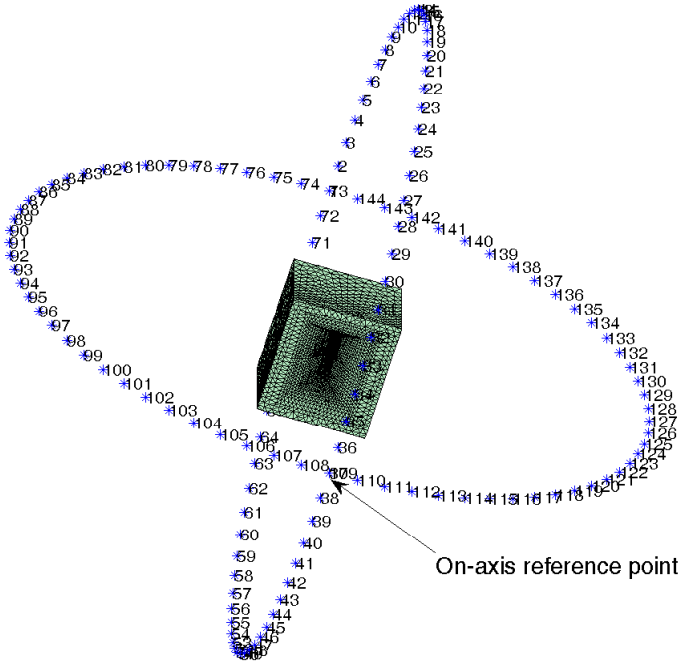

Figure 5.11: Definition of the horizontal and vertical circles of field points. The horn is magnified by a scaling factor of five for sake of visibility

Looking at the fundamental mode responses in Figure 5.12(a) and 5.12(b), the classification as 60x40 horn becomes clear. The off-axis horizontal frequency response at ± 30° is at -6 dB compared to the on-axis frequency response. The vertical direction off-axis drop-off is not that smooth and constant over frequency and covers the 40° only in the mid-frequency range. This is a typical result for such a small-sized horn. Besides the coverage of a constant spatial angle, it is also important that no significant side lobes are existent which might cause feedback problems in a stage-audience situation. Furthermore, an non-constant coverage, particularly in the horizontal direction, will lead to strong phasing effects at the audience area when clustering several loudspeakers. The phasing is a result of interference between two neighboured loudspeaker systems. This, actually, is the reason for the definition of the coverage angle at the -6 dB drop-off. Potentially, at this angle a combination of identical systems will work with a minimum of interference. In practice, this is, unfortunately, not exactly fulfilled. When combining the loudspeakers, the diffraction around the housing changes and thus the directional pattern can change in this particular frequency range. Accordingly, the coverage angle is only an indication and mainly serves as unique measure for classifying the spatial characteristics with some single numbers.

Another important property, especially when using only one pair of loudspeakers, is how smooth the off-axis response changes are. In listening tests, white or pink noise is reproduced by the loudspeaker and by walking around the loudspeaker it is determined if the off-axis drop-off changes smoothly at the audience area. This practical test corresponds

to determining if the “isobars” in the directivity plot are parallel to each other.

Looking at the normalized higher order mode results, it is obvious that they influence mainly the high frequencies. This is not surprising as the cut-off frequencies for the cylindrical tube indicated exactly this behaviour, namely that a power transmission is only possible above the cut-off. Of course, the cut-offs will drop a little bit when dealing with fast flaring geometries. It is also interesting to see, that for this horn only a few modes are necessary to use for simulations, as further increasing the order of the used eigenfunction will not contribute to the far field response. Similar properties are also observed at other geometries.

It is also worth mentioning here that with larger driver outlets more modes have to be taken into consideration and vice versa. As the results shown for a 1.4” horn indicate to use only the fundamental and maybe the first 8 eigenfunctions, one can conclude that smaller diameters do not require any higher order mode simulations or at least only two or three modes.

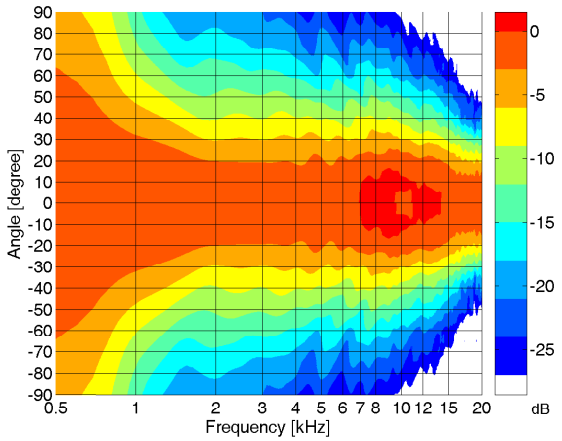

(a) Horizontal response with fundamental mode excitation Ψ_{00}

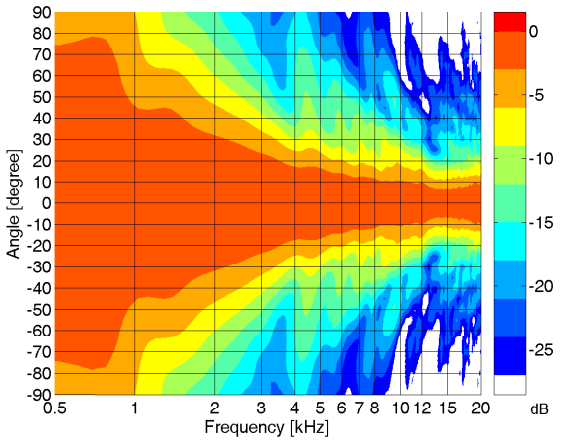

(b) Vertical response with fundamental mode excitation Ψ_{00}

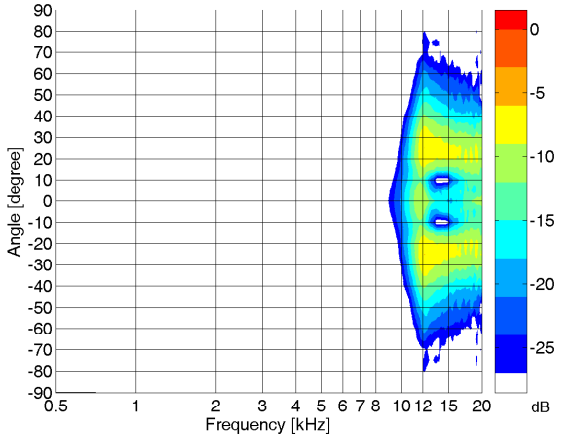

(c) Horizontal response with first radial mode excitation Ψ_{01}

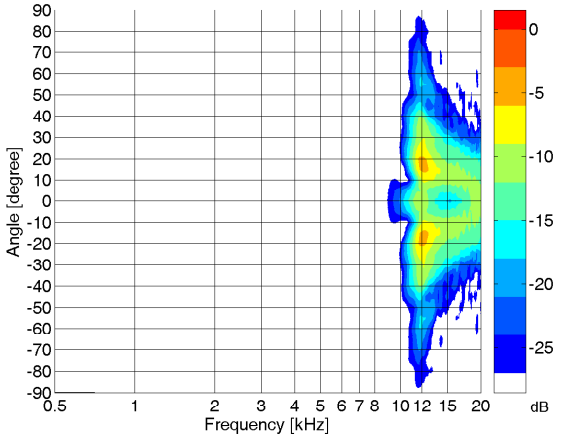

(d) Vertical response with first radial mode excitation Ψ_{01}

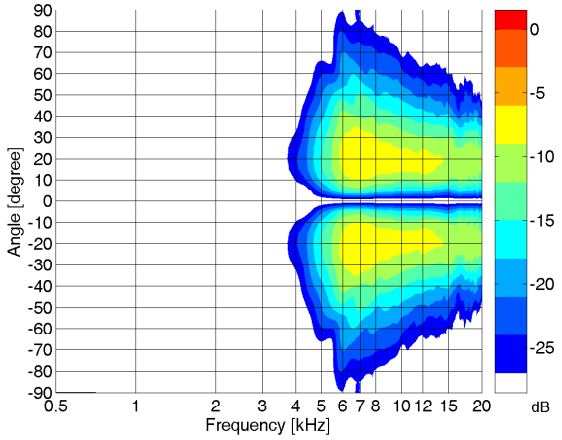

(e) Horizontal response with first angular mode excitation Ψ_{10sin}

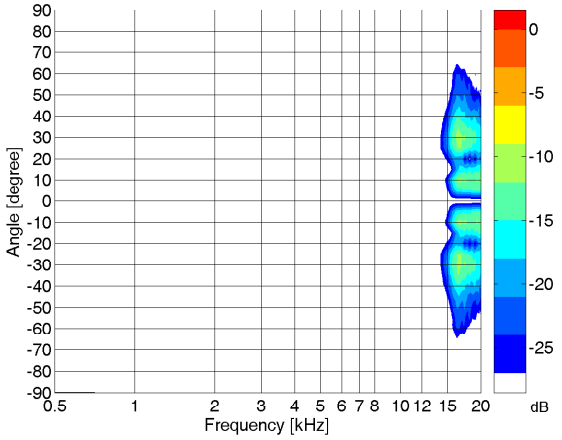

(f) Horizontal response with the first angular plus radial mode excitation Ψ_{11sin}

Figure 5.12: Modal directivity responses normalized to the 0° frequency response of the fundamental mode

Chapter 6

Determination of the Driver Parameters

In Chapter 4, a universal model based on a multi-port with orthogonal eigenfunctions for the acoustic port was described. If a feedback between all ports shall be considered, a huge number of unknowns is to be determined. It was pointed out that a model with a reduced number of unknowns should be used if a real horn driver shall be characterized by measurements. Several degrees of reduction for the full model were discussed and described.

Looking at the acoustic load that is represented by the horn throat impedance matrix, one can state that for common horn geometries, the throat impedance matrix is dominated by its diagonal elements. Even geometries with a diffraction unit which causes a significant modal conversion and reflection at the slot are dominated by the diagonal elements. The coupling observed at these geometries only affects some other modes. Hence, if a strong coupling between modes is existent, the matrix is dominated by the diagonal elements and some other elements. The particular structure of the matrix is, additionally, dependent on the modal basis used to describe the system.

If the importance of the modes has to be classified, one can clearly say that the fundamental mode excitation is of highest importance. This can be underlined by the investigation in Chapter 3 and the simulation of the spatial far field responses shown in 5.2.3. Both results show clearly that the fundamental mode dominates most of the frequency range and a modal influence at high frequencies requires at least rather high amplitudes of excitation at the driver's mouth. Additionally, the modal impedances underline these results.

In this thesis, two of the models proposed in section 4.2 are used:

- the fundamental mode model, and
- the reduced modal model

This Chapter describes in detail how the parameters of the fundamental mode model

can be acquired successfully. It will be demonstrated with a number of measurement and simulation results that the fundamental mode modal is a feasible approach.

The second model used in this thesis is the reduced modal description. It offers a good compromise between accuracy, measurement complexity and modelling effort. As it is merely a combination of the fundamental mode model and the normalized amplitudes of the measured velocity participation coefficients, it is not necessary to describe this method separately. Instead, its application is demonstrated in section 8.2.2 and a verification of the model is presented in section 8.3.1.

The measurement and the simulation of the more complex models is not discussed in this thesis as to the time of writing the investigation of suitable methods was not finished yet. First results indicate that the simulation of the full cross modal model is possible using similar methods as described in Chapter 5. Concerning the measurement of the modal source/impedance model it is indicated that the characterization seems possible using a modified scanning machine. The methods are currently under investigation.

6.1 Fundamental Mode Model

The practical measurement of two-port parameters at electro-acoustic transducers is not a new idea. One can find applications in ultrasonics, underwater acoustics and many examples of transducers for audio reproduction and measurement. In contrast to the measurements in this Chapter, it is a common method to characterize the parameters of a lumped element model by two-port measurements or to modify the topology of the network based on the measurement results. This is a rather effective method and very useful for analysis and development of new transducers, but in the case of horn drivers it is a rather difficult task to describe the behaviour of a propagating wave passing the phase plug by a lumped parameter model. Hence, the transducer is described here by a black-box via a transfer matrix as defined on page 50 and in section 6.1.1.

6.1.1 Definitions and Reciprocity

In general, a two-port can be used to describe any linear, time-invariant network with one input and one output (SISO). Applied to electro-acoustic networks the following definition will be used (Figure 6.1). The mathematical representation used here describes the connec-

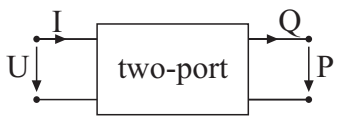

Figure 6.1: Electro-acoustic two-port

tion between the electric and the acoustic port via a two by two transfer matrix (eq. (6.1)). The parameters T_{ii} and the input and output quantities are complex vectors in the frequency domain. The operation between the input vector and the matrix is a complex multiplication.

$$\begin{pmatrix} P \\ Q \end{pmatrix} = \begin{pmatrix} T_{11} & T_{12} \\ T_{21} & T_{22} \end{pmatrix} \begin{pmatrix} U \\ I \end{pmatrix} = \mathbf{T} \begin{pmatrix} U \\ I \end{pmatrix} \tag{6.1}$$

P and Q are the acoustic pressure and the volume velocity, U denotes the electric voltage and I is the current. Inverting eq. (6.1) yields:

$$\begin{aligned} \begin{pmatrix} U \\ I \end{pmatrix} &= \frac{1}{\det \mathbf{T}} \begin{pmatrix} T_{22} & -T_{12} \\ -T_{21} & T_{11} \end{pmatrix} \begin{pmatrix} P \\ Q \end{pmatrix} \\ &= \mathbf{T^{-1}} \begin{pmatrix} P \\ Q \end{pmatrix} \end{aligned} \tag{6.2}$$

$$\det \mathbf{T} = T_{11}T_{22} - T_{12}T_{21} \tag{6.3}$$

A very important feature of electro-acoustic transducers is the reciprocity. Applied to a one-dimensional two-port model, a reciprocal transducer would behave such that transmitter and receiver could be reversed without a change in the transmission characteristic. This can be expressed by the following relations:

$$\frac{P}{U|_{I=0}} = T_{11} = \frac{I}{Q|_{P=0}} \tag{6.4}$$

$$\frac{P}{I|_{U=0}} = T_{12} = \frac{-U}{Q|_{P=0}} \tag{6.5}$$

$$\frac{Q}{U|_{I=0}} = T_{21} = \frac{-I}{P|_{Q=0}} \tag{6.6}$$

$$\frac{Q}{I|_{U=0}} = T_{22} = \frac{U}{P|_{Q=0}} \tag{6.7}$$

For example, the left side of eq. (6.4) is the quotient of pressure and voltage, while simultaneously the current is enforced to zero by terminating the electric side by an infinite electric impedance. For practical measurements these equations are very important. For instance, the reciprocal calibration of microphones is based on these relations (see for instance [VB94] and [BV04]). If they are fulfilled, the determinant of the matrix is 1 (or -1) for all frequencies.

6.1.2 Basic Considerations for the Measurement of the Fundamental Mode Model's Parameters

The model used here describes a Single Input Single Output system (SISO) considering only the fundamental mode velocity/pressure profile at the driver's outlet. As for high frequencies a superposition of different modes is found, the basic question is how to separate

the fundamental mode properties. Of course, using the modal decomposition technique together with the scanning of profiles at the driver's mouth, as described in Chapter 3, could be used to separate the modes. But, besides the fact that the additional information about higher order modes is not required for the fundamental mode model, the technique requires much time for the measurements and a complicated machine to automatically position the microphone probe. For fast practical development processes another, more intelligent technique is required. The idea for the two methods described in section 6.1.3 and 6.1.4 actually was a consequence of the first approaches described in [Mak01], [BM03] and the need to improve the quality of the two-port parameters.

"Historical" notes on direct acoustic measurements In the beginning of investigating two-port parameters for horn drivers, the characterization was done by directly measuring the acoustic properties. As the drivers are found in more or less standardized diameters, the measurements could be carried out using impedance tubes for the acoustic impedances. This measuring technique is normally used to characterize sound absorbing materials by its complex impedance [ISO96a], [ISO96b].

A basic problem of this method, however, is exactly the superposition of higher order modes. Above the cut-off frequencies, the sound pressure measured at certain positions in the tube does not belong to a one-dimensional sound field anymore and, thus, does not yield valid results at these frequencies. Accordingly, mode propagation is the reason for the upper frequency limit of standard impedance tube measurements. In a restricted frequency range, however, the measurements technique leads to valid results. It could be statistically shown that the method itself is free from systematic errors [BM03]. Figure 6.2 shows the

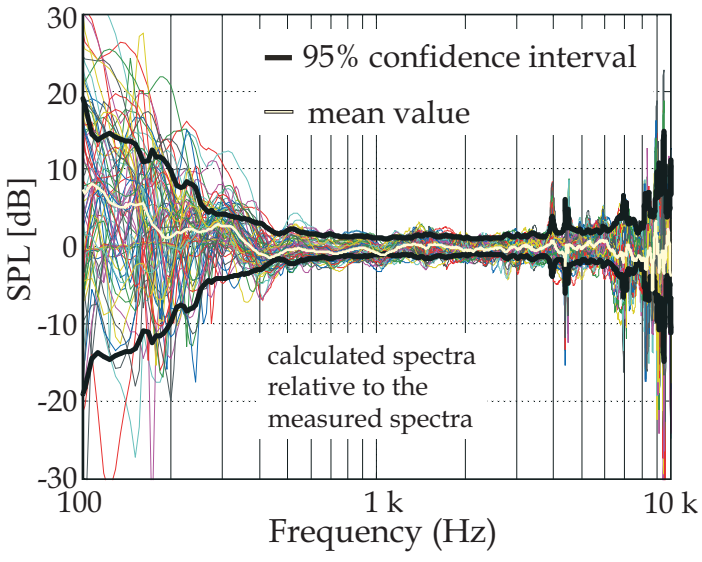

Figure 6.2: Difference level of measured and calculated sound pressure levels. The calculation is based on two-port descriptions obtained by direct acoustic measurements

difference level between measured and calculated sound pressure levels of 77 driver/horn combinations (the driver outlet of all drivers was 2”). The measurements were made in a semi-anechoic room. The horn was positioned in a height of 2 m and the microphone was at a distance of 2 m (same height as the horn). The differences at low frequencies are caused by the windowing technique which cuts off the ground plane reflections in the time domain.[1] Anyway, at these low frequencies a 2”-driver is, normally, not used for sound reinforcement. More interesting is the frequency range above 500 Hz. The mean value of all differences lies at about 0 dB and nearly all results are in the 95% confidence intervall. The errors introduced seem to be of statistic nature but besides this, the accuracy is quite high for such a complicated technique with many acoustic measurements involved. Above 4 kHz some peaks are visible. The first peak at 4 kHz is the cut-off frequency of the first angular mode with the eigenfunctions Ψ_{10cos} and Ψ_{10sin}. With increasing frequency the density of modes also increases which also explains the increasing deviations of the mean value from the 0 dB line. To cope with this, a technique has to be used avoiding direct acoustic measurements to circumvent the problem of higher order mode superposition. First results of this new method were presented in [Mak04a].

General approach The determination of two-port parameters requires four independent equations to solve the system of equations represented by eq. (6.1). The quantities can directly be accessed from the two ports: the acoustic port characterized by pressure and volume velocity and the electric port with voltage and current. The task is to make measurements at these ports that fulfil four linear independent equations which are derived from the transfer matrix eq. (6.1) or its inverse matrix in eq. (6.2). In general there are lots of possibilities to extract four linear independent equations, but one has to keep in mind that the physical quantities also have to be measurable in order to solve the system of equations later. For example, from eq. (6.7), the parameter T_{22} can be determined directly. Using the left side of eq. (6.7) requires the measurement of the volume velocity while the electric side is terminated by a short-circuit. As the measurement of volume velocity is not a trivial task, in particular for high frequencies, this approach does not seem to be practical. Using the right side of eq. (6.7) requires the measurement of pressure and voltage while the volume velocity is enforced to zero. The acoustic port has to be terminated by an infinite acoustic impedance. As the pressure profile might slightly deviate from the fundamental mode profile for higher frequencies this method will produce an incorrect pressure measurement.

A solution to this problem is to avoid making any direct acoustic measurements at

[1] The measurement technique is described in detail by Müller in [Mül99].

the interface horn driver/horn. Furthermore, a kind of acoustic integration over the junction area is required in order to acquire the fundamental mode parameters of the transducer. This "acoustic integrator" is, fortunately, already realized: the system of membrane, voice coil and magnetic system fulfils this requirement. The two-dimensional pressure-distribution within the cross section is reduced to a one-dimensional quantity via the electro-acoustic transformer. Taking all this into consideration, the huge amount of possible ways to determine the two-port parameters can be reduced to a reasonable amount[2]. In the following two methods are presented.

6.1.3 Method I - Using Two Different Drivers

This method uses two different horn drivers. Both drivers must have the same junction diameter. The first driver will be called driver **S**, the second one is driver **T**. The definition of input and output quantities is shown in Figure 6.3.

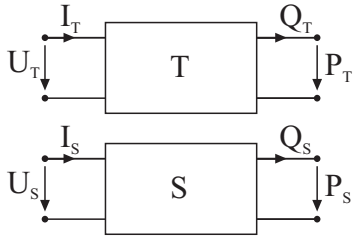

Figure 6.3: Two-ports **S** and **T**

The mathematical representation via two-port matrices is

$$\begin{pmatrix} P_S \\ Q_S \end{pmatrix} = \begin{pmatrix} S_{11} & S_{12} \\ S_{21} & S_{22} \end{pmatrix} \begin{pmatrix} U_S \\ I_S \end{pmatrix} = \mathbf{S} \begin{pmatrix} U_S \\ I_S \end{pmatrix} \tag{6.8}$$

$$\begin{pmatrix} P_T \\ Q_T \end{pmatrix} = \begin{pmatrix} T_{11} & T_{12} \\ T_{21} & T_{22} \end{pmatrix} \begin{pmatrix} U_T \\ I_T \end{pmatrix} = \mathbf{T} \begin{pmatrix} U_T \\ I_T \end{pmatrix}. \tag{6.9}$$

Measurements at two coupled drivers When connecting these two-ports as shown in Figure 6.4 the resulting two-port only has two remaining electric ports. The resulting cou-

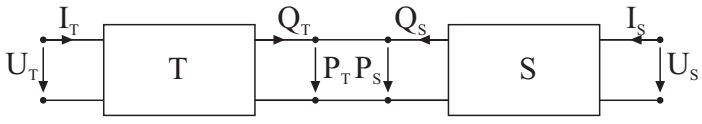

Figure 6.4: Two-port **S** and **T** connected via the acoustic ports

pling conditions are presented in eq. (6.10). It has to be noted that the sign of the volume velocity is changed due to the definition of its flow direction in Figure 6.3.

$$\begin{pmatrix} P_S \\ Q_S \end{pmatrix} = \begin{pmatrix} 1 & 0 \\ 0 & -1 \end{pmatrix} \begin{pmatrix} P_T \\ Q_T \end{pmatrix} \tag{6.10}$$

[2]The author tested about 10 different methods to find the best one: accurate and easy to carry out for drivers with arbitrary outlets

Using the inverse matrix $\mathbf{S^{-1}}$ the two-port $\mathbf{V}$ for this coupled system yields:

$$\begin{pmatrix} U_S \\ I_S \end{pmatrix} = \underbrace{\mathbf{S^{-1}} \begin{pmatrix} 1 & 0 \\ 0 & -1 \end{pmatrix} \mathbf{T}}_{\mathbf{V}} \begin{pmatrix} U_T \\ I_T \end{pmatrix} \tag{6.11}$$

Multiplying the three matrices yields the four elements of matrix $\mathbf{V}$:

$$V_{11} = S_{22}T_{11} + S_{12}T_{21} \tag{6.12}$$

$$V_{12} = S_{22}T_{12} + S_{12}T_{22} \tag{6.13}$$

$$V_{21} = -S_{21}T_{11} - S_{11}T_{21} \tag{6.14}$$

$$V_{22} = -S_{21}T_{12} - S_{11}T_{22}. \tag{6.15}$$

At a first glance, it seems that the original problem, determining the four parameters of one matrix, has become more complicated. Now eight equations are needed to solve the system of equations (6.12) - (6.15). But this configuration with two acoustically coupled drivers offers new ways to carry out pure electric measurements. One equation can be obtained by terminating the two-port by an electric short-circuit and measuring the electric impedance at the other port as shown in fig. 6.5.

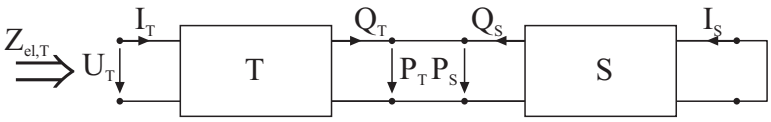

Figure 6.5: Two-port $\mathbf{V}$ terminated by an electric short-circuit

This configuration yields the first conditional equation.

$$Z_{el,T}|_{U_S=0} = -\frac{V_{12}}{V_{11}} = -\frac{S_{22}T_{12} + S_{12}T_{22}}{S_{22}T_{11} + S_{12}T_{21}} \tag{6.16}$$

In the same way one obtains the second equation when measuring the electric impedance $Z_{el,T}|_{I_S=0}$ while the other side is not terminated. This enforces the current $I_S = 0$. The resulting equation is

$$Z_{el,T}|_{I_S=0} = -\frac{V_{22}}{V_{21}} = \frac{S_{21}T_{12} + S_{11}T_{22}}{-S_{21}T_{11} - S_{11}T_{21}}. \tag{6.17}$$

Using reciprocity Another two equations result from the reciprocity of the driver - the determinants are equal 1:

$$\det \mathbf{T} = T_{11}T_{22} - T_{12}T_{21} = 1 \tag{6.18}$$

$$\det \mathbf{S} = S_{11}S_{22} - S_{12}S_{21} = 1. \tag{6.19}$$

In the following, the two drivers are not coupled anymore. Thus, the measurements are carried out at the two separate systems. Again, the reciprocity can be used to find two

conditional equations. Dividing eq. (6.7) by eq. (6.6) results in

$$-Z_{el,T}|_{Q_T=0} = \left.\frac{U_T}{-I_T}\right|_{Q_T=0} = \frac{T_{22}}{T_{21}} \tag{6.20}$$

$$-Z_{el,S}|_{Q_S=0} = \left.\frac{U_S}{-I_S}\right|_{Q_S=0} = \frac{S_{22}}{S_{21}}. \tag{6.21}$$

The electric input impedance is measured while the two-port is terminated by an acoustic impedance $Z_{ac} = \infty$ which enforces the volume velocity to zero. Such an acoustic impedance can be realized by a heavy stone slab, pressed at the driver's mouth or alternatively by pressing the driver on a granite floor while determining the electric input impedance.

Acoustic reference impedance Again, the two drivers are treated separately. In order to obtain the last two missing equations, the electric impedance has to be measured under well defined acoustic conditions. The driver is loaded by a known acoustic impedance $Z_{ac,ref}$. This impedance has to be of the same junction diameter as the horn drivers. Figure 6.6 illustrates the setup.

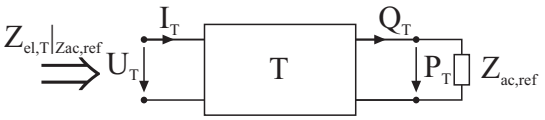

Figure 6.6: Two-port terminated by an acoustic reference impedance

The corresponding equations are

$$Z_{el,T}|_{Z_{ac,ref}} = \frac{T_{22}Z_{ac,ref} - T_{12}}{T_{11} - T_{21}Z_{ac,ref}} \tag{6.22}$$

$$Z_{el,S}|_{Z_{ac,ref}} = \frac{S_{22}Z_{ac,ref} - S_{12}}{S_{11} - S_{21}Z_{ac,ref}}. \tag{6.23}$$

The reference impedance must be selected carefully as it affects the solution of the whole system of equations. One possible impedance is a geometry that can be analytically calculated, like a baffled piston of same diameter as the investigated driver. But, remembering the results of Chapter 5.2, an abrupt cross sectional jump causes a strong modal coupling in the impedance matrix. As the intention is to characterize the fundamental mode model of the driver, an impedance with a minimum of modal coupling is needed. One possibility is to use a so-called spherical wave horn (or tractrix horn) as shown in Figure 2.1. The modal coupling is negligible and can be calculated accurately with numerical methods as described in section 5.2.2. Furthermore it offers a good loading without resonances even at low frequencies which minimizes the dynamic range needed for the measurements. Together with adapters for different junction diameters, this horn was used as reference

impedance. An interesting point to mention here is that the acoustic impedance, or more precisely, the modal basis chosen for the calculation of the fundamental mode impedance, is the only parameter which is directly related to the shape of the waveform leaving the driver's outlet. The results presented in the following are based on the cylindrical duct's eigenfunctions. This affects not only the acoustic reference impedance, but also the infinite impedance used in eq. (6.20) and (6.21). If, for example, a spherical system of coordinates is used, the infinite impedance must have the shape of a spherical cap to terminate the driver with an infinite load at the fundamental mode.

Hence, the fundamental mode impedance is in fact a plane wave throat impedance here. Fig. 6.7 shows the calculated and normalized fundamental mode throat impedance of the horn throat for four junction diameters.

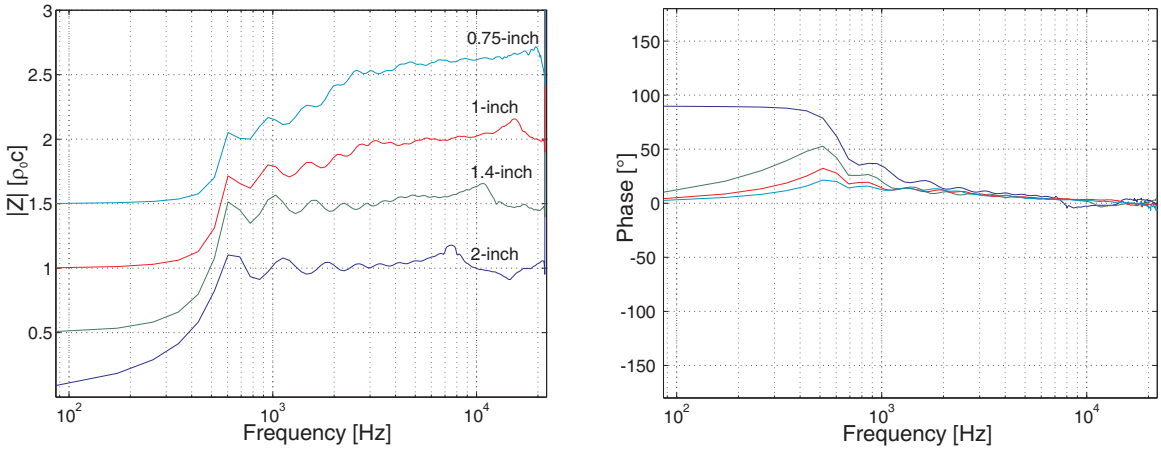

Figure 6.7: Normalized throat impedance for the used reference horns. The magnitude curves are shifted by 0.5 for sake of readability

Solution The system of equations defined by eq. (6.12) to (6.15) can be solved using the conditional equations (6.16) to (6.23). The solution and the used abbreviations are listed in Chapter C.

Measurement example Figure 6.8 shows a complete set of measurements to determine the two-port parameters as described in section 6.1.3. The two investigated drivers are an Electro Voice ND6-8 (driver **T**) and an Electro Voice ND6-16 (driver **S**). The junction diameter is 1.4". The rated electric impedance is 8 Ω for the ND6-8 and 16 Ω for the ND6-16. It is notable how much the electric impedance changes, when the transducer is loaded by different acoustic impedances. This is actually the reason why a method using only electric impedance measurements can work. The better the coupling of the investigated driver to

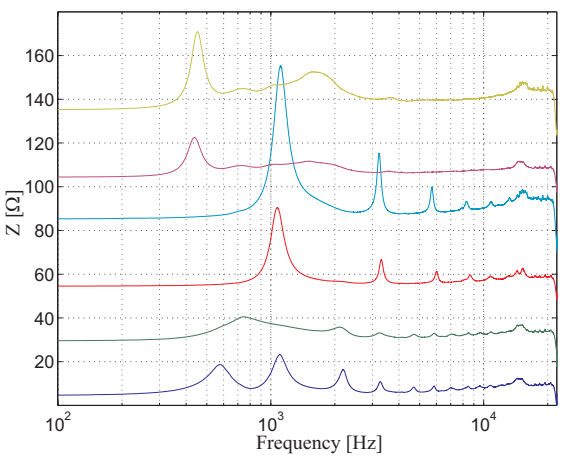

(a) Magnitude of the measured electric impedances according to eq. (6.16) - (6.23). The curves are shifted by 25 Ω for better readability. From bottom to top: $Z_{el,T}|_{I_S=0}$, $Z_{el,T}|_{U_S=0}$, $Z_{el,T}|_{Q_T=0}$, $Z_{el,S}|_{Q_S=0}$, $Z_{el,T}|_{Z_{ac,ref}}$, $Z_{el,S}|_{Z_{ac,ref}}$.

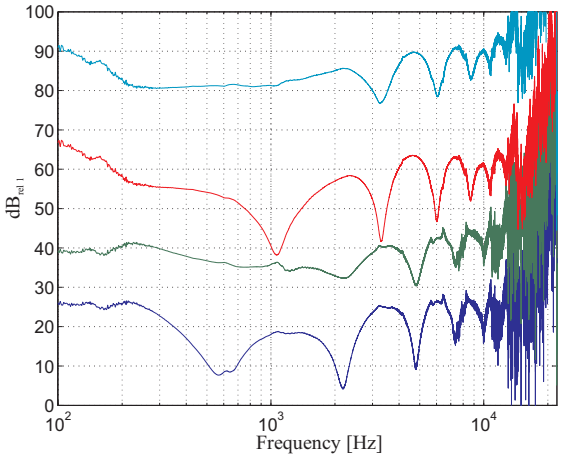

(b) Magnitude of the calculated Parameters of the Electro-Voice ND6-8 (driver **T**). From bottom to top: T_{11}, T_{12}, T_{21}, T_{22}. The curves are shifted for better readability.

Figure 6.8: Measurements (a) and calculated parameters (b) according to method I

the acoustic side the better will be the results obtained for the two-port parameters. The two-port parameters can be calculated using these measurements (Figure 6.8(b)). Above 13 kHz one notices a noise-floor disturbing the result. This can be traced back to the fact that for high frequencies the impedance is dominated by the inductance of the voice coil, so that the feedback from the acoustic side is masked. The second reason is the rather complicated calculation formula eq. (C.4) - (C.14). In order to reduce error propagation within this formula, it is necessary to measure the electric impedances with a high signal-to-noise ratio and additionally with a high precision.

In section 6.1.4, another method is presented leading to an easier solution for the system equations.

6.1.4 Method II - Using Two Identical Drivers

General approach and measurements The method described here also uses two drivers as method I does but two drivers of same type are required. It can be said that this method is a special case of method I. Only one two-port matrix is needed to describe the problem as both transducers should be identical . The definition of the input and output is according to Figure 6.3. The two-port matrix for both drivers is defined in eq. (6.9): the problem is reduced to find four conditional equations, as only one matrix with four coefficients is

used. Again two equations can be derived applying the reciprocity relationships:

$$\det \mathbf{T} = T_{11}T_{22} - T_{12}T_{21} = 1 \tag{6.24}$$

$$-Z_{el,T}|_{Q_T=0} = \left.\frac{U_T}{-I_T}\right|_{Q_T=0} = \frac{T_{22}}{T_{21}}. \tag{6.25}$$

A third equation is found using the set-up shown in Figure 6.6. The driver is loaded by a known reference impedance and the electric impedance is measured:

$$Z_{el,T}|_{Z_{ac,ref}} = \frac{T_{22}Z_{ac,ref} - T_{12}}{T_{11} - T_{21}Z_{ac,ref}} \tag{6.26}$$

The last missing equation can be derived using the following measurement setup:

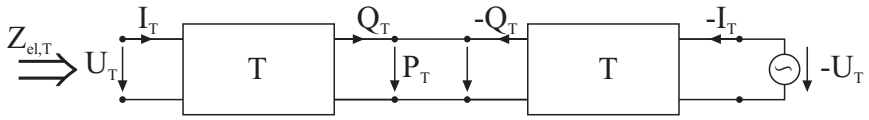

Figure 6.9: Measurement setup with second driver as active acoustic impedance to enforce the pressure to zero.

Both drivers are acoustically coupled. On one side, the electric impedance is measured while the other side is driven by the inverse voltage $-U_T$. This configuration yields a pressure of zero within the common junction. This can be explained by means of antisymmetry as both drivers should behave the same. But also using eq. (6.12) - (6.15) and replacing matrix **S** with **T** leads to this result. The second driver is used as an active acoustic impedance of zero for all frequencies. The corresponding equation can be found by dividing relationship (6.5) and (6.4):

$$-Z_{el,T}|_{P,T=0} = \frac{T_{12}}{T_{11}}. \tag{6.27}$$

Solution Using equation (6.24) to (6.27) the solution can be calculated (see section D).

Measurement example A BMS 4540-8 driver was investigated to demonstrate method II. This is a 1” neodymium type with a rated impedance of 8 Ω. Figure 6.10(a) shows the three impedance measurements that are needed. One can clearly see the difference between the electric impedances when the driver is loaded by different acoustic impedances. With these measurements the two-port parameters of the BMS driver can be calculated. The result is shown in Figure 6.10(c). It is not disturbed by noise and can be used for further calculations up to 20 kHz. In order to compare both methods, method I was also applied to the BMS driver. The calculated parameters are shown in Figure 6.10. Although partially the same measurements are used, the parameters are disturbed with noise below 500 Hz and

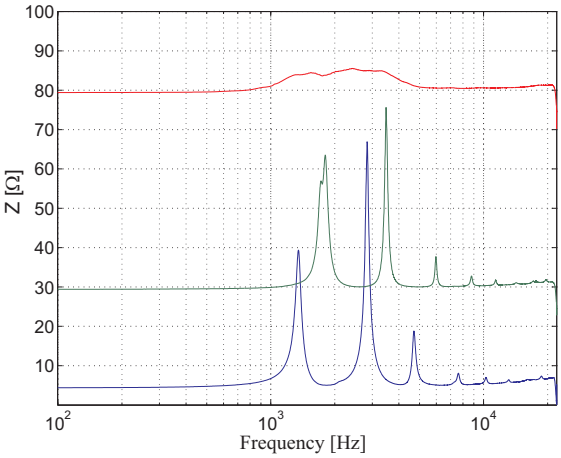

(a) Magnitude of the measured electric impedances according to eq. (6.24) - (6.27). The curves are shifted for better readability. From bottom to top: $Z_{el,T}|_{P_T=0}$, $Z_{el,T}|_{Q_T=0}$, $Z_{el,T}|_{Z_{ac,ref}}$.

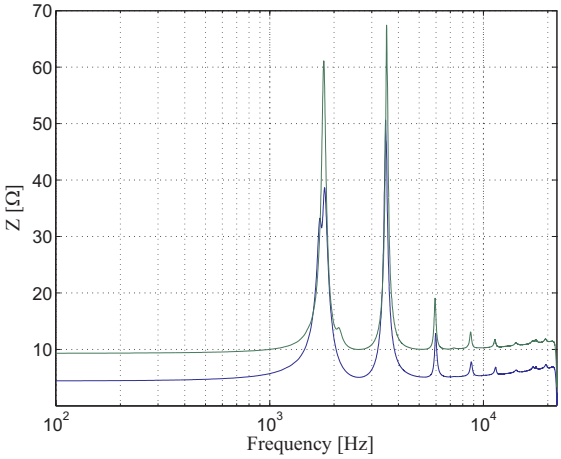

(b) Magnitude of the measured impedance of both BMS 4540-8 drivers. The drivers were terminated by a granite floor as infinite acoustic impedance. One curve is shifted by 5 Ω for better readability.

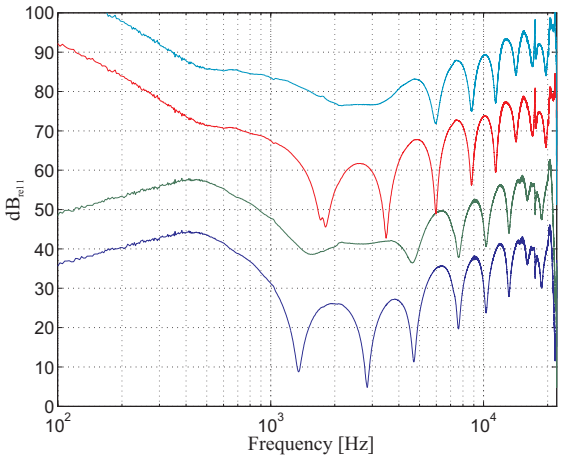

(c) T-Parameters Method II

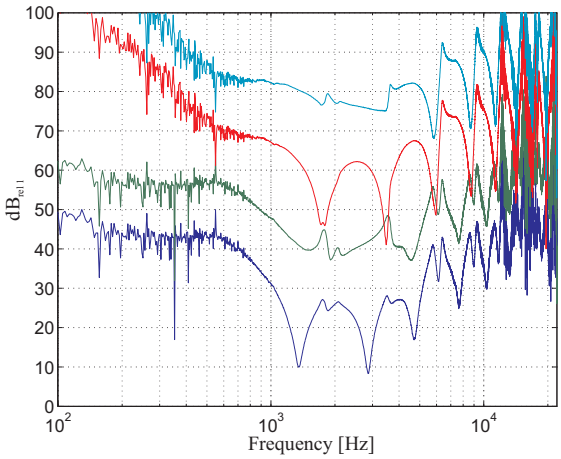

(d) T-Parameters Method I

Figure 6.10: Magnitude of the calculated parameters of the BMS 4540-8 using method I (d) and Method II (c). From bottom to top: T_{11}, T_{12}, T_{21}, T_{22}. The curves are shifted for sake of readability.

above 14 kHz. Furthermore some resonances are visible. This may be a consequence of the rather complicated calculation formula of method I. One can say that method II offers a more simple and reliable way to determine the two-port parameters, but when this method is used it is necessary to have two almost identical drivers.

To check if the drivers are suitable for this procedure, the electric impedance of both drivers can be measured under same acoustic conditions. This should yield the same result if the drivers are almost identical. Figure 6.10(b) shows a comparison of the two BMS drivers terminated by an infinite impedance. The resonances of both drivers should be located at exactly the same frequencies and additionally the impedance at low frequencies should be almost the same.

6.1.5 Some Application Examples for the Fundamental Mode Model

Simulation of driver/horn combinations The most popular application of two-port parameters is the simulation and evaluation of horn driver/horn combinations. The coupling of driver and horn is modeled by the throat impedance which represents the acoustic load $Z_{ac,throat}$ applied to the driver's junction[3]. With this impedance, it is possible to calculate the sound pressure within the junction area. Multiplying the sound pressure with the pressure transfer function H_P of the horn yields the sound pressure on axis P_{onaxis} in 1 m distance. This set-up is presented in Figure 6.11. A more detailed description was published in [BM03] and can also be derived by the modal description discussed in Chapter 4.

Using eq. (6.28) the frequency response can be calculated from the driver's two-port data.

$$P_{onaxis} = H_P U_T \frac{T_{11}T_{22} - T_{12}T_{21}}{T_{22} - \frac{T_{12}}{Z_{ac,throat}}}. \tag{6.28}$$

The data describing the horn's properties can either be measured directly[4] [Mak01], [MB01], or simulated numerically using BEM or other numerical methods (see Chapter 5). The following examples were computed using the latter method to calculate the horn throat impedance and the pressure transfer function of the horn.

The data of the Electro Voice horn driver was obtained using method I (see section 6.1.3), the data set of the BMS 4540-8 driver was obtained using method II (see section 6.1.4).

[3] To be compatible to the papers dealing with the fundamental mode model, the fundamental mode throat impedance is denoted as $Z_{ac,throat}$ instead of Z_h^{00}

[4] The measurement of the fundamental mode horn data is also disturbed by higher order modes, as direct acoustic measurements cannot be avoided. Furthermore it is not possible to separate the influence of higher order modes on the far field of the horn

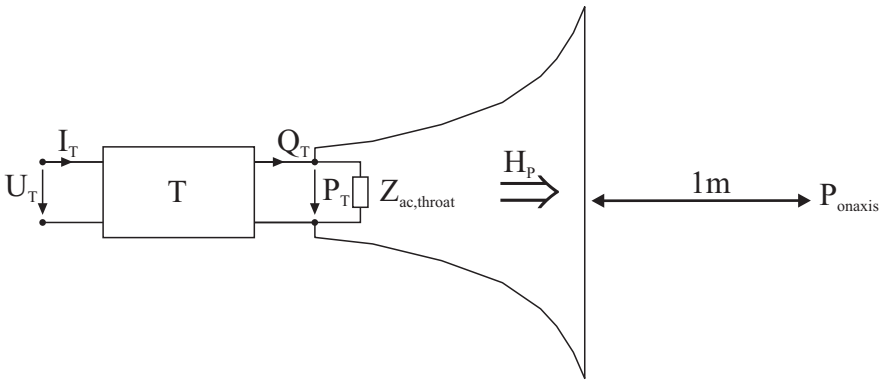

Figure 6.11: Simulation of horn driver/horn combinations

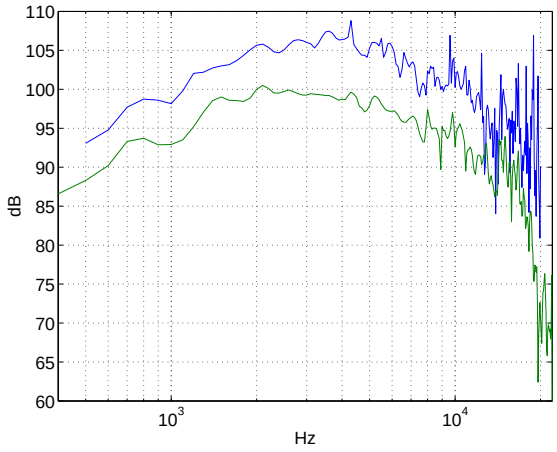

(a) Electro Voice ND6-8 and HP64 cd-horn

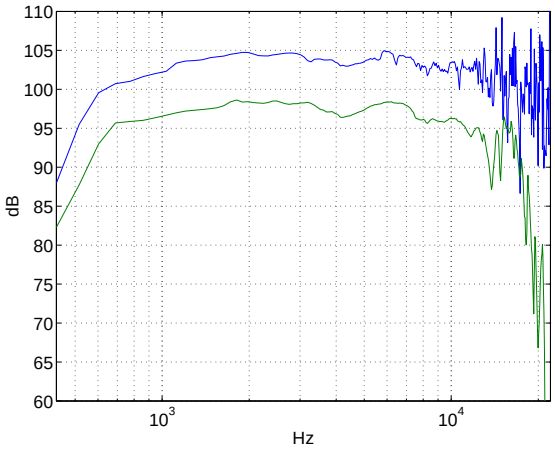

(b) Electro Voice ND6-8 and tractrix horn (see fig. 2.1)

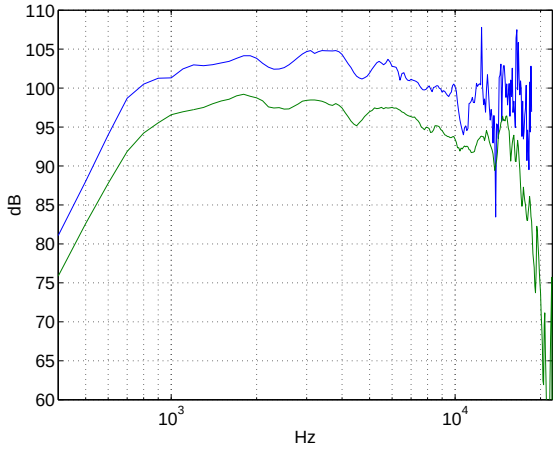

(c) Electro Voice ND6-8 and HP8055 horn

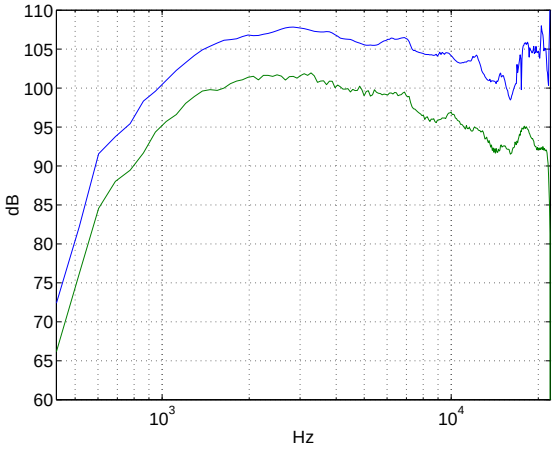

(d) BMS 4540-8 and tractrix horn

Figure 6.12: Simulated/measured on axis frequency response of horn driver/horn combinations. Top left: Electro Voice ND6-8 and HP64 cd-horn. The measured curves are shifted by -5 dB.

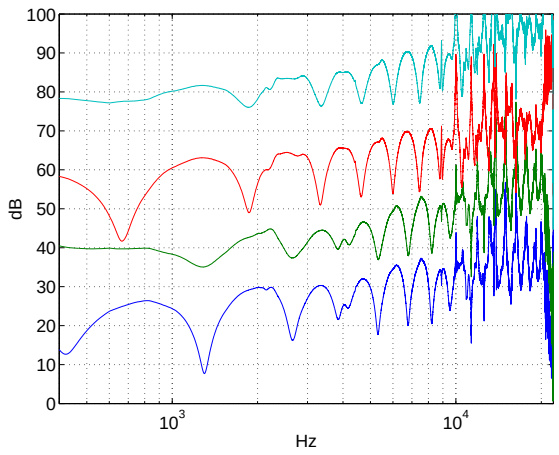

(a) Two-port data JBL 2545-76

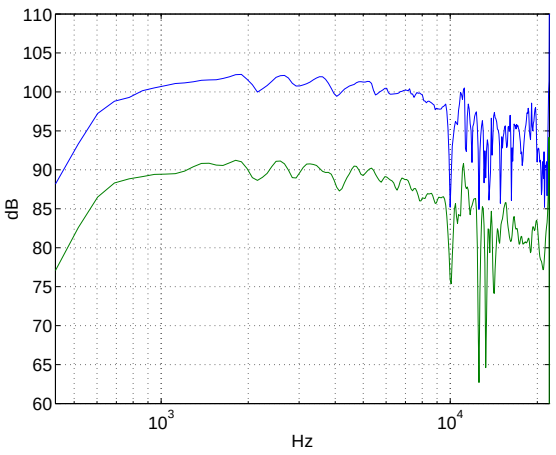

(b) JBL 2545-76 and tractrix horn

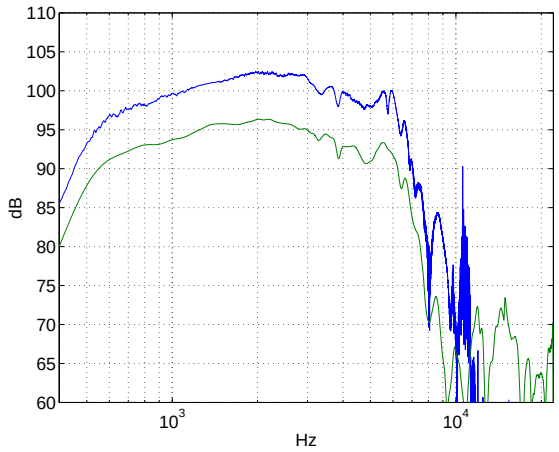

(c) BMS 4592-16 mid-range and tractrix horn

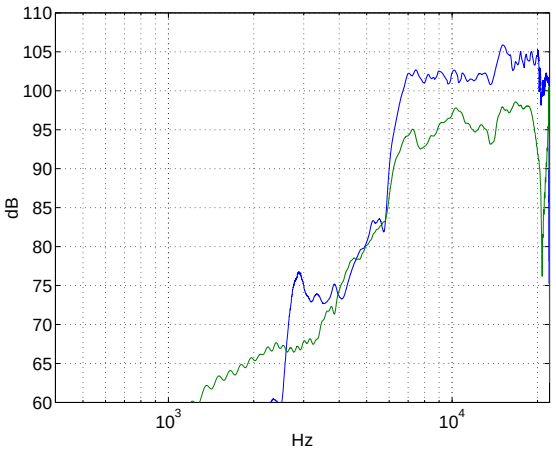

(d) BMS 4592-16 tweeter and tractrix horn

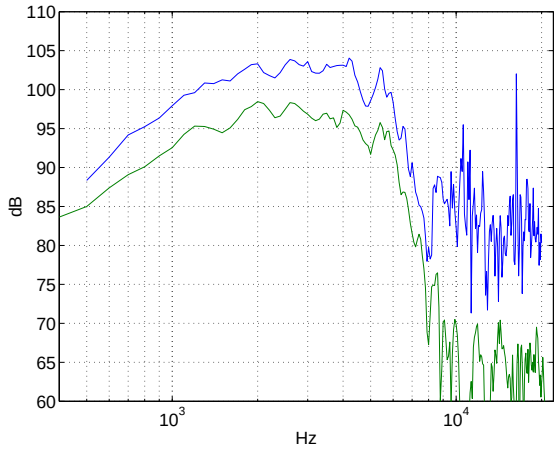

(e) BMS 4592-16 mid-range and HP64

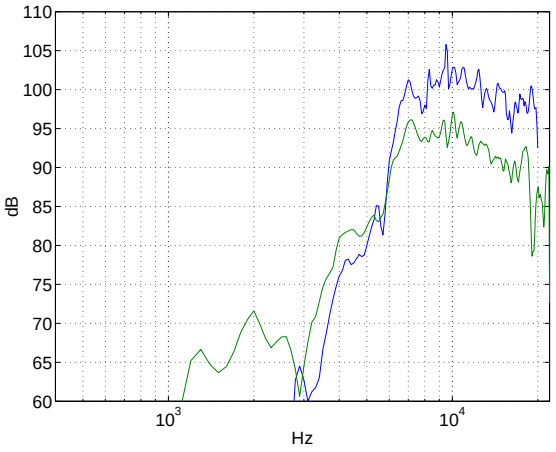

(f) BMS 4592-16 tweeter and HP64 cd-horn

Figure 6.13: Simulated/measured on-axis frequency response of horn driver/horn combinations. The measured curves are shifted by -5 dB. The measured curve in Figure (b) is shifted by -10 dB

Studying the examples (see Figure 6.12) using method I, one notices that the frequency responses are calculated with a high accuracy. Even small resonances are reproduced using this method. The noise in the frequency range above 14 kHz can be traced back to the noise of the driver's two-port parameters. Although the noise limits the overall frequency range it is notable that the upper limit has been extended to approximately 14 kHz for the here investigated 1.4" driver. The upper limit using the method described in [BM03] was about 8 kHz for the 2"-drivers. Looking at the frequency response of the BMS-driver calculated by method II, one can notice that the full frequency range is correctly simulated. There is no noise disturbing the result. Figure 6.13 shows some examples of measured and simulated driver/horn combinations with a diameter of 2". For both drivers, the BMS 4592-16 and the JBL2445-76, method II was used. The BMS driver is a two-way coaxial system. The parameters for the tweeter (6 kHz - 22 kHz) and the mid-range (400 Hz - 6 kHz) were separately acquired. The results show that the simulation frequency range can be extended up to 20 kHz, even when 2"-drivers are used.

Evaluation of horn drivers In professional loudspeaker development, it is necessary to compare properties of different horn drivers to find the most suitable one for the application. This can be done by measuring frequency responses, impedances, etc. of the drivers coupled to a horn or another well known acoustic impedance like an absorbing tube. But the results always will be influenced by the properties of the used acoustic load. It is even more difficult to compare drivers with varying junction diameters. Having obtained the two-port properties of the investigated drivers makes it easy to compare the properties or even to simulate frequency responses without having to build each combination of horn driver and horn.

In order to get a more descriptive representation of a horn driver, a simple acoustic source/impedance model may be extracted from the two-port parameters. The driver is, then, reduced to an ideal acoustic pressure source P_{source} and a source impedance $Z_{ac,source}$ (Figure 6.14(a)). The parameters can be derived from the two-port if it is connected to an

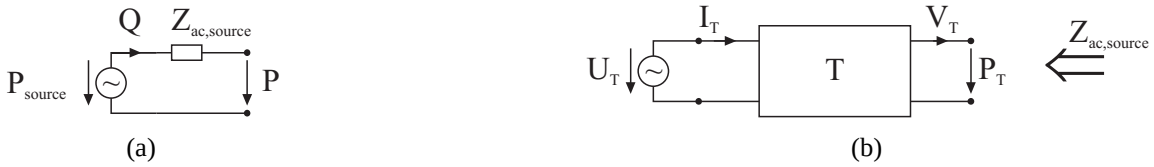

Figure 6.14: Source/impedance model of a horn driver (a) and two-port driven by an ideal voltage source U_T (b)

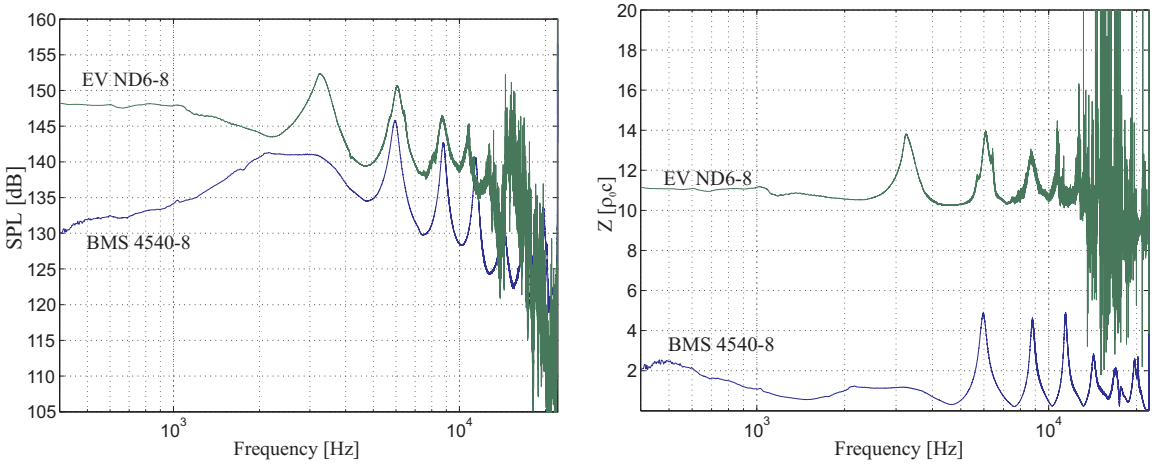

(a) Source pressure of the EV ND6-8 and BMS 4540-8 (shifted by -5 dB).

(b) Normalized source impedance of the EV ND6-8 (shifted by 10) and BMS 4540-8.

Figure 6.15: Source impedance and source pressure of two drivers

ideal voltage source U_T (Figure 6.14(b)). The elements of the equivalent network can be calculated by eq. (6.29) and (6.30).

$$P_{source} = \frac{U_T}{T_{22}} \tag{6.29}$$

$$Z_{ac,source} = -\frac{T_{12}}{T_{22}} \tag{6.30}$$

Comparing both source pressures in Figure 6.15(a), it comes immediately clear that the BMS driver is not capable to deliver as high sound pressures below 2 kHz as the Electro Voice driver does (this is not very surprising because the BMS driver is only a 1” type). Considering the source impedances shown in 6.15(b) one finds that both drivers are perfectly matched to a typical loading situation. The magnitude of the normalized source impedance is about 1 which is exactly the value of a typical fundamental mode throat impedance (see Figure 5.8 and 5.10).

6.1.6 Discussion

Section 6.1.3 and 6.1.4 describe methods to effectively measure the fundamental mode parameters of a horn driver with arbitrary mouth size and shape. By avoiding direct acoustic measurements, the valid frequency range is extended compared to methods using direct acoustic measurements. Although the fundamental mode description is not capable to deal with higher order mode excitation, it is the most suitable model to use in practical applications. The measurements can be carried out very fast and it is merely necessary to measure electric impedances. The only difficulty is to determine the acoustic reference impedance.

Using numerical methods as described in Chapter 5 together with a modal decomposition technique enables to exactly determine the modal impedances. As this has to be done only once for each type of driver outlet, this is not a serious problem. For this reasons, the methods (especially method II) have gained a significant importance in practical development processes of horn driver/horn combinations.

Besides the applications described in this Chapter, similar methods were successfully applied by the author and colleges to characterize particular piezo-electric actuators in a large frequency range [Bug02], [MGRS03], [Ste02].

Chapter 7

Simulation of Nonlinear Properties

The preceding sections of this thesis describe in detail how to model linear properties of the coupled system driver/horn. The used techniques enable to separately treat both systems. This section continues this idea but is focussed on the nonlinear properties.

In almost all professional sound reinforcement systems where horn driver/horn combinations are used, the two most important acoustical properties are the spatial coverage and the maximum sound pressure level that can be reached. The coverage is almost independent of the horn driver [1] , whereas the achievable sound pressure is dependent on driver and horn. It is limited primarily by

- electrical power handling capability
- nonlinearities of the force factor, suspension, etc...
- nonlinearities in compression chamber and horn, due to nonlinearity of the medium

The driver related distortions were investigated, for instance, in [Kli96], [SBSH95], [SBB97], [SB95], [Voi02], [SMPX99]. Common to all methods described in these papers is the high complexity and modelling effort making the models merely interesting for the development of new horn drivers. Hence, the application to the development of a new driver/horn combination, as it is an “every day” process, requires simpler and faster methods. Accordingly, the driver will not be modelled in detail here, but nonetheless considered by some simple measurements.

This Chapter is more focussed on the horn. The ideas described later are based on some new ideas and some rather old formulas known since hundred years or more. The influence of the horn on the distortion characteristic of a driver/horn combination is known

[1] The coverage is almost independent of the driver, as most of the frequency range is dominated by the fundamental mode velocity profile. Although the higher frequencies are sometimes dominated by higher order modes, the characteristic behaviour is normally not changed

for a long time. In 1935, Thuras [TJO35] investigated exponential, axisymmetric horns with the intention to improve the sound quality of the system. Although not yet obvious at this point, even a “distortionless” horn can significantly change the nonlinear properties via its particular radiation pattern. This special property was investigated by [KYS76] to find low distortion horn designs.

Analytical approaches for particular horn geometries, such as axisymmetric exponential horns of finite length, are described in [Bla40], [TJO35], [GM34] and [BM01b]. Although pure analytical approaches are interesting to study the elementary behaviour of distortion in horns, they are not very useful in practical horn development. To be more flexible concerning the flare rate of the horn, some authors use transmission line elements, conical or exponential, to characterize the nonlinear wave propagation within the horn [Kli95], [HM96]. This method is easy to handle, but it suffers from two characteristic problems: the frequency dependent gain of the horn is not taken into account, and, furthermore, the unknown radiation conditions for arbitrarily shaped horns cannot be predicted. This introduces an unpredictable error into the transmission line calculation, especially near the horn’s cut-off frequency. A pure numerical method based on (time domain) finite element modelling (FEM) to calculate nonlinear wave propagation is described by Tsuchiya [TKDT03]. This is the most universal approach to this problem, but one specific problem remains unsolved: as the FEM calculation is based on a finite volume, radiation into far field has to be modelled using other methods. Different approaches are described in [EGT87] and [KYM77]. Tsuchiya uses an artificial boundary with the specific impedance $\rho_0 c$ to limit the field-room for the calculation. It is obvious that the calculation of the nonlinear wave propagation also is limited to this field-room. Besides the error introduced by a too small field-room for FEM, a larger field-room also would produce an error due to dispersion effects of the FEM method in time domain.

The method proposed here is based on the Boundary Element Method. The application on radiation of loudspeakers and horns is described in literature in detail [Hen93], [GH96], [Bri03], [Joh94], [Mak04b], but only with respect to linear properties like frequency response, throat impedance, directivity or modal behavior. When the BEM is used for the purpose of horn optimization, a lot of different variants of geometries are simulated and the result of a BEM calculation is stored as surface pressure (see also section 5.1). From the surface pressure any linear property at any point of the sound field can be calculated using a simple and fast post-processing. The idea presented here is to use the stored surface pressure to calculate an estimation of the nonlinear properties of the horn. The method is

based on the fact that the exact sound field equation can be expanded into a Taylor series. From this expansion it is possible to derive relations between fundamental sound pressure and excited harmonics. Thus, if the linear part of a solution is known, the parts of higher degree can be calculated, as they depend only on the linear part. A complete solution for plane waves including viscosity of the medium was published in 1931 by Fay [Fay31]. The intention of this paper was to show that the energy transfer from fundamental wave to harmonic components finally leads to a stable waveform, as the harmonics are more attenuated by viscosity than parts of the wave with lower frequency. As these effects are only interesting for very large distances, it is convenient to use a more specialized (and not so complicated) solution.

7.1 Nonlinear Wave Equation

The wave equation used here is the exact one-dimensional wave equation for adiabatic changes in a non-viscous medium, based on Lagrangian coordinates, as introduced by Rayleigh in [SR45] and later used by Thuras [TJO35] and Goldstein [GM34] to calculate harmonic distortion in exponential horns.

$$\frac{\partial^2 \xi}{\partial t^2} = \underbrace{c_0^2 (1 + \frac{\partial \xi}{\partial x})^{-\gamma-1}}_{c'^2} \frac{\partial^2 \xi}{\partial x^2}, \tag{7.1}$$

where $c_0^2 = \gamma p_0/\rho_0$, p_0 is the equilibrium pressure, ρ_0 is the equilibrium density, γ is the adiabatic exponent and ξ is the displacement of a particle. Looking at c', it is clear that the phase velocity is dependent on the condensation of the fluid, which leads to the well-known wave steepening at high sound pressure levels.

To calculate harmonic distortion from linear simulation results a relationship between linear sound field properties and harmonic components is required. In [TJO35] Thuras used a relationship between the sound pressure of the fundamental and the sound pressure of the second, respectively, the third harmonic component in a plane wave. He found out that the second harmonic is calculated about 3 dB too low compared to real measurements in a plane wave tube. As exactly the same second order equation is used in the following, the author derived this equation in another way to ensure that the equation is free of errors (see section E).

Hence, the root mean square value (r.m.s.) of the second harmonic $\tilde{p}_2$ in a plane wave related to the r.m.s value of the fundamental $\tilde{p}_1$ is

$$\tilde{p}_2 = \frac{\gamma + 1}{2\sqrt{2}\rho_0 c_0^2} \tilde{p}_1^2 kx \tag{7.2}$$

where x is the distance form the acoustic source to the receiver. It has to be noted, that eq. (7.2) is the solution for large distances x in relation to the wavelength. The results presented in the following are calculated at 4 m distance which ensures that the approximation can be used even at very low frequencies (see section E). Thuras also gives an approximation for the third harmonic pressure in relation to the exciting fundamental:

$$\tilde{p}_3 = \frac{3}{16}\left(\frac{\gamma+1}{\rho_0 c_0^2}kx\right)^2 \tilde{p}_1^3 \tag{7.3}$$

He points out in his paper that even for a long distance x the third harmonic generated by the nonlinearity of the medium is significantly weaker than the second harmonic. This also corresponds to measurements of the author. Hence, in the following, the calculation of air generated distortion is restricted only to the second order. But it is clear that driver generated distortion can be of higher order, as the mechanisms of distortion generation are of another character (will also be briefly discussed). Hence, it is also interesting to be able to calculate how the distortion is transmitted by the horn.

7.2 Calculation of Harmonic Distortion in Horns

The equations in section 7.1, respectively, in section E show that the harmonic components in a one-dimensional pressure wave are only dependent on the pressure wave of first order. These higher order terms can be interpreted as source terms of higher order, caused by the pressure wave of first order. The idea described here is to estimate the source terms of the harmonics by calculating the linear part of the pressure wave using the standard BEM post-processing.

The horn and the outer field-room is theoretically divided into N slices of thickness Δx, where for each slice the linear part and the source terms of higher order are calculated. These source terms are finally integrated to the far field point to get the overall distortion. In order to calculate the linear part for each slice, a line of field points (Figure 7.1) is placed on the main axis of the horn, starting from the connection between driver and horn and ending at the far field of the horn, where the distortion is to be calculated. The distance between the field-points corresponds to the thickness Δx. The results shown below are calculated in $d = 4$ m distance from the horn throat using 2 cm for the slices, which results in 200 field-points to be calculated. Thus, the source term for the second harmonic generated within the i-th slice at frequency f is

$$\tilde{p}_{2,i} = \frac{\gamma+1}{2\sqrt{2}\rho_0 c_0^2}\tilde{p}_{1,i}(f)^2 k\Delta x_i. \tag{7.4}$$

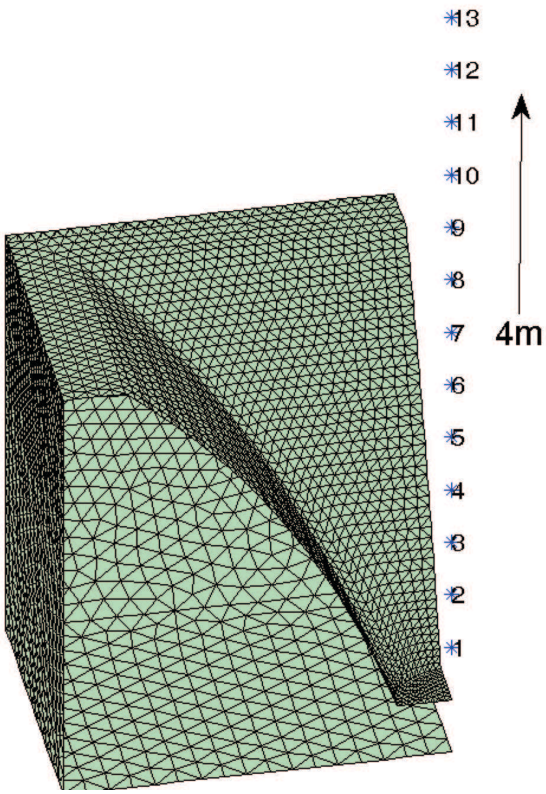

Figure 7.1: Field-points on-axis of a small 60x40 horn with 1.4” throat diameter (quarter sectional view)

As this is based on a plane-wave assumption a correction has to be introduced for each slice taking the frequency dependent gain and radiation pattern into account. This is realized by multiplying each source term by the corresponding pressure transfer-function from the *i*-th slice to the far field point. The distortion caused by the second harmonic at distance d on axis is accordingly calculated by

$$\tilde{p}_2 = \sum_{i=1}^{N} \tilde{p}_{2,i} \frac{\tilde{p}_{1,N}(2f)}{\tilde{p}_{1,i}(2f)} \tag{7.5}$$

In the same way, distortion of higher order can be calculated. As the driver related distortion is not included, the distortion will be a little bit smaller than in reality. This can be fixed by adding a source term for each harmonic caused by the used horn driver. Hence, the final formula for the second harmonic is

$$\tilde{p}_2 = \sum_{i=1}^{N} \left(\tilde{p}_{2,i} \frac{\tilde{p}_{1,N}(2f)}{\tilde{p}_{1,i}(2f)} \right) + \tilde{p}_{2,driver} \frac{\tilde{p}_{1,N}(2f)}{\tilde{p}_{1,1}(2f)}. \tag{7.6}$$

Figure 7.2 shows the simulated fundamental sound pressure level and the second harmonic at 7 kHz over the distance along the main axis of the horn presented in Figure 7.1. The total length of the horn is about 16 cm. The horn mouth (end of the horn) is indicated by

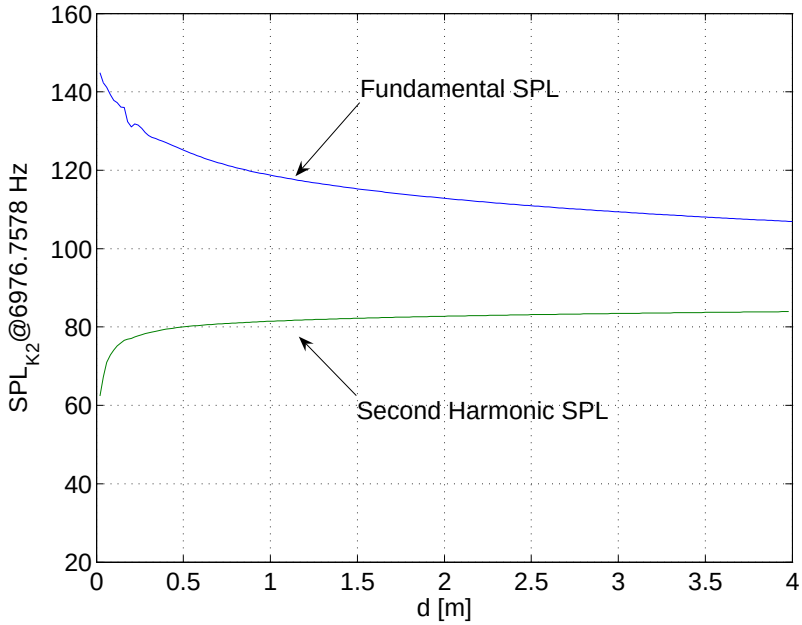

Figure 7.2: Fundamental and second harmonic over distance for a small 60x40 horn with 1.4” throat

the vertical line. As the harmonics are corrected by the corresponding transfer function to the far field reference point (here 4 m distance), the curve cannot be simply extrapolated to larger distances. Hence, the harmonics are already referred to the far field point in this plot. Most of the distortion is generated at the narrow end of the horn, as one would expect. Outside the horn, the distortion does not change as fast but it is obvious that it is not sufficient to simulate only a small portion of the sound field at the horn mouth as this was done by Tsuchiya in [TKDT03]. Especially when simulating (and also when measuring) distortion of horns with small coverage angles this fact has to be taken into account.

7.3 Calculation of the Maximum Sound Pressure Level

A common method to characterize harmonic distortion generated by electro-acoustic systems is plotting the total harmonic distortion (THD)[2] over frequency at a certain sound pressure level of the fundamental or at 1 W nominal input power. For several reasons, the THD is not a suitable measure to characterize distortion, at least, if public address systems are considered. First, the THD value changes with the level of the electric signal. Hence, cross-over filters and equalizing[3] will significantly modify the measured THD. Another problem of this most common measure is the bad correlation to real listening-tests. Several authors have pointed out this fact (see for instance [GL03]). One popular example is the

[2]The total harmonic distortion is the ratio of the summarized harmonic component’s rms values and the rms value of the fundamental.

[3]An equalizer allows to modify the frequency response of the system by inserting (digital or analog) filters into the signal path.

high acceptance of tube amplifiers, which are known for their “warm sound”. This is in fact a result of second order distortion generated by the characteristic curve of the electron tube. On the other side, it is known that odd order distortions are harmful for the sound. Finally, above a certain threshold of nonlinear distortion, everything starts to sound unpleasantly. As this Chapter mainly addresses professional sound reinforcement, the limit of a horn loudspeaker is of great interest. Of course, there is no hard threshold for this limit, but in practice several distortion thresholds are established in the audio community (at least in Germany), which are described in the following.

7.3.1 Horn Related Distortion

The method used here is to characterize the performance of the system via the maximum obtainable sound pressure level in 1 m distance at a certain allowed maximum overall distortion (Max-SPL). This method is more or less independent of the system controller's[4] settings and thus allows to evaluate the real performance of the loudspeaker. A typical maximum distortion level allowed within this measurement is the 10%[5] and the 3% limit for large scale sound systems and the 3% and 1% limit for studio and hifi equipement. The 10% limit can be interpreted as a kind of “threshold of pain for the audience”. The sound pressure at 3% distortion is about the maximum level allowed, where it still sounds pleasantly.

This method can be refined by measuring the Max-SPL for each harmonic separately.[6] Additionally, one can limit the maximum electrical input power during the measurement. This has to be done anyway to prevent the driver from thermal collapse. This limitation corresponds to the functionality of the peak limiter in the loudspeaker system controller.

The Max-SPL with distortion components of the k-th harmonic K_k [%] in 1 m distance is accordingly calculated by

$$L_{K_k} = 20\log_{10}\left|\frac{K_k}{\tilde{p}_k/\tilde{p}_1}\right|^{\frac{1}{k-1}} + 20\log_{10}\left|\frac{\tilde{p}_1(d-l)}{20\mu\,\mathrm{Pa\,m}}\right| \tag{7.7}$$

where l is the length of the horn and d is the distance from horn throat to the far field point used for the simulation. Figure 7.3 shows the simulated Max-SPL for the small 60x40 horn at 10% distortion of the second harmonic referred to 1 m distance. The driver

[4] A system controller is a kind of central processing unit for a large scale sound system: it processes the cross-over filters and equalizing filters and, at the same time, it is used as limiter to protect the loudspeaker from destruction. A state of the art controller is described in [Mül99]

[5] These thresholds are accepted in the audio community. Of course, it is possible to define other thresholds.

[6] A commercial software implementation to perform this kind of measurements is “Monkey Forest” [Goe99].

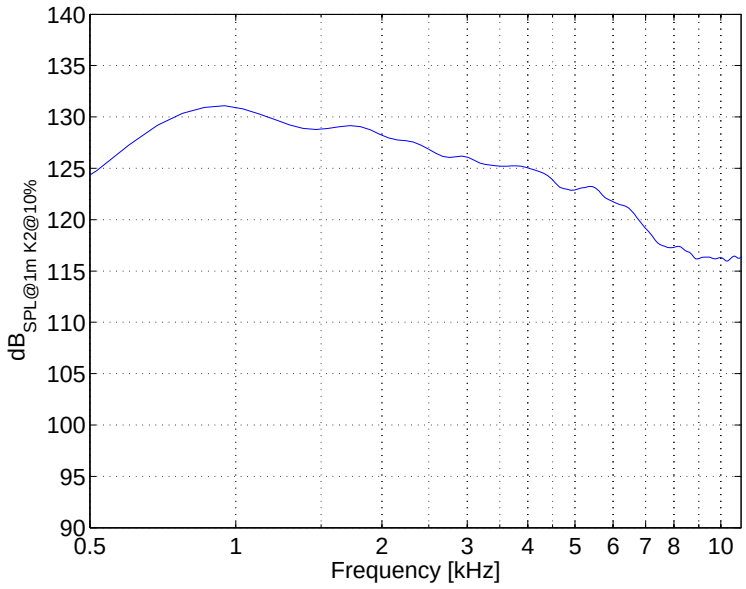

Figure 7.3: Max-SPL at 10% distortion of the second harmonic for a small 60x40 horn with 1.4" throat

related distortion is neglected here. Thus, this curve represents the physical limit for this particular horn as if it was used together with an ideal horn driver. The slope as well as the level of the curve is typical for small scale 1.4” horns of this type. It has to be noted that the difference between a simulation assuming an ideal, distortion-free horn driver and a measured result, respectively, a simulation which consideres driver generated distortion, may be rather large. At low frequencies, particularly below the lowest resonance frequency of the considered driver, the difference is significant. Hence, it is for practical purposes necessary to additionally consider the distortion generated by the acoustic source.

7.3.2 Driver Related Distortion

In Section 7.2, it was proposed to consider the driver related distortion by an additional source term in eq. (7.6). The intention of this section is to show under which assumptions, respectively, under which conditions this simple model will yield an accurate result.

The problem of this equation is, actually, that the influence of the horn on the driver is not considered. Hence, this equation will, in general, yield an accurate result if no influence exists (provided that the driver source term is correctly acquired). Accordingly, to estimate under which condition the horn provides a feedback on the distortion generation inside the driver, it has to be known how the horn influences the generation of distortion.

In the following, the mechanisms of distortion generation within the driver are briefly reviewed. For a more detailed review, it is referred to the literature cited in the introduction of this Chapter.

The mechanisms for generation of nonlinear distortion within the driver are manifold

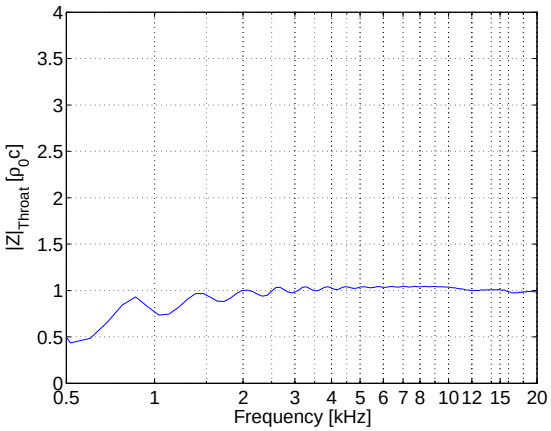

(a) 40x30 with 12x12” mouth

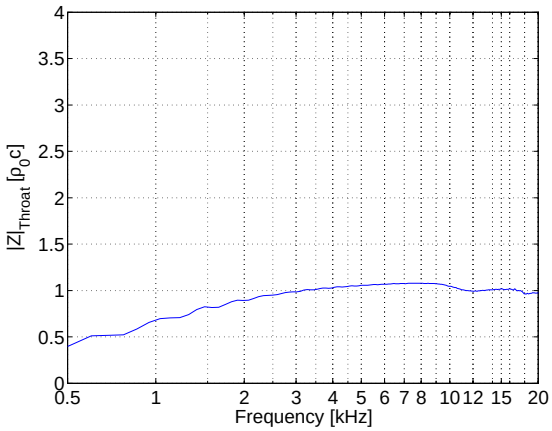

(b) 60x40 large format horn with 24x16” mouth

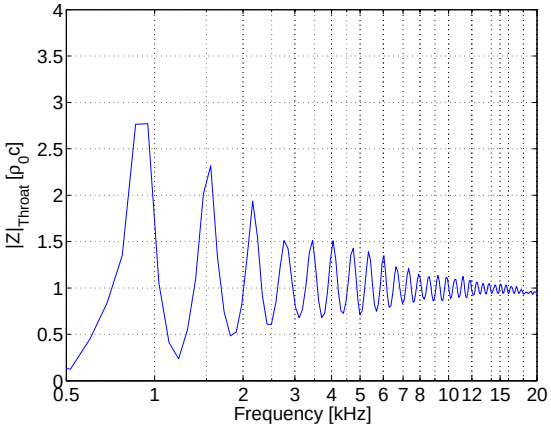

(c) very long 60x40 horn with 10x8” mouth

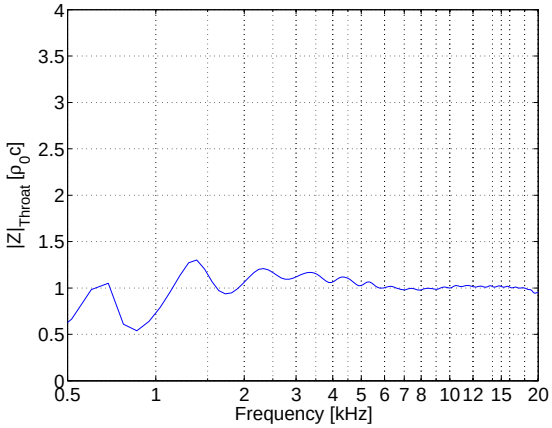

(d) 60x40 small format horn with 12x6” mouth

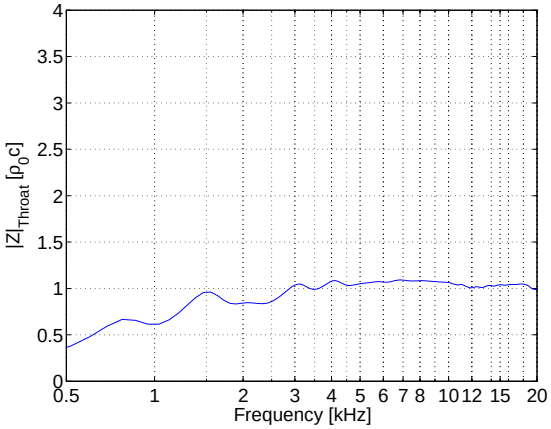

(e) 90x40 small format horn with 12x6” mouth

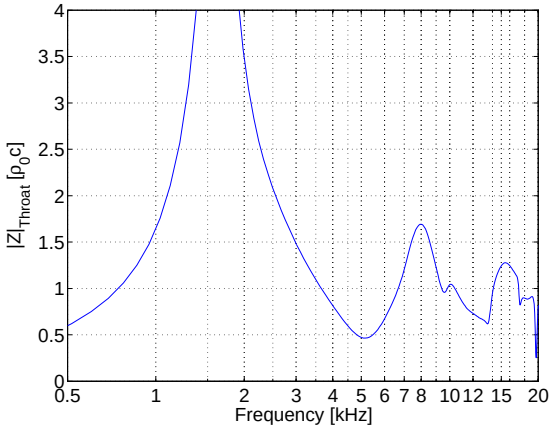

(f) 100x40 very small format horn with 4.7x4” mouth

Figure 7.5: Simulated fundamental mode throat impedances of the investigated horns. The results are normalized to $\rho_0 c$

and, furthermore, some of them are dependent on the acoustic load at the driver's outlet (see Figure 7.4). This load is transformed down to the membrane via the short tube/phase

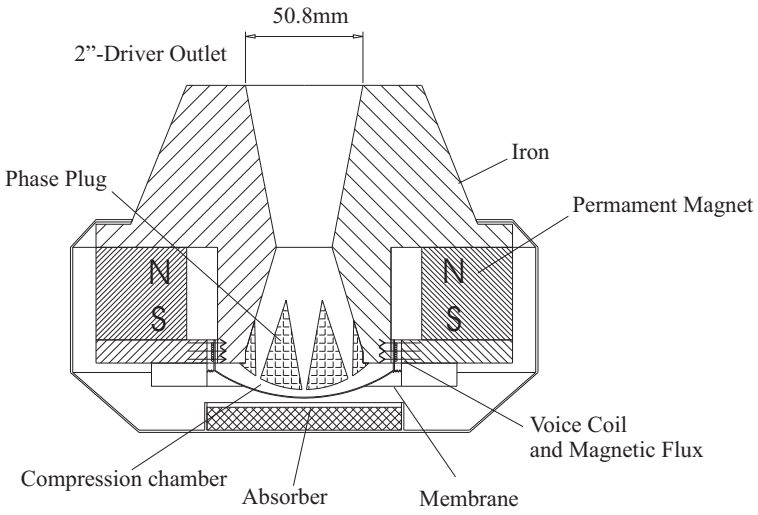

Figure 7.4: Sectional view of a typical (old-fashioned) horn driver.

plug in front of the membrane and, thus, represents a particular loading for the mechanical resonator. The displacement of the membrane is accordingly influenced by this load. Hence, any mechanism which generates distortion depending on the membrane excursion will be influenced by the horn loading. For instance, the compliance of the suspension and the force-factor are nonlinearly dependent on the membrane excursion (see for instance [Kli90]). It is obvious at this point that a simple model, as the driver source term in eq. (7.6) is, will not be capable to describe all these effects.

To estimate under which condition this simple model will be accurate, it is necessary to compare horn throat impedances of different horns to each other.

Figure 7.5 shows a selection of simulated fundamental mode throat impedances. For high frequencies, all impedances converge to the specific impedance of the fluid. At low frequencies, the impedances show a more or less resonant behaviour. Furthermore, smaller horns show larger deviations from the specific impedance. Hence, it has to be expected that the distortion calculated by simply considering a driver source term will yield to accurate results at high frequencies, respectively, for large horns connected to the driver.

Measurement of the driver source term With the extended post-processing described before, it is possible to estimate the distortion generated by the driver.

Figure 7.6 shows a simulated Max-SPL curve and a real measurement of the same horn connected to a horn driver. The simulation was calculated by eq. (7.7). The driver source term in eq. (7.6) was set to zero for this simulation. Hence, the curve represents the nonlinearities generated and transmitted by the horn. From 1 kHz to 20 kHz, the simulated

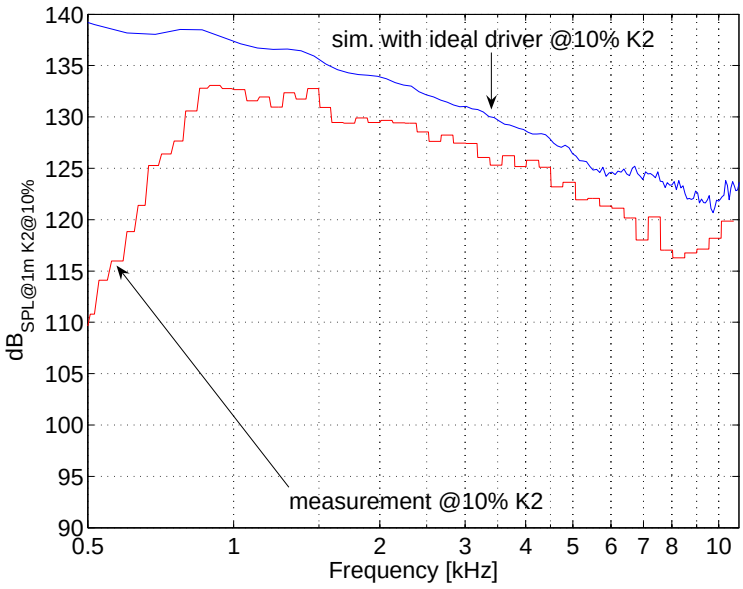

Figure 7.6: Simulation of the Max-SPL at 10% second harmonic distortion and measurement of the same horn connected to a horn driver

Max-SPL is only 3 dB to 4 dB too high, but at low frequencies the difference is rather large and increases with decreasing frequency. The difference between measurement and simulation can be used to calculate the distortion generated by the driver. The overall second harmonic distortion can be calculated by

$$\tilde{p}_2 = \frac{\tilde{p}_1^2(d-l)K_2}{\tilde{p}_{meas,K2}} \tag{7.8}$$

where $\tilde{p}_{meas,K2}$ is the measured second harmonic rms value at 10% distortion and $\tilde{p}_1$ is the fundamental sound pressure simulated at a distance d from the horn mouth. l is the length of the horn. Hence, for the second harmonic the driver source term is calculated using eq. (7.8) and eq. (7.6):

$$\tilde{p}_{2,driver} = \left(\tilde{p}_2 - \sum_{i=1}^{N} \tilde{p}_{2,i}\frac{\tilde{p}_{1,N}(2f)}{\tilde{p}_{1,i}(2f)}\right)\frac{\tilde{p}_{1,1}(2f)}{\tilde{p}_{1,N}(2f)} \tag{7.9}$$

As said before, the driver distortion is influenced by the horn throat impedance. To consider this effect, an empirical factor can be introduced to improve the accuracy of the simulation (at low frequencies and for small horns):

$$\tilde{p}_2 = \sum_{i=1}^{N}\left(\tilde{p}_{2,i}\frac{\tilde{p}_{1,N}(2f)}{\tilde{p}_{1,i}(2f)}\right) + \underbrace{\left(\frac{Z_{throat}(f)}{Z_{throat,ref}(f)}\right)^{1.4}}_{\text{empirical factor}} \tilde{p}_{2,driver}\frac{\tilde{p}_{1,N}(2f)}{\tilde{p}_{1,1}(2f)}. \tag{7.10}$$

This factor considers the difference between the throat impedance of the horn used to calculate the driver distortion and the horn under investigation. As it is just a “first order empirical factor”, based on a simple comparison between measurements and simulations, it has to be critically reviewed at the end of this Chapter. Anyhow, it is just a small correction and gives some improvements of the results at low frequencies.

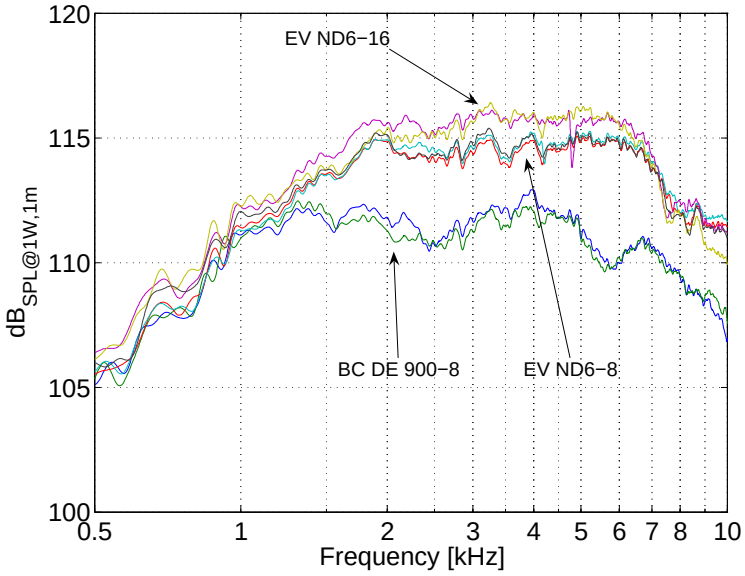

Figure 7.7: On axis frequency response for all drivers measured using a mid-size 40x30 horn as acoustical load

7.4 Measurements and Simulations

To verify the method described in this paper, a number of measurements with 1.4” drivers and horns were made and compared to simulation results. In a first step, the variance of the used drivers concerning their on-axis frequency response and their obtainable maximum sound pressure level were investigated. The transducers for the measurements were two BC DE900-8 drivers, manufactured in Italy, two Electro Voice EV ND6-16 and three Electro Voice ND6-8 drivers. The sound pressure level of those drivers (Figure 7.7) differs about 2 dB to 4 dB. Accordingly, it was expected that the Max-SPL would also differ by 2 dB to 4 dB.

Figure 7.8(a) shows the Max-SPL measurements for the seven drivers connected to the same 40x30 mid-size horn. The electrical input power was limited to 150 W for this measurements which can be a lot for a 1.4” driver. At frequencies below 1 kHz, the differences between the driver’s Max-SPL are about 10 dB, but for higher frequencies they reach almost the same sound pressure level. As the peak power is limited to 150 W it happens that, especially in the frequency range from 1 kHz to 4 kHz, the physical limit could not be reached. The limitation is, of course, necessary to prevent the voice coil from damage.

The same measurements were analysed concerning the total harmonic distortion of second *and* third harmonic. Figure 7.8(b) shows the result of the K_2 measurement and the K_2 plus K_3 measurement for the EV-ND6-8 and the 40x30 horn. As there is no noticeable difference within the Max-SPL results, it can be concluded that the second harmonic normally is predominant. Regardless of this fact, the measurements presented in the following were evaluated up to the third harmonic and the 3% limit was measured, too. It is possible to

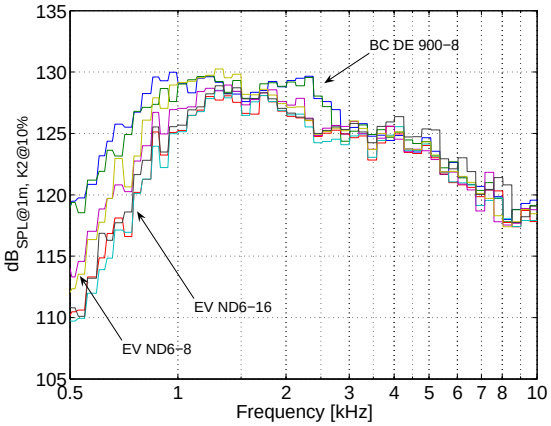

(a) Max-SPL referred to 1 m distance measured up to K_2 at 10% using a mid-size 40x30 horn referred to 1 m distance

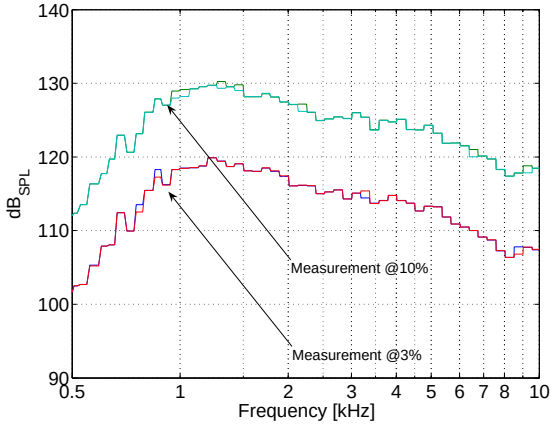

(b) Comparison of the Max-SPL of the EV ND6-8 referred to 1 m distance measured up to K_3 at 10% and 3% and measured up to K_2 at 10% and 3% using a mid-size 40x30 horn

Figure 7.8: Maximum sound pressure level of the investigated drivers

conclude from the 3% result if the third harmonic limits the measurement at 10%: if K_2 is predominant, the level difference of the 10% result and the 3% result has to be 10 dB. If the difference is smaller, the peak power limiter was activated or the third harmonic is dominant.

The horns used for this investigation ranged from very large to very small and also had different radiation patterns (40x30 to 100x40). A selection of results is presented in Figure 7.9. Each plot shows a measured 3% and 10% result, a simulation for the horn with the driver source term set to zero (ideal distortion free driver) and the simulation with driver source term considered (black bold curve). The horn used to calculate the driver's source term was the large format 60x40 horn (Figure 7.9(b)). It was selected as reference horn because it has a very smooth throat impedance. All results are calculated using the empirical correction for the throat impedances. The impedances of the horns are shown in Figure 7.5.

When comparing the simulation (black, bold curve) with the measurements one finds an excellent accuracy which makes this post-processing tool indispensable for the horn development. Of course, some deviations, mainly at low frequencies, are visible. But, if the simplicity of the whole procedure is compared to a complete nonlinear sound field simulation, it is a very surprising result. Furthermore, the errors can be explained by the loading properties of the horns as predicted by the considerations in section 7.3.2. The largest errors occur at the simulation of the smallest horn with the most resonant throat impedance

(Figure 7.9(f) and 7.5(f)). The large differences between ideal driver simulation and simulation with driver source term at low frequencies can also be explained by the influence of loading characteristic and displacement of the driver's membrane. Especially below the resonance frequency of the transducer, the system is very sensitive to changes in the loading impedance. Figure 7.9(c) additionally shows a comparison between a simulation with "empirical correction factor" (black, bold curve) and without considering this factor (grey, bold curve). At high frequencies, both curves are almost identical. Between 600 Hz and 1 kHz the result is improved a little bit, but below 600 Hz the deviations get larger with this factor. Hence, to cover all possible load cases (compare Figure 7.5(c) with 7.5(b)), it is necessary to replace the simple correction factor.

A further improvement could be achieved by measuring the driver source term under several different load cases. The horns or acoustic loads used for this measurement should significantly differ in their throat impedances. Due to the different loading conditions, these source terms should also show some differences. For a simulation, the driver source term is then to interpolate from this set of measurements according to the throat impedance of the considered horn. The practical implementation of this simple idea is, unfortunately, not such simple. Besides the influence of the magnitude of the throat impedance it is, of course, necessary to consider the influence of the phase. A promising impedance for this measurement is, for example, the "infinite impedance". Other useful configurations could be realized by using cylindrical ducts (also terminated by an infinite impedance) as loading device. Different magnitudes and phases of the "throat impedance" could be generated by varying the length of the duct.

Concerning the measurement itself it has to be stated that even small influences of the room change the result. A small reflection, which normally could be eliminated using a suitable windowing technique, is visible in the results. Looking at the result of the large reference horn in Figure 7.9(b) a small dip and peak occur at 7 kHz. If this was a property of the horn it should not be visible at the other measurements, too. Hence, a measurement error will also falsify the driver source term and may cause errors at other simulations. Finally, it has to be mentioned that the variances among drivers of the same type and the influence of the measurement conditions may cause larger errors than the simulation method itself.

7.5 Discussion

This method has some advantages over other methods (see the introduction) although it is not an exact nonlinear solution of the sound field. First of all, it is a fast method, as it is based on results which are already calculated. The second point is that the transfer functions into the far field and, thus, the frequency-dependent gain of the horn, are taken into account with this method. The accuracy is quite high especially for mid-size and large horns, as the distortion generated within the horn seems to dominate the overall distortion (at high frequencies). As this method enables to calculate the physical limit of a horn, independent of the driver, it allows an interesting insight during the development process of horn geometries. Especially the slope of the Max-SPL curve is simulated very accurately. Hence, it is possible to compare different horn geometries during the optimization process concerning their nonlinear behaviour. This, actually, was the main goal: to use the BEM method to estimate the nonlinear performance of different horn geometries. If a driver source term is measured and considered in the simulation results, the measured and simulated results are very close, even at low frequencies. Future work has to concentrate on improving the measurement set up to acquire the nonlinear driver source term in dependency of the complex throat impedance.

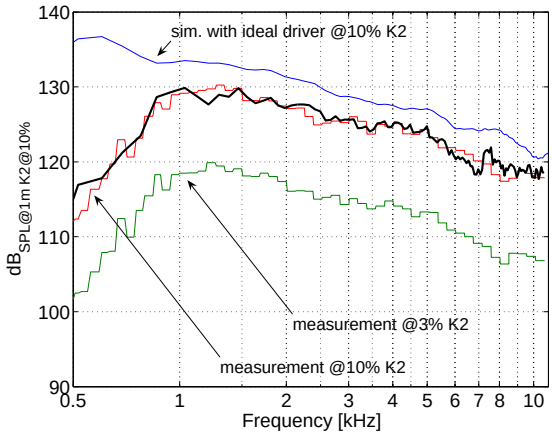

(a) 40x30 with 12x12” mouth

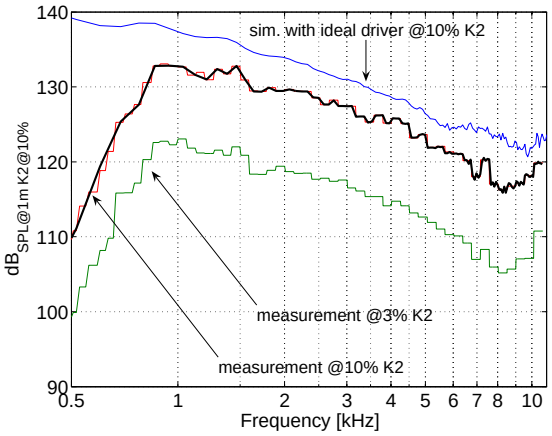

(b) 60x40 large format horn with 24x16” mouth

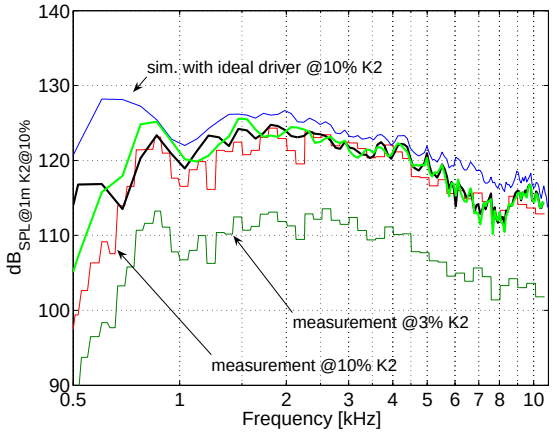

(c) very long 60x40 horn with 10x8” mouth

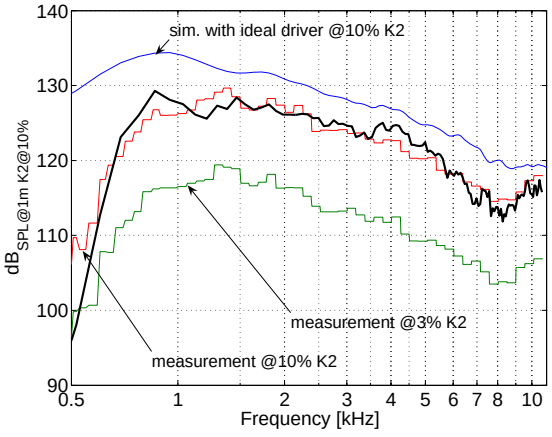

(d) 60x40 small format horn with 12x6” mouth

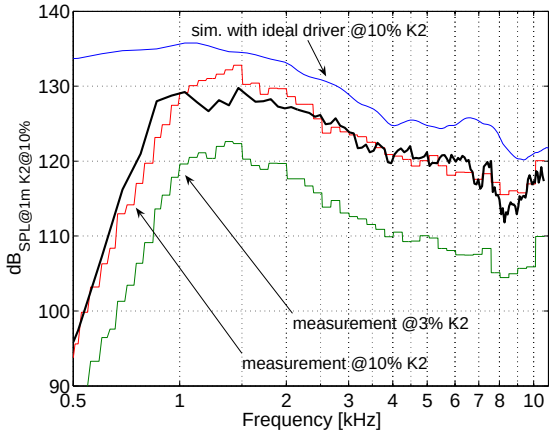

(e) 90x40 small format horn with 12x6” mouth

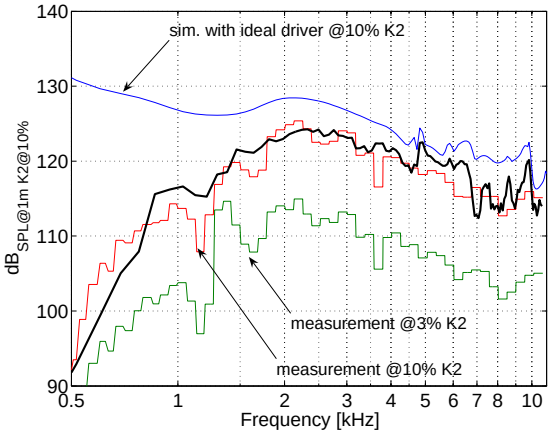

(f) 100x40 very small format horn with 4.7x4” mouth

Figure 7.9: Max-SPL at 10% distortion of the second harmonic simulated and measured with 10% and 3% threshold for K_2 and K_3. The electrical peak power was limited to 150 W. All results were measured and simulated at 4 m distance and are referred to 1 m distance to the horn mouth

Chapter 8

Professional Development of Loudspeakers

In this Chapter, it is demonstrated how the methods and parameters described in this thesis are applied to a typical development process: designing a horn driver/horn combination which has the desired acoustic properties.

At the very beginning of such a project the installation space for the horn is defined. The geometrical dimensions are, normally, coupled to the size of other components. In this fictive project, a 12” or a 10” woofer is used. Hence, the width of the horn must not exceed the diameter of the 10” woofer[1]. Accordingly, the horn geometry to be developed must not exceed the following dimensions:

- maximum front dimensions 250 mm x (approx.) 190 mm (overall width x height)
- flange width 20 mm (is needed for mounting the horn)
- maximum length of the horn, measured from the cut-plane of driver and horn 130 mm

Additionally, it has to be considered that in some cases the horn may be produced with a single part injection mould. Hence, the geometry must not have any undercuts. Otherwise it could not be removed from a single part mould.

For the acoustic properties, the parameters listed in the introduction are used here as design goal:

1. nominal angle of 60° x 40° (horizontal x vertical)
2. cut-off frequency of the horn as low as possible

[1] Of course, it is possible to combine a large horn with a small woofer, but a lot of space on the front baffle would be waisted using such a combination.

3. maximum sound pressure level (10% threshold for the harmonic distortion) should be about 125 dB to 130 dB in the mid-frequency range and must not be smaller than 120 dB at high frequencies[2]

4. the driver outlet diameter is 1.4” (35 mm)

8.1 Horn Optimization

At the beginning of the project, the driver might not be selected yet. Hence, for the moment this is a pure horn optimization task. Although it might sound strange to develop the horn without knowledge about the driver, it is the most common task. The reason is obvious: a horn is normally not used for only one particular loudspeaker, but it will be used in different families of loudspeaker systems together with different drivers. This trivial reason may underline the importance of knowing common driver properties.

8.1.1 Development of the Geometry

As the type of driver is not known at the beginning of this project, it is merely possible to use the common properties which resulted from the practical investigation (Chapter 3). Hence, a fundamental mode velocity profile should be used for excitation. In the following, the eigenfunctions of the cylindrical duct are used. Additionally, it is known from the pressure/velocity scanning that the modes start to dominate the profile above a certain transition frequency. Furthermore, the composition of modes is more or less an individual property of each type of driver. This frequency is about 14 kHz for 1.4” drivers. As the composition of dominating modes may influence the directivity in this frequency range (see Figure 5.12), it does not make any sense to optimize the directivity pattern from 14 kHz to 20 kHz with respect to the directivity results. But remembering the influence of the radiation pattern on the transmission of nonlinear driver and horn distortion, it may be interesting to optimize the frequency range above 14 kHz with respect to the nonlinearities (see also Chapter 7).

Another point to discuss is the definition of the lower cut-off frequency. Usually, it is defined together with a driver as the overall sensitivity has to be simulated together with the driver’s properties. The cut-off can be defined, for instance, at the -3 dB drop-off of the sensitivity. In this case, it makes sense to define the cut-off as -6 dB drop-off of the fundamental mode throat impedance because the coupling of driver and horn is determined

[2]To avoid confusion here: the sound pressure level is obtained in a full space measurement. Many vendors of PA-equipment give this value under semi-anechoic conditions which leads to a cosmetic gain of 6 dB maximum sound pressure level

by the throat impedance. This corresponds to -3 dB radiated sound power and gives a very good estimation, too.

The very first step is to make some rough “snapshots” of simulations. Although the results are not as accurate as fine simulations, the snapshots are of great importance. First of all, it is absolutely necessary to know if the outer dimensions of the horn are sufficient to create the defined acoustic properties. It is, of course, possible to estimate the lower cut-off by simply considering the length of the horn[3], but it is not such a trivial task (though possible) to know the lower cut-off of the nominal angles.

Snapshot simulations This kind of simulation is not a special technique, but it is a reduction of accuracy to accelerate the simulation. At first, the number of frequencies are reduced. In the following, the mid frequencies of 18 one-third-octave bands from 400 Hz to 20 kHz are used. Of course, some details may be hidden between these frequency bins, but it will give an almost complete picture of the properties. The second reduction is obtained by using a much too coarse mesh. In Chapter 5.1, it was explained that a linear interpolation of the surface potentials requires at least six nodes per wavelength. This configuration would lead to a node distance of about 3 mm to simulate a horn up to 20 kHz. But it is possible to use a particular mesh: the error introduced will be small if the node distance is distributed inversely to the level of the surface pressures. Hence, regions with vibrating faces have to be meshed with a smaller node distance and vice versa. This could be shown by some mathematical considerations, but the results presented later will show the feasibility of the snapshot method. The last simplification is, of course, to merely simulate quarter sections of the horn. This would not be possible with a full modal simulation, as the non-symmetric excitation distribution of the eigenfunctions requires a simulation without using planes of symmetry.

It is a good idea to start the first snapshot using a conical geometry which fits into the maximum dimensions given. The mesh is shown in Figure 8.1(a). It is made of 751 nodes. The snapshot simulation for the 18 frequencies and the post-processing requires about one to two minutes (Intel P4/3.2 GHz).

In Chapter 2, it was mentioned that the pure conical horn’s directivity is normally not very suitable. The results underline this statement. The directivity is far away from a constant coverage as it is usually needed for the high frequency reproduction. This particular

[3]The estimation is based on the fact that at low frequencies the horn is more or less a tube loaded by the radiation impedance of a vibrating piston at the mouth. As this impedance is very small at low frequencies, the first resonance of the horn can be found at a quarter wavelength fitting into the length of the horn. 13 cm gives a lower cut-off of about 650 Hz.

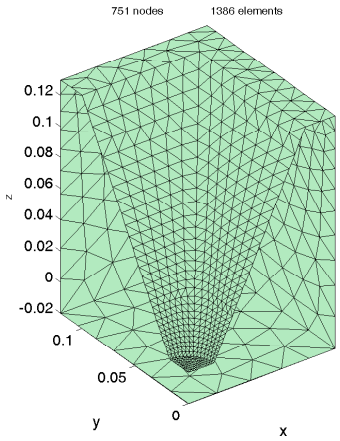

(a) Coarse mesh

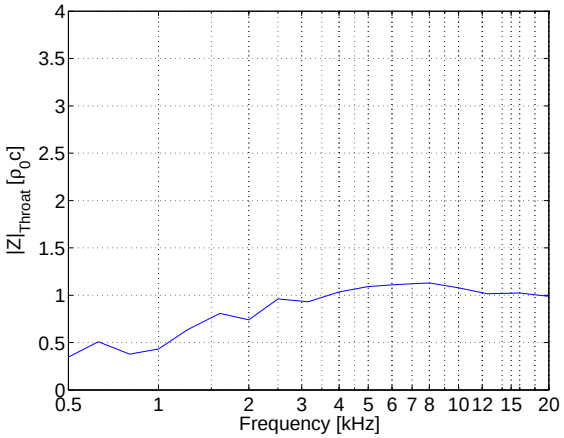

(b) Normalized magnitude of the fundamental mode throat impedance

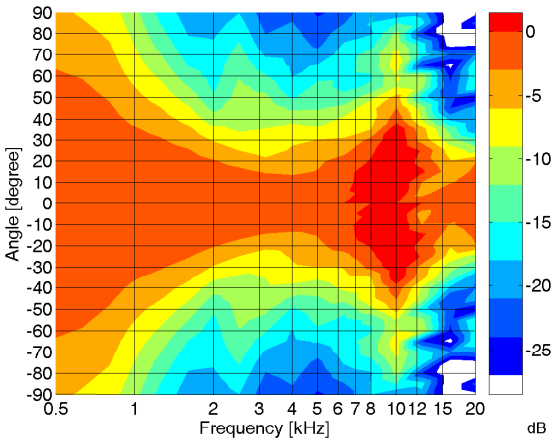

(c) Fundamental mode horizontal directivity

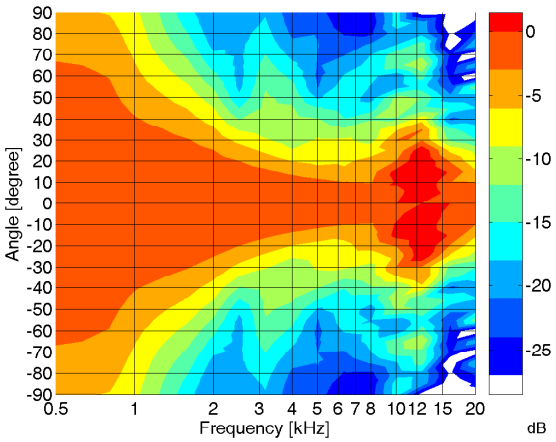

(d) Fundamental mode vertical directivity

Figure 8.1: A set of snapshot simulation results and the mesh of the conical horn

pattern created by conical horns is typical: a small coverage at mid-frequencies and a wide dispersion at high frequencies. Hence, it has an own name: midrange waist-banding. It gave also initiations to some investigations in the past to improve the directional characteristic, respectively, to find generalized designs for the so-called *constant directivity horns* (CD-horn) [Joh94], [HU78], [Sin80], [Kee83], [Hug99], [CD00], [SCD01], [CDS01]. The difficulty to create a constant coverage has mainly to do with the fact that, normally, 3 to 5 octaves are covered by a single horn. In the case considered here, the conical horn indicates that a 60° horizontal coverage is possible from about 2 kHz and the 40° coverage is possible above 4 kHz. Taking the upper limit of the directivity optimization (14 kHz) into account, a bandwidth of 3 octaves has to be considered in the directivity optimization.

To reach the design goal, the directivity has to be narrowed around 10 kHz and widened around 3 kHz. The focus is on the important mid-frequency range. Furthermore, the horizontal coverage should be optimised preferably. To modify the directional behaviour systematically, one has to consider the nature of wave propagation. A significant influence requires changes in the same dimension as the dimension of the wavelength is. Hence, it is evident that a modification of the high frequency pattern requires a small change and a mid-frequency modification needs larger changes of the geometry. At this point, it seems obvious to use an automated system to find the optimum. A system to exactly do this was investigated by Henwood and Geaves [GH96] for axisymmetric geometries. As the number of varieties are rather large in the full 3-dimensional case, a lot of additional expertise would be necessary to use for the algorithm. Anyhow, to investigate 3-D automated horn design is an interesting task for the future (not only as a lot of CPU power is required), but the author uses “manual optimization”. With some experience it is also possible to find suitable geometries.

Figures 8.2 and 8.3 show the first evolutionary steps of the horn. Version 2 (version 1 was the conical horn) shows a nearly perfect horizontal pattern (despite a very little waist-banding at 3 kHz). Looking at the vertical directivity, it has to be stated that the 40° are more or less 45°. Accordingly, the task of the further versions was an optimization of the vertical pattern and adding some slight corrections to the horizontal. Version 10 seems interesting enough to have a closer look at it. The vertical direction is narrow enough in the mid-frequency range and, at the same time, it shows an almost perfect horizontal behaviour.

High resolution simulations The high resolution simulations are needed for several reasons. The estimation of nonlinear properties, as described in Chapter 7, uses a lot of field points in the near-field of the geometry for the post-processing. A too coarse mesh could

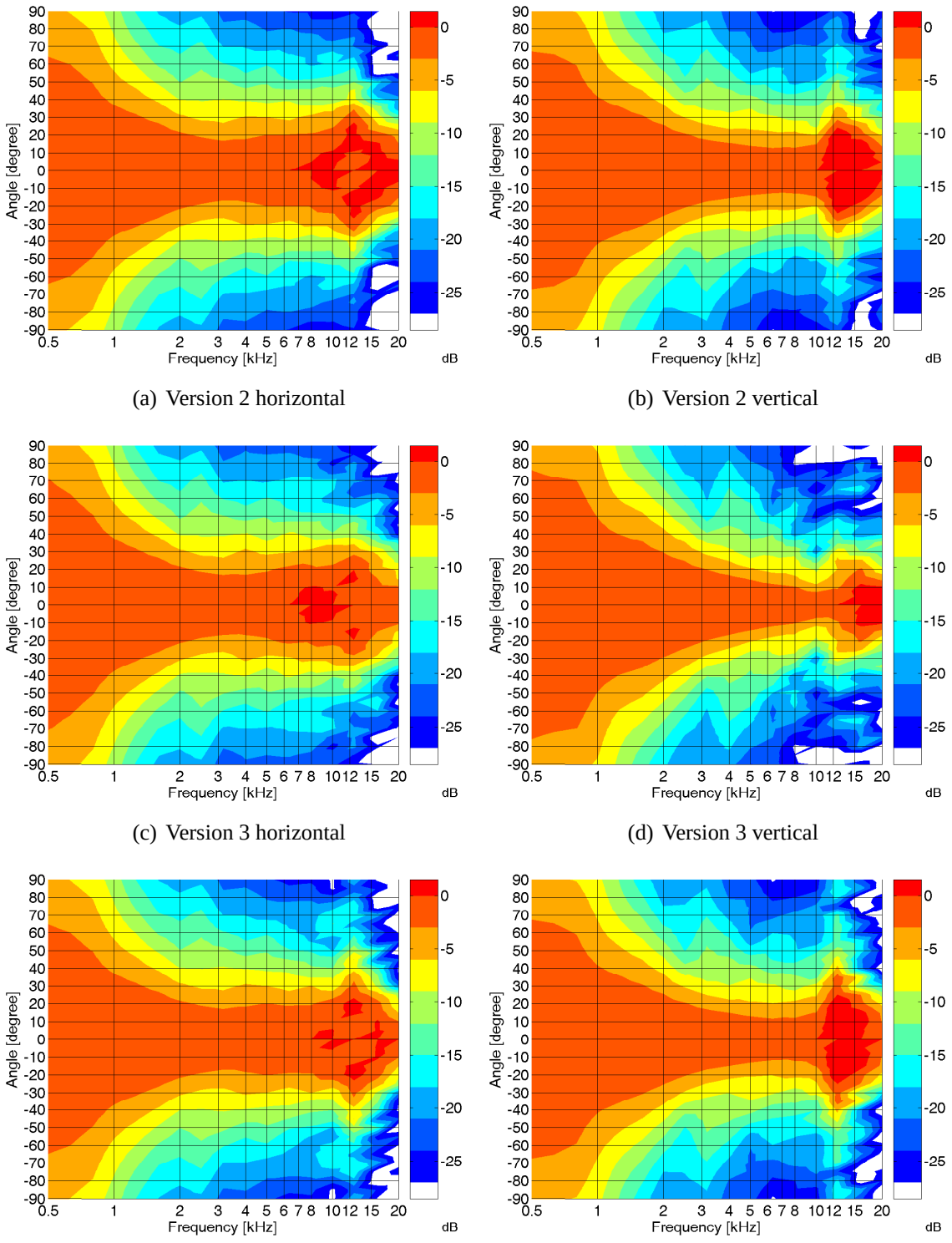

(a) Version 2 horizontal

(b) Version 2 vertical

(c) Version 3 horizontal

(d) Version 3 vertical

(e) Version 4 horizontal

(f) Version 4 vertical

Figure 8.2: Evolution of the horn version 2 to 4

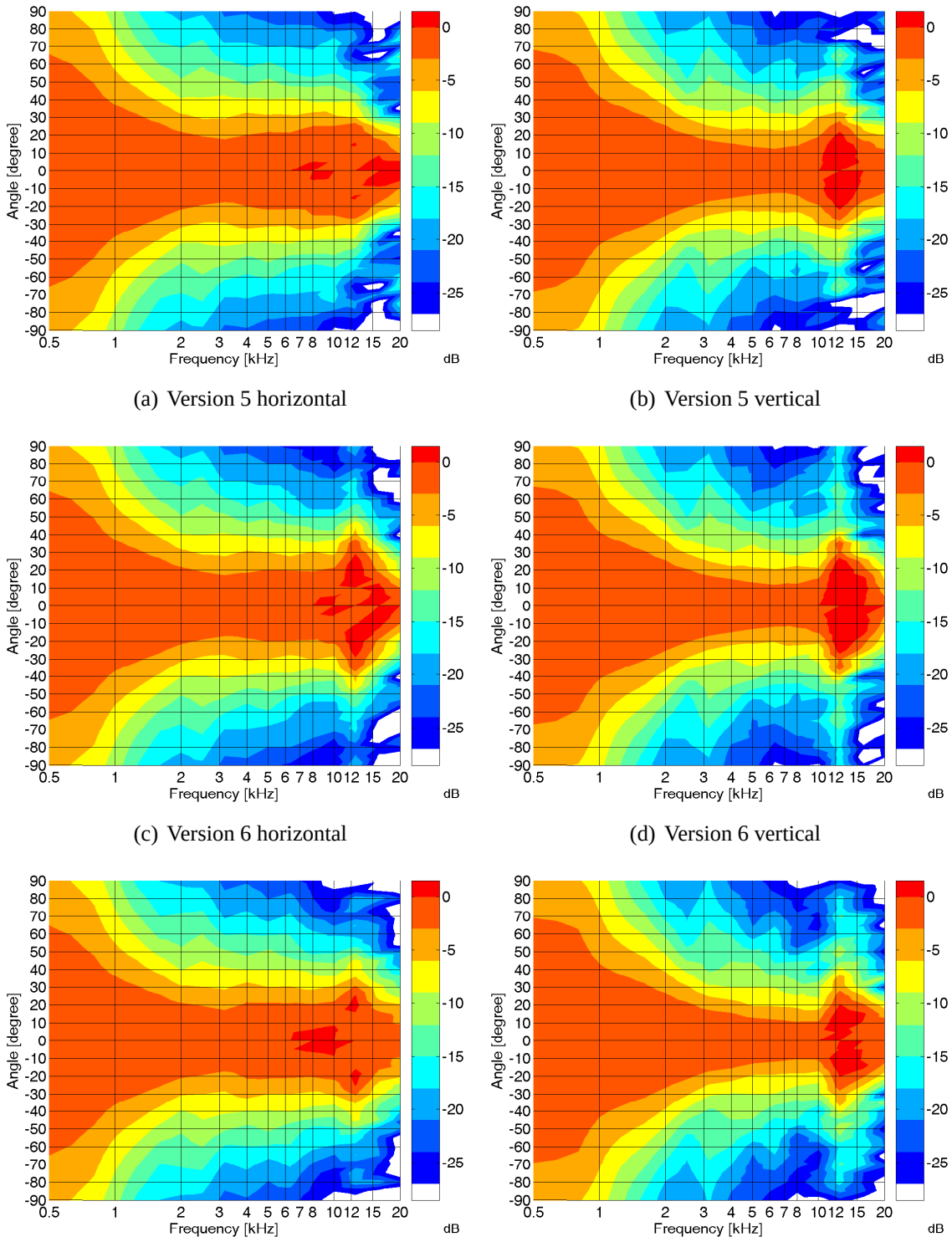

(a) Version 5 horizontal

(b) Version 5 vertical

(c) Version 6 horizontal

(d) Version 6 vertical

(e) Version 10 horizontal

(f) Version 10 vertical

Figure 8.3: Evolution of the horn version 5,6 and 10

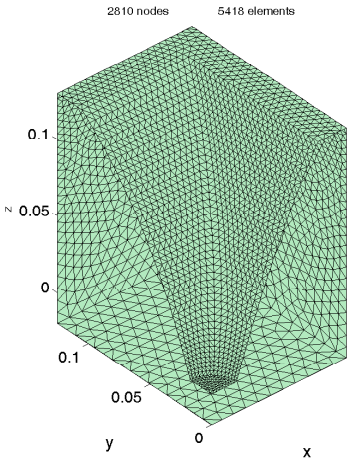

(a) Mesh version 10-hr

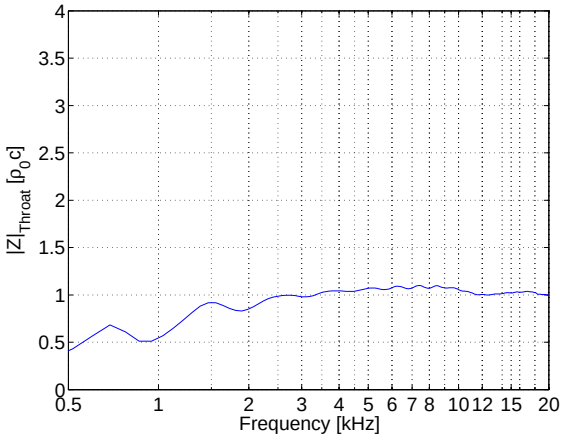

(b) Fundamental mode throat impedance version 10-hr

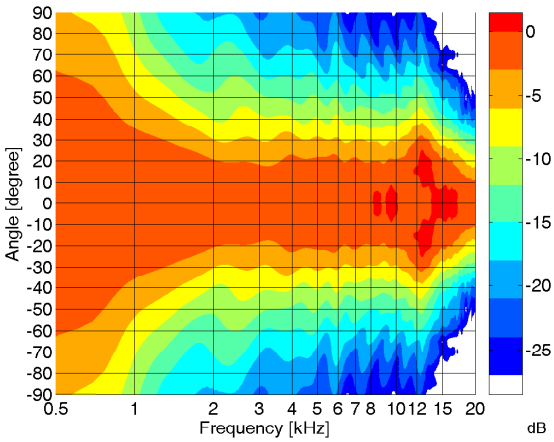

(c) Horizontal directivity version 10-hr

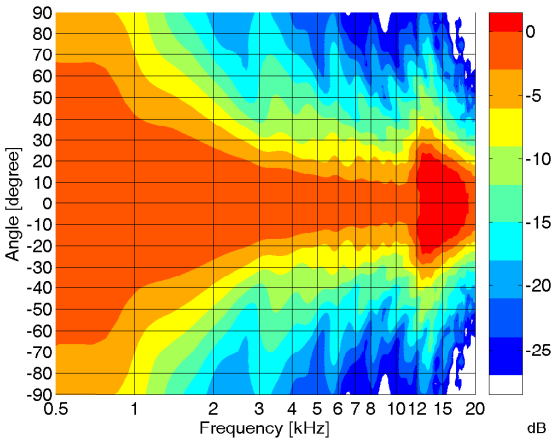

(d) Vertical directivity version 10-hr

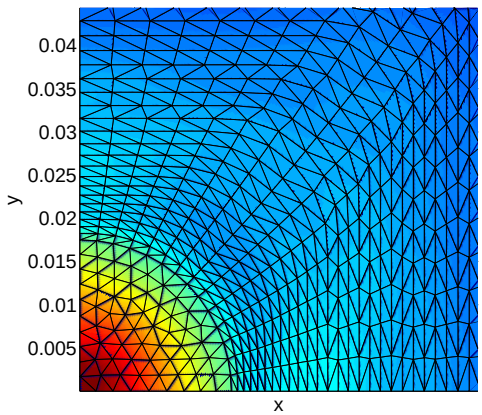

(e) Throat pressure distribution at 12 kHz

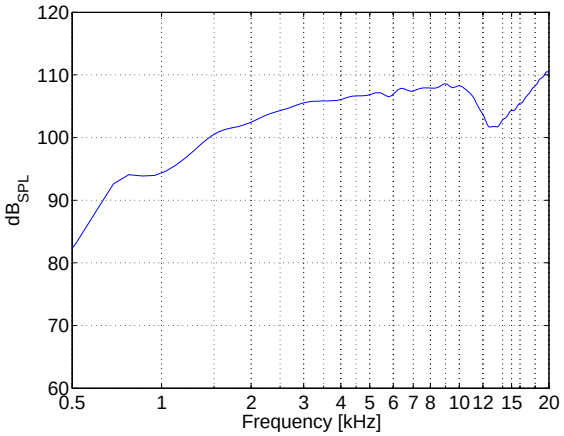

(f) Fundamental mode on-axis transfer function

Figure 8.4: High resolution results of the version 10

result in an unreliable simulation result. Besides this, a higher resolution is desirable to simulate properties of the horn if a driver is connected. Figure 8.4 shows a set of results of the version 10 with a mesh of 2800 nodes and 256 processed frequencies. The CPU-time for such a high resolution simulation is about 5 to 10 hours. The results validate the snapshots and it is now possible to begin with the fine tuning. The horizontal direction is almost perfect: the nominal angle is at exactly 60° above 2 kHz and the isobars are almost parallel. This promises a very smoothly distributed spatial sound. The only flaw is a small peak at 12 kHz. The vertical direction is almost perfect from 4kHz to 12 kHz. The peak at 12 kHz has to be removed. But how to remove the two peaks?

Before modifying the geometry, it is helpful to understand the reason of the sudden wide dispersion at 12 kHz in both directions. The on-axis fundamental mode transfer function shown in Figure 8.4(f) gives a first hint: an on-axis dip causes the directivity to widen in the horizontal as well as in the vertical direction (and all other directions, too). Looking at the surface pressure distribution at 12 kHz, the reason is identified as the first radial mode. Remembering the modal horn parameters described in Chapter 5, one finds that the only modes capable to transmit on-axis power are the fundamental and the pure radial modes. Obviously, the first radial mode is excited here and destructively interferes with the fundamental mode. The cause of this unwanted excitation is a too fast flaring at the very beginning of the horn. The wave front has to change in this way, in order to fulfil the geometrical boundary conditions. To suppress this mode, the flaring has to become more moderate.

Starting from this version, a series of snapshots with the indicated modifications at the beginning of the horn were done. The most promising versions were additionally simulated in a high resolution.

Figure 8.5 shows the data set of the horn version 10-08-04-hr. The dispersion peaks are now almost suppressed. This is also indicated by the transfer function shown in Figure 8.5(f). Besides the changes in the directivity, an interesting change can also be observed at the throat impedance: the loading at low frequencies could be increased which also lowers the cut-off frequency a little bit. This is also a result of changing the flaring at the beginning and can be understood without complicated mathematics. Imagine a rigid piston driving the horn. The more the horn geometry resembles a cylindrical tube, the more it will behave like this. The fundamental mode impedance of the tube is $\rho_0 c$. Thus, the fundamental mode throat impedance will converge to this value. A decrease of the flare rate to negative values will increase the throat impedance, too. The limit is, accordingly, an infinite impedance for

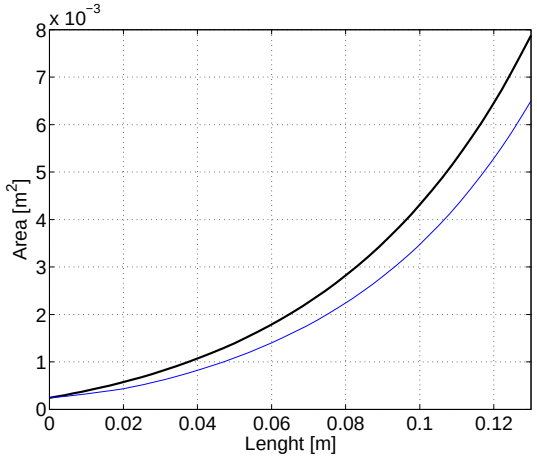

(a) Flaring of version 10 (bold) and version 10-08-04

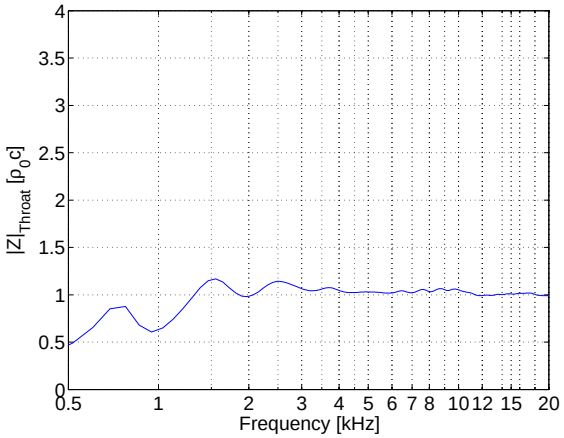

(b) Fundamental mode throat impedance version 10-08-04-hr

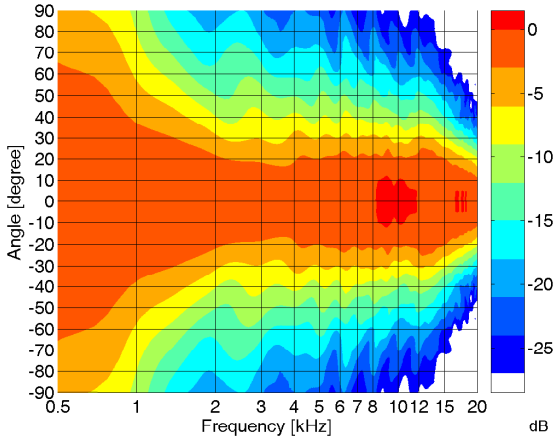

(c) Horizontal directivity version 10-08-04-hr

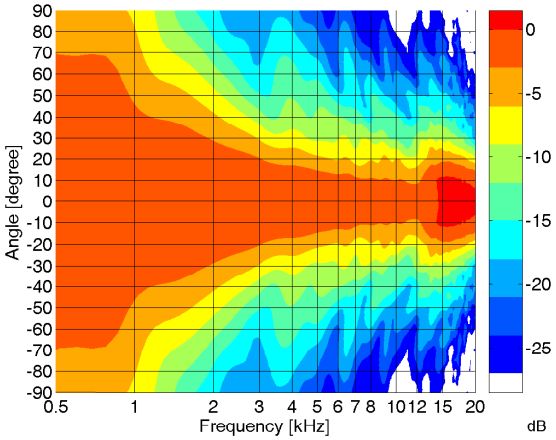

(d) Vertical directivity version 10-08-04-hr

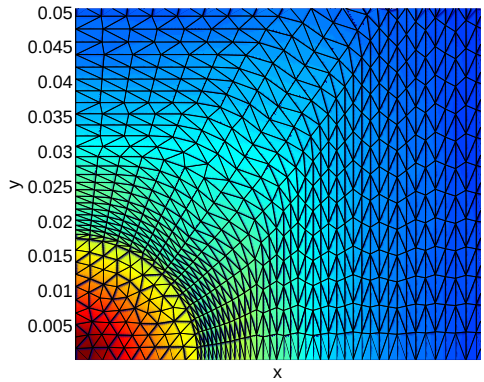

(e) Throat pressure distribution at 12 kHz

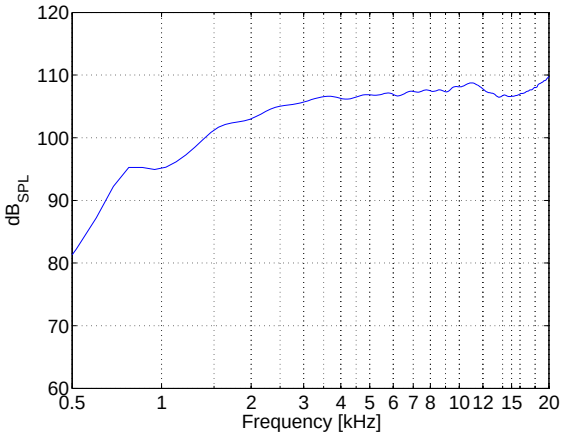

(f) Fundamental mode on-axis transfer function

Figure 8.5: High resolution results of the version 10-08-04

the hard wall. Naturally, this is just a simple explanation by the phenomena. In reality, the interactions with the complete geometry have to be considered.

At this stage of the horn optimization it seems that the geometry fulfils the development objectives: the directivity is (in the considered frequency range) 60°x40°, the isobars are almost parallel. The throat impedance does not show significant resonances and indicates a lower cut-off of about 600 Hz. The next step is to investigate the nonlinear properties.

8.1.2 Nonlinear Simulations

The goal of this project was, besides the linear property's optimization, to reach about 125 to 130 dB on-axis sound pressure at 10% distortion in the mid-frequency range. At high frequencies, about 120 dB should be the minimum. As the driver is not known, the horn has to be simulated assuming an ideal, distortion-free excitation at the throat. The technique to do this is described in Chapter 7. The advantage of this method becomes evident now: it is simply necessary to use the simulated surface pressures and to apply the extended post-processing to estimate the nonlinear properties of the horn.

This technique is used in the following to compare the two versions (10 and 10-08-04) in order to find out how they differ in their nonlinear behaviour. Although an experienced acoustic engineer could forecast that version 10 will generate less distortion, it is absolutely not possible to say how much they differ.

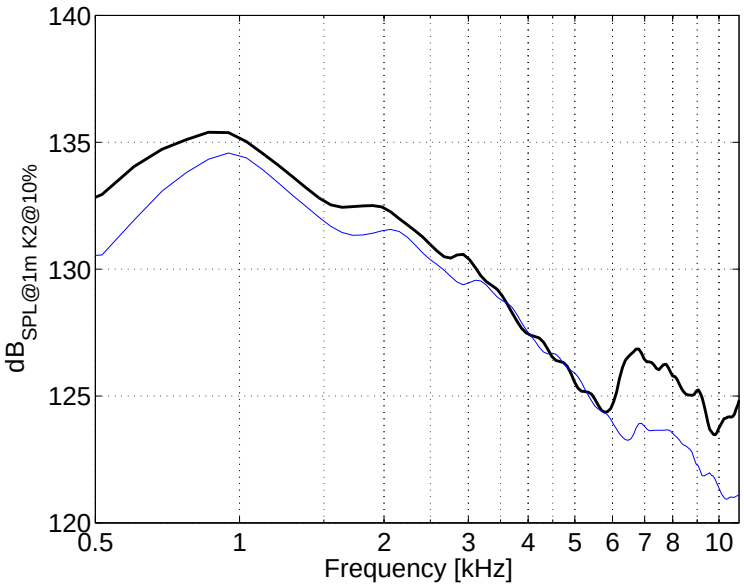

Figure 8.6: Sound pressure level at 10% second harmonic distortion on axis of version 10 (bold) and version 10-08-04

Figure 8.6 shows a comparison of the maximum SPL of both geometries. It is interesting to state that, although the changes in the geometry are not very large (see also the

comparison of the flaring in Figure 8.5(a)), they differ significantly in their nonlinear behaviour. In the important frequency range up to 3 kHz the version 10 reaches about 1 to 3 dB more SPL at the same distortion level of 10%. It is also worth mentioning that, especially, the change in the directivity causes the on-axis distortion of the version 10 to be smaller at 6 kHz. This can be traced back to the vertical dispersion at 12 kHz: the power of the second harmonic component is not concentrated on the main axis and, thus, the on-axis distortion is influenced.

Now, the development is in a state which allows to make some decisions. Both versions feature an almost perfect horizontal directivity. Version 10-08-04 provides a little bit more loading at low frequencies but this should not be overrated. The significant differences are the vertical dispersion and its interaction with the nonlinear behaviour. If the focus is on the directivity, version 10-08-04 should be preferred. If the distortion is more important, version 10 should be selected.

Besides these considerations, it is possible to forecast that version 10-08-04-hr will not reach the 120 dB Max-SPL at high frequencies together with a real source. A rule of thumb is that a high quality 1.4” driver adds about 3 dB distortion at high frequencies. Comparing the nonlinear simulation result once again, it becomes clear that version 10-08-04 will not reach the distortion level defined in this project.

8.2 Investigation of Horn Drivers and Properties of the Coupled System Driver/Horn

In this section, the “project” is continued with respect to the horn drivers. Two particular drivers (denoted as type A and type B) are investigated to find the most suitable driver/horn combination. The methods described in the previous Chapters are applied to simulate properties of the coupled system of driver and horn. At this stage of the project the horn is not yet built. Hence, any calculated property is based on simulation results as described in section 8.1 and Chapter 5.

The focus in this project is on the following properties:

- Sensitivity and lower cut-off frequency of both drivers coupled to both horn versions 10hr and 10-08-04-hr (see Chapters 4 and 6.1)
- Transition frequency for the higher order modes (frequency where modes dominate the velocity profile, see section 3.3)
- Influence of higher order modes on the directivity

- Estimation of the sound pressure level at 10% distortion of the four combinations (see Chapter 7)

With the two drivers and the two versions of the horn geometry, it is accordingly possible to simulate four combinations. This, actually, is one of the great advantages of treating driver and horn separately: the properties of the coupled system can be simulated. It is not necessary to build each horn and measure the combinations in reality. For instance, if the fundamental mode parameters or modal parameters of 10 drivers are known (by measurements) and 50 geometries of horns are simulated, it is possible to calculate the properties of 500 combinations.

8.2.1 Linear Properties Based on Fundamental Mode Two-port Measurements and Simulations

The two-port parameters for the results presented in the following were obtained by method II as described in section 6.1. With the measured parameters and the simulated horn data, it is possible to calculate the linear properties of the coupled system. Although many different properties could be calculated, like the electrical impedance[4], electro-acoustic efficiency[5] , pressure and volume flow at the horn throat area, etc., in the following only the sensitivity and the lower cut-off are considered.

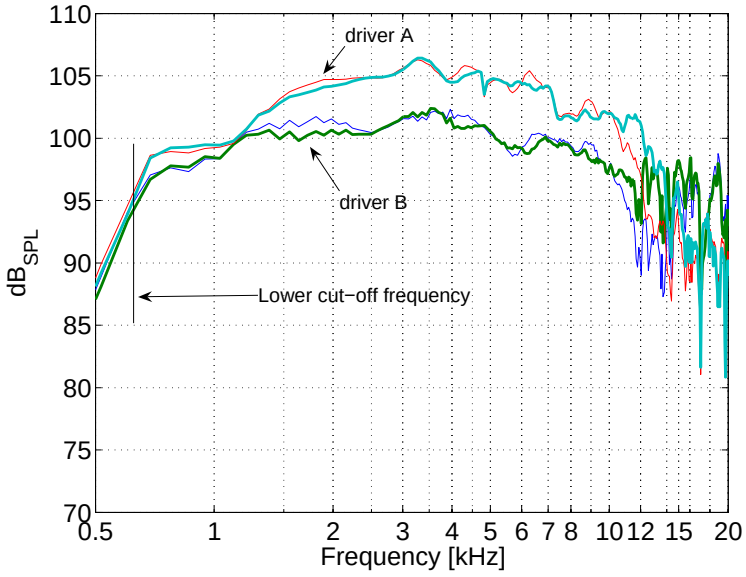

Figure 8.7: Simulated sensitivity (SPL in 1 m/1 V on-axis) of driver A and B combined with horn version 10 (fine curves) and version 10-08-04 (bold curves). The curves are based on measured fundamental mode two-port parameters of the drivers and simulated data of the two horns.

Figure 8.7 shows the simulated sensitivity for the four combinations. The equations used for the calculation are:

[4] In [Mak01] several examples for simulated and measured electric impedances are presented.
[5] In [BM01a] the efficiency is calculated for different driver/horn combinations.

- eq. (6.28) for the sensitivity
- eq. (5.13) for the fundamental mode transfer function

Both drivers have an almost smooth frequency response but a significant difference between driver A and driver B attracts the attention: the sensitivity of driver A is about 3 dB to 5 dB higher than the sensitivity of driver B. Accordingly, driver A needs only 25% to 50% of the input power of driver B to reach the same sound pressure level. In the introduction, it was pointed out that the electrical power is not a limiting factor in today's professional applications. But when considering lightweight and mobile applications, a high sensitiviy might become interesting. The second point of interest for the practical application is the lower cut-off frequency. It is for all combinations about 600 Hz to 650 Hz as this was predicted by the cut-off of the throat impedances. Hence, it is possible to combine the systems with the woofer at a cross-over frequency above approximately 1000 Hz. The third interesting difference is the sensitivity at high frequencies caused by the horn geometry: the horn version 10-04-08-hr provides about 3 dB to 5 dB more sensitivity. This increase of sensitivity can be explained by the on-axis transfer function of the fundamental mode: version 10 has a dip between 10 kHz and 15 kHz (please compare Figures 8.4(f) and 8.5(f)).

Summarizing the sensitivity results, it has to be stated that the driver of type A seems to be favourable.

8.2.2 Investigation of the Higher Order Mode Influence

The investigation of excited modes at the driver's outlet is done in three steps: first, the profiles are scanned as described in Chapter 3.1. Then, the modal decomposition technique is applied to the scanned velocity profiles to analyse the modal composition. This was described in section 3.2. The last step is to combine the scanned and decomposed profiles with the modal data sets. The simulation technique to obtain the modal horn data set is described in section 5.2.

Scanning and decomposition Both drivers were connected to a "neutral" tractrix horn and scanned in two planes with a distance of 2 mm. In section 3.1, it was pointed out that a two-plane measurement with such a small distance does not provide a good signal-to-noise ratio at low frequencies. Anyhow, the scanning was carried out in this configuration as the transition frequencies are at rather high frequencies and, thus, only in this frequency range a modal influence on the directivity has to be expected.

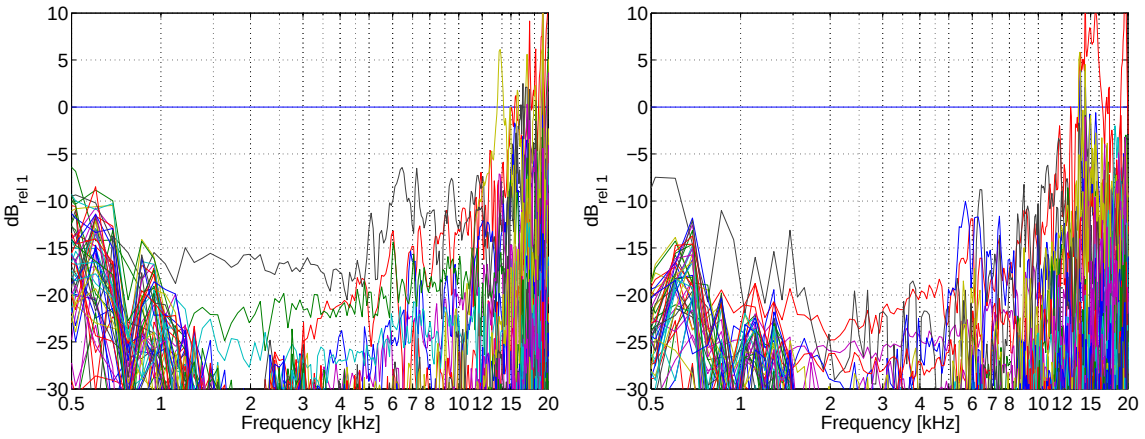

(a) Driver A (b) Driver B

Figure 8.8: Velocity participation coefficients of a two plane scanning measurement at the driver outlet. The coefficients are normalized to the fundamental mode. The decomposition was calculated up to order $m = 8$ and $n = 2$. (Order 8 of the Bessel function and the first two solutions of the boundary value problem)

Figure 8.8 shows the velocity decomposition result of driver A and driver B. At low frequencies, the measurement is disturbed by noise. Hence, in this frequency range the results are not relevant for further considerations. The transition frequency is about 13 kHz for driver A and about 14 kHz for driver B. In this point both drivers do not differ much. Accordingly, a significant deviation of the fundamental mode directivity response can be expected above 13 kHz for driver A and above 14 kHz for driver B. Looking at the level of the modes in this frequency range, it has to be noted that driver B excites one particular mode with a rather high level (01 mode). Hence, the influence of higher order modes excited by driver B are expected to be larger than that of driver A.

Higher order mode simulation Based on the scanning measurements of the velocity profiles, the modal directivity response of the four combinations is to be simulated. In section 4.2 several modal driver models are discussed. The model applied in the following is the *reduced modal description*: the fundamental mode parameters are measured using the technique described in section 6.1 and the higher order modes are treated as ideal velocity source. In order to couple the amplitude of higher order modes to the input voltage of the transducer, they are normalized to the fundamental mode amplitude as, for example, shown in Figure 8.8. This technique enables to calculate the coupled system's properties with a minimum of complexity. Of course, a modal feedback from horn to driver is not considered.

The horn's modal data are calculated using the techniques described in Chapter 5.2.

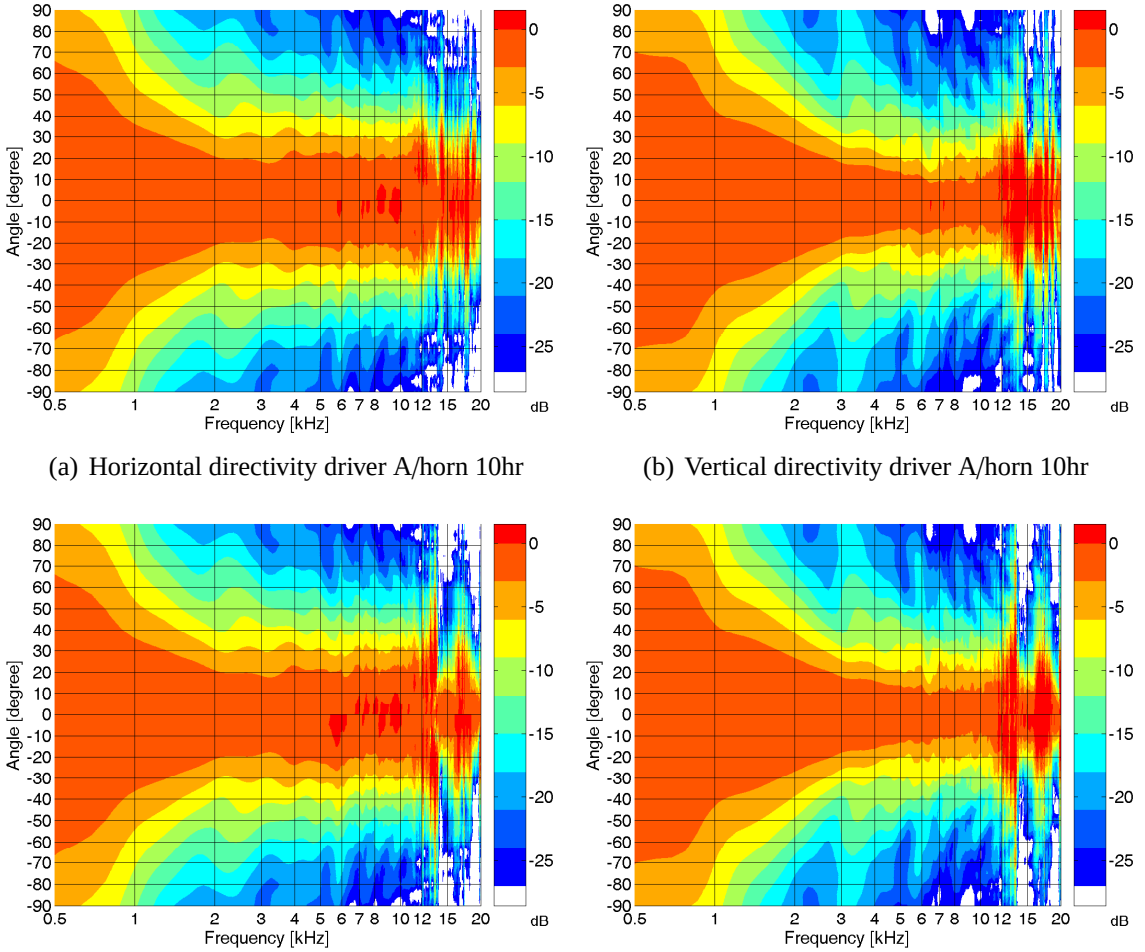

(a) Horizontal directivity driver A/horn 10hr

(b) Vertical directivity driver A/horn 10hr

(c) Horizontal directivity driver B/horn 10hr

(d) Vertical directivity driver B/horn 10hr

Figure 8.9: Modal directivity of driver A and driver B combined with horn 10hr

Although this might not be of great relevance for the practical implementation, the modal horn data were calculated for all modes: radial and angular modes. The modal surface pressures were stored which enables to calculate any sound field property with nearly arbitrary excitation profiles at the horn throat. With the normalised velocity participation coefficients V_{mn}/V_{00} it is, then, possible to calculated the resulting pressure distribution:

$$\mathcal{P} = \sum_{m,n} \mathcal{P}_{mn} \frac{V_{mn}}{V_{00}} \tag{8.1}$$

Using the standard post-processing of the BEM, the directivity and other properties of the particular driver/horn combination can be calculated.

Figure 8.9 shows the simulated directivity plots of the drivers combined with the horn 10hr. Comparing the modal results with the fundamental mode results (see also Figure 8.4), several differences are to be noted: firstly, the transition frequencies are also reproduced by the modal directivity simulation. Above this frequency, the results are dominated by

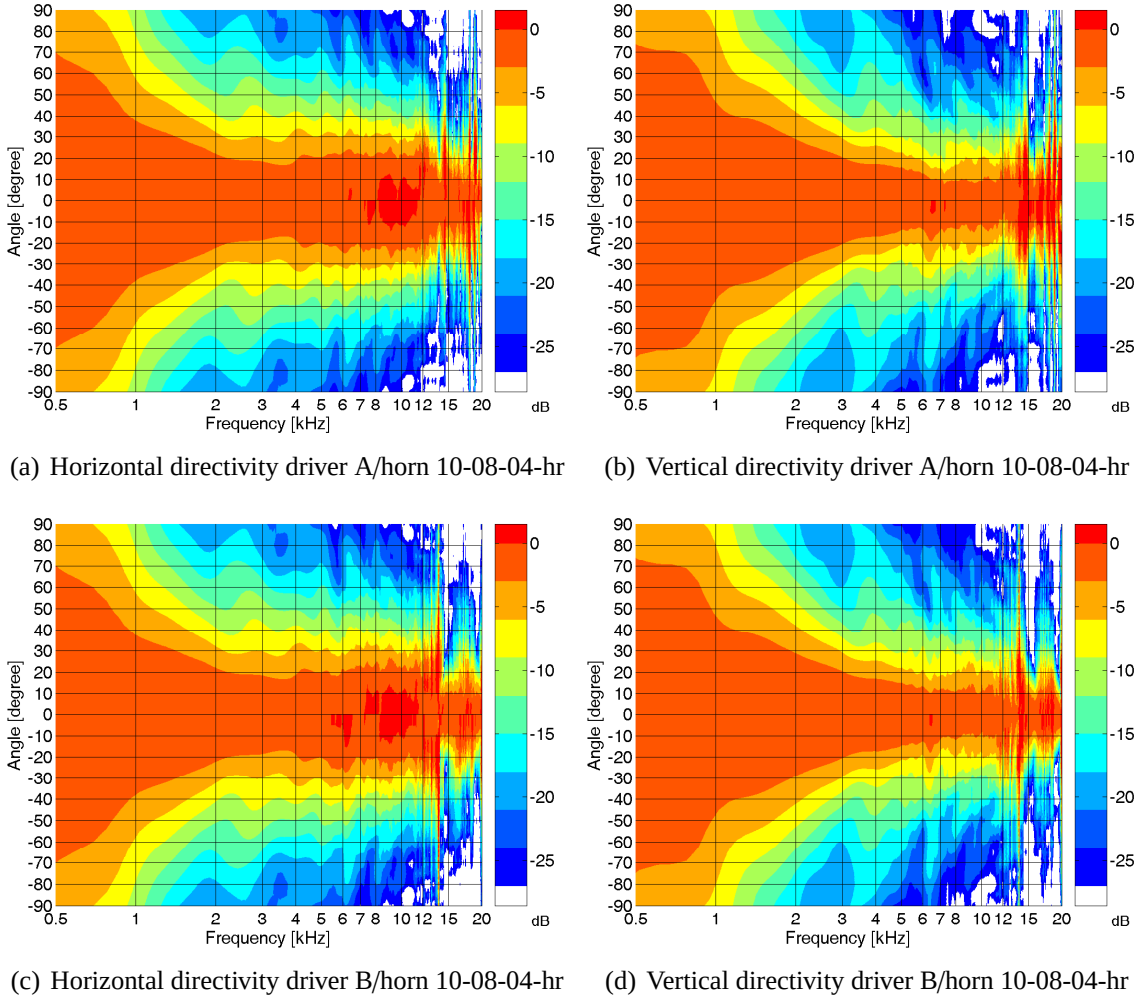

(a) Horizontal directivity driver A/horn 10-08-04-hr

(b) Vertical directivity driver A/horn 10-08-04-hr

(c) Horizontal directivity driver B/horn 10-08-04-hr

(d) Vertical directivity driver B/horn 10-08-04-hr

Figure 8.10: Modal directivity of driver A and driver B combined with horn 10-08-04-hr

excitation of higher order modes. This fact confirms that it is not useful to optimize the directivity above the transition frequency with respect to the fundamental mode directivity.

The second interesting result is the sharp dispersion peak at 14 kHz of driver B caused by the first radial mode excited at a rather high amplitude. Although driver A has a lower transition frequency, the overall result above 14 kHz looks smoother than the results of driver B.

The third interesting property is the asymmetrical vertical directivity of driver A between 6 kHz and 10 kHz: the whole directivity is bended. The deviation from a pure symmetrical directivity is approximately 3° to 5°. This is rather unusual, especially, in this frequency range. When the manufacturer of driver A was confronted with these results, it was admitted that during the production of these drivers problems occurred which caused the phase-plug to be mounted not symmetrically anymore. Anyhow, the author had the “luck” to get just some of those drivers. It opens a new field of commercial application

for the modal decomposition: as the scanning and decomposition technique offers to evaluate of how precise the components of the driver (membrane, suspension, and phase-plug) are mounted, it could be used for a non-invasive quality inspection to automatically sort the drivers by their quality. Of course, it would be possible to additionally measure the nonlinear driver properties at the same time.

Finally, it is investigated how the on-axis sensitivity changes when higher order modes at the interface driver/horn are considered. Basically, the same equations are used as for the fundamental mode sensitivity calculation, but now the parameters are calculated using the modal surface pressure for the particular driver/horn combination (see equation (8.1)).

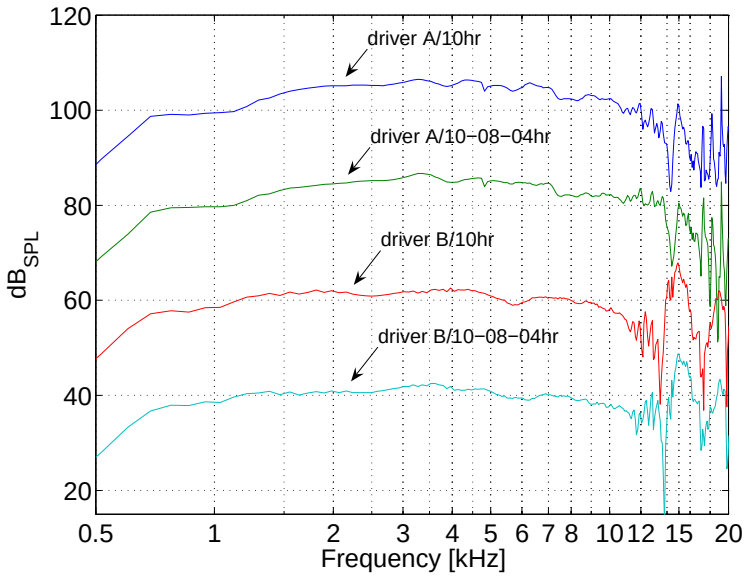

Figure 8.11: Simulated sensitivity (SPL in 1 m/1 V on-axis) of driver A and B combined with horn version 10 and version 10-08-04. The curves are calculated by the reduced modal model of the drivers and simulated data of the two horns. For sake of a better readability the curves are shifted by 20 dB.

Figure 8.11 shows the modal sensitivity results of the four combinations. The basic properties like the slope and the level of the curves are, of course, identical. But at high frequencies some changes are visible: the sensitivity of driver B shows a dip at 14 kHz followed by a 10 dB peak at 15 kHz. At 17 kHz another dip is visible.

Summarizing the results of this section: if the quality problem which caused the asymmetrical directivity is ignored, it can be stated that driver A is still the favourite. It offers a higher sensitivity and, additionally, a smoother directivity and a smoother on-axis frequency response in the frequency range were higher order modes are dominating.

8.2.3 Simulation of the Max-SPL

The last property to be investigated is the influence of the driver on the nonlinear behaviour of the complete system. In order to get an estimation, the driver's distortion is characterized by an additional nonlinear source term. In section 7.3.2 it was described how to obtain this

source term by calculating backwards from a real driver/horn measurement. This is also used in the following to get an estimate of the coupled system's nonlinear performance. The nonlinear sound generation and transmission caused by the horn geometry is simulated by the method described in 7.2.

Figure 8.12 shows the simulated sound pressure level at 10% second harmonic distortion for the four driver/horn combinations. The equations used to obtain these results are calculated by eq. (7.10) to obtain the overall second harmonic sound pressure level at the horn throat and eq. (7.7) was used to calculate the far field sound pressure level at 10% second harmonic distortion.

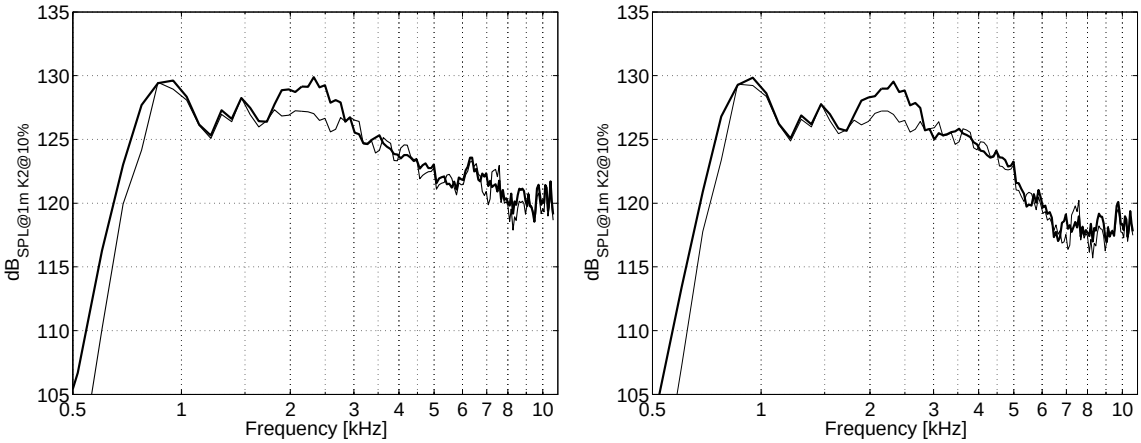

(a) Max SPL of the horn 10hr combined with driver A (fine curve) and driver B (bold curve)

(b) Max SPL of the horn 10-08-04-hr combined with driver A (fine curve) and driver B (bold curve)

Figure 8.12: Simulated sound pressure level in a distance of 1 m at 10% second harmonic distortion (Max SPL).

The overall performance of both drivers is almost the same. Between 2 kHz and 3 kHz driver B provides about 2 dB more Max-SPL. Additionally, it is interesting to note that the Max-SPL of driver B is 5 dB to 8 dB higher below 800 Hz. Although 1.4"-drivers are normally not used in this frequency range, it is an important feature and might be very useful for particular applications.

8.3 Final Conclusions and Measurements

The "project" is at a point, where a decision can be made: from the simulations and the driver measurements, two configurations will lead to driver/horn combinations with outstanding properties.

1. Driver A combined with horn version 10-08-04-hr will be a combination with a very

smooth horizontal and vertical coverage. Both components, the driver with the modal composition and the horn with the smooth fundamental mode directivity, contribute to this result. Additionally, driver A has a very high sensitivity.

2. Driver B combined with horn 10hr will be a “louder” combination: the horn, as well as the driver, are capable to reach higher sound pressure levels (measured at the same distortion threshold) than the other combination. This, of course, requires a rather high electric input power. Especially at low frequencies, driver B needs about 200 W input power to reach the simulated Max-SPL.

8.3.1 Measurements of the Combination Driver B/Horn 10hr

At the end of a development process, a prototype of the favourable horn version is built and characterized by a set of measurements or simulation of different parameters. The feasibility of the methods to simulate the parameters was shown in the corresponding Chapters of the thesis. The only model which is not verified yet is the reduced modal model of the horn driver (see page 50). This model combines the fundamental mode model (section 6.1) with a set of normalized velocity participation coefficients. The composition of the eigenfunctions in this model is not dependent on the modal impedances of the connected horn. This, actually, was motivated by the weak modal feedback found at the practical measurement results of different driver/horn combinations in Chapter 3.

Although this model introduces some simplifications, it promises accurate results. The intention of this section is to use the results of the fictive project to verify the modal simulation results based on the reduced modal model.

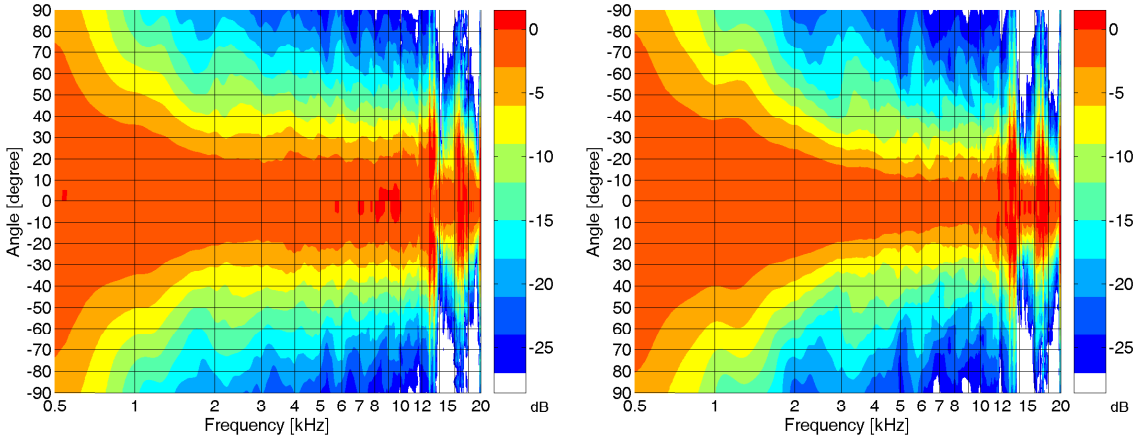

(a) Horizontal directivity driver A/horn 10hr (b) Vertical directivity driver A/horn 10hr

Figure 8.13: Measured directivity of driver B combined with horn 10hr

Figure 8.13 shows the measured directivity of driver B combined with horn 10hr. The set-up for the field points corresponds to the set-up used for the simulation of the directivity (described on page 67). The measurements were made in a semi-anechoic room. The horn loudspeaker was positioned at a height of 2 m (on a turn-table). The microphone was at a distance of 4 m (also at a height of 2 m). Ground-plane reflections were cut off using an appropriate window for the impulse response.

Comparing the measured results (Figure 8.13) with the simulation results (Figures 8.9(c) and 8.9(d)), it has to be stated that the accuracy is quite high. The measured nominal angles correspond exactly to the predicted radiation pattern: 60° in the horizontal plane above 2 kHz and 40° in the vertical plane above 4 kHz. Even small details of the measurement are visible in the simulation. For instance, the small asymmetric dip between 6 kHz and 7 kHz is simulated correctly and the two large dispersion peaks at 14 kHz and at 16 kHz are also very close to the measured results[6].

As a last example, the measured and simulated sensitivity of the combination driver B/horn 10hr are compared.

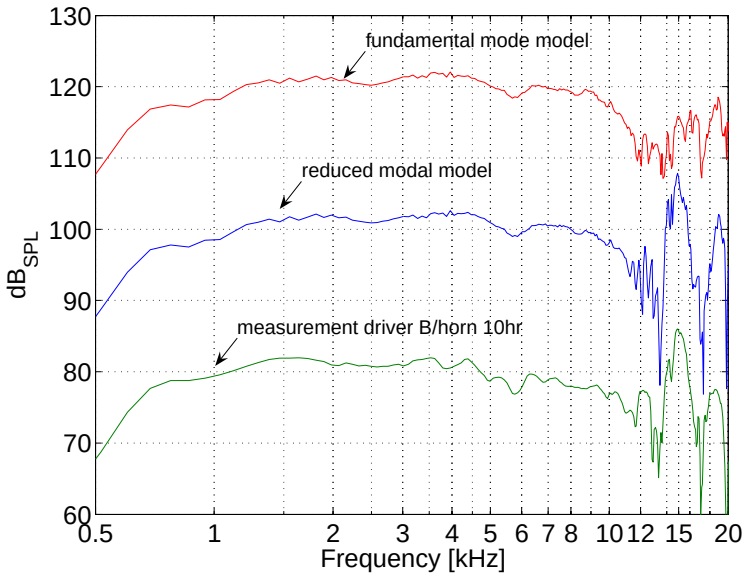

Figure 8.14: Comparison of simulated and measured sensitivity (SPL in 1 m/1 V on-axis) of driver B combined with horn version 10. For sake of a better readability the curves are shifted by 20 dB.

Figure 8.14 shows the result of the fundamental mode simulation, the reduced modal model result and the measured sensitivity. One can clearly see that the modal simulation adds the peak at 15 kHz which cannot be reproduced by the fundamental model. This result, actually, was predicted in section 6.1: if the fundamental mode dominates the excitation at the driver outlet, the parameter are simulated correctly. Using a modal model, even if it

[6]The deviations below 2 kHz are caused by diffraction. In the simulation, the horn was mounted in a small box, whereas the measurement was made with an unbaffled horn. Additionally, the windowing of the impulse response introduces errors at low frequencies.

is reduced to the minimum of complexity, the characteristic frequency response can be simulated also at higher frequencies.

Finally, it may be allowed to state that the “finger print” of the driver is reproduced correctly by the reduced modal model. Although the modal behaviour of drivers of the same type may vary due to the tolerances of the manufacturing process, some characteristic properties remain the same. Of course, a larger number of drivers must be scanned and with the averaged participation coefficients the characteristic modal properties can be found. For the “driver B”, the peak at 15 kHz and the two dips around the peak are characteristic. An experienced developer may be able to guess which driver is investigated here[7].

[7] This might be an interesting proposal for “Wetten, dass..?”: guessing the type of horn driver by analysing the on-axis frequency response.

Chapter 9

Summary

In this thesis, a number of methods for the professional development of horn loudspeakers are investigated and verified by extensive measurements. The tools provide an accurate modelling and are at the same time extremely effective to be used in practice.

Chapter 2 treats basic properties of driver/horn combinations and discusses the problems which occur when applying conventional methods (like lumped element networks for the driver or analytical approaches for the horn) to model a driver horn combination. At the end of this Chapter, the major aspects of the thesis are defined:

- the horn driver and the horn are to be treated as separate systems to provide a maximum of flexibility and reusability of the data
- the models have to consider the three dimensional properties of acoustic wave propagation and radiation
- the models should be as simple as possible and provide accurate results
- the methods have to consider a feedback from the horn to the driver as far as possible

For separating the acoustically coupled system of driver and horn, the velocity and pressure distribution at the driver outlet has to be known. Therefore, in Chapter 3, different driver/horn combinations are investigated. The wave front at the driver outlet is measured in the cut plane of driver and horn and analysed by decomposing the complex velocity and pressure profiles into a system of eigenfunctions. It turned out that the plane wave (fundamental mode) dominates the measured profiles, but at high frequencies an individual composition of modes is found at different types of drivers. Additionally, the velocity and pressure at the driver outlet is influenced by the horn but this seems to be negligible.

In Chapter 4, a driver model is described which is based on a modal multi-port approach: the 3-dimensional wave-front at the driver outlet is expressed as superposition of

orthogonal eigenfunctions and each eigenfunction is represented by one port of a multi-port. Additionally, one port is used to describe the electric properties. The interaction between the different ports is then described by a matrix. In this model, the horn is coupled to the driver multi-port by a modal impedance matrix. Generally, this approach leads to a large number of parameters to be determined. Considering the results of the investigation of pressure and velocity profiles, several simplified models are proposed to meet the requirements of practical applications. Two of the simplified models are then used to model the horn driver: a plane wave model (fundamental mode model) and a model which combines the plane wave model with measured velocity/pressure profiles (reduced modal model).

Chapter 5 deals with the horn. The essential point of this Chapter is to use a set of parameters based on the same eigenfunctions as used to describe the modal driver model. Two sets of parameters are proposed to store the horn's properties. The first method (a modal throat impedance matrix and a set of modal transfer impedance vectors) provides a very fast calculation of sound field properties but is restricted to a predefined set of field-points. Additionally, the storage space for the data set is negligible. The second method is a more universal approach. Based on this data set, it is possible to calculate any linear sound field property at any field-point for nearly arbitrary excitation profiles at the horn throat. Although this method requires more storage space (about 1 GB for each horn) and the computational time is longer compared to the first method, it is quite attractive due to its flexibility. To calculate these parameter sets the boundary element method (BEM) is used in this thesis. In general, any method which considers the 3-dimensional character of wave-propagation in the horn could be used to derive the parameters.

Chapter 6 describes a method to derive the fundamental mode model of a horn driver by measurements in detail. It is pointed out that many measurement methods exist, but most of these methods are disturbed due to higher order mode excitation at the driver outlet. The innovation of the method used in this thesis is to avoid any direct acoustic measurement at the driver outlet. Thus, the problems of the formerly used measurement methods can be reduced. Furthermore, the method requires a minimum of measurement devices: it is only necessary to measure the electric input impedance of the driver under exactly defined acoustic conditions. Several application examples and practical measurements show the feasibility of this method.

In Chapter 7, a method is developed to calculate the generation and transmission of the nonlinear pressure wave in the horn. The approach presented in this Chapter combines a

nonlinear plane wave approach with the post-processing capabilities of the BEM. Hence, this calculation scheme can be used with surface pressure distribution already processed. The distortion generated by the driver is considered by an additional term in the equations. A number of simulation and measurement results for different configurations show the power of this approach. It is pointed out that the dependency of the driver-related distortion on the throat impedance of the horn can be significant in some cases and an advanced measurement method is proposed to overcome this drawback.

Finally, Chapter 8 demonstrates how the methods are used in the professional development of a horn loudspeaker. As an example, the development of a 60°x40° high-frequency horn loudspeaker is described. First, the horn geometry is developed with respect to the common properties of real horn drivers. It is shown how the BEM and its post-processing features are applied to the optimisation of the geometry. This process results in two geometries to be analysed more closely by combining horn data sets obtained by simulation with the data sets of two drivers. The analysis of the four coupled system's properties concentrates on the sensitivity, the directivity, and the nonlinear performance of the systems. Using the driver models developed in this thesis, it is investigated how the modal composition at the driver outlet influences the linear properties and which combination leads to the best results. Lastly, a directivity and a sensitivity measurement of one of these combinations is presented. It is verified that this approach leads to accurate and detailed results even for frequencies where higher order modes dominate the velocity profile.

Figure 9.1 gives an overview of the different approaches described in this thesis and in which way they are combined to a powerful engineering tool. Furthermore, the figure shows the working flow in a development process of a horn loudspeaker and how the methods interact with the development objectives of a project.

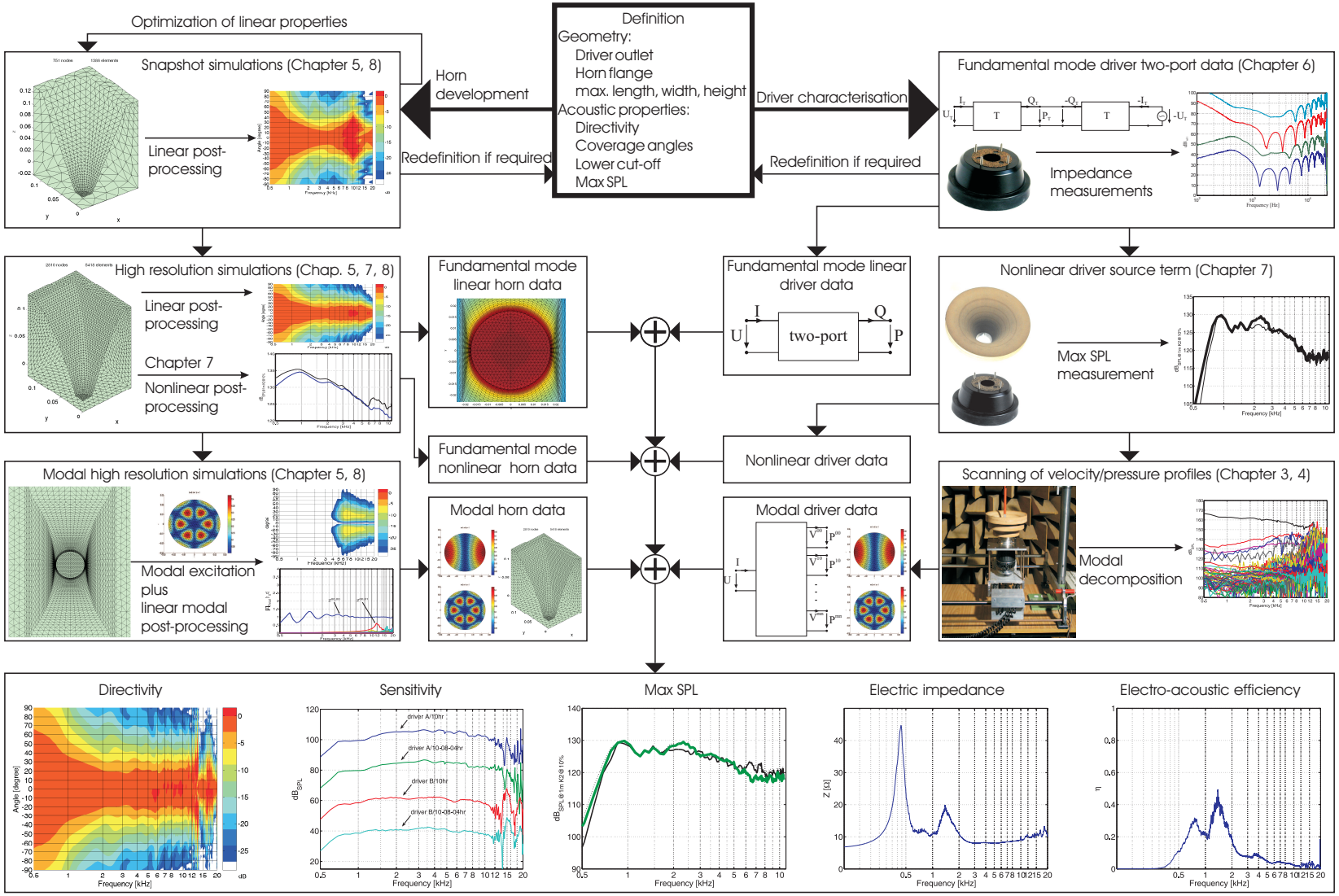

Figure 9.1: Interaction of the methods developed in this thesis

Outlook While writing this thesis, several methods to derive the advanced modal models by measurements and simulations were investigated. Although the simplest modal model leads to good results, a model which also considers the modal feedback would be desirable. As first results indicate, it will be possible to characterize at least the modal source/impedance model by measurements.

Besides the application on the development of horn loudspeakers, it is possible to use the scanning and decomposition technique for a non-invasive quality inspection of horn drivers. This new idea is briefly outlined in the following. The production and mounting of the different components of a horn driver is a highly complex process. For instance, the mounting of the phase plug is critical, as the distance from the membrane to the phase-plug is rather small. Hence, if the membrane and the phase-plug are not mounted axially the sound field may be asymmetric. This was observed in measurements, as well as in simulations based on scanned and decomposed velocity profiles. To determine if a driver is mounted correctly, scanned profiles can be decomposed and compared to a simulated modal multi-port model of this particular driver. To relate the mounting tolerances of the components to the participation coefficients, variants with the most common errors have to be simulated. Of course, the scanning technique as described in this thesis can not be applied directly (as it needs too much time), but it is possible to use a multichannel measurement technique with several microphone-probes positioned at the driver outlet. Furthermore, it is to be investigated how many probes are required and at which position the sound pressure should be acquired to identify a particular defect.

In this thesis, the standard BEM is used to simulate the radiation of the horn into the far field. Besides the acceleration of the method itself by using more advanced approaches (Multipol BEM and Padé expansion) another approach seems promising to be investigated: instead of simulating the complete horn geometry, it is also possible to divide the radiation problem into several parts which can be simulated separately. For instance, the radiation from the aperture of the horn could be simulated as one part and the interior of the horn is a second part. The coupling of both parts can be described by a modal impedance matrix at the common interface and the sound radiation from the aperture is also described in terms of the eigenfunctions of the aperture face. This technique would introduce some significant advantages:

- The modal aperture radiation and modal impedance matrix have to be calculated once and can be used for any horn geometry which ends with the same aperture. Hence, the aperture properties could be calculated in advance and used in subsequent projects.

- The calculation of wave propagation in the horn itself is then reduced to an interior problem which can be solved by the finite element (FEM) method. For several reasons, which shall not discussed here, the FEM provides a significant faster simulation for this particular boundary value problem.

Accordingly, it is also possible to subdivide the horn geometry in several parts which can be calculated separately if each part is described in its modal coordinates: the modal scattering matrix and the modal impedance matrix at the interface to the subsequent part. As a change of the geometry during the development process, normally, only affects two neighbouring elements, only these two elements would have to be simulated. Thus, a rather fast recalculation of the changes in the far field of the complete radiation problem would be possible. It is predicted here that this technique may be capable to provide “real-time horn development” in the future: a change of the geometry will more or less immediately be considered in the simulated directivity and sensitivity of the complete system. Besides the application on the particular problem of radiation described in this thesis, it may also be possible to apply this technique in room acoustics to effectively predict the sound field (at low frequencies) of coupled-room situations.

Kapitel 10

Kurzfassung

Die Nummerierung der Abschnitte in dieser Kurzfassung entspricht der Nummerierung der Kapitel der Dissertation. Wegen der Kürze des Textes ist hier lediglich die Übersichtsgrafik zu den entwickelten Verfahren abgebildet (Abb. 10.1). Daher sei zur Erläuterung der Abschnitte auf die Darstellungen in den entsprechenden Kapiteln der englischen Version verwiesen.

10.1 Einleitung

Der ”schallverstärkende Effekt” von Hörnern wird bereits seit Jahrtausenden in verschiedensten Anwendungen genutzt. Als wichtige historische Beispiele sind Musikinstrumente, Hörrohre und Trichter zur Sprachverstärkung zu nennen.

Im professionellen Beschallungsbereich werden für die Wiedergabe des Mittel- und Hochtonbereichs fast ausschließlich sogenannte Horntreiber[1]/Horn-Kombinationen verwendet, um die erforderlichen Schalldrücke und ein klar definiertes räumliches Abstrahlverhalten zu erzielen. Damit sind die Projektierung einer passenden Horntreiber/Horn-Kombination und der Entwurf der Horngeometrie die wichtigsten Teile der Entwicklung eines kompletten Beschallungssystems.

Obwohl in der Literatur verschiedene Modelle und Verfahren zur Berechnung von Hörnern und Horntreibern beschrieben sind, wird in der Praxis oft nur anhand von Faustformeln und mit empirischen Methoden, basierend auf der Erfahrung der beteiligten Ingenieure, entwickelt. Diese Vorgehensweise führt zu langen Entwicklungszeiten und hohen Entwicklungskosten, da viele Prototypen gebaut und akustisch vermessen werden müssen. Die Diskrepanz zwischen Theorie und Praxis lässt sich allgemein dadurch erklären, dass eine Methode entweder zu ungenau ist (z.B. konzentrierte Bauelemente für den Schallwandler)

[1] Ein Horntreiber ist ein speziell für den Einsatz mit einem Horn optimierter Schallwandler

oder zu eingeschränkt in der Anwendung ist (z.B. analytische Verfahren zur Berechnung der Wellenausbreitung im Horntrichter).

In dieser Arbeit werden Verfahren und Methoden entwickelt, die eine zielorientierte Entwicklung von Hornlautsprechern möglich machen. Grundlage der Methodik ist eine konsequente Trennung zwischen Schallquelle und Schallführung. Durch die getrennte Beschreibung beider Systeme wird ein Höchstmaß an Effektivität und Flexibilität in der praktischen Anwendung erzielt.

10.2 Funktionsweise einer Horntreiber/Horn-Kombination

In diesem Kapitel wird die Funktionalität eines Horntreibers und eines Horntrichters mit Hilfe von konventionellen, in der Literatur beschriebenen Modellen erklärt. Dabei werden die Grenzen und Schwierigkeiten bei der praktischen Umsetzung diskutiert. Daraus leiten sich für die weitere Vorgehensweise in dieser Arbeit folgende Forderungen ab:

- Schallquelle und Schallführung sollen als getrennte Systeme beschrieben werden
- Die Modelle und Verfahren müssen in der Lage sein, die dreidimensionalen Eigenschaften der Schallwelle, die sich im Übergang Horntreiber/Horn ausbreitet, abzubilden.
- Eine Rückwirkung der Schallführung auf die Schallquelle soll so gut wie möglich modelliert werden.
- Die Modelle müssen auch in die Praxis umsetzbar sein, entweder durch Messungen oder Simulationen.
- Für die praktische Anwendung ist es ausreichend, die Systeme anhand der physikalischen Ein- und Ausgangsgrößen zu beschreiben. Dafür kommen z.B. Zweitor- oder Mehrtormodelle in Frage.

10.3 Experimentelle Untersuchung der Schnittstelle von Horntreiber und Horn

Um die Auftrennung der akustisch gekoppelten Systeme vorzubereiten, werden in diesem Kapitel Eigenschaften der Schalldruck- und Schallschnelleverteilung unterschiedlicher Horntreiber/Horn-Kombinationen an der gemeinsamen Schnittstelle messtechnisch

und theoretisch untersucht. Ziel ist es folgende Kernfragen zu beantworten:

- Welche gemeinsamen Eigenschaften haben unterschiedliche Horntreiber/Horn-Kombinationen?
- Ist die Rückwirkung vom Horn auf den Horntreiber signifikant?
- Sind die Schnelle/Druckprofile der Schallwelle im Übergang Horntreiber/Horn eine Eigenschaft des Treibertyps oder des Horns?

Die Messung des Schallfeldes einer Horntreiber/Horn-Kombination erfolgt jeweils durch ein Abtasten des Schallfeldes in der gemeinsamen Schnittebene mittels einer computergesteuert positionierten Mikrofonsonde. Die so gewonnenen akustischen Profile werden anschließend durch eine modale Dekomposition in frequenzabhängige Partizipationsfaktoren zerlegt. Die hier verwendete modale Basis wird durch Lösung des Randwertproblems des schallharten, unendlich langen Zylinders gewonnen. Mit den so quantifizierten Messergebnissen ergeben sich folgende Schlussfolgerungen: Als wichtigste gemeinsame Eigenschaft unterschiedlicher Horntreiber/Horn-Kombinationen ist die Dominanz der Fundamentalmode für den größten Teil des Audiofrequenzbereichs festzuhalten. Eine Rückwirkung der Horngeometrie auf die Form der Schallwelle existiert zwar, ist aber schwach ausgeprägt und nur bei ungewöhnlichen Konfigurationen als signifikant zu bewerten. Weiterhin ist eindeutig festzustellen, dass die modale Zusammensetzung im modendominierten Frequenzbereich für jeden Treibertyp individuell ist.

10.4 Beschreibung der Schnittstelle von Horntreiber und Horn

Es wird zunächst eine allgemeine Beschreibung der Schnittstelle zwischen einem akustischen Wellenleiter und einem elektroakustischem Wandler als modales Mehrtor entwickelt. Mit diesem universellen Modell können alle Rückwirkungen der akustischen Last, dem Horn, zur elektrischen Seite des Horntreibers berücksichtigt werden. Die akustische Last wird in diesem Modell durch eine modale, voll besetzte Impedanzmatrix beschrieben. Da diese Beschreibung für eine messtechnische Umsetzung zu viele Freiheitsgrade besitzt, werden unterschiedliche Vereinfachungen diskutiert, die sich durch die in der messtechnischen Untersuchung gefundenen Eigenschaften begründen. Als wichtigste Vereinfachung ergibt sich somit das Modell für die Fundamentalmode. Als einfachstes Modell, was auch die modale Komposition der Schallwelle berücksichtigt, wird hier eine Kombination aus

dem Fundamentalmodenmodell und einer idealen, modalen Schnellequelle für die höheren Moden vorgeschlagen. Beide Modelle werden in den folgenden Kapiteln durch zahlreiche Messungen verifiziert.

10.5 Bestimmung der Parameter für das Horn

Die Berechnung der Schallabstrahlung von einem Horntrichter ist ein Standardproblem der numerischen Akustik.

Zur Lösung dieses Problems gibt es analytische Ansätze für bestimmte Horngeometrien (die durch separierbare Koordinatensysteme beschreibbar sind) und besondere Aperturkonfigurationen (z. B. planare, kreisförmige Apertur in unendlicher Schallwand etc.). Um vollkommen frei in der Entwicklung einer Horngeometrie zu sein, sind numerische Verfahren notwendig. In dieser Arbeit wurde zur Bestimmung der Hornparameter die Boundary Elemente Methode (BEM) implementiert und verwendet.

Die Eingangsdaten für eine BEM-Berechnung sind die Geometrie, die Wandadmittanz und die Schnelleverteilung auf der Oberfläche. Für das spezielle Problem einer Horntreiber/Horn-Konfiguration wird der Treiber in der Simulation durch eine Schnelleverteilung ersetzt. Da reale Schnelleverteilungen unterschiedlicher Treiber sich in ihrer modalen Zusammensetzung signifikant unterscheiden können, muss der Horndatensatz (d. h. das Ergebnis der Simulation) ebenfalls für beliebige Verteilungen eine Abstrahlungsberechung ermöglichen. Zu diesem Zweck wird die Anregung in der Simulation durch orthogonale Eigenfunktionen beschrieben. Die Kombination von BEM mit modaler Anregung und modaler Dekomposition ermöglicht so eine effektive Berechnung der Horndaten in modalen Koordinaten. Für eine Abstrahlungsberechnung werden die modalen Datensätze mit den entsprechenden Partizipationsfaktoren einer beliebigen Schnelleverteilung gewichtet und überlagert. Somit ermöglicht ein einmal berechneter Horndatensatz die Abstrahlungsberechnung für nahezu beliebige Eingangsdaten. Als weiterer Vorteil ist die Reduktion der benötigten Speicherplatzmenge um einen Faktor 200 zu nennen: eine vollständige Speicherung der numerischen Simulationsergebnisse eines mittelgroßen Horntrichters für 256 Frequenzlinien benötigt 200 GB Festplattenspeicher, für die Speicherung der modalen Ergebnisse sind höchstens 1 GB notwendig.

10.6 Bestimmung der Parameter für den Treiber

Dieses Kapitel beschreibt zwei messtechnische Verfahren, um die Parameter für das Zweitormodell der Fundamentalmode eines Horntreibers zu erfassen. In der Vergangenheit sind bereits verschiedene Verfahren zu diesem Zweck beschrieben worden, jedoch war eine breitbandige Messung, d.h. für den ganzen Audiofrequenzbereich, nicht möglich. Ursache für ein Versagen der bekannten Verfahren sind jeweils Störungen der akustischen Messungen durch Moden höherer Ordnung gewesen. Für die Anwendung in der professionellen Lautsprecherentwicklung ist ein eingeschränkter Gültigkeitsbereich jedoch nicht akzeptabel. Des Weiteren muss ein Verfahren schnell und sicher in der Anwendung sein.

Die Innovation der hier beschriebenen Verfahren beruht auf den vollständigen Verzicht akustischer Messungen. Die Methoden basieren auf elektrischen Impedanzmessungen, die mit moderner PC-Messtechnik hochpräzise bewerkstelligt werden können. Es wird hier ausgenutzt, dass eine akustische Last (z.B. ein Horn als akustischer Abschluss für den Horntreiber) eine Rückwirkung auf die elektrische Seite des Treibers hat. Durch Messungen der elektrischen Eingangsimpedanz für verschiedene, genau definierte akustische Konfigurationen können die Parameter schnell und mit verhältnismäßig geringem Aufwand bestimmt werden.

10.7 Simulation von nichtlinearen Eigenschaften

In diesem Kapitel wird ausführlich auf die Berechnung der wichtigsten nichtlinearen Eigenschaften einer Horntreiber/Horn-Kombination eingegangen. Es wird eine Methode entwickelt, die zum einen das Konzept der Trennung von Quelle und Schallführung konsequent auch auf die nichtlinearen Eigenschaften anwendet, zum anderen basiert dieses neuartige Verfahren auf bereits berechneten linearen Eigenschaften eines vorhandenen Horndatensatzes.

Da nach einer BEM-Simulation alle linearen Eigenschaften des Feldraumes mit einem schnellen Post-processing berechnet werden können, entstand die Idee, aus den linearen Schallfelddaten eine Abschätzung über die Verzerrungsprodukte der sich im Horn ausbreitenden Schallwelle zu berechnen.

Im ersten Schritt wird entlang der Hauptabstrahlachse der Verlauf des linearen Schalldrucks berechnet. Nun wird für jeden Feldpunkt aus dem Schalldruck der Grundwelle eine Abschätzung der Harmonischen berechnet. Diese Abschätzung kann aus der eindimensionalen Schallfeldgleichung für adiabatische Zustandsänderungen hergeleitet werden. Diese

so gewonnenen harmonischen Quellenterme müssen schließlich entlang der berechneten Feldpunktlinie, mit den Übertragungsfunktionen entsprechender Frequenz gewichtet, aufsummiert werden. Diese Gewichtung korrigiert den Fehler der eindimensionalen Abschätzung der harmonische Verzerrungsprodukte und berücksichtigt somit die dreidimensionale Verteilung der Schallleistung der harmonischen Verzerrungen im Feldraum.

Als Anwendung kann z.B. der Schalldruck bei einer definierten maximalen Verzerrungsgrenze simuliert werden. Da die Simulation keine Eigenschaften der Schallquelle berücksichtigt, stellt das Ergebnis die physikalisch maximal erreichbare Leistung der Horngeometrie dar. Es kann aber auch zusätzlich ein Verzerrungsterm für einen realen Treiber verwendet werden, um die nichtlinearen Eigenschaften der Schallquelle zu erfassen. Es wird ein Messverfahren beschrieben, um diesen Quellenterm zu erfassen.

Aus dem Vergleich von Simulations- und Messergebnissen ergibt sich, dass dieses Verfahren trotz seiner Einfachheit zu genauen Ergebnissen führt und somit die Entwicklung neuer Horngeometrien maßgeblich unterstützt.

10.8 Professionelle Entwicklung von Hornlautsprechern

Anhand eines typischen Entwicklungsprozesses wird in diesem Kapitel die Anwendung der in dieser Arbeit entwickelten Methoden demonstriert.

Ausgehend von der Definition der akustischen und geometrischen Eckdaten eines Beschallungslautsprechers, wird zunächst die Horngeometrie entwickelt. Es wird gezeigt, wie sich die BEM effektiv zur Optimierung der Abstrahlung einsetzen lässt. Es ergeben sich in diesem fiktiven Projekt zwei Kompromisse: ein Horn mit Nachteilen in der Abstrahlung, aber niedrigem Klirrfaktor und ein Horn mit besonders homogener Abstrahlung, aber etwas höherem Klirrfaktor.

In einem zweiten Schritt werden Eigenschaften zweier unterschiedlicher Horntreiber verglichen, um die Stärken und Schwächen beider Treiber auszuarbeiten. Dabei werden konsequent die Verfahren dieser Dissertation eingesetzt. Zunächst werden die linearen Eigenschaften anhand der Zweitordaten und der modalen Daten des Hornteibers in Kombination mit den Horndatensätzen der zwei Horngeometrien berechnet. Auch hier zeigt sich, dass signifikante Unterschiede existieren und dass sich diese Eigenschaften bereits in der Entwicklungsphase, d.h bevor ein Prototyp einer Horngeometrie für eine Messung zur Verfügung steht, prognostizieren lassen. Der Vergleich der nichtlinearen Simulationsergebnisse der Horntreiber/Horn-Kombinationen zeigt schließlich ebenfalls signifikante Leistungsunterschiede.

In einem realen Entwicklungsprozess könnten nun anhand der Simulationsergebnisse Horntreiber/Horn-Kombinationen mit besonderen Eigenschaften ausgesucht werden, wie z.B. eine Kombination mit einem sehr niedrigem Klirrfaktor, hoher Empfindlichkeit oder besonders homogener räumlicher Abstrahlung.

Schließlich werden anhand von Messungen einer dieser Kombinationen die Simulationsergebnisse verifiziert. Es wird gezeigt, dass insbesondere die modalen Simulationen im höherfrequenten Bereich zu sehr detailreichen Ergebnissen führen und dass sich so auch die charakteristischen Eigenschaften einer bestimmten Schallquelle vollständig in einen rechnergestützten Simulationsprozess integrieren lassen.

10.9 Zusammenfassung und Ausblick

In dieser Arbeit wurden Verfahren zur professionellen Entwicklung von Hornlautsprechern entwickelt und durch zahlreiche Messungen realer Hornlautsprecher verifiziert. Dieser ”Werkzeugkasten” ist aufgrund der getrennten Beschreibung von Schallquelle und Schallführung nicht nur flexibel, sondern erlaubt eine effektive und genaue Prognose der linearen und der wichtigsten nichtlinearen Eigenschaften einer Horntreiber/Horn-Kombination, ohne einen Hornprototyp bauen und vermessen zu müssen. Somit können Entwicklungsprozesse maßgeblich unterstützt werden und richtungsweisende Entscheidungen während der Entwicklung des Gesamtsystems anhand von Simulationsdaten gefällt werden.

Neben der Beschleunigung der numerischen Verfahren durch verfeinerte Methoden, ist die Erforschung weiterer Anwendungen der Schallfeldabtastung in Kombination mit modaler Dekomposition der Schallfeldverteilung ein zukünftiges Betätigungsfeld. Da sich auch scheinbar kleine Asymmetrien im mechanischen Aufbau des Treibers in der modalen Komposition des Schallfeldes am Treiberausgang abbilden, könnte diese Technik auch in der Fertigung zur Qualitätskontrolle verwendet werden, um z.B. bestimmte Defekte und Toleranzverletzungen in der Montage zu detektieren, oder um die Treiber nach verschiedene Güteklassen automatisch zu sortieren.

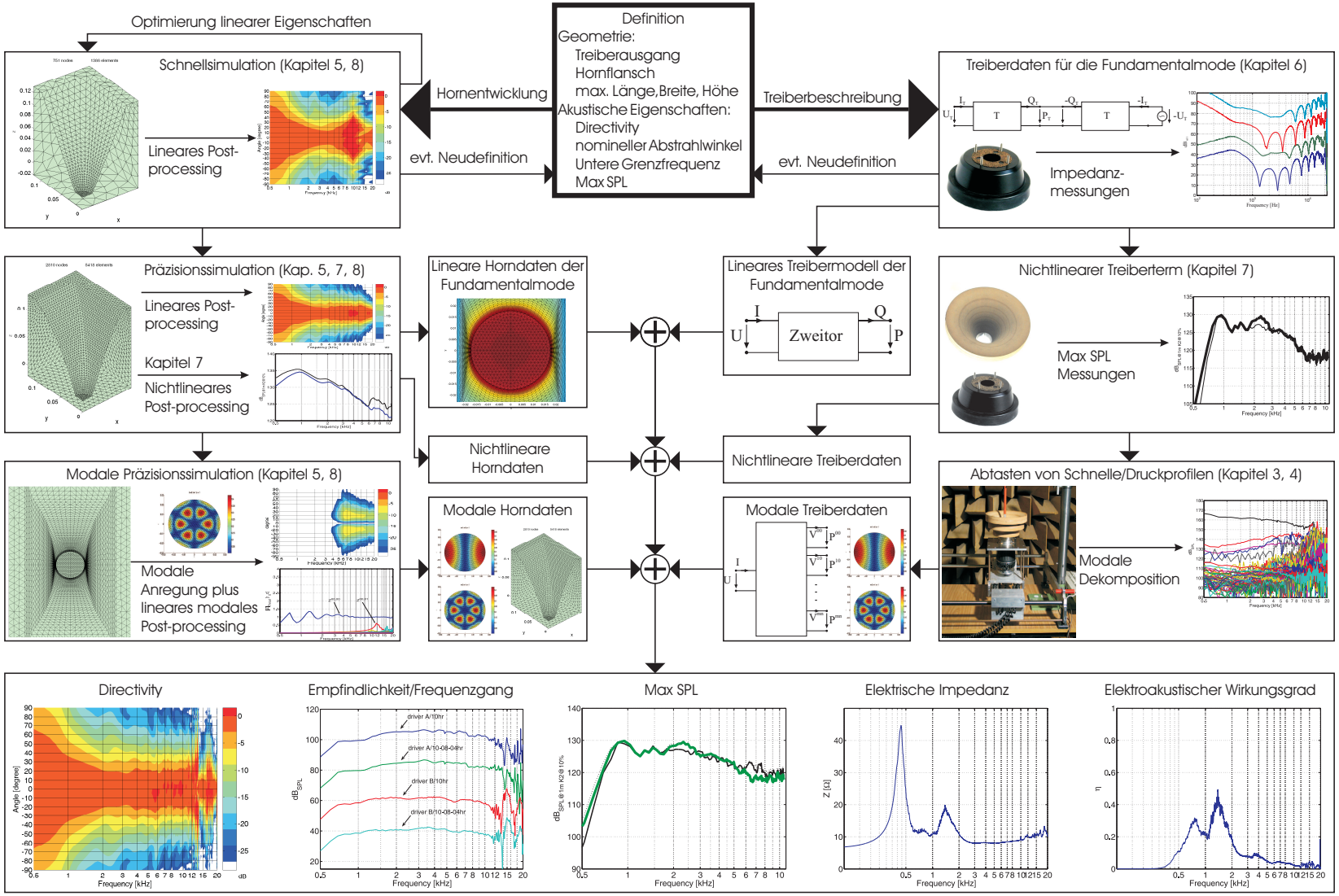

Abbildung 10.1: Zusammenspiel und Anwendung der entwickelten Verfahren

Appendix A

Glossary

Table A.1: Terms and abbreviations

Terms and abbreviations	Description
horn throat	geometrical beginning of the horn, the driver is connected to the horn throat
horn mouth	geometrical end of the horn, the mouth is the radiating aperture
horn driver	particular electro-acoustic transducer for the use with horns as loading device
throat impedance	ratio of pressure and velocity in the cut plane of the horn throat
PA, public address system	a sound reinforcement system for large audience areas
voice coil	coil in the air gap of a permanent magnet
coverage angle, nominal angle	angle where the sound pressure level is -6 dB referred to the main axis of the horn
sensitivity	on-axis frequency response of a loudspeaker referred to a distance of 1 m and 1 W input power

Table A.2: List of symbols

Symbol	Description	Unit
F	Mechanical Force	N
B	Magnetic flux density	N/A m
l	Length of the voice coil	m
I	Electric current	A
U	Electric voltage	V
V	Velocity	m/s
M	Force factor Bl	N/A
Z_e	Electric impedance	Ω
S	Membrane area	m^2
m	Mechanical mass	kg

Symbol	Description	Unit
n	Mechanical compliance	m/N
w	Mechanical losses	N s/m
R_0	DC-resistance of the voice coil	Ω
L_0	Voice coil inductance	H
Z_m	Mechanical impedance	N s/m
P	Sound pressure	N/m^2
Q	Volume velocity	m^3/s
Z_{ac}	Acoustic impedance	Pa s/m^3
Ψ	Velocity potential	m^2/s
Z_{mn}	Modal impedance of order m, n	Pa s/m^2
k	Wave number	1/m
ρ	Air density	kg/m^3
Φ	Angular eigenfunction	
J_m	Bessel function of order m	
κ_{mn}	Separation constant	1/m
Λ_{mn}	Normalization constant	
Ψ^{σ}_{mn}	Eigenfunction of order m, n, σ	
ζ	simplex coordinates	
J	Jacobian	
P^{σ}_{mn}	Pressure participation coefficient	Pa
V^{σ}_{mn}	Velocity participation coefficient	m/s
Φ_p	Interpolation function	
S_k	Area of the k-th surface element	m^2
f_{mn}	Cut-off frequency of mode with order m, n	Hz
$I_{z,mn}$	Intensity in z-direction of mode with order m, n	Pa s/m
$\mathbf{P}_{mn}$	Power of mode with order m, n	N m/s
P'_{mn}	Normalized power of mode with order m, n	
$\mathbf{P}$	Pressure participation coefficient vector	Pa
$\mathbf{V}$	Velocity participation coefficient vector	m/s
$\mathbf{Z_d}$	Driver matrix	
$\mathbf{Z_d^{U,V}}$	Electro-acoustic impedances vector	V s/m
$\mathbf{Z_d^{P,I}}$	Electro-acoustic impedances vector	Pa/A
$\mathbf{Z_d^{P,V}}$	Acoustic impedances sub-matrix	Pa s/m
$\mathbf{Z_h}$	Horn throat impedance matrix	Pa s/m
η	Electro-acoustic efficiency	
$\mathbf{H}$	Vector of modal transfer impedances	Pa s/m
H_{mn}	Modal transfer impedance	Pa s/m
$P\|_{1m,1W}$	Sensitivity of a transducer in 1 m distance at 1 W input power	Pa
$\mathcal{P}_{mn}$	Modal surface pressure distribution	Pa
$\mathbf{P_0}$	Modal source pressure vector	Pa
$\mathbf{Z_i}$	Inner impedance matrix	Pa s/m
$\mathbf{V_0}$	Modal source velocity vector	m/s
$\mathbf{T}$	Transfer matrix	
T_{ij}	Parameters of the transfer matrix	

Symbol	Description	Unit
g	Free space Green's function	1/m
C	Normalized solid angle	
n	Normal vector	m
ω	Frequency	1/s
v_n	Normal velocity	m/s
$\mathbf{D}$	Dipole matrix	
$\mathbf{M}$	Monopole matrix	Pa s/m
$\mathbf{C}$	Diagonal matrix of solid angles	
$\mathbf{A}$	BEM system matrix	
$Z_{ac,ref}$	Acoustic reference impedance	
c_0	Unperturbed fluid phase velocity of sound waves	m/s
p_0	Unperturbed fluid pressure	Pa
c'	Phase velocity	m/s
ζ	Particle displacement	m
$\tilde{p}$	RMS-value of sound pressure	Pa
γ	Adiabatic constant	
Δx_i	Thickness of the i-th slice	
L_{K_k}	Sound pressure level with distortion threshold K_k	dB
K_k	Distortion threshold for the k-th harmonic	

Appendix B

Discretised Decomposition

With the triangular structure used to define the measurement positions as nodes of the triangular elements, standard methods of numerical mathematics can be applied [Zie77]. Let's consider only one triangular element, as shown in figure B.1, which will be called simplex element in the following. At first, a coordinate transformation into simplex coordinates is

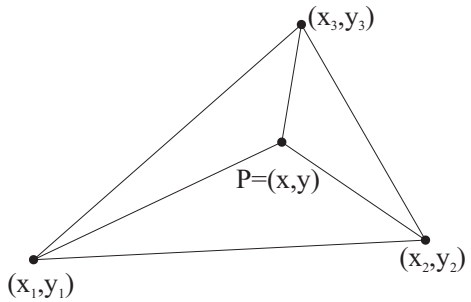

Figure B.1: Simplex element

performed. The transformation is defined as follows:

$$\zeta_1(x,y) = \frac{1}{J}\begin{vmatrix} 1 & x & y \\ 1 & x_2 & y_2 \\ 1 & x_3 & y_3 \end{vmatrix} \qquad \zeta_2(x,y) = \frac{1}{J}\begin{vmatrix} 1 & x_1 & y_1 \\ 1 & x & y \\ 1 & x_3 & y_3 \end{vmatrix} \qquad \zeta_3(x,y) = 1 - \zeta_1(x,y) - \zeta_2(x,y) \tag{B.1}$$

with the Jacobian

$$J = \begin{vmatrix} 1 & x_1 & y_1 \\ 1 & x_2 & y_2 \\ 1 & x_3 & y_3 \end{vmatrix}. \tag{B.2}$$

(x_{1-3}, y_{1-3}) are the node coordinates of one element, $P = (x,y)$ is the coordinate of a point within the triangle. Thus, the simplex coordinates describe the triangle in terms of triangle areas. For example, $\zeta_1(x,y)$ is the ratio of the triangle area $P, X2, X3$ to the area of the whole triangle.

For meshes with three nodes per element as used to define the measurement positions, a linear interpolation function has to be applied:

$$\Phi_p = \sum_{n=1}^{3} p_n \zeta_n \tag{B.3}$$

where p_n is the pressure measured at the n-th node. The integration over one surface element can now be performed in simplex coordinates:

$$\iint_{S_k} \Phi_p ds = \int_0^1 \int_0^{1-\zeta_1} \sum_{n=1}^{3} p_n \zeta_n J d\zeta_2 d\zeta_1 = \frac{S_k}{3} \sum_{n=1}^{3} p_n, \tag{B.4}$$

where S_k is the triangle area of k-th element of the mesh. The discretised decomposition formula applied on a linearly interpolated function over the cut plane is accordingly

$$\begin{aligned} P_{mn}^{\sigma} &= \left(\pi {r_0}^2 \Lambda_{mn}\right)^{-1} \sum_{k=1}^{N} \frac{S_k}{3} \sum_{n=1}^{3} p_0(k,n) \Psi_{mn}^{\sigma}(r,\varphi) \\ r &= \sqrt{x^2(k,n) + y^2(k,n)} \\ \varphi &= \arctan\left(\frac{y(k,n)}{x(k,n)}\right) \end{aligned} \tag{B.5}$$

$p(k,n)$ is the pressure measured at the n-th node of the k-th element and $\Psi_{mn}^{\sigma}(x(k,n), y(k,n))$ is the value of the transverse eigenfunction at the coordinate of the node.

Appendix C

Solution of the System of Equations using Method I, page 76

The system of equations defined by eq. (6.12) to (6.15) can be solved using the conditional equations (6.16) to (6.23). In order to increase the readability and save space the following abbreviations are used:

$$A := Z_{el,T}|_{U_S=0} \qquad B := Z_{el,T}|_{I_S=0} \qquad C := Z_{el,T}|_{Q_T=0} \tag{C.1}$$
$$D := Z_{el,S}|_{Q_S=0} \qquad E := Z_{el,T}|_{Z_{ac,ref}} \qquad F := Z_{el,S}|_{Z_{ac,ref}} \qquad G := Z_{ac,ref}$$

One obtains a set of four solutions, which only differ in the sign:

$$\left\{T_{11} = \mp\frac{1}{2}\,\%10, \qquad T_{12} = \pm\frac{1}{2}\,\%11, \qquad T_{21} = \pm\frac{\sqrt{\%8}}{\%9}, \qquad T_{22} = \mp\frac{C\,\sqrt{\%8}}{\%9}\right\} \tag{C.2}$$

$$\left\{S_{11} = \mp\frac{1}{2}\,\%5, \qquad S_{12} = \pm\frac{1}{2}\,\%6, \qquad S_{21} = \pm\frac{\sqrt{\%3}}{\%4}, \qquad S_{22} = \mp\frac{D\,\sqrt{\%3}}{\%4}\right\}. \tag{C.3}$$

The used abbreviations %1 – %11 are listed below:

$$\%1 := -BC + AC + BE - AE \tag{C.4}$$

$$\%2 := -CED + CDB + CFE - FAC - BFE - ADB + FAB + AED \tag{C.5}$$

$$\%3 := -2DG(-CDB + DAC + DBE - AED + BFC - FAC - BFE + FAE)\%2 \tag{C.6}$$

$$\%4 := -2D^2GAE - 2DGFAC - 2DGBFE + 2DGFAE + 2DGBFC - 2D^2GCB + 2D^2GAC + 2D^2GBE \tag{C.7}$$

$$\%5 := ((-CED - CDB - ADB - AED + 2DAC + 2DBE - BFE + CFE - FAC + FAB)\%4)/((D - F)\sqrt{\%3}\,\%1\,D) \tag{C.8}$$

$$\%6 := ((-CED + CDB - ADB + AED + FAC - 2BFC + CFE - 2FAE + FAB + BFE)\%4)/((D - F)\sqrt{\%3}\,\%1) \tag{C.9}$$

$$\%7 := C^2D - C^2F + FAC - CDB - DAC + BFC - FAB + ADB \tag{C.10}$$

$$\%8 := -2G(-FC^3 + C^3D + FC^2B + FAC^2 - AC^2D - C^2DB + FEC^2 - C^2DE - FABC + ACDB + ACDE - FEBC - FACE + CEDB + FABE - AEDB)\%2 \tag{C.11}$$

$$\%9 := 2DC^3G - 2FC^3G - 2DC^2BG + 2FC^2GE + 2FAC^2G - 2DAC^2G - 2DC^2EG + 2FC^2GB + 2CDABG + 2DCBEG - 2FACGE - 2FCGBE - 2CFAGB + 2DACEG + 2FAGBE - 2DABEG \tag{C.12}$$

$$\%10 := ((2C^2D - 2C^2F + FAC - CDB + CFE + 2BFC - CED - 2DAC + AED + ADB - FAB - BFE)\%9)/((-E + C)\sqrt{\%8}\,\%7) \tag{C.13}$$

$$\%11 := ((C^2DE + C^2DB - ACDB - ACDE - 2CEDB + 2AEDB - FAC^2 - FEC^2 + 2FACE + FEBC + FABC - 2FABE)\%9)/((-E + C)\sqrt{\%8}\,\%7). \tag{C.14}$$

Appendix D

Solution of the System of Equations using Method II, page 80

Using equation (6.24) to (6.27) the solution can be calculated (see section D). The following abbreviations are used:

$$C := Z_{el,T}|_{Q_T=0} \tag{D.1}$$

$$E := Z_{el,T}|_{Z_{ac,ref}} \tag{D.2}$$

$$G := Z_{ac,ref} \tag{D.3}$$

$$H := Z_{el,T}|_{P_T=0}. \tag{D.4}$$

The solution is:

$$T_{11} = \pm \frac{\sqrt{\%1\, G\, (-E + C)}}{\%1}, \tag{D.5}$$

$$T_{12} = \mp \frac{H\ \sqrt{\%1\, G\, (-E + C)}}{\%1}, \tag{D.6}$$

$$T_{21} = \mp \frac{\sqrt{\%1\, G\, (-E + C)}\, (E - H)}{\%1\, G\, (-E + C)}, \tag{D.7}$$

$$T_{22} = \pm \frac{C\ \sqrt{\%1\, G\, (-E + C)}\, (E - H)}{\%1\, G\, (-E + C)} \tag{D.8}$$

$$\%1 := C\, E - C\, H - E\, H + H^2. \tag{D.9}$$

Appendix E

Nonlinear wave equation

The wave equation used here is the exact one-dimensional wave equation for adiabatic changes in a non-viscous medium, based on Lagrangian coordinates, as introduced by Rayleigh in [SR45].

$$\frac{\partial^2 \xi}{\partial t^2} = \underbrace{c_0^2 (1 + \frac{\partial \xi}{\partial x})^{-\gamma-1}}_{c'^2} \frac{\partial^2 \xi}{\partial x^2}, \tag{E.1}$$

where $c_0^2 = \gamma p_0/\rho_0$, p_0 is the equilibrium pressure, ρ_0 is the equilibrium density, γ is the adiabatic exponent and ξ is the displacement of a particle. Looking at c', it is clear that the phase velocity is dependent on the condensation of the fluid, which leads to the well-known wave steepening at high sound pressure levels. Using a series expansion for c' yields the following equation:

$$c' = c_0 - c_0 \frac{\gamma + 1}{2} \frac{\partial \xi}{\partial x} + c_0 \frac{(\gamma + 1)(\gamma + 3)}{8} \left(\frac{\partial \xi}{\partial x} \right)^2 \ldots \tag{E.2}$$

The displacement ξ is written as asymptotic series

$$\xi = \xi_1 + \xi_2 + \xi_3 + \ldots \tag{E.3}$$

(E.4)

where

$$\xi_2 = C_2 f_2(x) \xi_1^2 \tag{E.5}$$

$$\xi_3 = C_3 f_3(x) \xi_1^3 \tag{E.6}$$

$$\vdots$$

C_i is a constant, and f_i is a function dependent only on x. The phase velocity can now be sorted by its degree in ξ:

$$c_0 = c_0 \tag{E.7}$$

$$c_1 = -c_0 \frac{\gamma+1}{2} \frac{\partial \xi_1}{\partial x} \tag{E.8}$$

$$c_2 = c_0 \left(-\frac{\gamma+1}{2} \frac{\partial \xi_2}{\partial x} + \frac{(\gamma+1)(\gamma+3)}{8} \left(\frac{\partial \xi_1}{\partial x} \right)^2 \right) \tag{E.9}$$

$$\vdots$$

Using the series expansion together with the wave equation yields the following equation:

$$\frac{\partial^2}{\partial t^2} (\xi_1 + \xi_2 + \xi_3 + \ldots) = (c_0 + c_1 + c_2 + \ldots)^2 \frac{\partial^2}{\partial x^2} (\xi_1 + \xi_2 + \xi_3 + \ldots) \tag{E.10}$$

Again, sorting by the degree in ξ yields:

$$O1: \quad \frac{\partial^2 \xi_1}{\partial t^2} = c_0^2 \frac{\partial^2 \xi_1}{\partial x^2} \tag{E.11}$$

$$O2: \quad \frac{\partial^2 \xi_2}{\partial t^2} = c_0^2 \frac{\partial^2 \xi_2}{\partial x^2} + 2c_0 c_1 \frac{\partial^2 \xi_1}{\partial x^2} \tag{E.12}$$

$$O3: \quad \frac{\partial^2 \xi_3}{\partial t^2} = c_0^2 \frac{\partial^2 \xi_3}{\partial x^2} + 2c_0 c_1 \frac{\partial^2 \xi_2}{\partial x^2} + (2c_0 c_2 + c_1^2) \frac{\partial^2 \xi_1}{\partial x^2} \tag{E.13}$$

$$\vdots$$

Equation E.11 is the linear equation which can be solved by:

$$\xi_1 = \hat{\xi}_1 \sin(\omega t - kx) \tag{E.14}$$

where $\omega = 2\pi f$ and $k = \omega / c_0$.

E.1 Second order equation

The second order equation is:

$$\frac{\partial^2}{\partial t^2} (C_2 f_2(x) \xi_1^2) = c_0^2 \frac{\partial^2}{\partial x^2} (C_2 f_2(x) \xi_1^2) + 2c_0 c_1 \frac{\partial^2 \xi_1}{\partial x^2} \tag{E.15}$$

In the following the abbreviation $()_x$ and $()_t$ are used for the partial derivatives. Carrying out the derivations and replacing c_1 leads to

$$C_2 f_2 (\xi_1^2)_{tt} - c_0^2 C_2 \left[(f_2)_{xx} \xi_1^2 + 2(f_2)_x (\xi_1^2)_x + f_2 (\xi_1^2)_{xx} \right] = -c_0^2 (\gamma+1)(\xi_1)_x (\xi_1)_{xx}, \tag{E.16}$$

where

$$\alpha = \omega t - kx \tag{E.17}$$

$$(\xi_1)_x = -k\hat{\xi}_1 \cos(\alpha) \tag{E.18}$$

$$((\xi_1)_x)^2 = k^2\hat{\xi}_1^2 \frac{1}{2}(1 + \cos(2\alpha)) \tag{E.19}$$

$$(\xi_1)_{xx} = -k^2\hat{\xi}_1 \sin(\alpha) \tag{E.20}$$

$$\xi_1^2 = \hat{\xi}_1^2 \frac{1}{2}(1 - \cos(2\alpha)) \tag{E.21}$$

$$(\xi_1^2)_{tt} = 2\hat{\xi}_1^2\omega^2 \cos(2\alpha) \tag{E.22}$$

$$(\xi_1^2)_x = -\hat{\xi}_1^2 k \sin(2\alpha) \tag{E.23}$$

$$(\xi_1^2)_{xx} = 2\hat{\xi}_1^2 k^2 \cos(2\alpha) \tag{E.24}$$

Equation (E.16) can be reorganized a little bit:

$$C_2 f_2 \underbrace{\left[(\xi_1^2)_{tt} - c_0^2(\xi_1^2)_{xx}\right]}_{=0} - c_0^2 C_2 \left[(f_2)_{xx}\xi_1^2 + 2(f_2)_x(\xi_1^2)_x\right] = -c_0^2(\gamma + 1)(\xi_1)_x(\xi_1)_{xx} \tag{E.25}$$

and solved for the unknown constant C_2

$$C_2 = \frac{(\gamma + 1)(\xi_1)_x(\xi_1)_{xx}}{(f_2)_{xx}\xi_1^2 + 2(f_2)_x(\xi_1^2)_x} \tag{E.26}$$

Using eq. (E.18) - (E.24) yields

$$C_2 = \frac{(\gamma + 1)(-k)\hat{\xi}_1 \cos(\alpha)(-k^2)\hat{\xi}_1 \sin(\alpha)}{(f_2)_{xx}\hat{\xi}_1^2 \frac{1}{2}(1 - \cos(2\alpha)) + 2(f_2)_x(-\hat{\xi}_1^2)k \sin(2\alpha)} \tag{E.27}$$

and simplifying the numerator yields

$$C_2 = \frac{(\gamma + 1)k^3 \frac{1}{2} \sin(2\alpha)}{(f_2)_{xx} \frac{1}{2}(1 - \cos(2\alpha)) + 2(f_2)_x(-k) \sin(2\alpha)} \tag{E.28}$$

A solution for the second order equation can be obtained for $f_2(x) = x$, as C_2 must not be a function of x or t:

$$C_2 = -\frac{\gamma + 1}{4}k^2 \tag{E.29}$$

Hence, the complete solution for the displacement up to order 2 with harmonic excitation is

$$\xi = \hat{\xi}_1 \sin(\alpha) - \frac{\gamma + 1}{8}k^2 x\hat{\xi}_1^2(1 - \cos(2\alpha)) \tag{E.30}$$

From the solutions for the displacement, one can obtain solutions for the pressure wave by using the relationship between density and pressure for adiabatic changes:

$$\rho = \rho_0(1 + \frac{\partial \xi}{\partial x})^{-1} \tag{E.31}$$

$$p = p_0 \left(\frac{\rho}{\rho_0}\right)^{\gamma} \tag{E.32}$$

As this relationship is nonlinear too, again a series expansion has to be used:

$$p = p_0 - \gamma p_0 \frac{\partial \xi}{\partial x} + 0.5\gamma p_0(\gamma+1)\left(\frac{\partial \xi}{\partial x}\right)^2 + \dots \tag{E.33}$$

Using the series for ξ yields:

$$p = p_0 - \gamma p_0 \frac{\partial}{\partial x}(\xi_1 + \xi_2 + \xi_3 + \dots) + 0.5\gamma p_0(\gamma+1)\left(\frac{\partial}{\partial x}(\xi_1 + \xi_2 + \xi_3 + \dots)\right)^2 + \dots \tag{E.34}$$

This yields the following solutions for the pressure wave, sorted by the degree in ξ

$$p_1 = -\gamma p_0 \frac{\partial \xi_1}{\partial x} \tag{E.35}$$

$$p_2 = -\gamma p_0 \frac{\partial \xi_2}{\partial x} + \gamma p_0 \frac{\gamma+1}{2}\left(\frac{\partial \xi_1}{\partial x}\right)^2 \tag{E.36}$$

$$p_3 = -\gamma p_0 \frac{\partial \xi_3}{\partial x} + \gamma p_0(\gamma+1)\frac{\partial \xi_1}{\partial x}\frac{\partial \xi_2}{\partial x} \tag{E.37}$$

$$\vdots$$

Using the solutions obtained for the first and second order displacement yields for the second order pressure wave:

$$p_2 = -\gamma p_0 C_2\left[\xi_1^2 + x(\xi_1^2)_x\right] + \gamma p_0 \frac{\gamma+1}{2}((\xi_1)_x)^2 \tag{E.38}$$

Together with equations (E.18) - (E.24) this results in

$$p_2 = \gamma p_0 \frac{\gamma+1}{4}k^2\left[\hat{\xi}_1^2\frac{1}{2}(1-\cos(2\alpha)) + x(-\hat{\xi}_1^2)k\sin(2\alpha)\right] + \gamma p_0 \frac{\gamma+1}{2}k^2\hat{\xi}_1^2\frac{1}{2}(1+\cos(2\alpha)) \tag{E.39}$$

which can be simplified

$$p_2 = \gamma p_0 \frac{\gamma+1}{4}k^2\hat{\xi}_1^2\left[\frac{3}{2} + \frac{1}{2}\cos(2\alpha) - xk\sin(2\alpha)\right] \tag{E.40}$$

For distances $x >> 4/k$ the equation can be simplified

$$p_2 = -\gamma p_0 \frac{\gamma+1}{4}k^2\hat{\xi}_1^2 xk\sin(2\alpha) \tag{E.41}$$

and finally expressed in terms of $\hat{p}_1$

$$p_2 = -\frac{\gamma+1}{4}\hat{p}_1^2 xk\sin(2\alpha), \tag{E.42}$$

where

$$\hat{p}_1 = \gamma p_0 k\hat{\xi}_1 \tag{E.43}$$

Thus, the r.m.s value of the second order pressure in terms of the first order pressure r.m.s value is

$$\tilde{p}_2 = \frac{\gamma+1}{2\sqrt{2}\gamma p_0}\tilde{p}_1^2 xk \tag{E.44}$$

Danksagung

An der Entstehung dieser Arbeit war eine Vielzahl von Personen direkt und indirekt beteiligt, denen ich im Folgenden meinen Dank aussprechen möchte.

Für die Betreuung dieser Arbeit und die Möglichkeit zur selbstständigen Bearbeitung des Themas danke ich Herrn Prof. Dr. rer. nat. Michael Vorländer. Für die Übernahme des Korreferats und die ungewöhnlich schnelle Durchsicht danke ich Prof. Dr.-Ing. Bernhard Rembold.

Den Mitarbeitern des Instituts für Technische Akustik sei gedankt für die entspannte Atmosphäre. Besonders hervorheben möchte ich an dieser Stelle Gottfried Behler, der einige wesentliche Ideen zu dieser Arbeit beigesteuert hat. Des Weiteren möchte ich Andreas Franck für die fachliche Unterstützung in numerischen Angelegenheiten danken. Heftig danken möchte meinem guten Freund Rainer Thaden, der per elektronischer Ferndiagnose aus den Niederlanden mein sehr mittelmäßiges Englisch verbessert hat und durch viele kritische Anmerkungen (“Wer soll das denn verstehen? Das versteht vielleicht noch der Günter Krauss, aber..”) wesentliche Verbesserungen erzwungen hat.

Den Werkstätten des Instituts möchte ich meinen Dank aussprechen für die Herstellung von etlichen Horntrichtern und speziellen Messvorrichtungen, die für die praktischen Untersuchungen unerlässlich waren.

Besonderer Dank gilt meinen Diplomanden Robert Joest und Oliver Strauch für die messtechnische Umsetzung und Ausarbeitung meiner Ideen. Weiterhin möchte ich Matthias Bösing für die Umsetzung einiger Ideen zur “Hornerzeugung” danken.

Anselm Goertz sei gedankt für die Unterstützung dieser Arbeit mit Horntreibern und Hörnern für Messzwecke und für die zahlreichen Kontakte zu den Herstellern von professionellen Lautsprechersystemen.

Günter Krauss und Bill Gelow von EVI Audio möchte ich an dieser Stelle für die vielen interessanten Hornprojekte und die Unterstützung dieser Arbeit durch die Versorgung mit zahlreichen Horntreibern danken.

Lebenslauf

Persönliche Daten

Michael Makarski
Morsbacher Str. 48
52146 Würselen

Tel.: (02 405) 489 589
E-Mail: mckarski@web.de

Geburtsdatum: 21. 4. 1975
Geburtsort: Mainz

Familienstand: Verheiratet

Nationalität: Deutsch

Schulbildung

1981–1983	Grundschule Koblenz-Neukarthause
1983–1985	Grundschule Koblenz-Moselweiß
1985–1994	Staatl. Eichendorff-Gymnasium Koblenz

Staatsdienst

1994–1995	1994-1995 Zivildienst in der Rhein-Mosel-Werkstatt für Behinderte gem. GmbH in Koblenz-Lützel

Studium

1995–2001	Diplomstudiengang Elektrotechnik an der RWTH Aachen

Beruflicher Werdegang

2001–2006	Wissenschaftlicher Mitarbeiter am Institut für Technische Akustik, RWTH Aachen

Bibliography

[AKP97] N. Amir, J. Kergomard and V. Pagneux, *A study of wave propagation in varying cross-section waveguides by modal decomposition. Part II. Results*, The Journal of the Acoustical Society of America **101** (1997), no. 5, 2504–2517.

[BBA99] R. Burger, R. Beyer and F. Arndt, *Rigourous Combined Mode-Matching Integral Equation Analysis of Horn Antennas with Arbitrary Cross Section*, IEEE Transactions on Antennas and Propagation **47** (1999), no. 11, 1641 – 1648.

[Bel98] C. I. Beltran, *Calculated Response of a Compression Driver Using a Coupled Field Finite Element Analysis*, Presented at the 105th Convention, San Francisco, September 1998.

[BJ74a] A. H. Benade and E. V. Jansson, *On Plane and Spherical Waces in Horns with Non-uniform Flare I. Theory of Radiation, Resonance Frequencies, and Mode Conversion*, Acustica **31** (1974), no. 3, 79–98.

[BJ74b] A. H. Benade and E. V. Jansson, *On Plane and Spherical Waces in Horns with Non-uniform Flare II. Prediction and Measurement of Resonance Frequencies and Radiation Losses*, Acustica **31** (1974), no. 4, 185–202.

[BK] Brüel and Kjaer, *Data Sheet Probe Microphone 4182*, http://www.bksv.com/pdf/Bp0659.pdf.

[Bla40] L. J. Black, *A Physical Analysis of Distortion Produced by the Nonlinearity of the Medium*, The Journal of the Acoustical Society of America **12** (1940), no. 2, 266–267.

[BM71] A. J. Burton and G. F. Miller, *The appliction of integral methods to the solution of some exterior boundary value problems*, Proceedings of the Royal Society of London **A** (1971), no. 323, 201–210.

[BM01a] G. K. Behler and M. Makarski, *Beschreibung der Schnittstelle Horntreiber - Horn mit Hilfe von Vierpol-Parametern*, Fortschritte der Akustik - DAGA '01 (Hamburg), 2001, pp. 398 – 399.

[BM01b] P. Bequin and C. L. Morfey, *Weak nonlinear propagation of sound in a finite exponential horn*, The Journal of the Acoustical Society of America **109** (2001), no. 6, 2649–2659.

[BM03] G. Behler and M. Makarski, *Two-Port Representation of the Connection Between Horn Driver and Horn*, The Journal of the Audio Engineering Society **51** (2003), no. 10, 883–897.

[BM04] G. K. Behler and M. Makarski, *On the Velocity Distribution at the Interface of Horn Driver and Horn*, Presented at the 116th AES Convention in Berlin, Preprint 6097, March 2004.

[Bri03] A. Bright, *Analysis of a Folded Horn*, Presented at the 114th AES Convention in Amsterdam, March 2003.

[Bug02] H. Bugge, *Kalibrierung von Piezo-Schallwandlern*, Diplomarbeit, Institute of Technical Acoustics, Aachen University (RWTH), Aachen, 2002.

[BV04] G. K. Behler and M. Vorländer, *Reciprocal measurements on condenser microphones for quality control and absolute calibration*, Acta Acustica united with Acustica **90** (2004), no. 1, 152 – 160.

[CD00] M. D. Cola and D. Doldi, *Horn's Directiviy Related to the Pressure Distribution at their Mouth*, Presented on the 109th AES Convention, preprint 5214, August 2000.

[CDS01] M. D. Cola, D. Doldi and D. Saronni, *Analysis of Directivity Anomalies in Mid and High Frequency Horn Loudspeakers*, Presented on the 111th AES Convention, preprint 5432, November 2001.

[CG87] D. Clark and E. Geddes, *Computer Simulation of Horn-Loaded Compression Drivers*, The Journal of the Audio Engineering Society **35** (1987), no. 7/8, 556.

[DHD91] J. N. Decarpigny, B. F. Hamonic and J. C. Debus, *Computation of the equivalent modal impedance matrix of a multiple degree of freedom electroelastic structure*

using antiresonance modes, The Journal of the Acoustical Society of America **90** (1991), no. 6, 2891–2894.

[DIN03] DIN EN 602628-5, *Elektroakustische Geräte - Teil 5*, Dezember 2003.

[Dod03] M. Dodd, *The Development of a Forward Radiating Compression Driver by the Application of Acoustic, Magnetic and Thermal Finite Element Methods*, Presented at the 115th Convention 2003 in New York, October 2003.

[EGT87] J. P. E. Geddes and Y. Tang, *A Boundary-Element Approach to Finite-Element Radiation Problems*, The Journal of the Audio Engineering Society **35** (1987), no. 4, 211–229.

[Eis66] E. Eisner, *Complete Solution of the "Webster's" Horn Equation*, The Journal of the Acoustical Society of America **41** (1966), no. 4, 1126–1146.

[Fah89] F. Fahy, *Sound Intensity*, Elsevier Science Publishers Ltd, 1989.

[Fay31] R. D. Fay, *Plane Sound Waves of Finite Amplitude*, The Journal of the Acoustical Society of America **3** (1931), no. 2, 222–241.

[Ged89] E. R. Geddes, *Acoustic Waveguide Theory*, The Journal of the Audio Engineering Society **37** (1989), no. 7/8, 554–569.

[Ged93] E. R. Geddes, *Acoustic Waveguide Theory Revisited*, The Journal of the Audio Engineering Society **41** (1993), no. 6, 452–569.

[Ged02] E. Geddes, *Audio Transducers*, Earl Geddes, 2002.

[GH96] G. P. Geaves and D. Henwood, *Horn Optimisation using Numerical Methods*, Presented at the 100th AES Convention in Copenhagen, preprint 4208, May 1996.

[GL03] E. Geddes and L. W. Lee, *Auditory Perception of Nonlinear Distortion - Theory*, Presented on the 115th AES Convention, October 2003.

[GM34] S. Goldstein and N. W. McLachlan, *Sound Waves of Finite Amplitude in an Exponential Horn*, The Journal of the Acoustical Society of America **6** (1934), no. 4, 275–278.

[Goe99] A. Goertz, *Monkey Forrest Anleitung 3.1D*, 1999.

[Hen93] D. Henwood, *The Boundary Element Method and Horn Design*, The Journal of the Audio Engineering Society **41** (1993), no. 6, 485–496.

[HM96] K. R. Holland and C. L. Morfey, *A Model of Nonlinear Wave Propagation in Horns*, The Journal of the Audio Engineering Society **44** (1996), no. 7/8, 569–580.

[HU78] C. Henricksen and M. Ureda, *The Manta-Ray Horns*, The Journal of the Audio Engineering Society **26** (1978), no. 9, 629.

[Hug99] C. E. Hughes, *A Generalized Horn Design to Optimize Directivity Control and Wavefront Curvature*, Presented on the 107th AES Convention, preprint 5016, August 1999.

[ISO96a] ISO 10534-1, *Acoustics - Determination of sound absorption coefficient and impedance in impedance tubes - Part 1: Standing-wave method*, 1996.

[ISO96b] ISO 10534-2, *Acoustics - Determination of sound absorption coefficient and impedance in impedance tubes - Part 2: Transfer-function method*, 1996.

[Joe04] R. Joest, *Untersuchung der akustischen Schnelleverteilung im Übergang Horntreiber-Horn*, Diplomarbeit, RWTH, RWTH Aachen University, May 2004.

[Joh94] T. F. Johansen, *On the Directivity of Horn Loudspeakers*, The Journal of the Audio Engineering Society **42** (1994), no. 12, 1008–1019.

[Kee77] D. Keele, *Low-Frequency Horn Design Using Thiele/Small Driver Parameters*, Presented at the 57th Convention of the Audio Engineering Society, May 10-13, 1977, Los Angeles, 1977.

[Kee83] J. D. B. Keele, *A Loudspeaker Horn that Covers a Flat Rectangular Area from an Oblique Angle*, Presented on the 74th AES Convention, preprint 2052, September 1983.

[Kel02] T. Kellert, *Numerische und experimentelle Untersuchung von Hörnern für die Schallabstrahlung*, Diplomarbeit, Institute of Technical Acoustics RWTH Aachen University, Aachen, Germany, April 2002.

[Kli90] W. Klippel, *Dynamic Measurement and Interpretation of the Nonlinear Parameters of Electrodynamic Loudspeakers*, Journal of the Audio Engineering Society **38** (1990), no. 12, 944 – 955.

[Kli95] W. Klippel, *Nonlinear wave propagation in horns and ducts*, The Journal of the Audio Engineering Society **98** (1995), no. 1, 431–436.

[Kli96] W. Klippel, *Modeling the Nonlinearities in Horn Loudspeakers*, The Journal of the Audio Engineering Society **44** (1996), no. 6, 470–480.

[KSH91] R. J. Kraszewski, R. A. Sigelmann and J. Herbertz, *Electrical multiport transfer functions and efficiency in layered media of piezoelectric and/or nonpiezoelectric materials*, The Journal of the Acoustical Society of America **90** (1991), no. 5, 2769–2774.

[Küp84] K. Küpfmüller, *Einführung in die theoretische Elektrotechnik*, 11. ed., Springer-Verlag, 1984.

[KYM77] Y. Kagawa, T. Yamabuchi and A. Mori, *Finite element simulation of an axisymmetric acoustic transmission system with a sound absorbing wall*, Journal of Sound and Vibration **53** (1977), no. 3, 357–374.

[KYS76] T. Kikkawa, A. Yukiyoshi and N. Sakamoto, *A New Horn Loudspeaker Design Yields Low Distortion and Wide Dispersion*, Presented on the 55th AES Convention, September 1976.

[Lük95] H. D. Lüke, *Signalübertragung*, 6 ed., Springer Verlag, 1995.

[Mak] M. Makarski, *Download link visualized velocity distribution*, http://www.akustik.rwth-aachen.de/pub/mma/moden.avi.

[Mak01] M. Makarski, *Theoretische und experimentelle Untersuchung der Schnittstelle Horntreiber-Horn*, Diplomarbeit, Institut für Technische Akustik, RWTH, Aachen, Deutschland, 2001.

[Mak03] M. Makarski, *Horndesign und Hornoptimierung mittels BEM*, Fortschritte der Akustik - DAGA ’03 (Aachen), März 2003, pp. 42–50.

[Mak04a] M. Makarski, *Determining Two-Port Parameters of Horn Drivers using only Electrical Measurements*, Presented at the 116th AES Convention in Berlin, Preprint 6098, March 2004.

[Mak04b] M. Makarski, *Do Higher Order Modes at the Horn Driver's Mouth contribute to the Sound Field of a Horn Loudspeaker?*, Presented at the 117th AES convention in San Francisco, Preprint 6188, October 2004.

[MB01] M. Makarski and G. K. Behler, *Messtechnische Bestimmung der Vierpolparameter von elektroakustischen Systemen*, Fortschritte der Akustik - DAGA '01 (Hamburg), 2001, pp. 410 – 411.

[Mec02] F. P. Mechel, *Formulas of Acoustics*, Springer Verlag, 2002.

[MGRS03] M. Makarski, J. H. D. Guimaraes, K. Reitz and C. Steinhusen, *Measurement of Transfer Path for Bearing Diagnostics*, Acta Acustica united with Acustica **89** (2003), no. 5, 799 – 808.

[MI68] P. Morse and K. Ingard, *Theoretical Acoustics*, McGraw-Hill, 1968.

[MKS79] S. Morita, N. Kyono and S. Sakai, *Acoustic Radiation of a Horn Loudspeaker by the Finite Element Method - A Consideration of the Acoustic Characteristic of Horns*, The Journal of the Audio Engineering Society **28** (1979), no. 7/8, 482–489.

[MM01] S. Müller and P. Masarani, *Transfer-Function Measurement with Sweeps*, The Journal of the Audio Engineering Society **49** (2001), no. 6, 443.

[MR93] D. Mapes-Riordan, *Horn Modeling With Conical and Cylindrical Transmission Line Elements*, The Journal of the Audio Engineering Society **41** (1993), no. 6, 471–484.

[Mül99] S. Müller, *Digitale Signalverarbeitung für Lautsprecher*, Ph. D. thesis, RWTH, 1999.

[NKP96] N.Amir, J. Kergomard and V. Pagneux, *A study of wave propagation in varying cross-section waveguides by modal decomposition. Part I. Theory and validation*, The Journal of the Acoustical Society of America **100** (1996), no. 4, 2034–2048.

[Pis03] R. Piscoya, *Die Beeinflussung der Richtwirkung von Schalltrichtern durch Impedanzbelegung der Wandung*, Ph. D. thesis, Technische Universität Berlin, Berlin Germany, Februar 2003.

[Pol] Polytec GmbH, *http://www.polytec.com/ger*.

[Put93] G. R. Putland, *Every One-Parameter Acoustic Field Obeys Webster's Horn Equation*, The Journal of the Audio Engineering Society **41** (1993), no. 6, 435–451.

[Put96] G. R. Putland, *Modeling of Horns and Enclosures for Loudspeakers*, Ph. D. thesis, Department of ELectrical and Computer Engineering, University of Queensland, Queensland, Australia, December 1996.

[RLK+97] M. Rausch, R. Lerch, M. Kaltenbacher, H. Landes, G. Krump and L. Kreitmeier, *Optimization of electrodynamic loudspeaker-design parameters by using a numerical calculation scheme*, ACUSTICA **83** (1997), no. 1-2, 1–8.

[SB95] C. H. Sherman and J. L. Butler, *Analysis of harmonic distortion in electroacoustic transducers*, The Journal of the Acoustical Society of America **98** (1995), no. 3, 1596–1611.

[SBB97] C. H. Sherman, J. L. Butler and A. L. Butler, *Analysis of harmonic distortion in electroacoustic transducers under indirect drive conditions*, The Journal of the Acoustical Society of America **101** (1997), no. 1, 297–314.

[SBSH95] H. Schurer, A. P. Berkhoff, C. H. Slump and O. E. Herrmann, *Modeling and Compensation of Nonlinear Distortion in Horn Loudspeakers*, The Journal of the Audio Engineering Society **43** (1995), no. 7/8, 592–598.

[SCD01] D. Saronni, M. D. Cola and D. Doldi, *Horn's Directiviy Related to the Pressure Distribution at their Mouth: part 2*, Presented on the 110th AES Convention, preprint 5319, April 2001.

[Sin80] R. Sinclair, *Two-section exponential acoustical horn*, The Journal of the Acoustical Society of America **68** (1980), no. 2, 736–736.

[SMPX99] M. C. T. S. M. Potirakis, G. E. Alexakis and P. J. Xenitidis, *Time-Domain Nonlinear Modeling of Practical Electroacoustic Transducers*, The Journal of the Audio Engineering Society **47** (1999), no. 6, 447–467.

[SR45] J. W. Strutt and F. R. S. S. B. Rayleigh, *The Theory of Sound*, First American ed., vol. II, Dover Publications, New York, 1945.

[Ste02] C. Steinhusen, *Untersuchung von Transferimpedanzen für die Wälzlagerdiagnose*, Diplomarbeit, Institute of Technical Acoustics, Aachen University (RWTH), Aachen, 2002.

[TJO35] A. L. Thuras, R. T. Jenkins and H. T. O'Neil, *Extraneous Frequencies Generated in Air Carrying Intense Sound Waves*, The Journal of the Acoustical Society of America **6** (1935), no. 3, 173–180.

[TKDT03] T. Tsuchiya, Y. Kagawa, M. Doi and T. Tsuji, *Finite element simulation of non-linear acoustic generation in a horn loudspeaker*, Journal of Sound and Vibration **266** (2003), no. 5, 993–1008.

[VB94] M. Vorländer and H. Bietz, *Reciprocity Technique for Simultaneous Free-Field and Diffuse-Field Microphone Calibration*, Acustica **80** (1994), 365 – 377.

[Voi02] A. Voishvillo, *Nonlinearity in Horn Drivers - Where the Distortion Comes From?*, Presented at the 113th AES Convention, Los Angeles, October 2002.

[Vor05] M. Vorländer, *Technische Akustik II*, Vorlesungsumdruck, September 2005.

[WML78] J. W. Marshall Leach, *On the Specification of Moving-Coil Drivers for Low-Frequency Horn-Loaded Loudspeakers*, The Journal of the Audio Engineering Society **27** (1978), no. 12, 951.

[Zie77] O. C. Zienkiewicz, *The Finite Element Method*, 3rd ed., McGraw-Hill, London, 1977.

[ZZ93] M. Zollner and E. Zwicker, *Elektroakustik*, 3. ed., Springer-Verlag, 1993.